

**UC Davis**

**UC Davis Electronic Theses and Dissertations**

**Title**

Understanding Affected Muscle Activity in Children with Unilateral Congenital Below-Elbow Deficiency for Intuitive Control of Dexterous Prostheses

**Permalink**

<https://escholarship.org/uc/item/85c7h7rw>

**Author**

Battraw, Marcus Aaron

**Publication Date**

2024

Peer reviewed|Thesis/dissertation

Understanding Affected Muscle Activity in Children with Unilateral Congenital Below-Elbow  
Deficiency for Intuitive Control of Dexterous Prostheses

By

MARCUS A. BATTRAW  
DISSERTATION

Submitted in partial satisfaction of the requirements for the degree of

DOCTOR OF PHILOSOPHY

in

Mechanical and Aerospace Engineering

in the

OFFICE OF GRADUATE STUDIES

of the

UNIVERSITY OF CALIFORNIA

DAVIS

Approved:

---

Jonathon S. Schofield, Chair

---

Wilsaan M. Joiner

---

Stephen K. Robinson

Committee in Charge

2024

## Abstract

There are many complex factors that will affect whether children with a unilateral congenital below-elbow deficiency (UCBED) will use a prosthetic limb to interact within their environment. Children face higher rates of prosthesis abandonment at 35-45%, compared to adults at 23-26%. Ultimately, for a child to wear and use their prosthesis, it must facilitate the effective performance of daily tasks and promote healthy social interactions. Although beginning to emerge, multiarticulate upper limb prostheses for children remain sparse despite the continued advancement of mechatronic technologies that have benefited adults with upper limb amputations. In contrast, pediatric devices typically provide a single open-close grasp (if a grasping function is available at all) and often offer non-anthropomorphic appearances, falling short of meeting the criteria essential to prosthesis adoption. Moreover, this population presents unique challenges, as they were born never having actuated a hand, and with forearm musculature that never fully developed—a stark departure from those with acquired limb absence. Due to the lack of investigation into how children with UCBED actuate their muscles coupled with the limited advancement in pediatric upper limb devices, the effective translation of dexterous prostheses remains a prominent issue.

This dissertation builds the fundamental groundwork necessary for the effective translation of dexterous prosthetic hands for children with UCBED. It begins with an examination of how typically developing children use their hands to interact within their environment to inform dexterous device development (Chapter 3). Here we found that children, like adults, use a small subset of hand movements to perform object manipulation in home settings. Subsequently, a child-sized dexterous prosthetic hand was developed to serve as a dedicated research platform (Chapter 4). A thorough benchmark of this research platform was performed to validate its functional

grasping ability and it was shown to be a robust device within a research environment. Prior to using this device, a cohort of children with UCBD were recruited, and an in-depth analysis of state-of-the-art prosthetic control, namely surface electromyography (sEMG) as a measure of affected muscle electrical activity, was conducted (Chapter 5). Upon investigation, participants exhibited a measurable degree of consistency and repeatability of their affected musculature as obtained through sEMG when they attempted missing hand and wrist movements. Furthermore, through tuning features, i.e., sEMG characteristics, and classification algorithms, we found a novel generalized feature set that provided increased classification to decode hand motor intent (Chapter 6). Moreover, we benchmarked the real-time performance of these children to execute hand movements, adding a translational dimension to our findings (Chapter 7). This forms a crucial foundation for understanding muscle actuation and use of advanced prostheses among children with UCBD.

Through this work, we have laid the foundation to understand the capacity of children with UCBD to control their affected musculature. This begins to address the translational aspect of child-size dexterous upper limb devices and has the potential to remove barriers to device acceptance.

## Preface

The research presented within this dissertation is an original work by Marcus A. Battraw, conducted within the Bionic Engineering and Assistive Robotics Laboratory at the University of California Davis, in collaboration with the Shriners Children's – Northern California.

All data collection methods and study procedures performed on the participants herein received approval from both Shriners Children's – Northern California and the University of California, Davis Research Ethics Board. Written informed consent and assent were obtained from all participants and legal guardians.

This research was primarily supervised by Dr. Jonathon Schofield in collaboration with Dr. Wilsaan Joiner, both from the University of California, Davis, and with Dr. Michelle James and Dr. Anita Bagley from Shriners Children's – Northern California. This research is part of a larger nationwide multi-site Shriners Hospital study. Additionally, this research received support from the National Science Foundation CISE-IIS Human Centered Computing Program under award number 2133879, and through the Shriners Children's Hospital Clinical Research Program under award number 79139-NCA-23.

The majority of Chapter 2 has been published as:

**Battraw MA**, Fitzgerald J, Joiner WM, James MA, Bagley AM, Schofield JS. (2022). A review of upper limb pediatric prostheses and perspectives on future advancements. *Prosthetics and Orthotics International*. 46(3): 267-273

Contributions as the first author: Conducted the literature search, led manuscript writing and organization, synthesized data, generated figures and tables, authored draft manuscript, and performed revisions during peer review. It is important to note that Fitzgerald J wrote

the majority of the section on Psychosocial functioning, and Schofield JS wrote a paragraph on neural-machine-interfaces.

The majority of Chapter 3 has been published as:

**Battraw MA**, Young PR, Welner ME, Joiner WM, Schofield JS. (2022). Characterizing pediatric hand grasps during activities of daily living to inform robotic rehabilitation and assistive technologies. IEEE International Conference on Rehabilitation Robotics.

Contributions as the first author: Led manuscript writing and organization, designed the experimental protocol, formulated and conducted data analysis, generated figures and tables, authored the draft manuscript, and performed revisions during peer review.

The majority of Chapter 4 has been published as:

**Battraw MA**, Young PR, Joiner WM, Schofield JS. (2022). A multiarticulate pediatric prosthetic hand for clinical and research applications. *Front. Robot. AI* **9**, 1–14.

Contributions as the first author: Designed and fabricated the device, developed the experimental protocol, conducted data collection and analysis, generated figures and tables, led the writing and organization of the draft manuscript, and performed revisions during peer review.

The majority of Chapter 5 has been published as:

**Battraw MA**, Fitzgerald J, James MA, Bagley AM, Joiner WM, Schofield JS. (2024). Understanding the capacity of children with congenital unilateral below-elbow deficiency to actuate their affected muscles. *Sci. Rep.*

Contributions as the first author: Designed the experimental protocol, performed data collection and analysis, generated figures and tables, led the writing and organization of the draft manuscript, and performed revisions during peer review.

The majority of Chapter 6 has been submitted for publication as:

**Battraw MA**, Fitzgerald J, Winslow E, James MA, Bagley AM, Joiner WM, Schofield JS. (2024). Surface electromyography evaluation for decoding motor intent in children with congenital upper limb deficiency. (SREP-24-01211) Under Review.

Contributions as the first author: Designed the experimental protocol, performed data collection, developed the analysis methodology, conducted data analysis, generated figures and tables, led the writing and organization of the draft manuscript, and performed revisions during peer review.

The majority of Chapter 7 is a draft for publication as:

**Battraw MA**, Fitzgerald J, James MA, Bagley AM, Joiner WM, Schofield JS. Real-time control of multiple movement patterns for children with unilateral congenital below-elbow deficiency: A Case Series

Contributions as the first author: Designed and developed the experimental protocol and methodology, performed data collection and analysis, generated figures and tables, led writing and organization, and authored the draft manuscript.

## Acknowledgements

I would like to express my gratitude to my advisors—Jonathon Schofield, Wilsaan Joiner, Michelle James, and Anita Bagley. Each of you has been instrumental in my development as a young academic, offering unique insights and helping me cultivate a multidisciplinary skillset.

A special thanks to my primary advisor, Jonathon Schofield. Your unwavering support has been invaluable in the journey towards becoming an independent researcher. I am particularly thankful for your assistance early on in my academic career when I needed it the most. It has been wonderful reflecting on the hard work you invested into my growth and how it has shaped me into the academic I am today. My graduate career would not have been possible without you. Thank you for always listening to me ramble and for articulating into words what I often struggled to say concisely. You are a wonderful advisor, and I could not have asked for a better mentor.

I appreciate my lab mates for providing much-needed distractions. I would like to acknowledge Justin Fitzgerald for all our technical conversations, which have greatly shaped my approach to data analysis. A big thanks to all the participants without whom this work would not be possible.

I want to express my heartfelt thanks to my wife, Yoana, for her unconditional support. Thank you for patiently listening to me explain and think through my research even if you weren't really listening at times. Your assistance in setting and adhering to deadlines, painstakingly reading through and helping edit my papers, and even creating some figures for me, has been invaluable.

I am grateful for your selflessness, as you helped shoulder my academic journey at the expense of yours. You are a truly remarkable and supportive wife.

This has been a very exciting season of my life, and I am beyond grateful and joyful for the research I have been able to conduct and the contributions I have made to the field.



# Table of Contents

Abstract .....	ii
Preface.....	iv
Acknowledgements.....	vii
List of Tables .....	xii
List of Figures .....	xiii
Chapter 1. Introduction .....	1
1.1. Problem definition.....	1
1.2. Objectives.....	2
1.3. Dissertation outline .....	2
1.4. References .....	5
Chapter 2. Current state-of-the-art conventional pediatric upper limb prostheses .....	7
2.1. Chapter preface .....	7
2.2. Introduction .....	7
2.3. Types of pediatric prostheses .....	8
2.3.1. Passive devices.....	10
2.3.2. Body-powered devices.....	10
2.3.3. Myoelectric devices .....	10
2.4. Quality of life and prosthesis use .....	11
2.4.1. Psychosocial functioning .....	13
2.4.2. Physical functioning.....	15
2.5. Discussion .....	17
2.5.1. Dexterous multi-grasp terminal devices .....	17
2.5.2. Advanced control interfaces .....	18
2.5.3. Current barriers to advanced pediatric devices.....	20
2.6. Conclusions .....	21
2.7. References .....	22
Chapter 3. Taxonomy of pediatric hand grasps during activities of daily living.....	27
3.1. Chapter preface .....	27
3.2. Introduction .....	27
3.3. Methods.....	29
3.3.1. Participants.....	29

3.3.2. Experimental equipment .....	30
3.3.3. Analysis and procedures .....	31
3.4. Results .....	33
3.4.1. Participant 1 .....	33
3.4.2. Participant 2 .....	36
3.5. Discussion .....	37
3.6. Conclusions .....	39
3.7. References .....	39
Chapter 4. Development of a research-based multiarticulate pediatric prosthetic hand.....	42
4.1. Chapter preface .....	42
4.2. Introduction .....	42
4.3. Materials and methods .....	45
4.3.1. Pediatric prosthetic hand criteria .....	45
4.3.2. Mechanical and electrical performance .....	46
4.3.3. Hand assessment protocol.....	51
4.4. Results .....	54
4.4.1. Pediatric prosthetic hand.....	54
4.4.2. Mechanical and electrical performance .....	57
4.4.3. Hand assessment .....	61
4.5. Discussion .....	63
4.6. Conclusions .....	67
4.7. References .....	67
Chapter 5. The capacity of children with UCBD to actuate their affected muscles.....	71
5.1. Chapter preface .....	71
5.2. Introduction .....	72
5.3. Methods.....	74
5.3.1. Participants.....	74
5.3.2. Data collection .....	75
5.3.3. Experimental protocol.....	75
5.3.4. sEMG per-processing.....	78
5.4. Analysis.....	79
5.4.1. Muscle excitation .....	79

5.4.2. Differences across limbs .....	83
5.5. Results .....	84
5.5.1. Muscle excitation .....	84
5.5.2. Across movement dissimilarity.....	90
5.5.3. Differences across limbs .....	94
5.6. Discussion .....	97
5.6.1. Visible patterns of muscle excitation.....	97
5.6.2. Reproducible attempted hand movements .....	98
5.6.3. Distinguishable attempted hand movements .....	99
5.7. Conclusions .....	101
5.8. References .....	102
Chapter 6. Decoding hand motor intent in children with UCBED .....	106
6.1. Chapter preface .....	106
6.2. Introduction .....	107
6.3. Methods.....	109
6.3.1. Participants.....	109
6.3.2. Experimental protocol.....	110
6.3.3. Data processing.....	111
6.4. Feature evaluation .....	115
6.4.1. Individual features .....	116
6.4.2. Individual domains and combined domains .....	117
6.4.3. Generalized congenital feature set .....	119
6.5. Analysis.....	119
6.5.1. Feature set comparisons.....	119
6.5.2. Congenital feature set assessment.....	121
6.6. Results .....	123
6.6.1. Individual features .....	123
6.6.2. Generalized congenital feature set .....	124
6.6.3. Feature set comparisons.....	125
6.6.4. Congenital feature set assessment.....	128
6.7. Discussion .....	134
6.7.1. Unique features can be identified for children with UCBED.....	134

6.7.2. Children with UCBED benefit from certain feature sets .....	134
6.7.3. The congenital feature set is an effective generalized set .....	136
6.8. Conclusions .....	138
6.9. References .....	139
Chapter 7. Real-time control of multiple grasp patterns for children with UCBED .....	144
7.1. Chapter preface .....	144
7.2. Introduction .....	144
7.3. Methods .....	147
7.3.1. Participants.....	147
7.3.2. Data collection .....	148
7.3.3. Motion Test.....	149
7.3.4. Feature space quality.....	151
7.4. Analysis.....	155
7.4.1. Offline evaluation .....	155
7.4.2. Motion Test.....	155
7.4.3. Feature space quality.....	156
7.5. Results .....	156
7.5.1. Offline evaluation .....	156
7.5.2. Motion Test.....	159
7.5.3. Feature space quality.....	165
7.6. Discussion .....	168
7.6.1 Children with UCBED can control dexterous prostheses.....	169
7.6.2 Feature space metrics follow similar behavior across limbs .....	171
7.7. Conclusions .....	172
7.8. References .....	174
Chapter 8. Conclusions and future directions .....	177
8.1. References .....	180
References.....	182
Appendix A: BEAR PAW movement assessment.....	201
Appendix B: Muscle excitation and visualization .....	205
Appendix C: Classification tables and analysis .....	232
Appendix D: Real-time feature space trial differences.....	259

## List of Tables

Table 2-1. Pediatric quality of life comparison .....	12
Table 3-1. Participant grasp duration and frequency .....	35
Table 4-1. Pediatric research platform design criteria .....	46
Table 4-2. Top 7 common generalized hand grasps configurations .....	47
Table 4-3. Different manipulandum used to characterize the force output of the BEAR PAW...	48
Table 4-4. BEAR PAW achieved specifications .....	56
Table 4-5. BEAR PAW's mechanical and electrical characteristics .....	60
Table 5-1. Demographic information for participants with UCBD .....	74
Table 5-2. Split-data representational dissimilarity analysis .....	92
Table 5-3. Relatedness of RDMs across limbs for each participant .....	96
Table 6-1. Participant demographics .....	110
Table 6-2. Extracted features from the time, frequency, and time-frequency domains.....	113
Table 6-3. Computational expense of the congenital feature set across classifiers .....	130
Table 7-1. Participant demographics for children with UCBD .....	147
Table 7-2. Average offline performance metrics .....	157
Table 7-3. Average real-time performance metrics .....	161

## List of Figures

Figure 2-1. Pediatric prosthetic hand options .....	9
Figure 3-1. Video camera harnessing equipment and setup .....	31
Figure 3-2. Adult generalized hand grasps .....	32
Figure 3-3. Tree maps of the combined dominant and non-dominant hand grasps.....	36
Figure 4-1. Depicts the testing platform for the BEAR PAW .....	49
Figure 4-2. Depicts the BEAR PAW during grasp actuation .....	50
Figure 4-3. Depicts the testing rig used to perform the AHAP .....	52
Figure 4-4. The BEAR PAW .....	55
Figure 4-5. A size comparison between the BEAR PAW and the HANDi Hand .....	57
Figure 4-6. A detailed illustration of the mechanical features of the BEAR PAW .....	58
Figure 4-7. BEAR PAW grasping comparison scores.....	62
Figure 4-8. BEAR PAW posture comparison scores.....	63
Figure 5-1. Participants with sEMG electrodes donned across limbs .....	76
Figure 5-2. Overview of the experimental outline.....	77
Figure 5-3. Dataflow to produce the split-data representation dissimilarity matrix .....	82
Figure 5-4. The box and whisker plots provide a visualization of the RMS muscle excitation ...	86
Figure 5-5. The box and whisker plots provide a visualization of the MNF muscle excitation ...	87
Figure 5-6. Within-movement consistency for median RMS and MNF .....	90
Figure 5-7. Visual representation of the correlation distances between hand movements .....	94
Figure 5-8. Comparison of across-limb consistency for the 10 hand movements.....	95
Figure 6-1. Experimental protocol.....	111
Figure 6-2. Feature evaluation flow diagram.....	116
Figure 6-3. Cumulative count of domain-specific high-performing individual features.....	124
Figure 6-4. Feature count for recommending the generalized congenital feature set.....	125
Figure 6-5. Investigation of feature set performance for participant SHR-I.....	127
Figure 6-6. Congenital feature set classifier comparisons .....	129
Figure 6-7. Impact of movement reduction .....	132
Figure 6-8. Count of the top five reduced hand movements.....	133
Figure 7-1. Illustration of the feature space metrics employed for analysis.....	152
Figure 7-2. Offline confusion matrices .....	159
Figure 7-3. Participant examples for the Motion Test and setup.....	160
Figure 7-4. Real-time performance metrics .....	164
Figure 7-5. Feature space quality metric trajectories.....	167
Figure 7-6. Feature space trial-to-trial separability trajectory differences .....	168

# Chapter 1. Introduction

## 1.1. Problem definition

There are roughly 1 in 500 live births in which an upper limb absence will occur<sup>1</sup>. Moreover, approximately 1 in 10,000 children will have a transverse limb deficiency<sup>2</sup>. Of these children, those with unilateral congenital below-elbow deficiency (UCBED), absence of the upper limb between the distal and proximal region of the forearm<sup>3</sup>, will typically exhibit limb characteristics amenable to prosthesis prescription. However, when children are prescribed a prosthesis, they often abandon the device at a rate of 35-45%, in contrast to adults at 23-26%<sup>4</sup>. This increased rate of device abandonment can be attributed to various factors which are broadly categorized into physical and psychosocial functioning<sup>5</sup>.

The current state-of-the-art for child-sized upper limb prostheses fails to provide sufficient functional benefit when compared to not wearing the device at all<sup>5</sup>. Even those who regularly use their device may be living with a prosthesis that provides insufficient functional benefit and may be motivated by other considerations, such as aesthetics and social factors. Interestingly, the primary focus of the field of upper limb prosthesis has been to restore the functional capacity of adults to control their device, this is a stark departure from the challenges faced by children, many of whom were born with limb absence, thus never having had an intact hand to actuate.

Current commercial and research-based techniques for decoding motor intent for the purpose of prosthetic control were developed with adult populations. These techniques use measures of muscle electrical activity captured at the skin's surface, electromyography (sEMG), and identify patterns in sEMG as participants perform various hand movements. These patterns serve as templates to predict the intended hand movement of the prosthesis user. Subsequently, this

prediction is used as a control signal to operate a prosthesis. Despite the success of these technologies with adults, the translation to children has yet to be investigated, specifically those individuals born with limb absence. These children present unique challenges in the prosthetics arena that should be addressed for the effective translation of dexterous upper limb prostheses.

## 1.2. Objectives

This dissertation primarily focuses on understanding how children born with limb deficiency actuate their affected muscles and how systematically tuning classification methods to decode missing hand motor intent may provide improved predictions for the control of multi-grasp prostheses.

To begin, a data annotation methodology was employed to investigate how typically developed children use their hands within daily activities, thus informing prosthesis development to enhance the functional capabilities a device may offer. Mechatronic technologies were leveraged for the design and development of a research-based prosthetic hand intended for real-time applications. Furthermore, measures of physiological activity through sEMG were used to explore the capacity of children with UCBED to consistently and reliably actuate their affected musculature. Following this, we applied and tuned sEMG classification techniques to investigate the ability to decode hand motor intent for this unique child population. This exploration culminates in investigating how children with UCBED control a multi-grasp prosthesis in real time, thereby initiating the translation of these techniques to children with UCBED.

## 1.3. Dissertation outline

Within this dissertation, we provide the foundational elements necessary to initiate the translation of dexterous upper limb devices to the pediatric UCBED population. First, we present an overview



of the current state of the art for pediatric upper limb prostheses. This overview serves as a starting point for investigation, highlighting the current gaps in knowledge concerning child-specific prostheses.

Next, we explore how children use their hands to manipulate objects within their environments. This aims to understand what types of hand movements may be beneficial for children with UCBD. It also informs the development of a child-sized multi-grasp prosthesis designed for use in research and clinical settings, marking the initial steps to begin the translation of these technologies to real-world use.

Prior to children effectively utilizing a dexterous device in real-time, we investigated their ability to actuate their affected musculature. Given the unique circumstances children with UCBD present, as they were born with their limb absence, techniques to decode hand motor intent become a focal point for investigation. Therefore, we explore how sEMG classification techniques may be used to enhance movement prediction for these children.

Finally, we explore real-time settings to begin the translation of these techniques. This work establishes a foundation for the effective translation of dexterous prostheses to children with UCBD. Future work includes investigating how children manipulate objects with a multi-grasp prosthesis and exploring the effects of training and long-term use. The research discussed above is presented in the following list of chapters.

## **Chapter 2. Current state-of-the-art conventional pediatric upper limb prostheses.**

This chapter provides a review of the current state of the art for pediatric prostheses. It discusses various types of prostheses, along with the current standard of care for prostheses prescription. The physical and psychosocial challenges faced by children with UCBD are highlighted. The

gap between emerging technology for children, especially those with UCBD, is presented as a significant barrier to the effective translation of dexterous devices. Avenues for future directions to begin removing barriers to device acceptance are then outlined.

### **Chapter 3. Taxonomy of pediatric hand grasps during activities of daily living.**

In this chapter, an investigation into how typically developed children grasp and manipulate objects within their home environments is conducted. A detailed analysis of hand grasps from video footage was performed to characterize grasp taxonomy by frequency and duration of use. The implication of this work begins to provide an understanding of how to develop functional dexterous prostheses and other rehabilitative devices.

### **Chapter 4. Development of a research-based multiarticulate pediatric prosthetic hand.**

This chapter covers the development and comprehensive benchtop testing of a multiarticulate child-sized prosthetic hand. Criteria for the development, along with a detailed investigation of the mechanical and electrical performance, are provided. Additionally, a validated functional test to explore the robotic hand's ability to grasp a variety of objects was conducted and discussed in relation to alternatively available adult-based research devices.

### **Chapter 5. The capacity of children with UCBD to actuate their affected muscles.**

This chapter investigates the capacity of children with UCBD to actuate their affected muscles. Standard amplitude and frequency measures of sEMG are used to explore their ability to consistently and reliably actuate their affected musculature during distinct attempted hand movements. This work provides a foundational understanding that children born with upper limb deficiency still retain the capacity to actuate their affected muscles—an essential first step prior to employing classification techniques to predict motor intent.

## **Chapter 6. Decoding hand motor intent in children with UCBED.**

Within this chapter, a systematic methodology was employed to determine which classification techniques and features, characteristics of sEMG signals, provided enhanced movement classification for children with UCBED. The training and testing times for classification were determined to address the potential for the real-time implementation for prosthetic control. As, individuals who use multi-grasp prostheses typically employ a subset of grasp movements to perform daily tasks, we investigated a reduced set from the total number of participant-attempted movements to understand the effects on prediction accuracy. This establishes a foundation for implementing real-time control of dexterous prostheses among children with UCBED.

## **Chapter 7. Real-time control of multiple grasp patterns for children with UCBED.**

A case series is presented to investigate how children with UCBED control multiple grasp patterns in real-time. Utilizing the classification techniques developed in Chapter 6, the real-time Motion Test to assess classification performance was conducted<sup>6</sup>, along with an assessment of the differences in feature space quality metrics<sup>7-9</sup> for real-time control. This work marks a significant step in the effective translation of real-time control techniques for multiarticulate prostheses to children with UCBED.

## **Chapter 8. Conclusions and future directions.**

This chapter synthesizes the presented work, exploring its implication for children with UCBED, and outlines future directions to enhance our understanding and development of prostheses, aiming to offer functional benefits.

### **1.4. References**

1. Giele, H., Giele, C., Bower, C. & Allison, M. The incidence and epidemiology of

- congenital upper limb anomalies: A total population study. *J. Hand Surg. Am.* **26**, 628–634 (2001).
2. Ekblom, A. G., Laurell, T. & Arner, M. Epidemiology of congenital upper limb anomalies in 562 children born in 1997 to 2007: A total population study from Stockholm, Sweden. *J. Hand Surg. Am.* **35**, 1742–1754 (2010).
  3. Davids, J. R., Wagner, L. V., Meyer, L. C. & Blackhurst, D. W. Prosthetic management of children with unilateral congenital below-elbow deficiency. *J. Bone Jt. Surg. - Ser. A* **88**, 1294–1300 (2006).
  4. Biddiss, E. & Chau, T. Upper limb prosthesis use and abandonment: A survey of the last 25 years. *Prosthetics and Orthotics International* vol. 31 236–257 (2007).
  5. Batraw, M. A. *et al.* A Review of Upper Limb Pediatric Prostheses and Perspectives on Future Advancements. *Prosthet. Orthot. Int.* **46**, 267–273 (2022).
  6. Kuiken, T. A. *et al.* Targeted muscle reinnervation for real-time myoelectric control of multifunction artificial arms. *JAMA - J. Am. Med. Assoc.* **301**, 619–628 (2009).
  7. Kristoffersen, M. B., Franzke, A. W., Sluis, C. K. Van Der, Murgia, A. & Bongers, R. M. The Effect of Feedback During Training Sessions on Learning Pattern-Recognition-Based Prosthesis Control. *IEEE Trans. Neural Syst. Rehabil. Eng.* **27**, 2087–2096 (2019).
  8. Franzke, A. W. *et al.* Exploring the Relationship between EMG Feature Space Characteristics and Control Performance in Machine Learning Myoelectric Control. *IEEE Trans. Neural Syst. Rehabil. Eng.* **29**, 21–30 (2021).
  9. Bunderson, N. E. & Kuiken, T. A. Quantification of feature space changes with experience during electromyogram pattern recognition control. *IEEE Trans. Neural Syst. Rehabil. Eng.* **20**, 239–246 (2012).

## Chapter 2. Current state-of-the-art conventional pediatric upper limb prostheses

The majority of this chapter has been published as:

Battraw MA, Fitzgerald J, Joiner WM, James MA, Bagley AM, Schofield JS. (2022). A review of upper limb pediatric prostheses and perspectives on future advancements. *Prosthetics and Orthotics International*. 46(3): 267-273

### 2.1. Chapter preface

This chapter highlights the current gap in knowledge that ultimately affects the use of child-specific upper limb prostheses and serves to provide a fundamental foundation for the remaining chapters of this dissertation. It discusses an overview of the types of prostheses that may be prescribed to children with upper limb deficiency and their limitations. The numerous physical and psychosocial factors affecting whether a child will choose to use their device are outlined. Additionally, it describes emerging technologies that have yet to be applied to children and the potential benefits they may provide to this population. Future directions to begin removing barriers to device acceptance and effectively translating dexterous devices to children with unilateral congenital below-elbow deficiency are then discussed.

### 2.2. Introduction

Approximately 1 in every 2,800 children in the United States will be born with an upper limb difference<sup>1</sup> and nearly 1 in 10,000 live births will present with a transverse upper limb deficiency (ULD)<sup>2</sup>. Of these children, those with a below-elbow deficiency may be prescribed an upper limb (UL) prosthesis as young as 6-18 months of age with the intention of helping the child learn to adapt early in life;<sup>3</sup> although early prescription has not been shown to be associated with the frequency of use or wear<sup>4</sup>. Parents influence how often their child wears their prosthesis while they are too young to make these decisions for themselves, and it is not uncommon for parents to

view their child's limb difference as a deficiency that must be addressed with an artificial limb<sup>5</sup>. However, when children become old enough to make decisions for themselves, prosthesis abandonment becomes a pervasive issue<sup>6</sup>.

Like adult UL prosthesis wearers, device abandonment is common in pediatric populations; however, it is far more prevalent. In a review of 25 years of UL prostheses literature, Biddiss and Chau determined that adult abandonment rates varied from 26% for body-powered devices to 23% for electric devices; yet, for children, these rates were 45% and 35%, respectively<sup>7</sup>. This suggests that development, acceptance, and use of pediatric UL prostheses are complex issues and multiple factors determine whether a child will use or abandon their prosthetic limb<sup>7</sup>. In this chapter, we will critically assess the state of current prosthetic UL options for children with congenital below-elbow deficiencies and the outcomes reported in literature. While experimental prostheses including those developed with 3D printing technologies have rapidly accelerated in recent years this narrative review empathizes clinically prescribed devices. Further, we summarize the prevailing technical and social challenges contributing to the high rates of prosthesis abandonment. Finally, we highlight emerging technologies on the clinical horizon that may begin to remove barriers to prosthesis acceptance for pediatric populations.

### 2.3. Types of pediatric prostheses

Numerous prosthesis options may be prescribed for children with transverse below-elbow deficiencies. These transradial prostheses have several common components that may include a prosthetic socket, liner, terminal device, and harness (Figure 2-1). The socket surrounds the wearer's residual limb and serves as the point of attachment between the prosthesis and the user's body. It is custom fabricated and contoured to accommodate the individual's morphology while strategically compressing pressure-tolerant regions on the residual limb to securely suspend the

prosthesis. An optional socket *liner* may be used to improve comfort and suspension in certain cases. The *terminal device* (TD) is the most distal component that may provide grasping functionality, or in some devices, be included solely for cosmetic appearance. Finally, *harnessing* is often used to further assist in prosthetic suspension and/or leverage body motion to actuate grasping functions in a TD.

Transradial pediatric prostheses can be categorized as *passive* (cosmetic) devices, that do not provide any grasping functionality and *active* devices that can be operated to perform grasping functions. *Active* devices are further subcategorized as *body-powered* and *myoelectric* devices (further described below). Figure 2-1 depicts commonly prescribed upper limb pediatric prostheses. Each category of device provides desirable qualities to the user; however, there are also inherent trade-offs and challenges associated with each. A final category of prostheses are activity-specific devices which are designed to enable children to participate in specific sports and recreational activities. Although there are a diverse variety of useful activity-specific prostheses, in this chapter we will focus on the active and passive devices prescribed for general use in daily living.

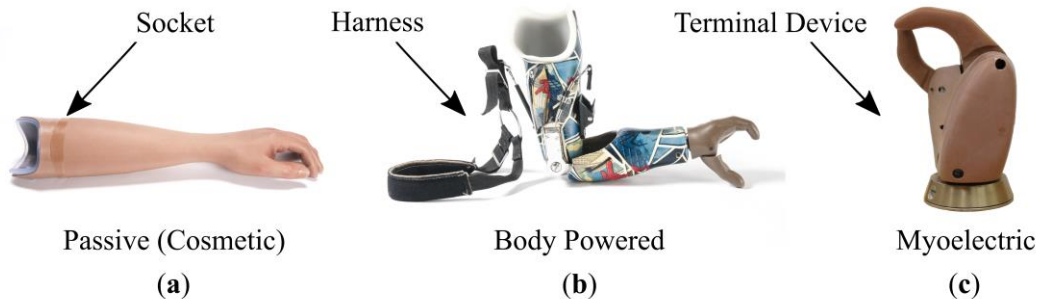


Figure 2-1. Pediatric prosthetic hand options. Arrows depict the socket, harnessing, and terminal device. **(a)** The cosmetic device provides a realistic appearance. **(b)** A body-powered device utilizes compensatory body motion to control the terminal device. Note: the prosthesis depicted accommodates a higher-level deficiency and includes a mechanical elbow. **(c)** An electric terminal device that, when coupled with sensors measuring muscle activity, allows for prehension control. **(a)** and **(b)** - Photos courtesy of Shriners Children's – Northern California. **(c)** - Photo courtesy of Michael Dawson at the BLINC Lab at the University of Alberta <https://blinclub.ca>.

### 2.3.1. Passive devices

A key benefit of passive devices is that they can provide life-like, anthropomorphic appearances. These devices do not actively move to accommodate grasping functions and are typically encased in a silicone or skin-like material that can be made to match the wearer's skin tone and closely resemble an intact hand and/or limb. For children, these prostheses may help in social situations when the child or parent is fearful or anxious about the reactions of others to their ULD; although there is evidence that hiding a limb difference is an ineffective coping strategy<sup>8</sup>. Further, they may help in supporting bimanual tasks, or when lifting or playing with large objects.

### 2.3.2. Body-powered devices

Body-powered prostheses offer wearers the ability to actively control grasp and release movements through a system of cables, elastic bands, and harnessing worn on the upper body. Typically, scapular motion pulls a cable attached to the terminal device, which can be set to either open the TD (normally closed device) or close the TD (normally open device). These relatively simple mechanical devices are lightweight, quick to actuate, robust, and simple to use, maintain, and repair. However, their function is limited to a single grasp and release motion, often necessitating compensatory strategies to achieve tasks<sup>9</sup>. Further, many body-powered devices are a split-hook design, bearing little aesthetic resemblance to an intact hand which may have social implications for the user<sup>5</sup>.

### 2.3.3. Myoelectric devices

Myoelectric TDs use electro-mechanical actuators to drive grasping motions. These devices use electromyography (EMG) to control the device's grasping function. This control technique employs sensors that measure the electrical activity of muscles on the palmar and dorsal aspects of the residual forearm skin. This measured activity is processed by a control system and the



resulting signals command the TD to actuate. Myoelectric devices provide the benefit of control using the muscles of the affected limb, often eliminating the need for harnessing and cables as well as body/shoulder movements to control the TD. Like cosmetic devices, these TDs may also be covered with a silicone cosmetic glove for cosmesis. Myoelectric devices have several practical challenges including increased weight, reduced robustness<sup>10</sup>, slower actuation speeds, challenges achieving intuitive control<sup>11</sup>, and remembering to recharge the battery<sup>12</sup> when compared to alternate devices. Additionally, consistent control is limited by electronic and physiologic characteristics e.g. noisy sensor signals<sup>13</sup> that are sensitive to small displacements on the residual limb<sup>14</sup>, changes in arm posture, and fatigue due to extended muscle use<sup>15</sup>. Commonly, myoelectric TDs are shaped like an intact hand and actuate the first three digits achieving a chuck pinch (3-finger tripod) grasp configuration, which is not suitable for many daily activities; less-anthropomorphic devices are also available. Nearly all current pediatric myoelectric devices offer only a single-degree-of-freedom open/closing action.

#### 2.4. Quality of life and prosthesis use

Independent from prosthesis research, studies have investigated multiple dimensions related to the quality of life for children with ULDs. In this review, we divide the challenges that these children may face into two categories: psychosocial and physical functioning. Table 2-1 presents an analysis of literature reporting the health-related quality of life for children with ULDs using a validated clinical inventory. The pediatric quality of life (PedsQL) inventory was employed by<sup>16-18</sup> to compare pediatric individuals with ULDs to the general population<sup>19-21</sup>. This self-reported survey can be completed either by the patient or their parent, is valid for patients aged 2-18 years, and contains 23 items that capture physical, emotional, social, and school functioning<sup>19,22</sup>. It is important to note that PedsQL has been validated in multiple populations and scoring using patient

or parent self-reports has been shown to achieve comparable results and the appropriate statistical significance needed to analyze patient data<sup>19</sup>. Participants respond by providing a score from 0-4 to questions that reflect the frequency of events in daily living, (0 indicating never, and 4 indicating almost always). Scores are translated to a percentage between 0-100% in 25% increments<sup>19,22</sup>. Interestingly, of the limited work making these comparisons, PedsQL inventory scores often suggest few statistically and/or clinically significant differences between affected and unaffected patient-matched groups<sup>16-18</sup>.

Table 2-1. Pediatric Quality of Life Comparison. Comparison of multiple health-related quality of life studies conducted for the pediatric ULD population. Categories span to assess both physical and psychosocial factors inherent to children with ULDs. Scores for the Shriners, Norway, and Dutch studies<sup>16-18</sup> were obtained through the implementation of PedsQL inventory<sup>22</sup> and compared to their respective general populations<sup>19-21</sup>. Here participants were asked a set of questions related to the frequency of events during daily activities in which they responded on a scale from 0 indicating never to 4 indicating almost always. These values were then converted to percentages between 0-100% in increments of 25%<sup>19,22</sup>. Note: \*Child reported results. †Clinically significant difference. ‡Statistically significant difference.

Populations	Age Group (years)	Number of Samples (n)	Physical Functioning (%)	Emotional Functioning (%)	Social Functioning (%)	School Functioning (%)
<b>Shriners<sup>16</sup></b>						
General Population <sup>19</sup>	2-16	8713	84.08	81.20	83.05	78.27
Wearers	2-20	317	88.5	77.9	82.2	55.1†
Non-wearers	2-20	132	88.6	74.3	80.1	46.7†
<b>Norway<sup>17</sup></b>						
General Population <sup>20</sup>	13-15	424	91.12	77.15	88.12	78.02
ULD*	6-16	46	87	82	87	82
<b>Dutch<sup>18</sup></b>						
General Population <sup>21</sup>	10-12	219	84.9	77.1	86.1	78.7
ULD*	10-12	77	87.1	76.0	85.6	78.6
General Population <sup>21</sup>	13-14	106	87.3	77.3	90.0	77.0
ULD*	13-14	39	89.5	74.9	81.8‡	74.4

Additionally, Ylimäinen et al. 2010, employed a cross-cultural health-related quality of life inventory to assess children with limb deficiencies compared to children with common chronic conditions<sup>23</sup>. This inventory was for patients aged 8-16 years and contains five categories to capture physical limitations, emotional function, independence, social inclusion, and social exclusion<sup>24</sup>. Participants respond to the inventory questions through a five-point Likert scale, with

response extremes at always (5 points) and never (1 point)<sup>24</sup>. This study showed that children with ULDs demonstrated little difference in social exclusion measures compared to children with common chronic conditions while showing improved quality of life measures in the remaining domains<sup>23</sup>.

#### 2.4.1. Psychosocial functioning

ULDs may impact a child on multiple complex levels. Although Table 2-1 suggests no significant difference in the larger psychosocial domain, James et al. 2006 showed that social functioning in the school environment can be significantly lower in children with ULDs than in the general population, suggesting there may be a social stigma when children with ULDs interact in a peer environment<sup>16</sup>. Ylimäinen et al. 2010 additionally found that measures of quality of life in children aged 8-16 with ULDs (n = 140) are generally higher than children with common chronic conditions (n = 1152) across multiple subdomains (physical limitations, emotional function, independence, among others), with the exception of social exclusion<sup>23</sup>. This further suggests that having a ULD may come with social and/or exclusionary implications.

It is common for children with upper limb differences to experience internal stressors related to self-perception and external stressors associated with peer or social interactions, and these can result in anxiety and/or depression<sup>8</sup>. Here, stress may arise not only from the physical differences associated with one's upper limb but may also be heavily influenced by the aesthetic differences. Internal stress related to aesthetics is more common in teenaged patients, whereas external aesthetic stress is more frequent in younger children<sup>8</sup>. When pediatric patients with upper limb differences reach adolescence, they undergo the same intellectual and emotional changes that other adolescents face, and a limb difference makes this adjustment much more difficult<sup>25</sup>. During the transition from childhood to adolescence, children experience significant development of their

self-identity, and “positive” development can often be correlated to self-esteem during childhood<sup>26</sup>. Coupling this with evidence that peer-related stress spikes around the time a child with an upper limb difference enters high school, it is evident that finding methods to mitigate external stresses becomes critical during this transitional period<sup>8,26</sup>.

Teasing and bullying are obvious external stressors that may reinforce the stigma of an upper limb difference as “non-normal” and create an “us” and “them” mentality<sup>8,26</sup>. However, less obvious, innocent interactions may also have lasting repercussions on a child’s mental state. When a child is repeatedly asked about their limb difference, stared at by peers, or even given unique social treatment (i.e. in school or sport), this may impact the child’s self-image<sup>8</sup>. Further, these interactions can leave the child feeling singled out and, even meeting new people, when coupled with feelings of self-consciousness or embarrassment, can create further stress. In fact, Franzblau et al. 2015 found 58% of their 33 pediatric patients with upper differences (ages 6 to 17 years) associated stress with social interactions<sup>8</sup>. Children are strongly influenced not only by their peers, but by how they interact with parents and other adult role models (e.g. teachers and health care providers). It is not uncommon for a parent to experience emotional strain due to the fact that their child has a congenital limb difference<sup>8,27,28</sup>. Adverse emotional reactions by parents can reinforce a child’s feeling of being “non-normal” or that they have inherent limitations that cannot be overcome<sup>8,29,30</sup>. This can have serious repercussions on self-image, magnify feelings of shame or anxiety, and result in declining social participation.

Although the above findings focus on a broader population of children with upper limb differences (independent of prosthesis use), they are highly relevant to complex challenges faced by pediatric prosthesis wearers. There are clear psychosocial implications of having a visibly different limb which may have an increased effect on adolescents. Like the limb deficiency itself, a prosthesis

may also create unwanted attention or feelings of being different, which can heavily influence whether it is worn or abandoned. However, these challenges are further complicated as simply wearing a prosthesis to cover or hide one's UL deficiency is not necessarily a desirable outcome since this may be an indication of problematic coping mechanisms<sup>8</sup>.

#### 2.4.2. Physical functioning

Children with ULDs often present little to no significant differences in measures of physical functioning when compared to the general population as shown in Table 2-1<sup>16-18</sup>. Further, these individuals have shown increased function when compared to children with common chronic conditions<sup>23</sup>. Specifically evaluating the impact of prosthesis use in this population, James et al. 2006 performed a study that employed both survey-based and functional measures of 489 children with a unilateral congenital below-the-elbow deficiency (321 prosthesis wearers and 168 non-wearers)<sup>16</sup>. No clinically relevant differences were found between prosthesis wearers and non-wearers in functional outcomes and quality of life<sup>16</sup>. Furthermore, non-wearers scored higher on the performance of age-appropriate daily tasks than prosthesis wearers, and wearers performed better when not wearing their prosthesis. This drove their conclusion that pediatric prostheses may provide a cosmetic benefit for social acceptance or may be useful tools for specialized activities, but they do not appear to improve performance of daily activities or self-reported quality of life<sup>16</sup>.

The potential physical-functioning benefits and drawbacks a prosthesis offers the wearer may be linked to the type of device prescribed. In a retrospective study, it was found that pediatric wearers often prefer body-powered prostheses to myoelectric devices when performing functional tasks<sup>31</sup>. Crandall et al. 2002 surveyed the satisfaction of pediatric patients and their parents in relation to prosthesis use during daily activities. In their cohort of 34 wearers (ages 1 to 12 ½ years), those who wore body-powered devices were able to achieve more functional tasks to the wearers'

satisfaction than those who wore passive and myoelectric devices. However, in a long-term follow-up more than a decade later, most of these same subjects were wearing a passive device<sup>31</sup> suggesting that the grasping function provided by active prostheses offered limited benefit relative to no-grasping function at all. Here again, a trade-off can be made when using passive devices; although they do not provide grasping function, they may provide improved aesthetics to help facilitate social integration. Furthermore, Huizing et al. 2010 addressed the outcomes of pediatric prosthetic fittings, with 11 of their 20 participants rejecting their device because it provided no functional gain to offset the inconveniences associated with its use<sup>32</sup>. Somewhat intuitively, it has been suggested that the limited function offered by current devices impact their usefulness<sup>6,32,33</sup>. In the absence of sufficient functional gains, pediatric prosthesis wearers may be content with no grasping function and opt for a passive device or choose not to wear a device at all.

When taken together, the decision to wear a prosthesis is dependent on it facilitating improved physical and/or psychosocial functioning. That is, it must provide utility (prosthetic function) and aesthetics that allow the child to feel comfortable participating in social activities with their peers<sup>5,28,30</sup>. The degree to which this is achieved must be sufficient to offset any drawbacks associated with wearing the device, such as increased weight<sup>6,10,34,35</sup>, wearing harnesses, cables, and straps<sup>34</sup>, warmth and perspiration<sup>34</sup>, and the potential for discomfort or tissue irritation<sup>6,33,34</sup>. Further, the financial costs, frequency, and time associated with regular prosthetic maintenance, adjustments to prosthetic fit, and other service-related device requirements can vary across devices and dramatically impact a child's disposition to wearing their device. It is a challenging task to provide a child with a prosthesis that meets these many demands. Unlike the smaller population of children with acquired limb amputations, children born with congenital ULDs learn effective one-handed compensatory strategies for most daily tasks early in life. This in itself may influence

a child's willingness to wear a prosthesis as often there is no real sense of limb loss<sup>36</sup>, although they may feel a sense of being different. Here, a prosthesis is simply an aid rather than a limb replacement, and if it does not actually assist in the often near-normal abilities of the wearer, it will be rejected<sup>25</sup>. Therefore, these children have close to normal function, and evidence suggests current prostheses do not further normalize their physical functioning<sup>16</sup>. Therefore, providing a prosthesis capable of truly augmenting a child's physical functioning, providing satisfactory aesthetics, and overall facilitating social integration, remains an important challenge.

## 2.5. Discussion

### 2.5.1. Dexterous multi-grasp terminal devices

Challenges impacting the pediatric population living with congenital ULDs are often complex and multi-faceted. In this population, current prosthetic UL devices are frequently abandoned, which strongly suggests that many fall short of meeting user needs and/or providing sufficient benefit to warrant their wear. It has been suggested that device function and aesthetics (cosmesis) are two key areas contributing to the high rates of rejection<sup>25</sup>. Functionally, unlike the simple open-close grasping offered by active pediatric prostheses, intact hands move with 27 degrees of freedom<sup>37</sup>. Although it is possible to achieve a multitude of complex postures, most daily activities are performed using a limited number of common grasp configurations<sup>38,39</sup>. Nearly 80% of common daily tasks may be accomplished with as few as 6-9 standard grasp configurations<sup>39</sup>. Therefore, we suggest that a significant functional benefit may be provided to pediatric prosthesis wearers if their devices offer a strategic repertoire of grasping configurations. This is not unique to children and closely parallels very active work being performed with adult amputee populations. Like pediatric prostheses, adult devices may be cosmetic, body powered, or myoelectric; however, there has also been an acceleration in prosthetic mechatronic technologies resulting in devices that more closely resemble the form and function of intact hands, including offering multiple grasp

configurations<sup>40</sup>. As mechatronic technologies continue to evolve, similar smaller-proportioned prostheses are beginning to emerge for pediatric patients. For example, the Vincent Young 3 (Vincent Systems, Karlsruhe, Germany) is sized for children age 8 and up and is capable of 13 individual grasp patterns. Similar devices have begun to emerge and will persist as multi-grasp prostheses continue to mature and become increasingly available. Further, as these devices typically include individually articulating digits, they may also offer more anthropomorphic, hand-like appearances to soften social integration challenges.

### 2.5.2. Advanced control interfaces

Although multi-grasp prostheses are becoming a promising new option for pediatric wearers, several limitations remain to be addressed. Here, prosthesis control interfaces become a crucial factor in device use as in adults, even the most advanced prostheses rapidly promote frustration and disuse if the control is unintuitive, or overly difficult to learn<sup>12</sup>. In conventional myoelectric prostheses, device control presents numerous limitations, namely noisy control signals<sup>13</sup> and sensitivity to small electrode displacements<sup>14</sup>, changes in arm posture, and muscle fatigue<sup>15</sup> among others. In adult multi-grasp hands, standard myoelectric control schemes measure activity in the wearer's residual wrist-flexion and wrist-extension muscle groups as signals to open and close the prosthetic hand, respectively. By co-contracting both muscle-sets together, wearers may toggle and select from a list of pre-programmed hand grasp configurations. Here, we suggest it is doubtful that this toggle-and-select strategy will translate effectively to pediatric devices, as it does not replicate typical muscle contraction patterns used for grasping. We argue that toggling creates an increased cognitive load and may negatively reinforce wearers to default to a single primary grasp configuration in an effort to limit the amount of toggling they perform.



Recently, advanced adult prosthesis control strategies have become available that may address limitations in conventional EMG control for pediatric wearers. In the past 10 years, myoelectric pattern recognition techniques transitioned from a promising experimental control strategy to commercially available prosthesis control systems<sup>41-44</sup>, that are largely unavailable for the pediatric population. EMG pattern recognition uses multiple electrodes that are applied on the skin's surface over the wearer's affected musculature. Machine learning algorithms are then trained to recognize patterns in the electrical-muscle activity and infer the wearer's intended movements<sup>45</sup>. Following a short algorithm training session, the real-time classifications of muscle patterns are used to command the appropriate hand movements in a prosthesis<sup>45</sup>. Both in the laboratory and in real-world prostheses, this technique has largely been shown to improve adult-user control over multiple prosthesis movements and/or grasp patterns<sup>46-48</sup>. These techniques continue to evolve to the benefit of more robust control over multiple prosthesis movements with methods now capable of accommodating traditional challenges such as movement and positioning of the prosthesis affecting control consistency<sup>49-51</sup>. However, myoelectric prosthesis control is still beset with limitations, and although more promising than traditional EMG control, it has yet to be translated to pediatric populations.

Other experimental control techniques exclusive to adult populations have begun to emerge as options for intuitive control of multiple prosthesis movements<sup>12</sup>. For example, sonomyography employs a small ultrasound sensor to capture muscle deformations in the affected limb and infer the wearer's intention<sup>52</sup>. Here, image processing and supervised learning algorithms are employed to predict intended grasp configurations that generate the pattern of muscle deformation captured in the ultrasound data. This happens in near real-time and the output predictions are encoded to drive the prosthesis<sup>53</sup>. Sonomyography may provide a more accurate control signal as, unlike

myoelectrics, it measures activity deep beyond the skin's surface<sup>12,52</sup>. However, sonomyography, like many other experimental control techniques, is still maturing, needs to be further tested as a prosthesis control system, and has yet to be translated to pediatric populations.

A final category of advanced control interfaces that have begun to emerge for adults are neural-machine-interfaces (NMIs). NMI techniques interface or manipulate the affected neural anatomy of adult prosthetic users to restore physiologically relevant control and sensation. For example, targeted muscles and sensory reinnervation<sup>54,55</sup> redirect affected nerves to new target muscle and skin sites in the residual limb. After, attempting to move the missing limb creates unique patterns of muscle activity which are measured and used to intuitively control EMG prostheses<sup>54</sup>. Further simulation of the reinnervated skin sites can create sensations of touch experienced as occurring in the missing limb<sup>56</sup> and strategic vibration of reinnervated muscles produces sensations of missing hand movements<sup>57</sup>. Further, multiple peripheral nerve interfaces have been described in literature that measure and decode affected nerve activity for prosthetic control and even stimulate nerves to provide prosthetic sensory feedback<sup>58,59</sup>. Although many NMIs have shown significant promise in achieving intuitive prosthesis control and the restoration of sensation, the invasiveness, requisite surgeries, and experimental nature of these techniques will likely limit their immediate relevancy for pediatric patients.

### 2.5.3. Current barriers to advanced pediatric devices

As advanced multi-grasp prosthetic hands and intuitive control strategies continue to develop, a new subset of challenges unique to pediatric wearers will arise. **Device cost** is a significant and prohibitive barrier for pediatric populations since children's limbs and bodies are ever-growing. Therefore, unlike adults, where purchasing a single device may be a long-term investment, the cost of children's prostheses must reflect the fact that children outgrow prostheses in a few short years

and multiple devices will be purchased over their childhood. Further, with advancements in additive manufacturing numerous 3D printable UL devices are available; yet, it is important to distinguish these as separate from clinically prescribed devices that receive rigorous engineering development and regulatory approvals prior to being made commercially available. ***Child growth*** presents a further set of challenges in achieving consistent device control. As affected limb proportions change, so will the fit of a prosthetic socket. This may compromise the contact and placement of any sensing technologies and result in diminished, inconsistent, or intermittent device control. Further ***training and learning*** will likely play an important role in the success of future prostheses. Individuals with congenital ULDs likely have never had a need to activate their affected muscles as their limb did not finish developing. Although advanced biosensors and intelligent control algorithms may offset some of these difficulties, structured training and learning of these systems will be a necessity for effective use. Finally, device ***robustness and bulk*** will foreseeably be important factors. Children will inevitably require robust devices to facilitate the physical nature of childhood play, which include but are not limited to physical durability, waterproof/weather-resistance, extended playtimes, and susceptibility to external contaminants. However, robustness typically comes at the cost of more rugged designs with often increased weight and size. Children are more affected by the weight of a device <sup>6,10,35</sup> since they are smaller and do not possess the same strength as a grown adult. Here, creative lightweight low-bulk design principles must be employed.

## 2.6. Conclusions

Pediatric UL prosthesis wearers face a number of complex challenges. Presently, device abandonment is pervasive because many prostheses fail to offer wearers sufficient benefit to warrant their use. Ultimately, for a child to adopt their device, it must facilitate the effective

performance of daily activities and help alleviate stigmas associated with having a limb deficiency. Therefore, both the psychosocial and physical functioning of a child plays a key role. As upper limb prostheses continue to evolve, there are many technological advancements in the adult arena that have yet to be leveraged for pediatric patients. However, these solutions may not be directly applied to children with ULDs as their challenges are often unique. These may include practical issues related to growth, prosthesis control systems measuring activity in muscles that never actuated an intact limb, and the cost of purchasing multiple devices as a child grows. Further, although technological approaches have the potential to positively impact physical function, psychosocial factors also have a heavy influence on device adoption. Here, children may face both internal and external stressors as they navigate social situations, potential peer exclusion, and both direct and indirect attention drawn to their limb deficiency. Factors such as aesthetics may drive a child to opt for a less functional but more visually appealing prosthesis or choose not to wear a device at all. When taken together, the field of pediatric prostheses may see a technological boom much like adult prostheses have recently experienced. However, several technical, practical, and social challenges must first be addressed to unlock the potential of this next generation of devices.

## 2.7. References

1. Parker, S. E. *et al.* Updated national birth prevalence estimates for selected birth defects in the United States, 2004-2006. *Birth Defects Res. Part A - Clin. Mol. Teratol.* **88**, 1008–1016 (2010).
2. Ekblom, A. G., Laurell, T. & Arner, M. Epidemiology of congenital upper limb anomalies in 562 children born in 1997 to 2007: A total population study from Stockholm, Sweden. *J. Hand Surg. Am.* **35**, 1742–1754 (2010).
3. Shaperman, J., Landsberger, S. & Setoguchi, Y. Early Upper Limb Prosthesis Fitting: When and What Do We Fit. *Prosthet. ORTHOTIC Sci.* **15**, 11–17 (2003).
4. Davids, J. R., Wagner, L. V., Meyer, L. C. & Blackhurst, D. W. Prosthetic management of children with unilateral congenital below-elbow deficiency. *J. Bone Jt. Surg. - Ser. A* **88**, 1294–1300 (2006).

5. Vasluian, E. *et al.* Opinions of Youngsters with Congenital Below-Elbow Deficiency, and Those of Their Parents and Professionals Concerning Prosthetic Use and Rehabilitation Treatment. *PLoS One* **8**, (2013).
6. Postema, K. *et al.* *Prosthesis rejection in children with a unilateral congenital arm defect. Clinical Rehabilitation* vol. 13 (1999).
7. Biddiss, E. & Chau, T. Upper limb prosthesis use and abandonment: A survey of the last 25 years. *Prosthetics and Orthotics International* vol. 31 236–257 (2007).
8. Franzblau, L. E. *et al.* Coping with congenital hand differences. *Plast. Reconstr. Surg.* **135**, 1067–1075 (2015).
9. Valevicius, A. M. *et al.* Compensatory strategies of body-powered prosthesis users reveal primary reliance on trunk motion and relation to skill level. *Clin. Biomech.* **72**, 122–129 (2020).
10. Egermann, M., Kasten, P. & Thomsen, M. Myoelectric hand prostheses in very young children. *Int. Orthop.* **33**, 1101–1105 (2009).
11. Englehart, K. & Hudgins, B. A Robust, Real-Time Control Scheme for Multifunction Myoelectric Control. *IEEE Trans. Biomed. Eng.* **50**, 848–854 (2003).
12. Castellini, C. *et al.* Proceedings of the first workshop on peripheral machine interfaces: Going beyond traditional surface electromyography. *Front. Neurorobot.* **8**, 1–17 (2014).
13. Chowdhury, R. H. *et al.* Surface electromyography signal processing and classification techniques. *Sensors (Switzerland)* **13**, 12431–12466 (2013).
14. Young, A. J., Hargrove, L. J. & Kuiken, T. A. Improving myoelectric pattern recognition robustness to electrode shift by changing interelectrode distance and electrode configuration. *IEEE Trans. Biomed. Eng.* **59**, 645–652 (2012).
15. Castellini, C. & Van Der Smagt, P. Surface EMG in advanced hand prosthetics. *Biol. Cybern.* **100**, 35–47 (2009).
16. James, M. A. *et al.* Impact of Prostheses on Function and Quality of Life for Children With Unilateral Congenital Below- the-Elbow Deficiency. *J. Bone Jt. Surgery-American* Vol. **88**, 2356–2365 (2006).
17. Johansen, H., Dammann, B., Øinæs Andersen, L. & Andresen, I. L. Children with congenital limb deficiency in Norway: issues related to school life and health-related quality of life. A cross-sectional study. *Disabil. Rehabil.* **38**, 1803–1810 (2016).
18. Ardon, M. S., Janssen, W. G., Hovius, S. E., Stam, H. J. & Selles, R. W. Low impact of congenital hand differences on health-related quality of life. *Arch. Phys. Med. Rehabil.* **93**, 351–357 (2012).
19. Varni, J., Burwinkle, T., Seid, M. & Skarr, D. The PedsQL 4.0 as a Pediatric Population Health Measure: Feasibility, Reliability, and Validity. *Ambulatory. Ambul. Pediatr.* **3**, 329–341 (2003).
20. Johansen, H., Dammann, B., Andresen, I. L. & Fagerland, M. W. Health-related quality of

- life for children with rare diagnoses, their parents' satisfaction with life and the association between the two. *Health Qual. Life Outcomes* **11**, 1 (2013).
21. Engelen, V., Haentjens, M. M., Detmar, S. B., Koopman, H. M. & Grootenhuis, M. A. Health related quality of life of Dutch children: Psychometric properties of the PedsQL in the Netherlands. *BMC Pediatr.* **9**, 68 (2009).
  22. Varni, J. W. The PedsQL Measurement Model for the Pediatric Quality of Life Inventory. <https://www.pedsql.org/> (1998).
  23. Ylimäinen, K., Nachemson, A., Sommerstein, K., Stocksélius, A. & Norling Hermansson, L. Health-related quality of life in Swedish children and adolescents with limb reduction deficiency. *Acta Paediatr. Int. J. Paediatr.* **99**, 1550–1555 (2010).
  24. Schmidt, S. & The DISABKIDS group. *The DISABKIDS questionnaires: quality of life questionnaires for children with chronic conditions. Handbook.* (Lengerich: Pabst Science Publishers, 2006).
  25. Bowker, J. & American Academy of Orthopaedic Surgeons. *Atlas of Limb Prosthetics: Surgical, Prosthetic, and Rehabilitation Principles.* (Mosby Year Book, 1992).
  26. Lumsdaine, S. & Thurston, M. Growing up in a Mainstream World: A Retrospective Enquiry into the Childhood Experiences of Young Adults with a Physical Disability. *Int. J. Disabil. Dev. Educ.* **64**, 182–197 (2017).
  27. Kerr, S. M. & McIntosh, J. B. Disclosure of disability: Exploring the perspective of parents. *Midwifery* **14**, 225–232 (1998).
  28. Oliver, J., Dixon, C. & Murray, C. D. Being the parent of a child with limb difference who has been provided with an artificial limb: an interpretative phenomenological analysis. *Disabil. Rehabil.* **0**, 1–8 (2018).
  29. Andrews, E. E., Williams, J. L., VandeCreek, L. & Allen, J. B. Experiences of Parents of Children with Congenital Limb Differences With Health Care Providers: A Qualitative Study. *Rehabil. Psychol.* **54**, 217–221 (2009).
  30. De Jong, I. G. M. *et al.* Activity and Participation of children and adolescents with Unilateral Congenital Below Elbow Deficiency : An online focus group study. *J. Rehabil. Med.* **44**, 885–892 (2012).
  31. Crandall, R. C. & Tomhave, W. Pediatric unilateral below-elbow amputees: Retrospective analysis of 34 patients given multiple prosthetic options. *J. Pediatr. Orthop.* **22**, 380–383 (2002).
  32. Huizing, K., Reinders-Messelink, H., Maathuis, C., Hadders-Algra, M. & Van Der Sluis, C. K. Age at first prosthetic fitting and later functional outcome in children and young adults with unilateral congenital below-elbow deficiency: A cross-sectional study. *Prosthet. Orthot. Int.* **34**, 166–174 (2010).
  33. Wagner, L. V., Bagley, A. M. & James, M. A. Reasons for Prosthetic Rejection by Children With Unilateral Congenital Transverse Forearm Total Deficiency. *Am. Acad. Orthotists Prosthetists* **19**, 51–54 (2007).

34. Routhier, F., Vincent, C., Morissette, M. J. & Desaulniers, L. Clinical results of an investigation of paediatric upper limb myoelectric prosthesis fitting at the Quebec Rehabilitation Institute. *Prosthet. Orthot. Int.* **25**, 119–131 (2001).
35. Pylatiuk, C., Schulz, S. & Döderlein, L. Results of an internet survey of myoelectric prosthetic hand users. *Prosthet. Orthot. Int.* **31**, 362–370 (2007).
36. Jain, S. Rehabilitation in limb deficiency. 2. The pediatric amputee. *Arch. Phys. Med. Rehabil.* **77**, (1996).
37. Agur, A. M. R. & Lee, M. J. *Grant's Atlas of Anatomy*. (Lippincott Williams and Wilkins, 1999).
38. Feix, T., Romero, J., Schmiedmayer, H. B., Dollar, A. M. & Kragic, D. The GRASP Taxonomy of Human Grasp Types. *IEEE Trans. Human-Machine Syst.* **46**, 66–77 (2016).
39. Zheng, J. Z., De La Rosa, S. & Dollar, A. M. An Investigation of Grasp Type and Frequency in Daily Household and Machine Shop Tasks. in *IEEE International Conference on Robotics and Automation* (2011). doi:10.1109/TOH.2013.6.
40. Vujaklija, I., Farina, D. & Aszmann, O. New developments in prosthetic arm systems. *Orthop. Res. Rev.* **8**, 31–39 (2016).
41. IBT. Sense. <https://www.i-biomed.com> (2020).
42. Ottobock. Myo Plus. <https://www.ottobockus.com> (2020).
43. COAPT. CoApt Complete Control. <https://coaptengineering.com> (2020).
44. LTI. MYOTRAINER. <https://liberatingtech.com/> (2020).
45. Ortiz-Catalan, M., Brånemark, R. & Håkansson, B. BioPatRec: A modular research platform for the control of artificial limbs based on pattern recognition algorithms. *Source Code Biol. Med.* **8**, 1–18 (2013).
46. Toledo, C. *et al.* A comparison of direct and pattern recognition control for a two degree-of-freedom above elbow virtual prosthesis. *Proc. Annu. Int. Conf. IEEE Eng. Med. Biol. Soc. EMBS* 4332–4335 (2012) doi:10.1109/EMBC.2012.6346925.
47. Franzke, A. W. *et al.* Users' and therapists' perceptions of myoelectric multi-function upper limb prostheses with conventional and pattern recognition control. 1–13 (2019) doi:10.5281/zenodo.2585639.
48. Resnik, L. J., Acluche, F. & Klinger, S. L. *User experience of controlling the DEKA Arm with EMG pattern recognition*. *PLoS ONE* vol. 13 (2018).
49. Fougner, A., Scheme, E., Chan, A. D. C., Englehart, K. & Staudahl, Ø. Resolving the limb position effect in myoelectric pattern recognition. *IEEE Trans. Neural Syst. Rehabil. Eng.* **19**, 644–651 (2011).
50. Beaulieu, R. J. *et al.* Multi-position Training Improves Robustness of Pattern Recognition and Reduces Limb-Position Effect in Prosthetic Control. *J. Prosthetics Orthot.* **29**, 54–62 (2017).

51. Betthausen, J. L. *et al.* Limb Position Tolerant Pattern Recognition for Myoelectric Prosthesis Control with Adaptive Sparse Representations from Extreme Learning. *IEEE Trans. Biomed. Eng.* **65**, 770–778 (2018).
52. Akhlaghi, N. *et al.* Real-Time Classification of Hand Motions Using Ultrasound Imaging of Forearm Muscles. *IEEE Trans. Biomed. Eng.* **63**, 1687–1698 (2016).
53. Dhawan, A. S. *et al.* Proprioceptive Sonomyographic Control: A novel method for intuitive and proportional control of multiple degrees-of-freedom for individuals with upper extremity limb loss. *Sci. Rep.* **9**, 1–15 (2019).
54. Kuiken, T. A., Dumanian, G. A., Lipschutz, R. D., Miller, L. A. & Stubblefield, K. A. The use of targeted muscle reinnervation for improved myoelectric prosthesis control in a bilateral shoulder disarticulation amputee. *Prosthet. Orthot. Int.* **28**, 245–253 (2004).
55. Hebert, J. S. *et al.* Novel targeted sensory reinnervation technique to restore functional hand sensation after transhumeral amputation. *IEEE Trans. Neural Syst. Rehabil. Eng.* **22**, 765–773 (2014).
56. Kuiken, T. A., Marasco, P. D., Lock, B. A., Harden, R. N. & Dewald, J. P. A. Redirection of cutaneous sensation from the hand to the chest skin of human amputees with targeted reinnervation. *Proc. Natl. Acad. Sci. U. S. A.* **104**, 20061–20066 (2007).
57. Marasco, P. D. *et al.* Illusory movement perception improves motor control for prosthetic hands. *Sci. Transl. Med.* **10**, (2018).
58. Yildiz, K. A., Shin, A. Y. & Kaufman, K. R. Interfaces with the peripheral nervous system for the control of a neuroprosthetic limb: A review. *J. Neuroeng. Rehabil.* **17**, (2020).
59. Svensson, P., Wijk, U., Björkman, A. & Antfolk, C. A review of invasive and non-invasive sensory feedback in upper limb prostheses. *Expert Rev. Med. Devices* **14**, 439–447 (2017).



## Chapter 3. Taxonomy of pediatric hand grasps during activities of daily living

The majority of this chapter has been published as:

Battraw MA, Young PR, Welner ME, Joiner WM, Schofield JS. (2022) Characterizing Pediatric Hand Grasps During Activities of Daily Living to Inform Robotic Rehabilitation and Assistive Technologies. in IEEE International Conference on Rehabilitation Robotics.

### 3.1. Chapter preface

This chapter presents an initial investigation into how typically developed children use their hands within home environments. This work begins to build an understanding of how children use their hands to interact and manipulate objects, enabling us to better develop devices that provide and promote meaningful functional benefits. The frequency and duration of performed hand grasps were tabulated from video footage and discussed. The characterization described in this chapter marks a meaningful step toward the development of both dexterous prostheses and assistive/rehabilitative devices.

### 3.2. Introduction

Our hands play an important role in how we engage with the world around us. Our abilities to perform daily tasks, work-related functions, and many social interactions are largely influenced by our hand function. The importance is perhaps most strongly emphasized when hand function is chronically impaired, often compromising physical independence and reducing the quality of life for affected individuals<sup>1</sup>. In recent years advances in robotics and mechatronics have facilitated the development of numerous technological approaches to address challenges associated with impaired hand motor function. These include rehabilitation systems to improve hand mobility, strength, and dexterity<sup>2</sup>, assistive technologies such as powered exoskeletons to drive impaired

digits<sup>3,4</sup>, and even highly dexterous prostheses to provide a variety of grasping options when an upper limb is lost<sup>5,6</sup>.

For children, healthy hand and upper limb function are crucial not only to their independence<sup>7</sup>, but to their physical development<sup>8</sup>, and participation in social environments<sup>9</sup>. Much like the recent emergence of robotic rehabilitative and assistive devices for adults many similar technologies are on the clinical and research horizons for pediatric patients with hand motor impairments. However, the nature of childhood play and daily activities means that children use their hands in fundamentally different ways than adults. Further, as children develop so do their motor systems. Here, age-appropriate and activity-specific tasks are important considerations when developing treatment protocols for this unique population<sup>10-12</sup>. It is imperative that rehabilitative and assistive devices can facilitate these needs; yet there remains a knowledge gap in which hand grasps or movements may be of the highest priority during rehabilitation or daily tasks to provide the most effective outcomes and functional independence.

Hands have immense dexterity as they have the ability to move with up to 27 degrees of freedom and are actuated by more than 30 muscles<sup>13</sup>. Hand motor control relies on multiple inputs including proprioceptive and tactile sensory feedback<sup>14</sup> and may even be coordinated with the activity of the other hand during bimanual tasks. Even as robotic technologies advance and continue to be miniaturized, the most sophisticated robotic manipulators and rehab devices are still challenged to achieve the same levels of dexterity and control. Yet interestingly, in adults, it has been shown that we use a reduced repertoire of hand movements to achieve most daily tasks. This taxonomy of common movements can be simplified to 17 generalized configurations<sup>15</sup>. It has been further shown that in home and industrial settings 6-9 common grasps can account for nearly 80% of all hand

activity with Wrap, Lateral Tripod, Lateral Pinch, and Tripod grasps being the top 4 most frequently used grasps among adults<sup>15,16</sup>.

Although currently, it may be impractical for rehabilitative and assistive devices to offer dexterity that rivals an intact healthy hand, it is feasible that significant functional gains may be provided. This can be done by targeting specific aspects of the motor impairment related to strategic grasping patterns and hand movements. Yet, unlike adults, a common pediatric hand grasp taxonomy has yet to be developed. This gap in knowledge presents barriers to making informed device design decisions that promote the overall effectiveness and function of newly emerging robotic devices offered to pediatric patients. The effectiveness of a device and resulting function are among the most important factors when considering user-based needs<sup>14</sup> and are driving factors influencing the adoption or abandonment of clinical technologies.

The objective of this work was to explore how healthy able-bodied children use their hands in daily tasks and how this may differ from adult literature. We investigated two pediatric participants and characterized their hand grasping movements in a home environment. We evaluated the duration and frequency of hand grasps across their dominant and non-dominant sides. Further, we hypothesized that children would exhibit a unique set of grasps that may be different from those reported in adult literature as their motor systems are still developing and their daily activities differ from an adult.

### 3.3. Methods

#### 3.3.1. Participants

Two female children participated in this study. Research protocols were approved by the Institutional Review Board at the University of California, Davis. Participants provided written informed assent and their parents/legal guardians provided written informed consent. Participants

PARC1 and PARC2 were 7 and 10 years old at the time of the study, respectively. Both participants had a dominant right hand with the same results of L.Q.= +100, Decile R.10 as determined by the Edinburgh Inventory<sup>17</sup>. Additionally, enrolment in this study required participants to be healthy with no neuromuscular or motor impairments that may impact hand or upper limb use.

### 3.3.2. Experimental equipment

To record the participants' hand activities, a video camera was mounted to the child's head using an elastic strap harness (Figure 3-1). Guardians and participants were instructed on how to properly don the camera prior to data collection. A GoPro Hero5 video camera with a 1080 resolution at 60 frames per second (fps) was used with the field of view set to wide mode. This camera configuration was chosen due to its lightweight nature, large field of view, reduced invasiveness, and ease of data analysis. To ensure the video camera was recording at the correct angle to capture the child's action space, guardians observed the GoPro's video stream and adjusted the camera mount as necessary. Participants and guardians were instructed to record footage in the home environment during regular daily activities. They were encouraged to avoid recording daily events that would result in long periods of hand inactivity such as watching television, resting, or sleeping. Approximately 2 hours of video data were obtained for each participant over the course of 2-3 days. It was confirmed by the guardians that wearing the camera resulted in no noticeable changes in daily activity performed by the children.

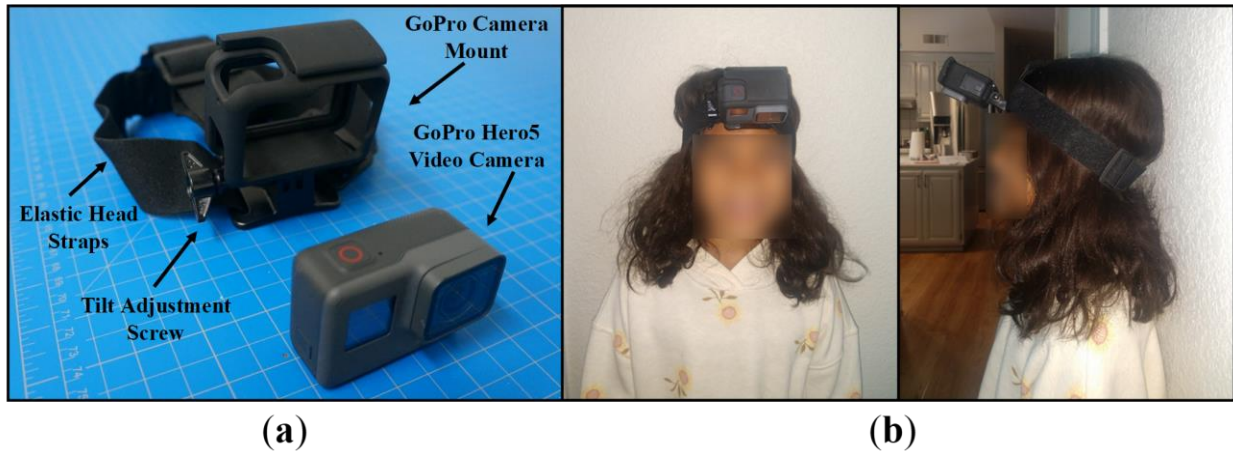


Figure 3-1. Video camera harnessing equipment and setup. (a) The elastic strap allows for comfortable and adjustable mounting. GoPro Hero5 is attached to the camera mount which allows for angled tilt adjustment. (b) Depicts a front and side view of the camera setup worn by a participant.

### 3.3.3. Analysis and procedures

To categorize hand activity from the video footage, we adopted previously defined grasp taxonomies from *Feix et al.* Consistent with their work, we simplified the total number of hand grasps to 17 generalized configurations<sup>15</sup>. We then broke down grasps into three main categories: power, intermediate, and precision<sup>15</sup>. We further separated grasps based on digit opposition and defined a ‘virtual finger’ when multiple digits actuated together<sup>15</sup>. The final inventory upon which hand movements were classified is depicted in Figure 3-2. Our adopted grasp taxonomy includes the frequency and duration in which hand grasps were used irrespective of object shape and size<sup>15</sup>. This definition is relevant within the context of rehabilitative and assistive devices, as they are often programmed to achieve digit actuation from a fully extended to a flexed position rather than intermediate degrees of digit movement for individual objects that may be manipulated.

Using the grasping movements depicted in Figure 3-2, video footage was manually reviewed to classify the hand grasping movements of participants. Two raters were trained to recognize and classify hand grasp data from the footage. Further, in conjunction with the generalized grasp taxonomy we adopted and for clarity, raters used a reference of supplemental material depicting

grasps in everyday scenarios<sup>18</sup>. Prior to video analysis, a grasp inclusion/exclusion methodology was determined as follows:

- Grasps that were in the video frame and clearly distinguishable were readily classified.
- Open hand configurations were not considered grasps.
- Any hand movements that were not clearly identifiable were reviewed by 2 raters who came to a consensus on the grasp. In the unlikely event, the grasp was unidentifiable, it was flagged and not tabulated.
- Grasps that were covered by obstacles and/or poor video resolution were not tabulated.

		Power		Intermediate		Precision	
		Palm	Pad	Side	Pad	Side	
Opp	Abduction	1: Wrap VF: 2-5 Frequency: 21.6% Duration: 30.5%	2: Ring VF: 2 Frequency: 2.0% Duration: 2.0%	6: Adduction Grip VF: 2 Frequency: 2.2% Duration: 0.9%	8: Pinch VF: 2 Frequency: 4.8% Duration: 2.7%		
			3: 3-Finger Sphere VF: 2-3 Frequency: 1.6% Duration: 0.7%	7: Tripod Variation VF: 3-4 Frequency: 0.0% Duration: 0.0%	9: Tripod VF: 2-3 Frequency: 14.8% Duration: 10.4%		
			4: 4-Finger Sphere VF: 2-4 Frequency: 3.8% Duration: 2.0%		10: Prismatic 3 Finger VF: 2-4 Frequency: 4.5% Duration: 3.7%		12: Writing Tripod VF: 3 Frequency: 0.7% Duration: 1.0%
			5: Distal VF: 2-5 Frequency: 0.0% Duration: 0.0%		11: Prismatic 4 Finger VF: 2-5 Frequency: 11.3% Duration: 26.9%		
Opp	Adduction	13: Index Finger Extension VF: 3-5 Frequency: 3.4% Duration: 5.6%		15: Lateral Pinch VF: 2 Frequency: 10.1% Duration: 6.9%	17: Parallel Extension VF: 2-5 Frequency: 2.0% Duration: 2.3%		
		14: Hook Grip VF: 2-5 Frequency: 6.8% Duration: 5.1%		16: Lateral Tripod VF: 3 Frequency: 10.4% Duration: 5.1%			

Figure 3-2. Adult generalized hand grasps reported in and adapted from [15]. Grasps presented are irrespective of object shape and size. Grasps are defined by three categories, power, intermediate, and precision. They are further broken down by opposition (Opp) type and a virtual finger (VF). The generalized percent grasp frequency and duration for adults are tabulated.

Video data were analyzed using the VSDC Video Editor (*Flash-Integro LLC*) software allowing for frame-by-frame playback. A similar study using two raters has shown such rating methods to achieve high inter-rater agreement with minor inconsistencies<sup>19</sup>. Raters tabulated video data in a shared spreadsheet that included grasp identification, side-of-hand use, the beginning and ending frames, and any additional notes. Finally, to analyze the tabulated data, a MATLAB (The MathWorks, Inc.) script was written to extract the duration and frequency along with their corresponding percentages for participants' dominant and non-dominant hands.

We analyzed the data by assigning a grasp identification number from 1 to 17 corresponding to the generalized grasps in Figure 3-2. The duration of a grasp was calculated using the difference between the corresponding beginning and ending frame number and converting this value to seconds by dividing by the frame rate (60 fps). Duration was defined as the time a grasp was held, which began once the hand was securely holding an object and ended at the onset of release. The total duration of a specific grasp was calculated by summing the duration times, and its percent duration was defined by the ratio of a specific grasp's total duration to the total duration of all grasps<sup>16</sup>. The duration and percent duration were calculated for both the dominant and non-dominant hands. Furthermore, data included grasp frequency, the number of times a grasp was performed by the participant, which was further separated by hand dominance. The percent frequency was obtained for each grasp by the ratio of a single grasp's frequency to that of the total instances all grasps were used<sup>16</sup>.

## 3.4. Results

### 3.4.1. Participant 1


















PARC1 used their hands to manipulate objects related to drawing/coloring, turning book pages, and retrieving food from a refrigerator, among many other activities. Of the more than 120 minutes of

footage obtained, an aggregate of 107 minutes captured the participant using either their dominant or non-dominant hand performing grasps. Out of the 107 active minutes, the child used their dominant and non-dominant hand for approximately 91 and 16 minutes, respectively. The total number of performed grasps was 1115 with 696 from the dominant hand and 419 from the non-dominant hand. The duration and frequency of individual grasps according to hand dominance along with their percentage are given in Table 3-1.

When combining the dominant and non-dominant hands it was found that 90% of the time the child frequently used a set of seven generalized grasp configurations. Additionally, over 90% of the duration could be accounted for by these same seven grasps. Interestingly, it was found that 74% of the duration was attributed to a single generalized grasp, Tripod. However, this same grasp only accounted for 30% of the total grasp frequency. Figure 3-3a displays the total combined grasp frequency and Figure 3-3b displays the total combined grasp duration.



Table 3-1. Participant grasp duration and frequency. The table illustrates the grasp duration (Dur) and frequency (Freq) for both child participants. The grasp identification (ID) number followed by the grasp picture are displayed. Data presented were separated by participant, hand dominance, and broken into duration and frequency. The duration and frequency are defined as the time in seconds and total number of instances each grasp was performed, respectively. Additionally, the percentage of duration and frequency out of all the grasps performed are provided in the parenthesis.

ID	Grasp	PARC1 Hand				PARC2 Hand			
		Dominant		Nondominant		Dominant		Nondominant	
		Dur (%)	Freq (%)	Dur (%)	Freq (%)	Dur (%)	Freq (%)	Dur (%)	Freq (%)
1		106 (1.9)	54 (7.8)	295 (30.4)	26 (6.2)	205 (5.8)	51 (6.9)	224 (6.6)	66 (10.6)
2		0 (0.0)	0 (0.0)	0 (0.0)	0 (0.0)	10 (0.3)	3 (0.4)	0 (0.0)	0 (0.0)
3		0 (0.0)	0 (0.0)	0 (0.0)	0 (0.0)	49 (1.4)	3 (0.4)	8 (0.2)	4 (0.6)
4		111 (2.0)	42 (6.0)	222 (22.8)	70 (16.7)	79 (2.2)	23 (3.1)	59 (1.8)	23 (3.7)
5		0 (0.0)	0 (0.0)	6 (0.6)	5 (1.2)	110 (3.1)	9 (1.2)	0 (0.0)	0 (0.0)
6		10 (0.2)	7 (1.0)	37 (3.8)	3 (0.7)	3 (0.1)	2 (0.3)	1 (0.0)	1 (0.2)
7		0 (0.0)	0 (0.0)	0 (0.0)	0 (0.0)	0 (0.0)	0 (0.0)	0 (0.0)	0 (0.0)
8		117 (2.1)	120 (17.2)	44 (4.6)	45 (10.7)	903 (25.3)	221 (29.7)	1804 (53.4)	194 (31.2)
9		4739 (86.5)	300 (43.1)	37 (3.8)	29 (6.9)	1315 (36.8)	239 (32.1)	97 (2.9)	68 (10.9)
10		36 (0.7)	26 (3.7)	38 (3.9)	26 (6.2)	85 (2.4)	16 (2.2)	277 (8.2)	89 (14.3)
11		63 (1.2)	25 (3.6)	83 (8.5)	46 (11.0)	68 (1.9)	15 (2.0)	354 (10.5)	77 (12.4)
12		15 (0.3)	2 (0.3)	0 (0.0)	1 (0.2)	58 (1.6)	3 (0.4)	0 (0.0)	0 (0.0)
13		6 (0.1)	3 (0.4)	3 (0.3)	2 (0.5)	6 (0.2)	3 (0.4)	40 (1.2)	6 (1.0)
14		17 (0.3)	6 (0.9)	8 (0.9)	5 (1.2)	62 (1.7)	23 (3.1)	145 (4.3)	30 (4.8)
15		144 (2.6)	55 (7.9)	119 (12.2)	111 (26.5)	592 (16.6)	118 (15.9)	301 (8.9)	57 (9.2)
16		29 (0.5)	18 (2.6)	15 (1.5)	8 (1.9)	5 (0.2)	7 (0.9)	1 (0.0)	1 (0.2)
17		83 (1.5)	38 (5.5)	65 (6.7)	42 (10.0)	19 (0.5)	8 (1.1)	69 (2.0)	6 (1.0)

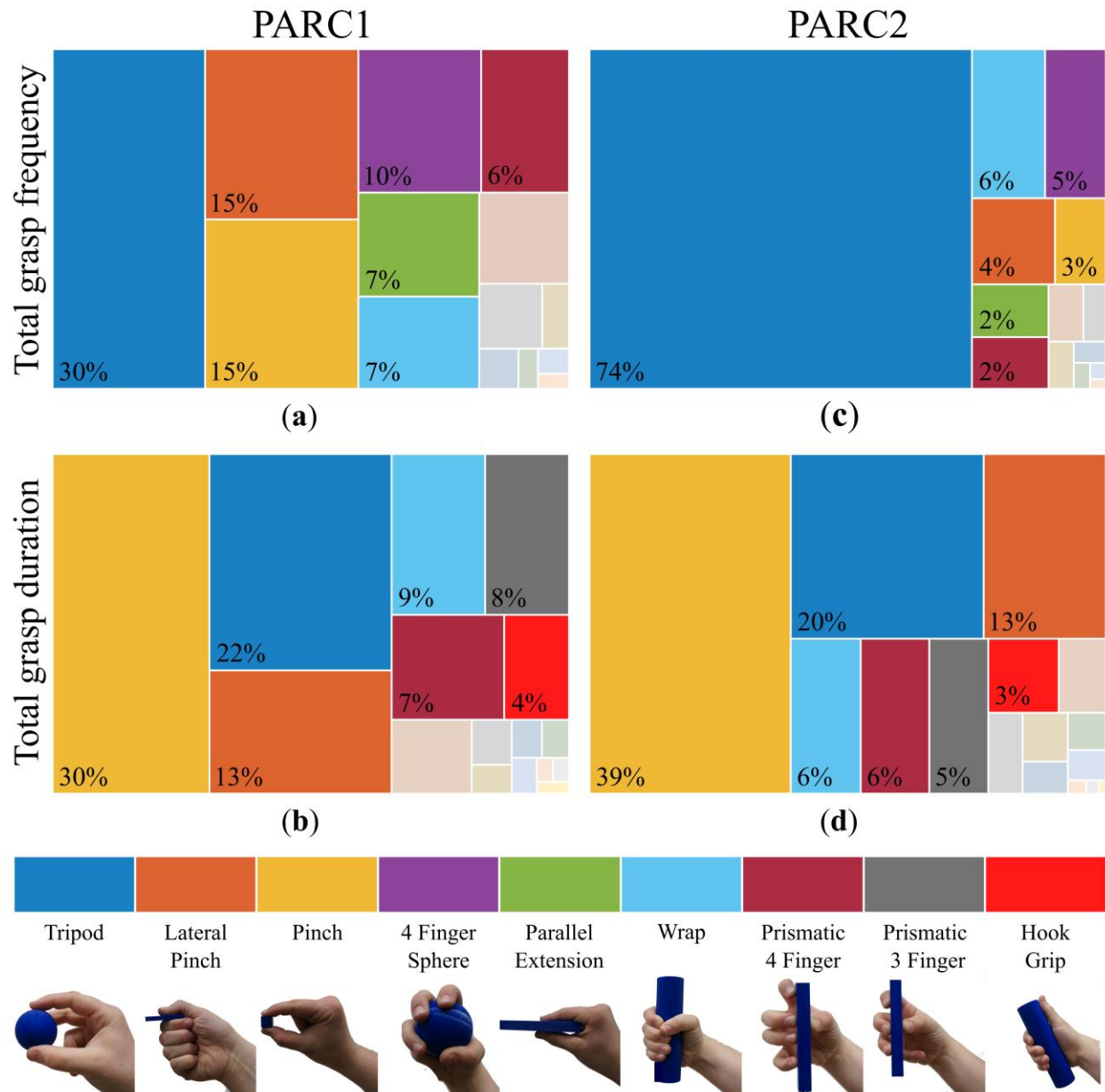


Figure 3-3. Tree maps of the combined dominant and non-dominant hand grasps, depicting the frequency and duration for PARC1 and PARC2. (a) Depicts PARC1’s combined total percent frequency with 90% of the total frequency accounted for by seven hand grasps. (b) PARC1’s combined total percent duration where the same seven hand grasps attributed to 96% of the duration. (c) Illustrates PARC2’s combined total percent frequency with 93% accounted for by seven hand grasp configurations. (d) PARC2’s combined total percent duration with 92% of the duration attributed to the same seven hand grasps.

### 3.4.2. Participant 2

Data were obtained from analyzing approximately 132 minutes of video footage in which the child used their hands to manipulate objects related to knitting, preparing hot chocolate, and playing with

art supplies such as clay, among many other activities. There was a total of about 115 active minutes where the child performed grasps with either their dominant hand or non-dominant hand. Moreover, the participant used their dominant and non-dominant hand for approximately 59 and 56 minutes, respectively, out of the total active time. The number of performed grasps was 1366, exceeding the total of PARC1 by 251. Here, 744 were attributed to the dominant hand and 622 were from the non-dominant hand. Results from Table 3-1 show the compiled duration and frequency data for individual grasps based on hand dominance and their corresponding percentages.

Data synthesized across hands indicated 7 generalized grasps that accounted for 93% of their frequency. Upon analysis of the duration, it was found that 92% could account for these same grasp configurations. Grasp frequency and duration were more homogenous across combined data than that of PARC1. Here, 65% and 72% of the grasp frequency and duration, respectively, can be attributed to Pinch, Tripod, and Lateral Tripod. Data can be seen in Figure 3-3c and Figure 3-3d.

### 3.5. Discussion

A common set of hand grasps was obtained for each child as they performed their daily activities. Data from both PARC1 and PARC2 are in agreement with similar adult studies which suggested that 6-9 standard grasps can account for nearly 80% of common activities<sup>16</sup>. Here 7 generalized grasps accounted for 90% or more of daily activities in both frequency and duration across both participants when handedness was not considered. This high percentage supports that a strategic repertoire of grasp configurations may be pertinent when developing rehabilitative and assistive devices.

For PARC1 the dominant hand accounted for about 85% of the total grasp duration yet the frequency of the dominant and non-dominant hands were approximately 62% and 38%, respectively. Further, PARC2's dominant and non-dominant hands accounted for 51% and 49%

of the total grasp duration, respectively while the frequency of use was 54% for the dominant and 46% for the non-dominant. Even though the frequency and duration of the non-dominant hands are generally lower than that of the dominant hands, results suggest they still play a vital role in supporting everyday object interactions. These results further emphasize the importance of understanding the role both hands play when developing rehabilitative and assistive devices. For example, in populations of children with unilateral motor impairments, the unaffected side often assumes the dominant role while the affected side offers support and stabilization of objects. Therefore, it is critical to recognize how laterality may impact the desired function a patient wishes to accomplish with a robotic technology. Those with unilateral impairments may have very different demands than those affected bilaterally.

Interestingly, the results from both participants share the same top 3 frequently used generalized grasp configurations, Pinch, Lateral Pinch, and Tripod. These 3 grasps can be found within the top 7 generalized grasps used by adults and account for approximately 80% of their frequency<sup>15</sup>. Intriguingly, PARC1 performed 5 out of the 7 generalized grasps, and PARC2 performed 6 out of the 7. It was expected that children may use a variety of hand grasps to accomplish tasks. Although our limited data set of two children exhibited similarities to how adults use their hands, this may not be entirely representative of the whole pediatric population. Our data supports that a common repertoire of grasp configurations accounts for much of a child's hand activity and further investigation with a larger sample size across ages and sexes is warranted.

While limited, the data collected here suggests that as robotic rehabilitative and assistive technologies continue to emerge for children, consideration of key hand grasping movements will be vital to their effectiveness. For example, the current standard of care pediatric upper limb prostheses typically provides a single-degree-of-freedom tripod grasp. This aligns well with

PARC1's data in which a tripod grasp accounted for 74% total duration of hand use. However, PARC1's frequency data, shows 4 hand grasp types are needed to achieve 70% of the total grasp frequency. Thus, evaluating the effectiveness of mechatronic assistive devices requires data-rich approaches that account for both the frequency and duration of grasp type in real-world settings.

### 3.6. Conclusions

This study explored how two children used their hands in daily activities and if they are inclined to use a strategic set of grasp patterns. It was found that 7 unique grasp configurations accounted for the vast majority of hand use in both frequency and duration across participants. Taken together, these results lay the foundation to further understand the stereotypical hand activity of children. Further, this work may help inform the development and evaluation of pediatric rehabilitative and assistive devices. However, there are a few limitations and future directions that must first be considered. A larger sample size is currently under investigation and will allow us to understand how hand grasps differ across age ranges, sexes, and daily activities. Moreover, due to the categorical nature of the generalized grasp taxonomy, additional data analysis can be achieved including analyses of digit opposition type, and virtual finger units among many others. Linking the activities the children performed to grasps may also provide a more comprehensive picture of hand use during specific activities of daily living. This may also include expanding the study environment beyond the home to social, school, and childcare settings.

### 3.7. References

1. Kim, E. S. *et al.* Longitudinal Impact of Depression on Quality of Life in Stroke Patients. *Psychiatry Investig.* **15**, 141–146 (2018).
2. Maciejasz, P., Eschweiler, J., Gerlach-Hahn, K., Jansen-Troy, A. & Leonhardt, S. A survey on robotic devices for upper limb rehabilitation. *J. NeuroEngineering Rehabil.* **2014** *111* **11**, 1–29 (2014).
3. Plessis, T., Djouani, K. & Oosthuizen, C. A Review of Active Hand Exoskeletons for

- Rehabilitation and Assistance. *Robot. 2021, Vol. 10, Page 40* **10**, 40 (2021).
4. Heo, P., Gu, G. M., Lee, S. jin, Rhee, K. & Kim, J. Current hand exoskeleton technologies for rehabilitation and assistive engineering. *Int. J. Precis. Eng. Manuf. 2012 135* **13**, 807–824 (2012).
  5. Mendez, V., Iberite, F., Shokur, S. & Micera, S. Current Solutions and Future Trends for Robotic Prosthetic Hands. *Annu. Rev. of Control, Robot. Auton. Syst.* **4**, 595–627 (2021).
  6. Belter, J. T., Segil, J. L., Dollar, A. M. & Weir, R. F. Mechanical design and performance specifications of anthropomorphic prosthetic hands: A review. *J. Rehabil. Res. Dev.* **50**, 599–618 (2013).
  7. Falzarano, V., Marini, F., Morasso, P. & Zenzeri, J. Devices and protocols for upper limb robot-assisted rehabilitation of children with neuromotor disorders. *Appl. Sci.* **9**, 1–22 (2019).
  8. Simon-Martinez, C. *et al.* Age-related changes in upper limb motion during typical development. *PLoS One* **13**, 1–15 (2018).
  9. Franzblau, L. E. *et al.* Coping with Congenital Hand Differences. *Plast Reconstr Surg.* **135**, 1067–1075 (2015).
  10. Bassini, L. & Patel, M. *Fundamentals of Hand Therapy: Clinical reasoning and Treatment Guidelines for Common Diagnoses of the Upper Extremity.* (Mosby, 2007).
  11. Charles, J. & Gordon, A. M. Development of hand-arm bimanual intensive training (HABIT) for improving bimanual coordination in children with hemiplegic cerebral palsy. *Dev. Med. Child Neurol.* **48**, 931–936 (2006).
  12. Peck-Murray, J. A. Utilizing everyday items in play to facilitate hand therapy for pediatric patients. *J. Hand Ther.* **28**, 228–232 (2015).
  13. Agur, A. M. R. & Lee, M. J. *Grant's Atlas of Anatomy.* (Lippincott Williams and Wilkins, 1999).
  14. Ritter, H. & Haschke, R. *Humanoid Robotics and Neuroscience: Science, Engineering and Society.* (Taylor & Francis, 2015).
  15. Feix, T., Romero, J., Schmiedmayer, H. B., Dollar, A. M. & Kragic, D. The GRASP Taxonomy of Human Grasp Types. *IEEE Trans. Human-Machine Syst.* **46**, 66–77 (2016).
  16. Zheng, J. Z., De La Rosa, S. & Dollar, A. M. An Investigation of Grasp Type and Frequency in Daily Household and Machine Shop Tasks. in *IEEE International Conference on Robotics and Automation* (2011). doi:10.1109/TOH.2013.6.
  17. Oldfield, R. C. The Assessment and Analysis of Handedness the Edinburgh Inventory. *Neuropsychologia* **9**, 97–113 (1971).
  18. Liu, J., Feng, F., Nakamura, Y. C. & Pollard, N. S. A Taxonomy of Everyday Grasps in Action. *IEEE-RAS Int. Conf. Humanoid Robot.* (2014).
  19. Bullock, I. M., Zheng, J. Z., De La Rosa, S., Guertler, C. & Dollar, A. M. Grasp frequency

and usage in daily household and machine shop tasks. *IEEE Trans. Haptics* **6**, 296–308 (2013).

## Chapter 4. Development of a research-based multiarticulate pediatric prosthetic hand

The majority of this chapter has been published as:

Battraw MA, Young PR, Joiner WM, Schofield JS. (2022). A multiarticulate pediatric prosthetic hand for clinical and research applications. *Front. Robot. AI* 9, 1–14.

### 4.1. Chapter preface

The development and validation of a multiarticulate child-sized prosthetic hand for research and clinical applications is presented in this chapter. Mechanical and electrical characteristics were assessed to provide a performance benchmark for the device. A validated functional test was conducted to understand the grasping capabilities of the hand, which were compared to adult-based research devices. Our device serves as a research platform to begin investigating the abilities children with congenital upper limb deficiency have to control dexterous prosthetic hands (those that offer multiple grasping movements) during functional activities. The robotic prosthetic hand described in this chapter was later employed in Chapter 7 to demonstrate the feasibility for children born without a hand to control multiple grasping movements offered by a dexterous device.

### 4.2. Introduction

It is estimated that congenital upper limb differences occur in up to 1 in 500 live births<sup>1</sup>, and those with unilateral congenital below-elbow deficiencies typically present malformations amenable to prosthesis prescription. These children will have one typical upper limb and one that ends below the elbow, at the level of the proximal or mid-forearm<sup>2-4</sup>. Prosthesis prescription for these children is a complex challenge, and presently 35% to 45% of prescribed upper limb pediatric prostheses will be abandoned<sup>5</sup>. Regardless of age, factors that affect prosthesis adoption are related to the device offering sufficient function while promoting healthy social interactions<sup>6</sup>. The high rate of pediatric prosthesis abandonment suggests that current devices fall short of achieving these



demands and specific reasons for abandonment include the lack of useful function offered by the device<sup>6-8</sup>, device weight<sup>6,9</sup>, discomfort<sup>7,8</sup>, and social aspects related to device cosmesis<sup>6,7,10,11</sup>.

Standard-of-care pediatric prostheses provide limited functionality, typically offering only a single-degree-of-freedom open/close grasping function. This is a stark departure from the immense dexterity of an intact hand that moves with 27 degrees of freedom<sup>12</sup>, and the 6-9 common hand grasp movements (pulp pinch, cylindrical grasp, among others) that have been shown to account for nearly 80% of grasping movements when performing activities of daily living<sup>13,14</sup>. In recent years, multi-articulating motorized prosthetic hands for adults have become increasingly available. These assistive devices offer adults significant functional benefits by providing a multitude of hand grasp configurations<sup>15</sup>. Beyond their added function, an additional advantage inherent to their hand-like designs is the anthropomorphic or more life-like appearances when compared to their hook or grasper-style counterparts. Similarly, dexterous devices have begun to emerge for children, namely, the Vincent Young 3 (Vincent Systems, Karlsruhe, Germany) which is sized for an 8-year-old and offers up to 13 individual grasp configurations, or the Hero Arm (Open Bionics, Bristol, United Kingdom) which offers children 8 years and older 6 grasp configurations.

As dexterous pediatric prostheses continue to emerge there remain many unanswered questions such as which control techniques may be most effective in operating these devices, the degree to which children can use the newly available dexterity for improved functional outcomes, and how best to translate many effective innovations for adults to meet the unique demands of children<sup>16</sup>. For example, it is not known which grasping motions may be most effective to support age-appropriate daily activities and childhood play. Additionally, it is unknown how conventional adult muscle-based prosthesis control (surface EMG) may be translated to this population given that many were born with their limb difference and their affected muscles have never actuated an intact

limb<sup>16</sup>. Although control of dexterous prostheses for adults with congenital upper limb deficiencies has been investigated<sup>17</sup>, it is uncertain how these findings may translate to developing children. Furthermore, limited work has been done to illustrate changes in cortical activation during prosthesis control<sup>18,19</sup>. Addressing these knowledge gaps requires rigorous scientific investigations and supporting research platforms; hardware such as dexterous child-sized prostheses with open access to its programming and the mechanical capabilities to interact with daily objects to perform clinical or research-based activities. While there are no robust pediatric research platforms, there are numerous experimental or non-clinical pediatric prostheses that have been reported in literature; however, data characterizing their use, functional capabilities, and effectiveness remain sparse<sup>20</sup>. Furthermore, researchers and clinicians often have limited access to these devices as they are not commercially available, and few are released open-source such that they can be fabricated and programmed by individuals outside of their development teams.

Our objective was to develop a child-sized multi-grasp prosthesis that may serve as a robust research platform to address many of the critical gaps in translating dexterous upper limb prostheses to pediatric populations. Supporting our open-source release of the device, we performed a comprehensive set of benchtop and validated functional tests manipulating common objects to quantify the performance of our device. Here we present the development of a cable-driven, underactuated, adaptive grasp, multi-articulate pediatric hand termed the Bionic Engineering and Assistive Robotics Pediatric Assistive Ware (BEAR PAW). The mechanical and electrical characteristics of individual digit articulation and 7 commonly used hand grasps<sup>13</sup> are presented, followed by the functional performance benchmarked against other multi-grasp devices using an established assessment protocol<sup>21</sup>.

### 4.3. Materials and methods

We performed three tasks that were designed to develop, characterize, and evaluate the performance of the BEAR PAW. Design criteria were derived to inform the development and fabrication of our pediatric device. We performed benchtop testing to evaluate the device's mechanical and electrical characteristics, and we evaluated the BEAR PAW while grasping common objects to benchmark its performance against other comparable adult devices.

#### 4.3.1. Pediatric prosthetic hand criteria

In developing a robust research platform, delivering a device capable of achieving multiple hand grasp configurations to a similar degree of dexterity as current research-based adult devices was the crux of the challenge. The size of the device was an important first step to consider, as this directly impacted the feasibility of device development. As emerging dexterous devices have been targeted to no younger than the 8-year-old population and off-the-shelf componentry is limited in size, the minimum age of 8 provides us with an ideal size constraint. Furthermore, to achieve comparable dexterity, individual digit actuation was needed along with an active opposable thumb. Weight was another important consideration during device development because children do not yet have the strength of an adult<sup>9</sup>. Even in a research setting, it is important to carefully consider this constraint as fatigue, soreness, and/or discomfort can significantly diminish a child's engagement with experimental activities. Here, the mass of an Ottobock Electrohand 2000 for children 8-13 years old was used as a baseline for comparison (130 g) as it is among the lightest commercially available terminal devices for children. Additionally, the force output of the device was of high importance as in biological hands, it has been shown that most hand grasping configurations on average hold objects less than 500 g in weight during most activities of daily living<sup>13</sup> making this an ideal design target value for a pediatric prosthesis. Further, the time to fully

close the hand was set to be less than 1 s, reflecting values found among commercially available prosthetic systems<sup>22</sup>. Finally, a budget value of less than \$1000 for parts was selected to promote the accessibility of our system to other research laboratories. A detailed summary of the design criteria is outlined in Table 4-1.

Table 4-1. Pediatric research platform design criteria.

Design Requirement	Specification Metric	Quantitative Value
Size	Anatomical proportions	8-year-old child
Mass	Low mass	< 130 g
Inexpensive	Low cost	< \$1000
Degrees of actuation	Digit actuation and thumb opposition	6 degrees of actuation
Active actuation	Servo control	Servo motors
Electronics	Compact design	Enclosed in hand
Extended operation	Continuous power	Grid power
Control	Ease of actuation	Bluetooth protocol
Ease of use	High usability	Graphical interface
Finger speed	Time to close	< 1 s
Load	Target mass	500 g

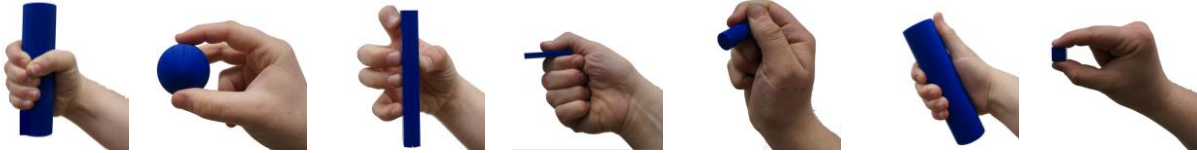
#### 4.3.2. Mechanical and electrical performance

##### 4.3.2.1. Experimental setup

We characterized the mechanical and electrical performance of the BEAR PAW while performing a set of the most frequently used generalized hand grasps along with individual digit actuations. Feix et al. suggests that the vast majority of human object manipulations are accomplished using 33 different grasp types which can be simplified to 17 generalized hand grasp configurations<sup>13</sup>. This simplification can be made when considering that objects of different shapes and sizes may

actually require the hand to move in similar ways, just to differing degrees of hand closure<sup>13</sup>. This is a relevant consideration as the BEAR PAW is programmed to conform to objects regardless of their size. Of the 17 generalized hand grasps some are used far more frequently than others, and a subset of 7 accounts for 80% of total activity (Table 4-2). Furthermore, these 7 grasps also accounted for over 80% of the time duration in which a hand is used to grasp objects in daily living. Table 4-2 shows the top 7 generalized hand grasps that were used to characterize the BEAR PAW's performance.

Table 4-2. Top 7 common generalized hand grasps configurations, percent frequency (Freq), and duration (Dur).










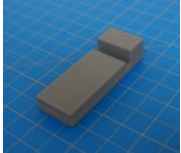
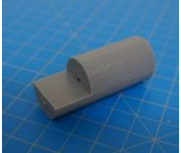
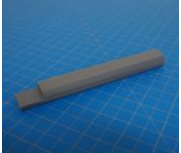
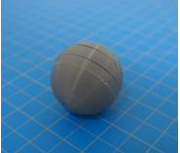
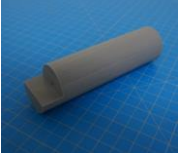
1. Cylindrical Grip	2. Tripod Pinch	3. Prismatic 4 Finger	4. Lateral Pinch	5. Lateral Tripod	6. Hook Grip	7. Pulp Pinch
Freq: 21.6%	Freq: 14.8%	Freq: 11.3%	Freq: 10.5%	Freq: 10.4%	Freq: 6.8%	Freq: 4.8%
Dur: 30.5%	Dur: 10.4%	Dur: 26.9%	Dur: 6.9%	Dur: 5.1%	Dur: 5.1%	Dur: 2.7%

A set of 6 custom manipulanda were designed and fabricated to measure the force characteristics of the BEAR PAW while performing the 7 grasp configurations and individual digit actuations. These consisted of a series of 3D printed enclosures that housed one to two calibrated 8mm diameter SingleTact capacitive force sensor(s) with a range of 10 Newtons (SingleTact CS8-10, PPS UK Limited, Glasgow, United Kingdom) (Table 4-3).

A testing platform was assembled with 15mm x15mm MakerBeam and included a custom 3D-printed mount for the BEAR PAW. The platform was designed to fixate the BEAR PAW which allowed for repeated consistent testing of the various hand motions during data collection. Additionally, the platform accommodated the set of manipulanda to capture the mechanical force

output. These were either mounted to the platform or on an external gooseneck for strategic object placement (Figure 4-1).

Table 4-3. The different manipulandum used to characterize the force output of the BEAR PAW for individual finger articulation and common generalized hand grasp configurations. The hand grasp (HG) used and the number of sensors (NS) for each manipulandum are noted and each square on the blue background is 1 cm by 1 cm.

<b>Top View</b>						
<b>Isometric</b>						
<b>Description</b>	<b>HG:</b> Finger Articulation <b>NS:</b> 1	<b>HG:</b> Pulp Pinch, Lateral Pinch <b>NS:</b> 1	<b>HG:</b> Lateral Tripod <b>NS:</b> 1	<b>HG:</b> Prismatic 4 Finger <b>NS:</b> 2	<b>HG:</b> Tripod Pinch <b>NS:</b> 1	<b>HG:</b> Hook Grip, Cylindrical Grip <b>NS:</b> 2

Beyond the mechanical force measurements obtained using the manipulanda, the electrical characteristics of the BEAR PAW were recorded during testing. This included capturing the current obtained with an ACS723 current sensor which recorded the current load of the BEAR PAW's servo motors during the experimental procedure. Further, the voltage across the servo motors during actuation was recorded. Lastly, to synchronize the data during post-hoc analysis a timing voltage was used. An Arduino script was written to actuate the BEAR PAW and the voltage values produced from the force, servo current, servo voltage, and time voltage were passed into a National Instruments USB-6210 data acquisition system sampling at 4000 Hz. This data was stored for further analysis in a table format using a MATLAB (The MathWorks, Inc., Natick, MA) script.



Figure 4-1. Depicts the testing platform for the BEAR PAW. It illustrates the hand mount used to hold the BEAR PAW stable during testing, the gooseneck which strategically held manipulanda, and the MakerBeam platform which supported the manipulandum used for individual digit articulation.

#### 4.3.2.2. Experimental procedures

The BEAR PAW was tested to determine the mechanical and electrical performance when completing individual digit and grasp actuations. In both configurations, the BEAR PAW was mounted to the testing platform to assess the grasping movements shown in Figure 4-2. To test individual digit flexions, the manipulanda was placed at a fixed distance and was then aligned with the digit so that it would press down on its center. For each hand grasp configuration, the appropriate manipulandum was attached to the gooseneck (Figure 4-1) and was strategically placed in front of the BEAR PAW (Figure 4-2).

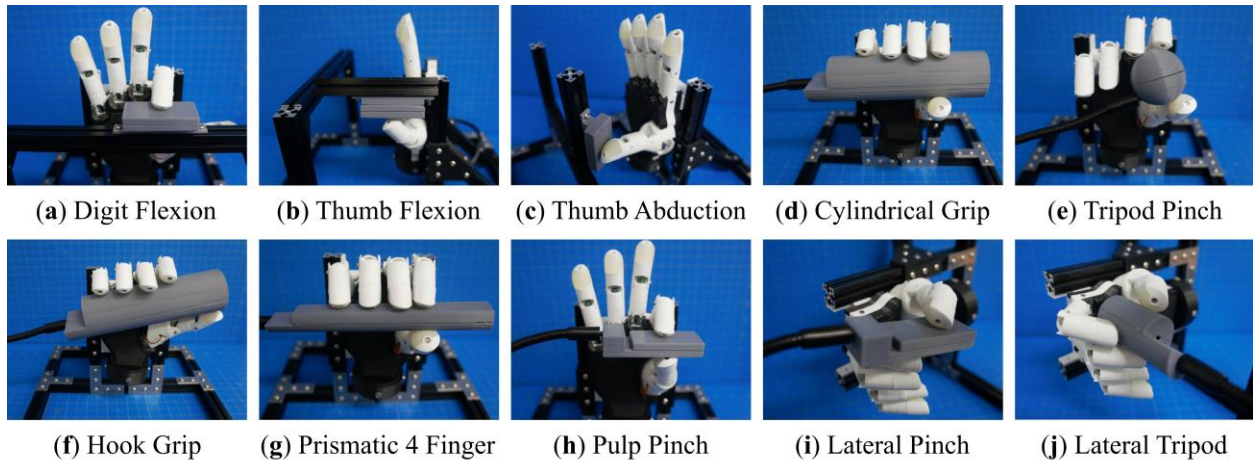


Figure 4-2. Depicts the BEAR PAW during grasp actuation on the various manipulanda. **(a)** represents individual digit articulation for digits 2-5 and **(b-c)** represents both thumb palmar abduction and flexion. **(d-j)** shows each manipulandum used for the 7 common generalized hand grasp configurations.

Testing was performed in accordance with ANSI/ISA testing protocols<sup>23</sup>. The test procedure consisted of performing single-digit actuations and the hand grasp configurations 10 times each. Here one cycle consisted of the BEAR PAW actuating for a total of 5 seconds to grasp/load the manipulanda and then unload it. The current from the servo motors, voltage across the servo motors, force applied to the manipulandum, and a reference voltage used for data synchronization, were measured and stored for each testing cycle. Together, these data allowed for post-hoc calculations relating force, current, and power each time the BEAR PAW performed a grasping movement (see below).

#### 4.3.2.3. Data analysis

A separate MATLAB script was written to read the stored data for analysis. First, the voltage output from the force sensor(s) in the manipulanda was converted to force using the line of best fit for each of the calibrated sensors<sup>24</sup>. Further, in the case of two force sensors, a point load was assumed at each sensor, and data were summed together after conversion to include the total force value. The voltage from the current sensor output was converted to amperes using the provided IC



sensitivity of 400mV/A<sup>25</sup>. Finally, Watt's law was used to calculate power draw from the measured voltage across the servo motors and the corresponding current.

To align data across the 10 trials a reference timing voltage was used, during the 5 seconds of actuation, that was set to low until the BEAR PAW began to actuate at which point it was set to high. Once this occurred, 1 second of the data directly after the high was omitted followed by 2.5 seconds of recorded data to ensure that the BEAR PAW was fully actuated on the manipulanda. For individual digit actuations and generalized hand grasp configurations, these 2.5 seconds were averaged for a total of 10 values, one per each actuation cycle. Here, the mean and standard deviation of these measures were obtained. Measures obtained during the flexion of digits 2-5 were averaged together as these fingers are identical in size and mechanical design. Values for thumb flexion and opposition were captured separately. Additionally, all generalized hand grasp configuration measures were averaged on an individual grasp basis.

#### 4.3.3. Hand assessment protocol

##### 4.3.3.1. Experimental setup

To assess the BEAR PAW's functional capabilities, we used the validated Anthropomorphic Hand Assessment Protocol (AHAP)<sup>21</sup>. The protocol consists of 8 different grasp types of which there are 3 different objects associated with each. The 8 grasps are Hook Grip, Spherical Grip, Tripod Pinch, Extension Grip, Cylindrical Grip, Diagonal Volar Grip, Lateral Pinch, and Pulp Pinch. Furthermore, there are 2 postures – Index Pointing and Platform – for a total of 26 objects that must be grasped and/or maintained. A further explanation of the objects used during the AHAP test can be found in<sup>21</sup> and a subset of these objects are depicted in the results section.

We preprogrammed grasp configurations into the BEAR PAW in accordance with the definitions used in<sup>21</sup>. These definitions explained the proper posture for each grasp and indicated the correct

contact between an object and various locations on a robotic hand. With these definitions, the BEAR PAW's hand grasp configurations were created in software by adjusting individual digit positions which allowed for it to appropriately conform to the test objects. This was achieved using a custom-developed graphical user interface (GUI) that allowed the investigators to fine-tune the digit movements for each grasp configuration using virtual buttons and knobs. The final settings were stored, and the GUI offered the ability to then simply press a virtual button to actuate the final grasping configurations. To perform the AHAP protocol a testing rig was developed which consisted of the BEAR PAW mounted to a forearm frame through a wrist mount (Figure 4-3) which could then be held by the investigator to perform necessary object manipulations.



Figure 4-3. Depicts the testing rig used to perform the Anthropomorphic Hand Assessment Protocol, highlighting the BEAR PAW, wrist adapter mount, and forearm frame grip.

#### 4.3.3.2. Experimental procedures

The AHAP test required that 26 test objects be manipulated 3 times which was then repeated by 3 test investigators<sup>21</sup>. Replicating the test with 3 separate investigators is the standard AHAP procedure and ensures that collected data accounts for the minor potential variability in the way

objects may be manipulated. Here, investigators included laboratory personnel who acted as the lead investigator and test investigators. Prior to conducting the protocol the test investigators were instructed by the lead investigator as to the correct hand grasp for the object and were allowed to familiarize themselves for approximately 1 minute<sup>21</sup>. Each trial of the AHAP protocol began with the lead investigator holding 1 of the 26 objects in front of a test investigator in a predefined orientation. The test investigator used the GUI to actuate the BEAR PAW to achieve a desired grasp configuration and grasp the object. Afterwards, the lead investigator would release the object such that it was held exclusively by the BEAR PAW. For each grasp type (excluding postures), the BEAR PAW started in the palm-faced-up direction in which it attempted to hold the corresponding object for 3 seconds (known as the grasping phase) and then was rotated 180° with the palm faced down again attempting to hold the object for 3 seconds (known as the maintaining phase). The index posture consisted of starting a timer for the grasping phase and stopping it after 3 seconds for the maintaining phase. Additionally, the platform posture only involved the grasping phase which entailed holding a plate for 3 seconds. The grasping and maintaining phases for each grasp type and posture are further described in<sup>21</sup>.

#### 4.3.3.3. Data analysis

During the grasping and maintaining phases for each object, the lead investigator scored the BEAR PAW's performance<sup>21</sup>. Accordingly, a score of 1 was received if the object was held with the specified grasp for the allotted time. A score of 0.5 was received if the BEAR PAW held the object for the designated time but was done with a different grasp and 0 was received if it could not hold the object. Then, while the BEAR PAW performed the maintaining portion, if there was no movement of the object with respect to the hand over the time constraint a score of 1 was awarded. If the object moved but did not drop, then a score of 0.5 was received and a score of 0 was received

if it was not able to maintain the object. The BEAR PAW's raw AHAP scores are provided in Appendix A.

These scores were then used to compare the BEAR PAW's grasping and maintaining abilities to previously published values from 4 research-focused adult prosthetic hands performing the same experimental procedure<sup>26</sup>. These 4 adult hands (Dextrus, IMMA, InMoov, and Limbitless) were all underactuated systems with a range from 14-17 degrees of freedom and 1-6 degrees of actuation<sup>26</sup>. Here, scores obtained from the BEAR PAW and the 4 adult prosthetic hands were separated based on which phase (grasping or maintaining) the prosthetic hand was in. The scores for each prosthetic hand were further separated into 10 categories for grasping and 9 categories for maintaining in accordance with the grasp type/posture. These scores were aggregated across the 3 test investigators such that individual grasping and maintaining comparisons could be made between the BEAR PAW and the 4 adult prosthetic hands.

To accommodate the ordinal (non-parametric) AHAP scoring data, statistical analyses were conducted using a Mann-Whitney U test to perform pairwise comparisons between the BEAR PAW and each of the 4 adult prosthetic hands (for the 10 grasps and 9 postures, 40 and 36 comparisons, respectively). For each comparison, the null hypothesis  $H_0$  stated that there was no statistically significant difference in the central tendency or median score between the BEAR PAW and the corresponding adult hand for a particular grasp. A confidence interval of 95% was selected and  $p < 0.05$  was taken to indicate statistical differences.

## 4.4. Results

### 4.4.1. Pediatric prosthetic hand

The BEAR PAW is a multi-articulating pediatric prosthetic hand developed in the computer-automated design software SolidWorks 2020 and fabricated with a SigmaX R19 3D Printer using

PLA material. The BEAR PAW uses a 3.3V Arduino Pro Mini with an ATmega328 microcontroller, HC-05 wireless Bluetooth module, and a custom breakout board to interface with the six KST-X08 series servo motors. Further, it internally houses its electronics, has 6 independently programmable degrees of actuation, is an under-actuated system with 11 degrees of freedom, and is therefore capable of a multitude of common grasping movements. In summary, the BEAR PAW is a dexterous pediatric prosthetic hand that was designed using off-the-shelf components, highly accessible design and fabrication techniques, and open access to programming which includes a graphical user interface for intuitive control. A detailed depiction of the BEAR PAW is presented in Figure 4-4 and a detailed list of its performance characteristics is supplied in Table 4-4.

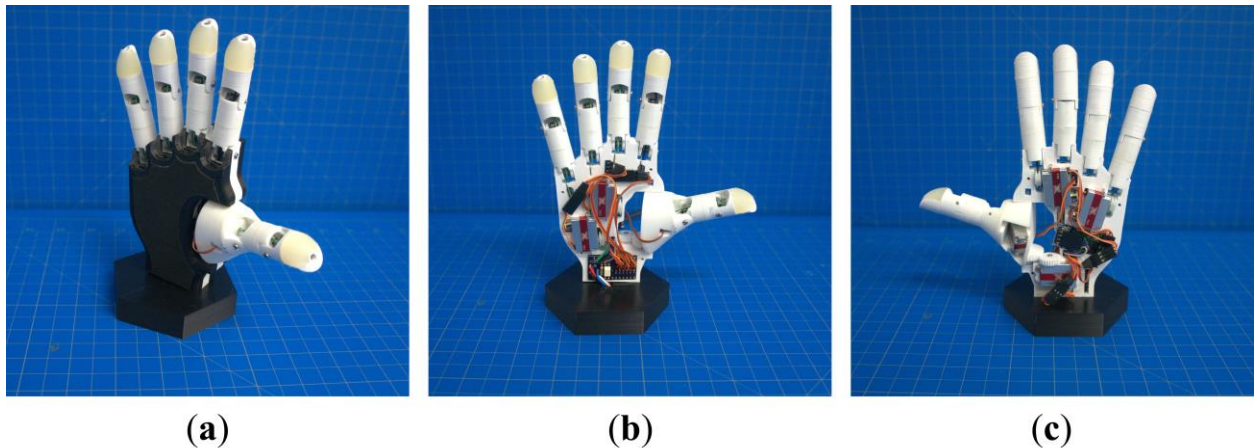


Figure 4-4. The BEAR PAW: A pediatric multiarticulate prosthetic hand with six degrees of actuation and programmable hand grasp configurations. Shown in an isometric (a), front (b), and back (c) view.

Table 4-4. BEAR PAW achieved specifications. \*Values obtained as explained in the Materials and Methods section 4.3.2 on Mechanical and Electrical Performance and the detailed analysis are provided in the corresponding results section 4.4.2. †The STL files and assembly guide can be found at <https://github.com/BEAR-Labs/BEAR-PAW>.

<b>Specification</b>	<b>Achieved Value</b>
<b><i>Size/Appearance</i></b>	
Anatomical proportions	8 years old child
<b><i>Electrical</i></b>	
Operating voltage	5 V
Actuation power	3.388 – 8.718 W*
<b><i>Mechanical</i></b>	
Time to grasp	0.67 s
Force	0.424 – 7.216 N*
Number of actuators	6
Type of actuators	Servo motors
Actuation type	Underactuated
Actuation mechanism	Tendon driven
<b><i>Range of motion</i></b>	
Degrees of freedom	11
Digit 2-5 flexion	120 degrees
Thumb flexion	90 degrees
Thumb abduction	90 degrees
<b><i>Control</i></b>	
Able-bodied control	Graphical interface
Communication	Bluetooth, UART
<b><i>Weight</i></b>	
Mass	177 g
<b><i>Ease of access</i></b>	
Cost	500 USD
Componentry	Off the shelf
STL Files	Available online†
Assembly guide	Available online†

The BEAR PAW’s design and development was inspired by the HANDi Hand and was sized to 50<sup>th</sup> percentile 8-year-old male and female anthropometric hand data (Figure 4-5)<sup>27–29</sup>. Similar to the HANDi Hand the BEAR PAW is accessible to researchers and clinicians, and provides open-

source 3D printable files, a bill of materials, assembly instructions, microcontroller code, and GUI which can be found via <https://github.com/BEAR-Labs/BEAR-PAW>.



Figure 4-5. A size comparison between the BEAR PAW (left), a pediatric prosthetic hand, and the HANDi Hand (right), an adult prosthetic hand. Each square in the background is 1cm by 1cm.

#### 4.4.2. Mechanical and electrical performance

The BEAR PAW uses an underactuated tendon-driven design in each digit to achieve flexion, and torsion springs incorporated into each joint to return digits to their extended position when not being actuated (Figure 4-6a). Here flexion is caused by a servo motor rotating a pulley to which a tendon is attached. One challenge with conventional tendon-driven actuation is managing the slack that may present in the tendon. Therefore, we developed a tensioning mechanism in which a tensioner screw translates a tendon mount to compensate for the slack. Moreover, the digits 1-5 are all actuated and controlled independently; while thumb abduction uses gearing for motion and is also actuated independently.

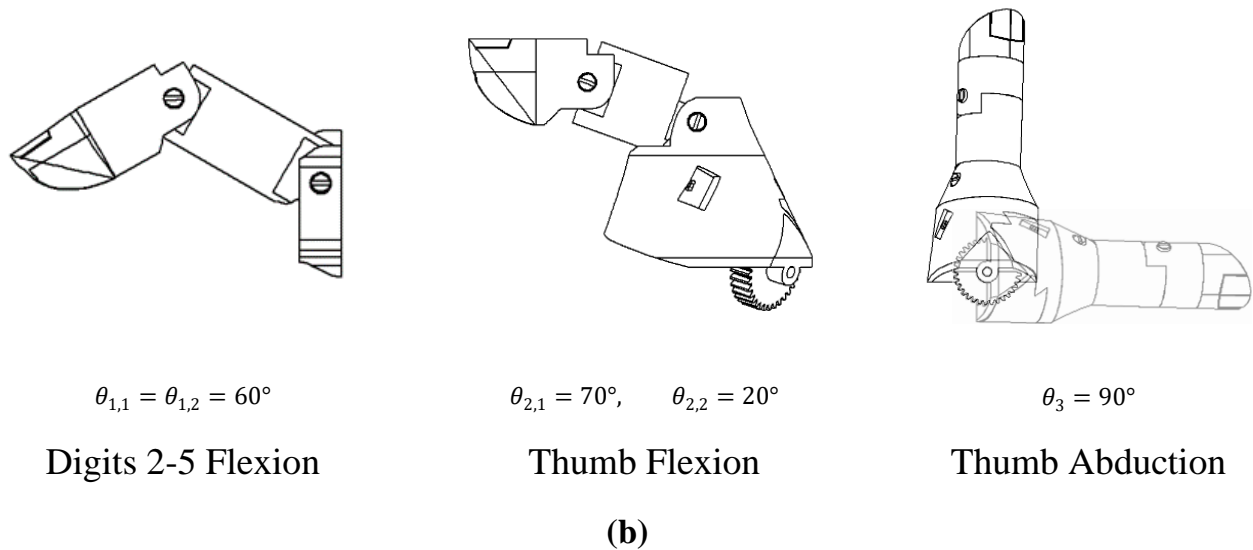
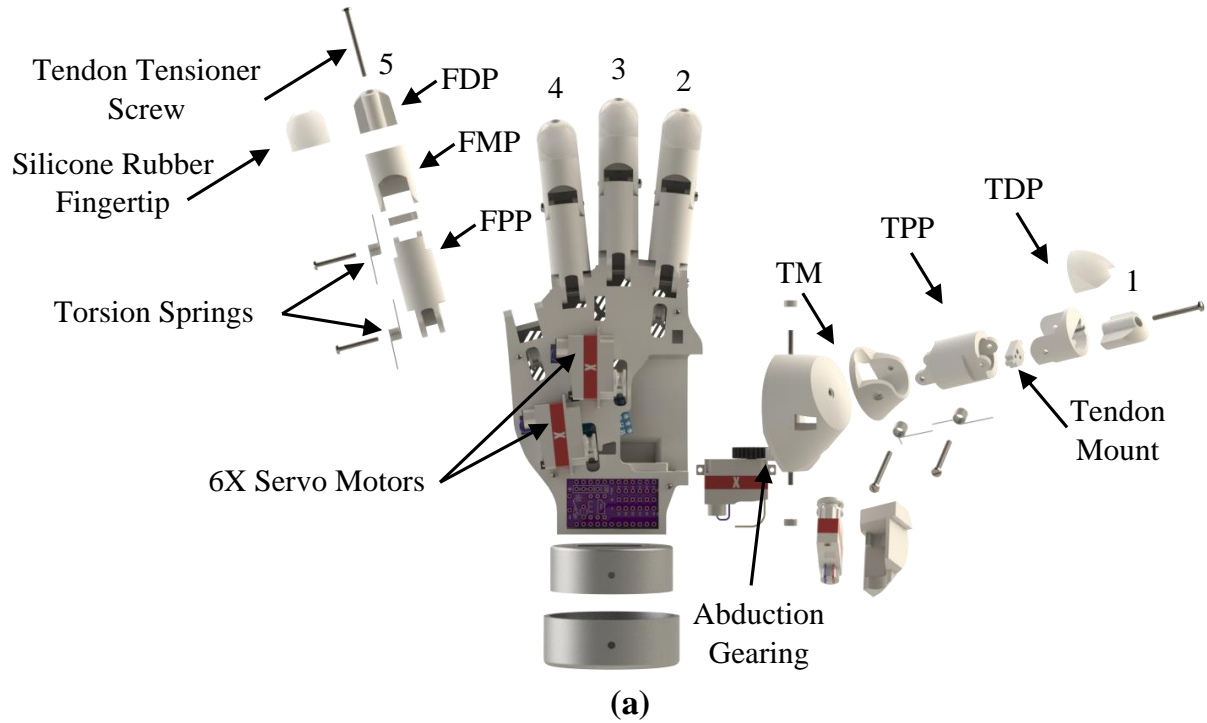


Figure 4-6. A detailed illustration of the mechanical features of the BEAR PAW. (a) shows an exploded view of individual digits 1-5 highlighting key components of the mechanical design. (b) provides the range of motion for each degree of actuation. Digits 1-5 are labeled with acronyms: finger distal phalanx (FDP), middle phalanx (FMP), proximal phalanx (FPP), thumb distal phalanx (TDP), proximal phalanx (TPP), and metacarpal (TM).

The anatomical design of digits 2-5 for the BEAR PAW included the distal, middle, and proximal phalanx where the distal and middle are coupled to accommodate the small size required of a



pediatric hand. The range of motion for these digits during flexion (while not contacting objects) was approximately 60° for the proximal and middle-distal phalanx. Further, digit 1 included the distal and proximal phalanx along with the thumb metacarpal. During thumb flexion, a 70° range of motion for the proximal and 20° for the distal was achieved, respectively. Finally, thumb abduction had a 90° range of motion (Figure 4-6b).

The measured force outputs for the BEAR PAW while performing the 7 grasping configurations and individual digit articulations ranged from 0.424 N to 7.216 N. The maximum value of 7.216 N was achieved during the Cylindrical Grip while the minimum value of 0.424 N was achieved during the Lateral Pinch (Table 4-5). The electrical performance ranged from 0.675 A to 1.789 A and 3.388 W to 8.718 W across the different grasp configurations. The minimum values of 0.675 A and 3.388 W corresponded to the individual digit flexion of digits 2-5. The maximum values of 1.789 A and 8.718 W were achieved from the Cylindrical Grip which also achieved the highest grasping forces (Table 4-5).

Table 4-5. BEAR PAW’s mechanical and electrical characteristics for the six degrees of actuation and the top seven generalized hand grasp configurations. \*Hook Grip and Diagonal Volar Grip have the same gross hand motion, yet in the AHAP test, these are considered separate motions that include a different set of objects.

Motion Posture	Motion Picture	Mechanical and Electrical Characteristics		
		Force (Newtons)	Current (Amperes)	Power (Watts)
Digits 2-5 Flexion		$1.709 \pm 0.076$	$0.675 \pm 0.069$	$3.388 \pm 0.343$
Thumb Flexion		$0.761 \pm 0.042$	$0.751 \pm 0.002$	$3.763 \pm 0.010$
Thumb Abduction		$2.454 \pm 0.069$	$0.729 \pm 0.003$	$3.656 \pm 0.014$
Cylindrical Grip		$7.216 \pm 0.578$	$1.789 \pm 0.052$	$8.718 \pm 0.242$
Tripod Pinch		$2.989 \pm 0.253$	$1.433 \pm 0.035$	$7.030 \pm 0.166$
Prismatic 4 Finger		$5.714 \pm 0.190$	$1.644 \pm 0.068$	$8.011 \pm 0.316$
Lateral Pinch		$0.424 \pm 0.011$	$0.841 \pm 0.008$	$4.115 \pm 0.042$
Lateral Tripod		$0.629 \pm 0.072$	$0.840 \pm 0.005$	$4.097 \pm 0.024$
Hook Grip/Diagonal Volar Grip*		$1.415 \pm 0.158$	$1.083 \pm 0.020$	$5.276 \pm 0.109$
Pulp Pinch		$2.043 \pm 0.025$	$0.949 \pm 0.004$	$4.649 \pm 0.020$

#### 4.4.3. Hand assessment

When statistically comparing the BEAR PAW's grasping performance to published values of the 4 research-focused adult prosthetic hands, its performance scored better or equivalent for 33 of the 40 comparisons made (10 grasp types/postures for 4 adult hands) (Figure 4-7 and Figure 4-8). Further, 31 times out of 36 the BEAR PAW performed statistically better or equivalent during the maintaining phase for the 9 grasp type/posture categories (results are included in Appendix A). That is, minor differences exist between the BEAR PAW and the 4 adult prosthetic hands when comparing grasping and maintaining capabilities.

For the grasping phase of the AHAP test, the statistical analysis showed the BEAR PAW performed significantly better a total of 9 times across the 4 adult prosthetic hands. Further, 24 times there were no statistically significant differences observed during the grasping phase. Finally, when comparing the BEAR PAW to each adult prosthetic hand the analysis showed statistically worse performance for 7 of the grasp types/postures. A detailed analysis of the grasping comparisons from the BEAR PAW to each of the 4 adult prosthetic hands across the 10 grasp types/postures can be seen in Figure 4-7 and Figure 4-8. In this figure, the number of times the hand scored a 1, 0.5, or 0 for a grasp type/posture was tallied and plotted. Further, this figure depicts a subset of the 27 objects used in the AHAP test as a reference.

The statistical analysis for the maintaining phase of the AHAP test showed significant differences between the BEAR PAW and each of the 4 adult prosthetic hands. There was a significantly better performance for 16 grasp types/postures, 15 were shown to have no significant differences, while 5 showed statistically worse performance. The detailed statistical comparison for the maintaining phase of the test can be viewed in Appendix A.

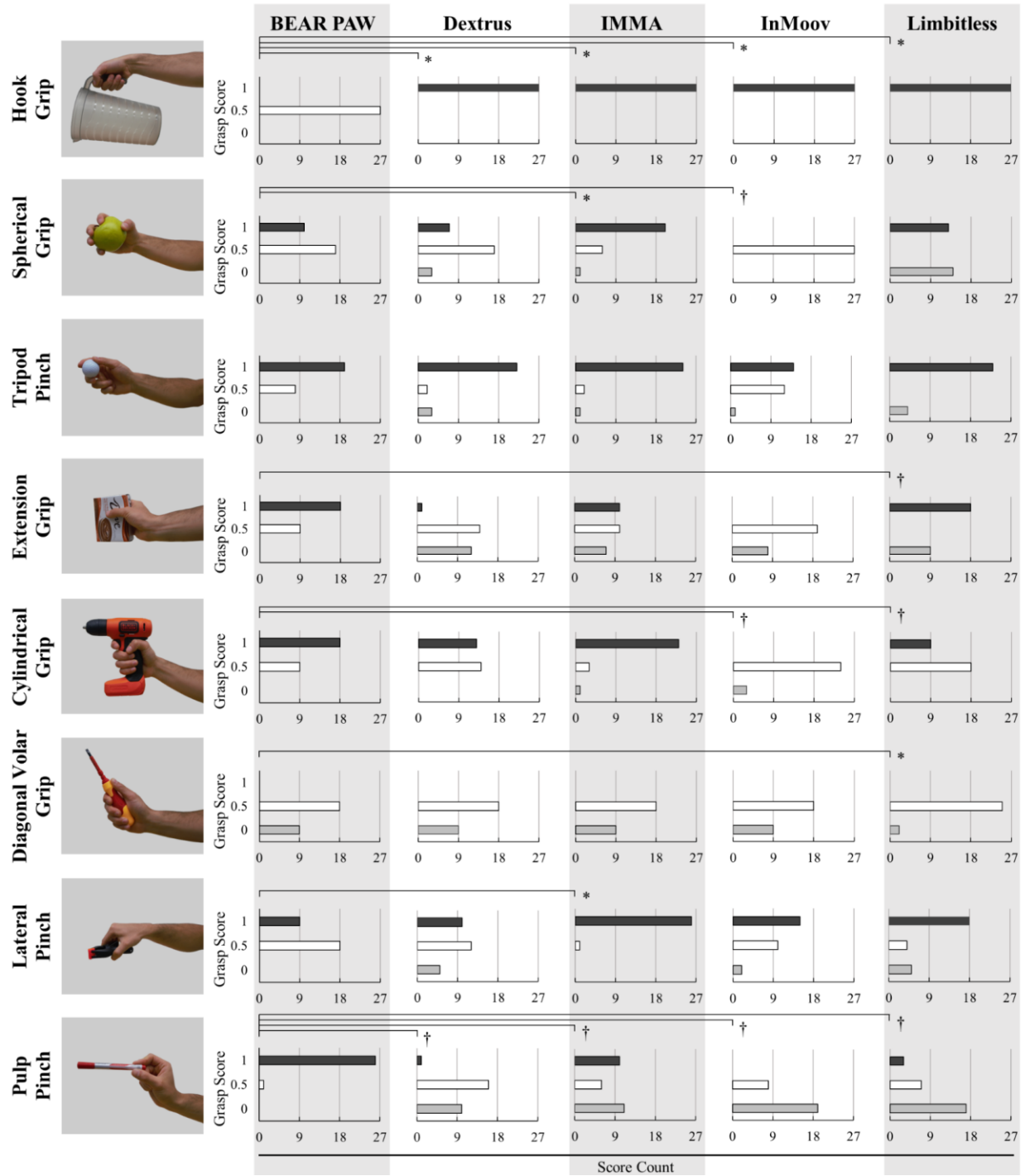


Figure 4-7. BEAR PAW grasping comparison scores for 8 different grasp types across the 4 adult hands. For each grasp type, the number of times each hand scored a 1, 0.5, or 0 was plotted. \*Represents when the BEAR PAW performed statistically worse. †Represents when the BEAR PAW performed statistically better.

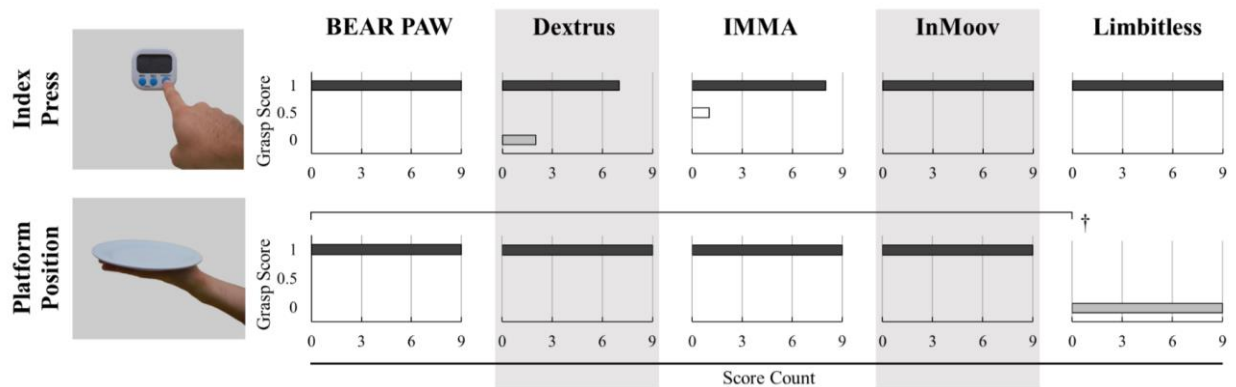


Figure 4-8. BEAR PAW posture comparison scores for 2 different postures across the 4 adult hands across the 4 adult hands. For each grasp type/posture, the number of times each hand scored a 1, 0.5, or 0 was plotted. †Represents when the BEAR PAW performed statistically better.

For both the grasping and maintaining phases of the AHAP test, the BEAR PAW performed significantly worse for the Hook Grip a majority of the time with only one comparison that showed no significant difference. Additionally, the BEAR PAW performed significantly better for the Pulp Pinch across all adult prosthetic hands. Finally, for the maintaining phase, the Cylindrical Grip of the BEAR PAW showed significantly better results than the other prosthetic hands. In summary, the BEAR PAW performed similarly to the 4 adult prosthetic hands and in some cases better, making it an effective platform to examine prosthetic control in pediatric populations.

#### 4.5. Discussion

This work presents the design and characterization of a multiarticulate pediatric-sized prosthetic hand that may serve as a robust and accessible research platform. The series of benchtop tests performed in this study provide a benchmark analysis of the device. Its performance, when compared to research-focused adult prosthetic hands, suggests that the BEAR PAW has the potential to serve as a useful tool in exploring the multitude of questions and unique challenges surrounding the effective translation of advanced mechatronic prostheses to children.

Multiple, clinically relevant design criteria were employed to inform the design and fabrication of the BEAR PAW and to ensure its utility as a research platform. These criteria included a size and weight limit, device dexterity, control methods, and accessibility. Intuitively, these criteria are interconnected and directly influence one another. A prominent example of this relationship is as dexterity increases, the number of actuators must also increase, and with that, the weight and the compact size of the device become difficult to address. This issue is vital to the BEAR PAW as it is a highly dexterous device that is tailored to conform to the anthropomorphic nature of an 8-year-old child to meet the need for a child-sized dexterous device. Although it is possible to develop smaller dexterous devices targeted at a younger population (less than 8 years old), commercial devices have yet to emerge, and it is unlikely a research platform with off-the-shelf componentry could exist as the next step to miniaturization would require hardware development. Furthermore, while the BEAR PAW exceeded the target weight limit of 130 g (weighing 177g), the device weighs less than comparable dexterous pediatric hands such as the Hero Arm hand (280–345g<sup>30</sup>), and is designed to be used in a research setting, allowing the researcher opportunities to make necessary adjustments to test procedures thereby minimizing subject fatigue.

As children's motor systems are still developing and they are often still exploring interactions within their environments, a more dexterous device is vital to allow them to interact with objects in different ways using a multitude of hand gestures<sup>31</sup>. The BEAR PAW can achieve similar dexterity to that of the comparable adult prosthetic hands, providing researchers control over individual digit movements and thus, the ability to explore the effects of providing users multiple grasping configurations. Further, the BEAR PAW can accommodate multiple communication protocols and incorporates affordable off-the-shelf componentry to provide ease of use and accessibility to research groups. The 3D printable files, assembly instructions, bill of materials,

and necessary code are openly available to further facilitate this access (<https://github.com/BEAR-Labs/BEAR-PAW>). Well-documented and tested open-source pediatric hands are scarce making experimentation with these devices difficult. Furthermore, current commercially available devices inhibit researchers' ability to manipulate device hardware/software to push the boundaries of the current state of pediatric prostheses. Here, we begin to address this gap by disseminating an open-source research platform with documented performance characteristics and benchmarking it to well-known adult research devices.

Feix et al. suggest that the majority of objects that adults commonly manipulate in daily life do not exceed 500 g, and the grasping force of the hand is largely driven by the mass of the object<sup>13</sup>. The BEAR PAW achieved a maximum grasping force output of 7.216 N which exceeded the typical force required to statically grasp a 500 g object<sup>13</sup>. This maximum force output was obtained from the Cylindrical Grip configuration, which was anticipated, as all the digits actuated around the object to perform the grasp thereby utilizing the combined outputs of all servo motors. Conversely, the minimum force output of 0.424 N was associated with the Lateral Pinch grasp and the low force was likely due to the nature of the index finger's range of motion which was limited by the servo motor to 120°. This limited range of motion caused restricted contact between the thumb and index finger. When taken together, the BEAR PAW was able to perform 7 common generalized hand grasp configurations successfully, although the device could not achieve the necessary force required to manipulate 500g objects for every hand grasp configuration. Further design refinements including incorporating high-performance servo motors may be warranted in future work.

Additionally, the electrical characteristics of current and power were tabulated to provide a baseline of electrical performance. It was found during testing that the lowest current and power

draw were 0.675 A and 3.388 W, respectively. These results corresponded to the actuation of digits 2-5, which was anticipated as a single digit was being activated and with minimal frictional forces present when compared to individual thumb flexion or geared thumb opposition. Likewise, the value for the maximum current and power draw was 1.789 A and 8.718 W which were recorded from the Cylindrical Grip. Similar to the maximum force, these values were expected as all the servo motors were under load causing an increase in the current and power. Overall, these values provide the necessary information to allow for future untethered battery-operated control.

The AHAP test allowed for the BEAR PAW's grasping and maintaining ability to be evaluated when manipulating common household objects and benchmarked against the adult prosthetic hands. The objective of performing the comparisons was to validate the BEAR PAW's performance and viability as a research platform. Here it was found that the BEAR PAW performed similar to or better than comparable adult devices across the test. While it outperformed the tested adult prosthetic hands for Pulp Pinch during both the grasping and maintaining phases, this was likely attributed to the silicone fingertips that allow for increased friction when performing pinch-type manipulations. During the Cylindrical Grip maintaining phase, the BEAR PAW performed better than the other comparable adult prosthetic hands which is intuitive when viewing the mechanical force output of the Cylindrical Grip as it exhibited the highest force output of 7.216 N. However, the BEAR PAW was challenged in performing some functions. The main limitation was the size constraints required to accommodate the pediatric population. Off-the-shelf micro servo motors that meet these size demands are often restricted in their range of motion, thereby affecting the BEAR PAW's ability to adequately grasp and maintain certain objects, i.e., the Hook Grip could not fully wrap around smaller objects in the AHAP test. Both the small nature of the



design and the limited range of motion affected the AHAP test as certain objects were too big for the BEAR PAW to reach around and too small for the range of motion.

#### 4.6. Conclusions

Our data suggest that it is plausible for the BEAR PAW to be used in research and clinical settings to perform tasks and object interactions that may not be overly mechanically demanding such as box and blocks<sup>32,33</sup>, Jebsen/Taylor hand function<sup>34</sup>, clothespin relocation<sup>35</sup>, and the SHAP test<sup>36</sup>, among others. However, with the exception of the SHAP test<sup>36</sup>, the remaining standardized tests are not designed to challenge the patient to perform more than one grasp type/posture. Although the SHAP test<sup>36</sup> allows for multiple grasps, it uses everyday objects that may not translate effectively to the pediatric population e.g., small hand compared to object size and lack of participant engagement during testing. Therefore, the BEAR PAW can be used to begin exploring the functional benefits that children have with the provided multi-grasp dexterity, but like the need for a robust research platform, standardized functional tests that challenge children to perform age-appropriate multi-grasp tasks are also needed. As multi-grasp pediatric devices continue to emerge a rigorous evidence base is required to facilitate clinical adoption and inform the prosthetic approaches to ensure the best functional outcomes for these children. The BEAR PAW provides an accessible, open-source research platform to begin assessing validated outcome measures, refining prosthetic control systems, and examining the degree to which multi-articulating prostheses may make a difference for the users.

#### 4.7. References

1. Giele, H., Giele, C., Bower, C. & Allison, M. The incidence and epidemiology of congenital upper limb anomalies: A total population study. *J. Hand Surg. Am.* **26**, 628–634 (2001).
2. Davids, J. R., Wagner, L. V., Meyer, L. C. & Blackhurst, D. W. Prosthetic management of

- children with unilateral congenital below-elbow deficiency. *J. Bone Jt. Surg. - Ser. A* **88**, 1294–1300 (2006).
3. Krebs, D. E. & Fishman, S. Characteristics of the child amputee population. *J. Pediatr. Orthop.* **4**, 89–95 (1984).
  4. Edmonds, L. D. *et al.* Congenital malformations surveillance: two American systems. *Int. J. Epidemiol.* **10**, 247–252 (1981).
  5. Biddiss, E. & Chau, T. Upper limb prosthesis use and abandonment: A survey of the last 25 years. *Prosthetics and Orthotics International* vol. 31 236–257 (2007).
  6. Vasluiian, E. *et al.* Opinions of Youngsters with Congenital Below-Elbow Deficiency, and Those of Their Parents and Professionals Concerning Prosthetic Use and Rehabilitation Treatment. *PLoS One* **8**, (2013).
  7. Postema, K., Van Der Donk, V., Van Limbeek, J., Rijken, R. & Poelma, M. J. Prosthesis rejection in children with a unilateral congenital arm defect. *Clin. Rehabil.* **13**, 243–249 (1999).
  8. Wagner, L. V., Bagley, A. M. & James, M. A. Reasons for Prosthetic Rejection by Children With Unilateral Congenital Transverse Forearm Total Deficiency. *J. Prosthetics Orthot.* **19**, 51–54 (2007).
  9. Egermann, M., Kasten, P. & Thomsen, M. Myoelectric hand prostheses in very young children. *Int. Orthop.* **33**, 1101–1105 (2009).
  10. Oliver, J., Dixon, C. & Murray, C. D. Being the parent of a child with limb difference who has been provided with an artificial limb: an interpretative phenomenological analysis. *Disabil. Rehabil.* **0**, 1–8 (2018).
  11. Franzblau, L. E. *et al.* Coping with Congenital Hand Differences. *Plast Reconstr Surg.* **135**, 1067–1075 (2015).
  12. Agur, A. M. R. & Lee, M. J. *Grant's Atlas of Anatomy*. (Lippincott Williams and Wilkins, 1999).
  13. Feix, T., Romero, J., Schmiedmayer, H. B., Dollar, A. M. & Kragic, D. The GRASP Taxonomy of Human Grasp Types. *IEEE Trans. Human-Machine Syst.* **46**, 66–77 (2016).
  14. Zheng, J. Z., De La Rosa, S. & Dollar, A. M. An Investigation of Grasp Type and Frequency in Daily Household and Machine Shop Tasks. in *IEEE International Conference on Robotics and Automation* (2011). doi:10.1109/TOH.2013.6.
  15. Belter, J. T., Segil, J. L., Dollar, A. M. & Weir, R. F. Mechanical design and performance specifications of anthropomorphic prosthetic hands: A review. *J. Rehabil. Res. Dev.* **50**, 599–618 (2013).

16. Battraw, M. A. *et al.* A Review of Upper Limb Pediatric Prostheses and Perspectives on Future Advancements. *Prosthet. Orthot. Int.* **46**, 267–273 (2022).
17. Kryger, M., Schultz, A. E. & Kuiken, T. Pattern recognition control of multifunction myoelectric prostheses by patients with congenital transradial limb defects: A preliminary study. *Prosthet. Orthot. Int.* **35**, 395–401 (2011).
18. Copeland, C., Mukherjee, M., Wang, Y., Fraser, K. & Zuniga, J. M. Changes in Sensorimotor Cortical Activation in Children Using Prostheses and Prosthetic Simulators. *Brain Sci.* **11**, (2021).
19. Da Paz, A. C. & Braga, L. W. Brain activation in a myoelectric prosthetic hand: The role of the brain in the rehabilitation of amputees. *J. Pediatr. Orthop.* **27**, 947–951 (2007).
20. Ten Kate, J., Smit, G. & Breedveld, P. 3D-printed upper limb prostheses: a review. *Disabil. Rehabil. Assist. Technol.* **12**, 300–314 (2017).
21. Llop-Harillo, I., Pérez-González, A., Starke, J. & Asfour, T. The Anthropomorphic Hand Assessment Protocol (AHAP). *Rob. Auton. Syst.* **121**, 103259 (2019).
22. Vujaklija, I., Farina, D. & Aszmann, O. New developments in prosthetic arm systems. *Orthop. Res. Rev.* (2016) doi:10.2147/ORR.S71468.
23. *ANSI/ISA Process Instrumentation Terminology, ANSI/ISA Standard 51.1.* (1979).
24. User Manual: SingleTact Miniature Force Sensors. [https://www.singletact.com/SingleTact\\_Manual.pdf](https://www.singletact.com/SingleTact_Manual.pdf) (2017).
25. High Accuracy, Galvanically Isolated Current Sensor IC With Small Footprint SOIC8 Package. <https://download.mikroe.com/documents/datasheets/ACS723.pdf> (2018).
26. Llop-Harillo, I., Pérez-González, A. & Andrés-Esperanza, J. Grasping Ability and Motion Synergies in Affordable Tendon-Driven Prosthetic Hands Controlled by Able-Bodied Subjects. *Front. Neurobot.* **14**, 1–15 (2020).
27. Cheng, I. F., Kuo, L. C., Lin, C. J., Chieh, H. F. & Su, F. C. Anthropometric Database of the Preschool Children from 2 to 6 Years in Taiwan. *J. Med. Biol. Eng.* **39**, 552–568 (2019).
28. Snyder, R. G. *et al.* *Anthropometry of Infants, Children, and Youths to Age 18.* (1977).
29. Brenneis, D. J. A., Dawson, M. R. & Pilarski, P. M. Development of the Handi Hand : an Inexpensive , Multi-Articulating , Sensorized Hand for Machine Learning Research in Myoelectric Control. in *Myoelectric Controls Symposium* (2017).
30. Featured Technology: Open Bionics Hero Arm. <https://hangerclinic.com/blog/featured-technology/open-bionics-hero-arm/#:~:text=The Hero Arm weighs less,the lightest bionic hand available.&text=Up to six easy-to,provide outstanding versatility and control> (2019).

31. Battraw, M. A., Young, P. R., Welner, M. E., Joiner, W. M. & Schofield, J. S. Characterizing Pediatric Hand Grasps During Activities of Daily Living to Inform Robotic Rehabilitation and Assistive Technologies. in *IEEE International Conference on Rehabilitation Robotics* (2022).
32. Hebert, J. S., Lewicke, J., Williams, T. R. & Vette, A. H. Normative data for modified box and blocks test measuring upper-limb function via motion capture. *J. Rehabil. Res. Dev.* **51**, 919–931 (2014).
33. Mathiowetz, V. & Weber, K. Adult Norms for the Box and Block. *Am. J. Occupational Ther.* **39**, 387–391 (1985).
34. Jebsen, R., Taylor, N., Trieschmann, R., Trotter, M. & Howard, L. An objective and standardized test of hand function. *Arch. Phys. Med. Rehabil.* **50**, 311–319 (1969).
35. Kyberd, P., Hussaini, A. & Maillet, G. Characterisation of the Clothespin Relocation Test as a functional assessment tool. *J. Rehabil. Assist. Technol. Eng.* **5**, 1–7 (2018).
36. Light, C. M., Chappell, P. H. & Kyberd, P. J. Establishing a standardized clinical assessment tool of pathologic and prosthetic hand function: Normative data, reliability, and validity. *Arch. Phys. Med. Rehabil.* **83**, 776–783 (2002).

## Chapter 5. The capacity of children with UCBED to actuate their affected muscles

The majority of this chapter has been published as:

Battraw MA, Fitzgerald J, James MA, Bagley AM, Joiner WM, Schofield JS. (2024). Understanding the capacity of children with congenital unilateral below-elbow deficiency to actuate their affected muscles. *Sci. Rep.*

### 5.1. Chapter preface

Children with unilateral congenital below-elbow deficiency (UCBED) display unique characteristics that may hinder the effective use of current dexterous prosthetic upper limb devices. These individuals were born without ever having actuated an intact hand; thus, before investigating dexterous prosthetic control techniques, this chapter aims to help further understand their ability to purposefully activate their affected muscles. This is an essential step since the control signals necessary for operating a dexterous prosthesis are derived from the affected muscle activity. Our investigation involves analyzing physiological signals of muscle electrical activity through surface electromyography (sEMG) as participants attempted a series of missing hand movements. Standard measures of amplitude and frequency were extracted from the sEMG data to understand participants' ability to consistently and reliably actuate their affected musculature. Furthermore, an investigation into movement distinguishability was performed to determine whether participants could actuate their muscles in patterned ways that can be linked to missing intended hand movements. Consistent and distinguishable patterns of affected muscle activity serve as a proxy for assessing the potential control of multiple hand movements with a prosthesis. In summary, this work provides a fundamental foundation for understanding the degree to which children with UCBED can actuate their affected musculature—a crucial step before exploring dexterous prosthetic control.

## 5.2. Introduction

Approximately 1 in 500 live births will present with an upper limb deficiency<sup>1</sup>, which is the most common reason for limb absence in children<sup>2</sup>. Among those born with upper limb deficiencies, children with unilateral congenital below-elbow deficiency (UCBED) will most typically present with limb characteristics amenable to prosthesis prescription. Although there are a variety of upper limb prostheses available for these children, they are regularly abandoned with 35%-45% of prescribed devices not being used<sup>3</sup>. In fact, these devices often fall short of meeting the wearers' needs and typically don't provide sufficient function and/or improve quality of life<sup>4</sup>. Encouragingly, dexterous prostheses that resemble the form and function of intact hands are becoming widely available for adults and more recently for children<sup>5,6</sup>. These devices achieve a variety of grasping movements and as a result, hold the potential to offer additional functional benefits. However, limited research has been performed to address and refine these systems for the unique challenges and demands of children.

With increased prosthetic dexterity comes the need for more sophisticated control systems to manage the newly available function. State-of-the-art control systems for adult prostheses use machine learning to predict the user's motor intent from patterns of muscle electrical activity (surface electromyography, sEMG) and map these predictions to corresponding prosthetic movements<sup>7-10</sup>. Despite promising results in adults with acquired amputation, few studies have been performed in those with congenital limb absence. One study recruited N = 4 adults with congenital limb absence and demonstrated limited success, applying sEMG and machine learning to predict 11 hand movements and finding classification accuracies of  $52.1\% \pm 15.0\%$ <sup>11</sup>. Additionally, in a cohort of children (N = 5, <21 years old) and adults (N = 2) with UCBED, a commercially available control system was used to predict missing limb movements<sup>12</sup>. Such

systems have been primarily designed for those with acquired limb loss and have yet to be refined for individuals with congenital limb differences. Only 2 of the 5 children demonstrated a classification accuracy greater than 80% for a limited repertoire of only 3 degrees of freedom<sup>12</sup>. Of these two publications, one studied and recruited children in a limited setting; however, an adult-specific prosthesis control system was employed which is unlikely to be directly applicable to children<sup>13</sup>. Collectively, these limitations restrict the translation of their findings to a more comprehensive understanding of affected muscle activity in children with UCBD.

The translation of advanced sEMG techniques to decode motor intent and control prostheses for children with UCBD requires a more thorough understanding of the capabilities of their affected muscles. sEMG characteristics such as root mean squared (RMS), moving average, linear envelope, mean frequency (MNF), and median frequency are often used to investigate the biological control an individual has over their limb(s)<sup>14-17</sup>. These characteristics have yet to be investigated in children born with limb absence and therefore the capacity for these children to actuate their affected muscles is unknown.

In this chapter, we investigated muscle activity using surface electromyography of children's affected and healthy unaffected-contralateral muscles while they attempted to perform a variety of hand movements. We evaluated measures of within-limb and across-limb consistency, and distinguishability using RMS and MNF measures. Our study had three main objectives to identify if children with UCBD could consistently and distinguishably actuate their affected muscles, and to examine how this actuation might compare to their unaffected side. First, we assessed children's ability to perform various distinguishable hand movements using split-data representational dissimilarity analysis, aiming to determine whether there was distinguishable structure in attempted movements. Second, we sought to quantify statistically significant differences in the

consistency of movements by comparing the affected and unaffected limbs. Lastly, we expanded our investigation to determine if a statistically significant relationship existed in the hand movement structure between the affected and unaffected limbs using representational dissimilarity randomization analysis.

### 5.3. Methods

#### 5.3.1. Participants

Nine participants (8 male, 1 female) with UCBD aged 8 to 20 years old participated in this study (mean = 14 years; SD = 4.4 years). Research protocols were approved by the Institutional Review Board at the Shriners Children’s – Northern California and were performed in accordance with the relevant guidelines and regulations. Participants provided written informed assent and/or their legal guardians provided written informed consent. Participant details can be found in Table 5-1. Additionally, participants exhibiting only a unilateral congenital upper limb deficiency in the forearm region were included. Children with UCBD otherwise underwent typical maturation and development. All potential candidates were clinically screened, and those with atypical development aside from UCBD were excluded. Therefore, we treated the data collected from the unaffected limb of each participant (described below) as a control for comparison.

Table 5-1. Demographic information for participants with unilateral congenital below-elbow deficiency. PA = Passive device. BP = Body-powered device. Myo = Myoelectric device. †Activity specific device.

Subject ID	Age	Sex	Affected Limb	Limb Length (cm)		Limb Circumference (cm)		Prosthesis Use
				Right	Left	Right	Left	
SHR-A	20	Male	Left		13		15	PA
SHR-B	8	Male	Right	14	16	20	21.5	PA
SHR-C	11	Male	Right	18	21	18	20	None
SHR-D	9	Male	Left	21.5	12.5	22.5	18.5	None
SHR-E	18	Male	Right	15	28	21	23	BP†
SHR-F	16	Female	Left	26.5	11.5	26.5	23.5	PA
SHR-G	19	Male	Left	26.5	13	25.5	21.5	Myo & PA
SHR-H	14	Male	Left	25	8	26	23	BP
SHR-I	12	Male	Right	10	24	21	24	BP



### 5.3.2. Data collection

A 16-Channel Delsys Trigno surface EMG System (Delsys, Natick, USA) was used to capture affected and unaffected forearm muscle activity. The system consisted of wireless Trigno Mini Sensors with an inter-electrode spacing of 10 mm and dual on-board differential references. The sEMG signal input was set to a range of  $\pm 11\text{mV}$  and the data were bandpass filtered at 20 Hz to 450 Hz<sup>18,19</sup>. A National Instruments USB-6210 data acquisition system (National Instruments Corp., Austin, USA) sampled sEMG data at 6,000 Hz and stored data in a MATLAB (MathWorks, Inc., Natick, USA) file structure for postprocessing and analysis. Additionally, a Logitech C922 high-definition camera (Logitech International S.A., Lausanne, Switzerland) sampled at 15 frames per second was synchronized with the sEMG data.

### 5.3.3. Experimental protocol

We first performed “conceptual training” with each participant in which we introduced our experimental equipment, described terminology used during testing, provided a simple overview of sEMG, and allowed them to familiarize themselves<sup>20</sup>. After, we adhered the sEMG electrodes to their skin over the affected and unaffected forearm muscles using double-sided adhesive. The participants were asked to contract their affected limb as if they were making a fist while we palpated to find where the superficial muscles on their ventral side were most firm and we placed the first sEMG electrode there. If participants had a small residual limb length, less than about 10 cm, then the first sEMG electrode was placed in the center of their residual limb starting on the ventral side. In either case, the remaining sEMG electrodes were placed around the circumference of the participants’ forearm muscles following the typical circumferential equidistant protocol<sup>21-23</sup>. This procedure was repeated in the unaffected limb and electrodes were placed on the most proximal two-thirds of the forearm musculature (Figure 5-1). As reported in prior work, 7 sEMG

electrodes were used on each side<sup>24</sup> (with the exception of SHR-A's affected limb where 4 sEMG electrodes were adhered due to size limitations).



Figure 5-1. Participants with sEMG electrodes donned across unaffected and affected limbs with sex and age in years old (y/o) specified.

Participants were then informed of which hand movement was to be performed and were allowed to familiarize themselves before proceeding to data collection. A strategic set of 10 hand movements was selected, which included commonly used hand grasps in daily living<sup>25</sup>, individual digit motions, and wrist movements: index flexion (IF), key pinch (KP), pulp pinch (PP), index point (IP), cylindrical wrap (CW), cylindrical wrap wrist rotate (CR), tripod pinch (TP), wrist extension (WE), wrist flexion (WF), and wrist rotation (WR) (Figure 5-2a). To ensure rich data sets for analysis of the muscle activity and due to the potential cognitive demands of attempting to

move their missing limb, 10 repetitions of each movement were performed. Participants were tasked with envisioning and attempting the prompted hand movement with their affected limb while simultaneously mirroring this action with their unaffected limb. Participants performed the 10 repetitions across 2 trials where a single trial began with the participant in the relaxed phase for 4 seconds followed by 3 seconds of contraction as indicated by an auditory tone. The relaxation (no tone) and contraction (tone) phases were repeated 5 times each in a single trial ([5 relaxations and contractions] \* 2 trials = 10 relax and contract repetitions for each hand movement). All participants were provided multiple opportunities for rest to mitigate fatigue. The structure of the experimental trials is illustrated in Figure 5-2b.

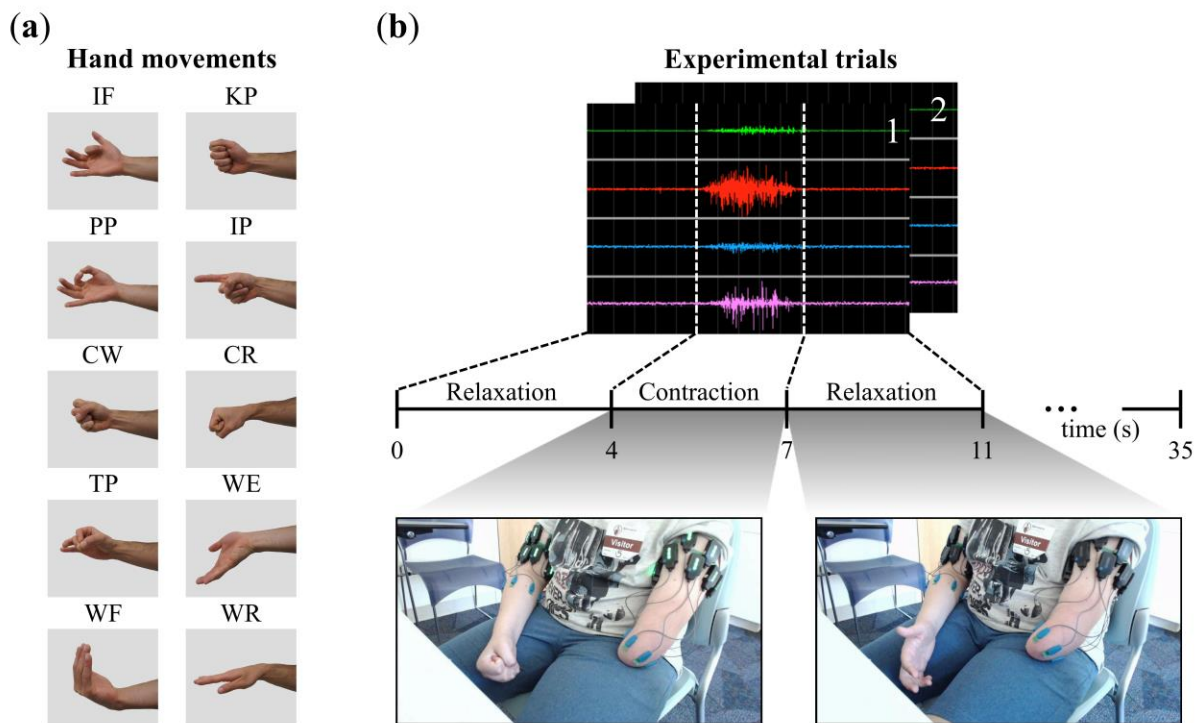


Figure 5-2. Overview of the experimental outline. (a) The 10 hand movements used in the experimental procedures. (b) An illustration of the experimental paradigm depicting a trial consisting of relaxation and contraction phases. There were two trials each consisting of alternating phases of four seconds of relaxation and three seconds of contraction for a total of ten contraction and relaxation phases across trials. Participant photo shows a cylindrical warp (CW) contraction and relaxation phase. Figure layout adapted from<sup>39</sup>.

#### 5.3.4. sEMG per-processing

A program was written in MATLAB to pre-process (condition) the data collected from the sEMG electrodes by first concatenating data across the 10 repetitions for individual movements. Additionally, to remove the effect of participant reaction times (i.e., from when they first hear the tone to when they contract their muscles), 15% of the data over the relevant time interval (contraction/relaxation) was discarded from both the onset and recession of the movement<sup>26</sup>.

We first performed analysis across sEMG channels, defined as the time-series voltage data produced from an individual sEMG electrode. From each channel, we assessed RMS and MNF characteristics, features that are commonly implemented and are sensitive to capturing the biological phenomenon of muscle excitation during hand movements<sup>15,27,28</sup>. For a given limb, movement, and sEMG channel the RMS and MNF were calculated with Equation 5-1 and 5-2, respectively. Where  $x_i$  is the  $i$ -th of  $N$  samples from a single conditioned contraction (3 s) or relaxation (4 s) repetition (e.g.  $N = 6,000 \text{ Hz} * 3 \text{ s} * 0.7 = 12,600$  samples for contraction)<sup>29</sup>. Additionally,  $f_j$  and  $p_j$  are the frequency variable and power spectrum, respectively, at a given bin  $j$  of  $M$  frequency bins<sup>29,30</sup>. The frequency range of interest was from 0-1,000 Hz, and the bin size was chosen as 0.4 Hz; therefore, the total number of bins was  $M = 2,500$ .

$$RMS = \sqrt{\frac{\sum_{i=1}^N x_i^2}{N}} \quad \text{Equation 5-1}$$

$$MNF = \frac{\sum_{j=1}^M f_j p_j}{\sum_{j=1}^M p_j} \quad \text{Equation 5-2}$$

For a given limb, the RMS and MNF were normalized to their corresponding maximum across all movements, on an individual channel basis. All data presented here is therefore a percentage of the maximum characteristic per channel.

## 5.4. Analysis

RMS and MNF characteristics were evaluated in both limbs. This included muscle excitation visualizations, investigating within-movement consistency with Kendall's Coefficient of Concordance<sup>31,32</sup> (see below for more details), and performing dissimilarity analysis to understand the distinguishability of hand movements. Furthermore, comparisons of hand movement consistency and the relatedness of movement characteristics across limbs with the RDM condition-label randomization analysis<sup>33</sup> were conducted. All analyses were performed on an individual participant basis.

### 5.4.1. Muscle excitation

#### 5.4.1.1. Visualization

The visualization of muscle excitation across hand movements and limbs was done to observe patterns in muscle activity across sEMG channels for RMS and MNF characteristics. The Shapiro-Wilk Test<sup>34</sup> was used to assess the normality of the RMS and MNF for each movement on an individual sEMG channel basis. This method was chosen due to its common application with limited sample sizes, as was the case in our study. The majority of the data were found to not be normally distributed. Therefore, all data were plotted using box and whisker plots for each sEMG channel and hand movement which included the relaxation phase.

#### 5.4.1.2. Movement excitation consistency

To understand the degree to which muscle excitation during individual movements were reproducible, measures of consistency were evaluated. We quantified the within-movement consistency given the RMS and MNF muscle excitation across sEMG channels for participants each time the same movement was performed. Due to the nonparametric nature of the RMS and MNF data, the within-movement consistency was determined with Kendall's Coefficient of

Concordance,  $W^{31,32}$ . This test produces a value of agreement from the ranked order of the 10 repetitions for RMS and MNF characteristics across the number of entities (sEMG channels). Therefore, Kendall's  $W$  provides a measure of agreement (with 0 indicating no agreement and 1 indicating complete agreement) in muscle excitation across sEMG channels (i.e., reproducibility of muscle excitation patterns.) The strength of agreement/consistency adapted from<sup>35-37</sup> are defined as:  $W < 0.20$  (poor consistency),  $0.20 \leq W < 0.40$  (minimal consistency),  $0.40 \leq W < 0.60$  (weak consistency),  $0.60 \leq W < 0.80$  (moderate consistency), and  $W \geq 0.80$  (strong consistency).

#### 5.4.1.3. Across movement dissimilarity

To examine the distinguishability of muscle response when children with UCBD attempted to perform each hand movement, the spread (given by the interquartile range (IQR)) and median amplitude of both RMS and MNF characteristics were analyzed. In literature, representational geometry is often applied to quantify the distinguishability in measures of physiological activity (e.g., sEMG, EEG, fMRI)<sup>33,38-40</sup> when participants are presented with different stimuli. Here, we applied and adapted the techniques outlined in<sup>33,38-40</sup> to assess the distinguishability of muscle excitation (sEMG channels). In this context, we treated the hand movements as the stimuli. Additionally, we illustrated this distinguishability through a qualitative visual representation.

To perform these analyses, a split-data representational dissimilarity matrix (sdRDM) was produced and analyzed. The data generated from performing a hand movement multiple times was first split into two equal data sets containing even and odd repetitions. Then the median and IQR of the RMS and MNF were obtained for each data set on a per-channel basis. Each entry of the sdRDM represented the rank-correlation distance between two data sets for every pair of hand movements across the sEMG channels. This distance was calculated from Kendall's Tau-b ( $\tau_b$ ) rank correlation coefficient, to account for ties, and is defined as  $(1 - \tau_b)$ . Kendall's correlation

coefficient was used to accommodate the fact that our data sets were not normally distributed when checked with the Shapiro-Wilk Test<sup>34</sup>. Here the “objects” of Kendall’s correlation coefficient test were defined as the median or IQR of the RMS or MNF for each sEMG channel (depending on which measure was being tested), and the two “variables” were any two pairs of hand movements. Additionally, a representational dissimilarity matrix (RDM) was produced as described above, without splitting the data into two datasets, and multidimensional scaling (MDS) was applied for visualization as adapted from<sup>41</sup>. A depiction of the dissimilarity dataflow as described above is given in Figure 5-3.

To determine a distinguishable structure of hand movements across the characteristics, the non-parametric RDM-level condition-label randomization test for exemplar discriminability index (EDI) was performed on the sdRDMs<sup>40</sup> (hereby referred to as the sdRDM analysis). The EDI was defined as the average between-exemplar dissimilarity estimate (the sdRDM off-diagonals) minus the average within-exemplar dissimilarity estimate (the sdRDM diagonal):  $EDI = \text{mean}(\text{between-exemplar dissimilarity}) - \text{mean}(\text{within-exemplar dissimilarity})$ , as adapted from<sup>40</sup>. A larger EDI was an indication that the hand movements may be more discriminable, and alternatively, smaller EDI values suggested hand movements are less discriminable. The sdRDM analysis consisted of simulating the null distribution by performing an exhaustive permutation of the rows of the sdRDM and calculating the EDI for every permutation. Therefore, we define the null hypothesis  $H_0$  as there being no structure to the data and pairwise distances of hand movements being equal (i.e., the intra-movement and inter-movement dissimilarities can be shuffled without change to the sdRDM structure). The EDI of the unshuffled sdRDM was then calculated and used to estimate the  $p$ -value by a proportion, i.e., by taking the EDIs in the null distribution that were greater than the unshuffled EDI. A significance level of  $\alpha = 0.05$  was used. A  $p$ -value less than this threshold

would indicate that there is significant structure in the data and that pairwise distances of hand movements are not equal. This would suggest that as participants performed missing hand movements the muscle excitation derived from these motions were distinguishable from one another.

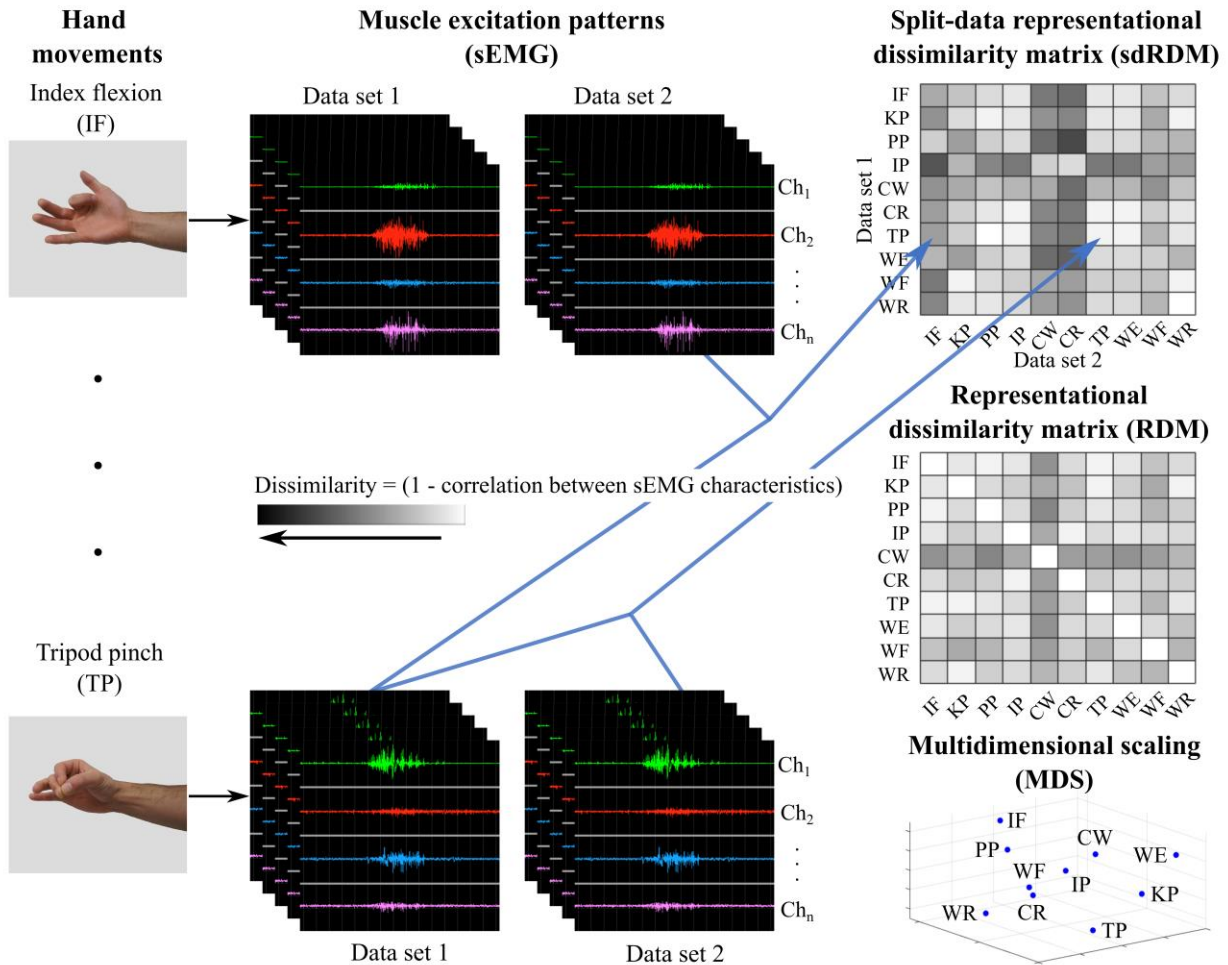


Figure 5-3. Dataflow to produce the split-data representation dissimilarity matrix (sdRDM) and RDM which are used to understand and visualize distinguishability. Participants attempted various hand movements, and muscle excitation was recorded through sEMG. Data for the sdRDM were split into two data sets containing even and odd trials, and measures of amplitude and spread were calculated from each. Then the sdRDM and RDM were produced with 1 minus the correlation between hand movements for split and unsplit data, respectively. As the dissimilarity increases the color gets darker and as it decreases the color gets lighter. The RDM was produced from unsplit data and used for multidimensional scaling (MDS) visualization and distinguishability across limbs (described further below).



To qualitatively visualize the distinguishability across hand movements, the RDM constructed from both data sets (i.e., unsplit data) was used and multidimensional scaling (MDS) was applied (Figure 5-3). MDS is a dimensionality reduction technique with the objective of reflecting the dissimilarity between items by projecting their distances in a lower dimensional space<sup>38</sup>. Nonmetric MDS was applied to the dissimilarity matrices (RDMs) through the MATLAB function *mdscale* with the squared stress criterion (*sstress*)<sup>39</sup>. The *statset* parameter for the maximum number of iterations (*MaxIter*) was increased to allow for convergence of the MDS solution.

#### 5.4.2. Differences across limbs

##### 5.4.2.1. Consistency across limbs

To further understand if the consistency of the children's affected muscle excitation was similar to that of their unaffected limb, across-limb comparisons were made. The previously-discussed within-movement consistency (across all hand movements), was used to determine overall consistency for each limb. Therefore, all movement consistencies for the affected limb were compared to all movement consistencies for the unaffected limb of a given participant. First, we assessed the normality for measures of consistency across the 10 movements for each limb with the Shapiro-Wilk Test<sup>34</sup>. Then, due to the non-parametric nature of the data, a Wilcoxon Signed Rank test with an  $\alpha = 0.05$  was used for comparisons. The null hypothesis,  $H_0$ , was defined such that the difference between the median movement consistency across the two limbs is zero. In this way, we were able to determine if there were any statistical differences in the participants' ability to attempt repeatable missing hand movements with their affected limb compared to their unaffected limb.

#### 5.4.2.2. Relatedness across limbs

In order to understand if attempted hand movements were related across the affected and unaffected limbs, measures of the RMS and MNF characteristics were evaluated with the non-parametric RDM label randomization analysis adapted from<sup>33</sup>. The affected limb RDM was selected, and 50,000 random permutations of both the rows and columns were performed. At each permutation, the RDM of the affected limb and the unaffected limb were compared with Kendall's Tau-a ( $\tau_a$ ) correlation, provided in the representational similarity analysis toolbox<sup>42</sup>, thereby allowing for simulation of the null distribution. The null hypothesis,  $H_0$ , is defined as two RDMs being unrelated. We calculated the correlation between two RDMs, which were subject to no label permutations, and found an estimate for the  $p$ -value through the proportion of correlations in the null distribution greater than the non-permuted correlation<sup>33</sup>. A significance level of  $\alpha = 0.05$  was selected and if the estimated  $p$ -value was less than the significance level then there was favor for the alternative hypothesis  $H_1$  that there is relatedness between the two RDMs. This suggests that the muscle excitation produced when participants performed missing hand movements is statistically related to that of their unaffected limb.

### 5.5. Results

#### 5.5.1. Muscle excitation

##### 5.5.1.1. Visualization

To visualize sEMG patterns across channels, the median RMS and MNF muscle excitation across limbs and hand movements were calculated as participants attempted to perform each motion (Figure 5-4, Figure 5-5, and Appendix B). For the RMS characteristic, the unaffected limb exhibited visual signs of normal muscle function. That is, as participants performed various movements, only a subset of sEMG channels recorded muscle excitation. This subset varied based on the attempted movement, indicating coordinated patterns of muscle excitation were being

enacted, which is considered normal in unaffected healthy limbs<sup>43</sup>. For example, during wrist extension and flexion, the extensor carpi radialis longus and flexor carpi radialis muscles are activated separately for each wrist movement<sup>43</sup>. A similar phenomenon can be seen in Figure 5-4 as exemplified by participant SHR-C and throughout participant data sets (Appendix B). Different patterns of sEMG activity were observed for the RMS characteristic across attempted hand movements of participants' affected limbs, thereby providing a visual indication of the extent to which children with UCBED could actuate their affected muscles. Interestingly, although not in all cases, when the participants were asked to attempt a hand movement with their affected limb the majority of sEMG channels recorded muscle excitation above the relaxed state (see Figure 5-4 and the RMS figures in Appendix B). Additionally, it is important to note that for some participants the affected limb RMS characteristic across the sEMG channels demonstrated relatively large degrees of variability, e.g., participant SHR-B produced a large RMS spread across sEMG channels for most hand movements (see Appendix B Figure B-3). In contrast, participant SHR-D had very few visual patterns of RMS muscle excitation with similar spread across movements. Therefore, we observed varied visual sEMG patterns of RMS muscle excitation across hand movements and participants. This visual inspection was crucial prior to performing statistical evaluations, particularly for identifying patterns within the sEMG voltage data. It played a key role in guiding the subsequent statistical analyses conducted in the proceeding sections.

For the MNF characteristic, patterns were illustrated in frequency-based muscle excitation for the unaffected and affected limbs among participants across sEMG channels. The MNF muscle excitation for both limbs showed parallels to their RMS counterparts. While the unaffected excitation differed across sEMG channels from movement to movement, the majority of the affected excitation was above the relaxed state, as illustrated by participant SHR-C in Figure 5-5

and Appendix B. Although there were variations in the degree of visual patterns for the RMS characteristics across movements, the MNF characteristics revealed additional patterns for most participants across both limbs (see MNF figures in Appendix B). This indicates that separately and together RMS and MNF characteristics may provide sufficient information to differentiate between hand movements.

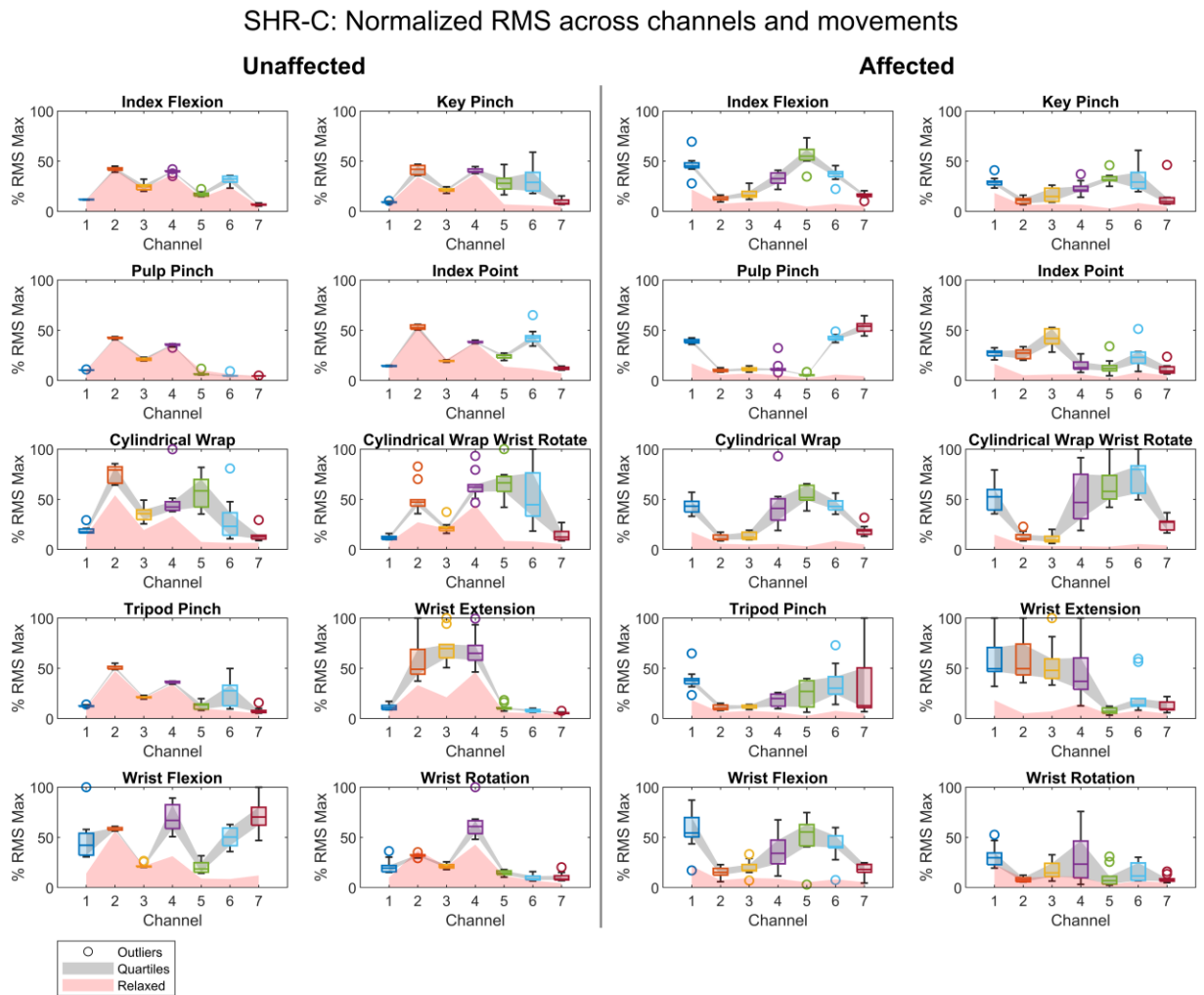


Figure 5-4. The box and whisker plots provide a visualization of the RMS muscle excitation patterns and relaxed states seen for the various hand movements across the unaffected and affected limbs for participant SHR-C.

## SHR-C: Normalized MNF across channels and movements

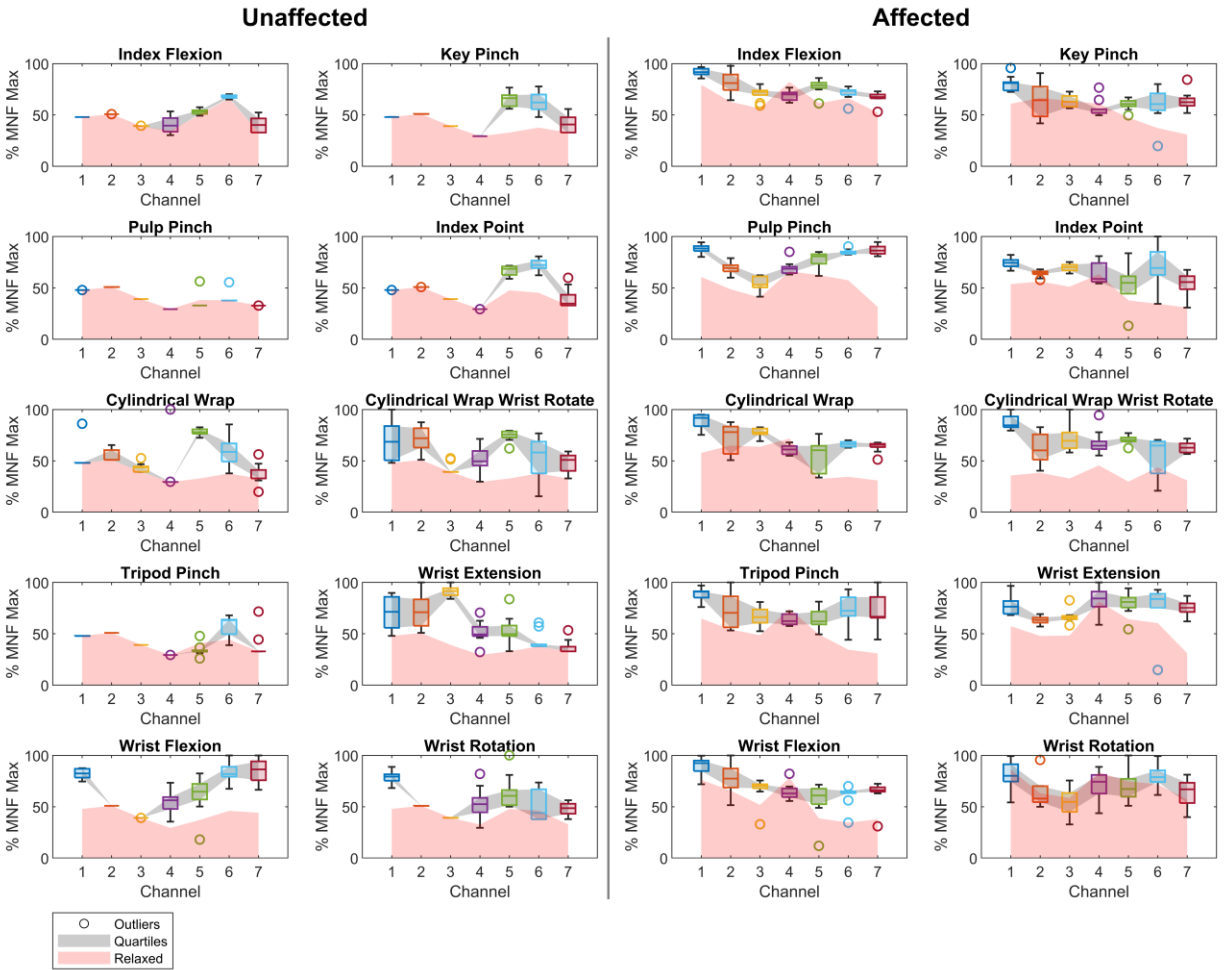


Figure 5-5. The box and whisker plots provide a visualization of the MNF muscle excitation patterns and relaxed states seen for the various hand movements across the unaffected and affected limbs for participant SHR-C.

### 5.5.1.2. Movement excitation consistency

Within-movement consistency was calculated from Kendall's Coefficient of Concordance,  $W$ , to quantify participants' ability to consistently perform patterns of RMS and MNF muscle excitation for each limb over the multiple trials of hand movements. Here consistencies ranged from  $W < 0.20$ ,  $0.20 \leq W < 0.40$ ,  $0.40 \leq W < 0.60$ ,  $0.60 \leq W < 0.80$ , and  $W \geq 0.80$  with poor, minimal, weak, moderate, and strong consistency, respectively. The definition of consistency in this work was adapted from<sup>35-37</sup> and represents a novel measure not previously applied in this context. These

values were utilized to demonstrate consistency and assess the affected limb in reference to the healthy, unaffected limb as a control. In general, for the unaffected limb, measures of consistency ranged from moderate to strong ( $0.60 \leq W \leq 0.99$ ), providing a baseline for healthy, typical, repetitive muscle actuation; few participants had poor to weak consistency ( $0.16 \leq W \leq 0.59$ ). Specifically, for the RMS consistency, all participants except for SHR-B had at least 9 hand movements with moderate to strong consistency i.e., a  $W$  of greater than 0.60. Interestingly, SHR-B had the top two lowest RMS consistencies in the unaffected limb for the movement-type cylindrical wrap with wrist rotated (CR) and cylindrical wrap (CW), with values of  $W = 0.25$  and  $W = 0.27$ , respectively. SHR-B only had 4 out of 10 hand movements with moderate to strong consistencies. Similarly, participant SHR-I had the third lowest consistency of  $W = 0.30$  for wrist flexion (WF). Alternatively, for the MNF unaffected limb within-movement consistency, all participants except SHR-B had moderate to strong consistency values for at least 5 hand movements while SHR-B had only 2. The top three lowest consistencies were present in participants SHR-F ( $W = 0.16$  for wrist extension (WE)), SHR-A ( $W = 0.21$  for pulp pinch (PP)), and SHR-B ( $W = 0.24$  for wrist rotation (WR)) in the poor to minimal consistency range. All hand movement consistency values for the unaffected limb can be seen in the first column of Figure 5-6.

When attempting to move their missing limb, participants were able to produce repeatable patterns of affected muscle excitation, although there was variability across participants. Repeatable patterns are an important facet for robust control of prostheses given that 6-9 common hand movements can account for nearly 80% of activities in daily living<sup>25,44</sup>, indicating the efficacy of prosthesis use in this population. When evaluating the RMS within-movement consistency in the affected limb, we found at least 5 of the 10 hand movements had moderate to strong consistency.

Here, participant SHR-A had the lowest consistency value of  $W = 0.14$  for the cylindrical wrap (CW). Participant SHR-B had the second and third lowest consistency values:  $W = 0.17$  in the cylindrical wrap (CW) and  $W = 0.22$  in the cylindrical wrap with wrist rotated (CR). Additionally, the MNF within-movement consistency for the affected limb showed that all participants except SHR-B had moderate to strong consistency values for 4 or more hand movements. SHR-G had the lowest consistency value of  $W = 0.13$  for index flexion (IF). Participant SHR-B had only 1 hand movement, wrist flexion (WF), with a moderate consistency value, and had the second through the sixth lowest consistency values from poor to weak. All other consistency values for the affected limb can be seen in the second column of Figure 5-6. Together, we see that 5 of 10 movements for RMS and 4 of 10 movements for MNF approached moderate to strong consistency (i.e., nearing the consistency for 6-9 hand movements). In conclusion, this may indicate that participants were able to perform reproducible attempted hand movements in their affected limb with a consistency range similar to that of their healthy unaffected limb ( $0.60 \leq W \leq 0.99$ ). Statistical comparisons of consistency measures are further investigated in section 5.5.3.1 to gain a deeper understanding of the differences across limbs.

### Within-movement consistency across participants

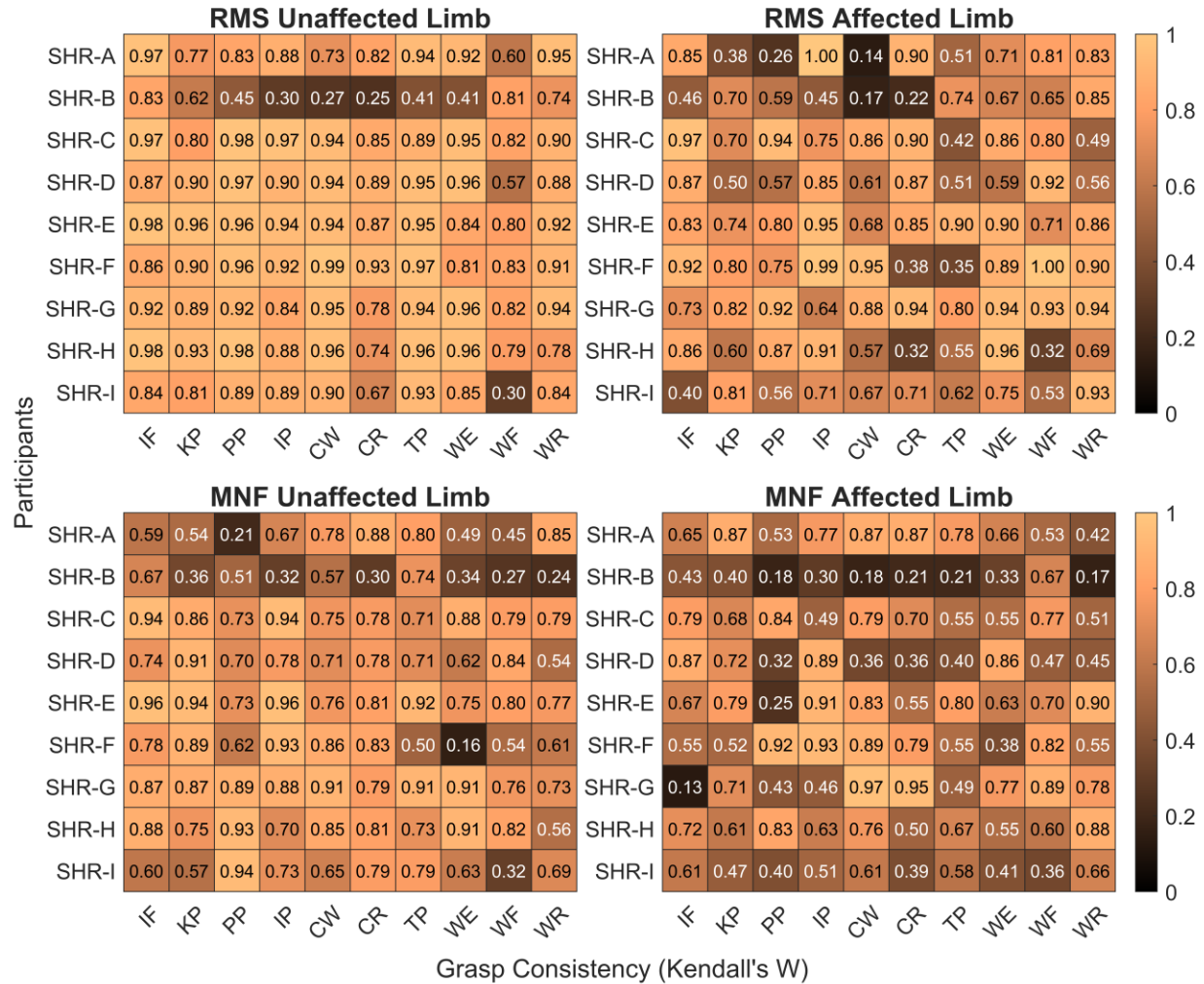


Figure 5-6. Within-movement consistency for median RMS and MNF data across repetitions obtained from Kendall’s Coefficient of Concordance, W. As the color gets darker this indicates a decrease in within-movement consistency, and the lighter the color an increase in consistency. The ranges of consistency are defined as  $W < 0.20$  (poor consistency),  $0.20 \leq W < 0.40$  (minimal consistency),  $0.40 \leq W < 0.60$  (weak consistency),  $0.60 \leq W < 0.80$  (moderate consistency), and  $W \geq 0.80$  (strong consistency).

#### 5.5.2. Across movement dissimilarity

To further understand whether the hand movements were dissimilar or distinguishable from one another, sDRDM analysis was performed. This assessment was motivated given the emergence of different muscle excitation patterns observed across hand movements in section 5.5.1.1. The objective was to determine whether there was sufficient information for distinguishable structure



across hand movements within the measures of RMS and MNF characteristics. The investigation of the median RMS and MNF enabled us to understand whether the central tendency of the hand movement muscle excitation exhibited distinguishable structure. Additionally, assessing the spread/variability (i.e., interquartile range (IQR)) of these characteristics allowed us to determine whether the reliability of hand movement muscle excitation also exhibited a distinguishable structure. Collectively, this analysis provided an indication of typical muscle excitation by assessing the distinguishability between movements for measures of RMS and MNF. It is noteworthy that typical muscle excitation involves the variability in sEMG signals across channels from task to task, or even within the same movement<sup>15</sup>. Furthermore, we employed multidimensional scaling (MDS) to qualitatively visualize the distinguishability across hand movements.

The sDRDM analysis of the median and IQR measures for RMS and MNF indicated that distinguishable structures of sEMG data were present when the participants with UCBD attempted to perform missing hand movements. This analysis also showed distinguishable structures of sEMG data were present in participants' unaffected limbs, as is expected of typical muscle contractions. However, this was not the case for all participants e.g., the analysis did not provide sufficient evidence to suggest there was a distinguishable structure for the median RMS of SHR-B's unaffected and affected limbs with  $p = 0.188$  and  $p = 0.267$ , respectively. Additionally, sDRDM analysis of the affected limb did not provide sufficient evidence to suggest a distinguishable structure for the following participants: SHR-D ( $p = 0.106$ , RMS IQR), SHR-F ( $p = 0.118$ , MNF IQR), and SHR-I ( $p = 0.163$ , RMS IQR). All other sDRDM analyses for the affected and unaffected limb showed a distinguishable structure of the hand movements; all  $p$ -values for each limb across participants and characteristics can be found in Table 5-2.

Table 5-2. Split-data representational dissimilarity analysis to distinguish the structure of amplitude and spread of RMS and MNF characteristics for participants (Par). \*Red  $p$ -values from the sDRDM analysis indicate a failure to reject the null hypothesis (i.e., there was not sufficient evidence to suggest a distinguishable structure of the hand movements), given a significance level of  $\alpha = 0.05$ . †Green EDI values indicate the maximum within a column. ‡Yellow EDI values indicate the minimum within a column.

Par	Unaffected				Affected			
	RMS EDI		MNF EDI		RMS EDI		MNF EDI	
	Median	IQR	Median	IQR	Median	IQR	Median	IQR
SHR-A	0.552 $p < 0.001$	0.483 $p < 0.001$	0.629 $p < 0.001$	0.235 $p = 0.005$	0.319 $p = 0.003$	0.459 $p = 0.006$	0.519 $p < 0.001$	0.452 $p < 0.001$
SHR-B	0.095‡ $p = 0.188^*$	0.546 $p < 0.001$	0.252‡ $p = 0.018$	0.728† $p < 0.001$	0.047‡ $p = 0.267^*$	0.256 $p = 0.036$	0.167‡ $p = 0.023$	0.510† $p < 0.001$
SHR-C	0.550 $p < 0.001$	0.472 $p < 0.001$	0.720 $p < 0.001$	0.377 $p < 0.001$	0.535 $p < 0.001$	0.294 $p = 0.003$	0.571 $p < 0.001$	0.423 $p < 0.001$
SHR-D	0.455 $p < 0.001$	0.463 $p < 0.001$	0.667 $p < 0.001$	0.205‡ $p = 0.020$	0.466 $p < 0.001$	0.114‡ $p = 0.106^*$	0.665† $p < 0.001$	0.199 $p = 0.015$
SHR-E	0.421 $p < 0.001$	0.453 $p < 0.001$	0.648 $p < 0.001$	0.235 $p = 0.007$	0.489 $p < 0.001$	0.273 $p < 0.001$	0.599 $p < 0.001$	0.212 $p = 0.018$
SHR-F	0.554 $p < 0.001$	0.459 $p < 0.001$	0.438 $p < 0.001$	0.603 $p < 0.001$	0.474 $p < 0.001$	0.254 $p = 0.004$	0.590 $p < 0.001$	0.119‡ $p = 0.118^*$
SHR-G	0.635† $p < 0.001$	0.578† $p < 0.001$	0.783† $p < 0.001$	0.449 $p < 0.001$	0.629† $p < 0.001$	0.519† $p = 0.002$	0.529 $p < 0.001$	0.303 $p = 0.007$
SHR-H	0.457 $p < 0.001$	0.368‡ $p < 0.001$	0.468 $p < 0.001$	0.214 $p = 0.007$	0.351 $p < 0.001$	0.212 $p = 0.008$	0.233 $p = 0.005$	0.364 $p < 0.001$
SHR-I	0.552 $p < 0.001$	0.497 $p < 0.001$	0.453 $p < 0.001$	0.366 $p < 0.001$	0.474 $p < 0.001$	0.116 $p = 0.163^*$	0.309 $p < 0.001$	0.180 $p = 0.021$

Further investigation of the sDRDM exemplar discriminability index (EDI) highlighted participants that may be good candidates for control of dexterous prostheses i.e., large amplitude-based (median) EDI values suggest increased distinguishability of prompted missing hand movements. Additionally, the large EDI values for IQR measures indicated two findings. First,

typical muscle excitation, which is indicative of distinguishable movements and therefore potentially effective control of dexterous prostheses. Second, variability may be too large across sEMG signals which may indicate poor consistency, upon which the muscle excitation plots and measures of consistency should be further investigated. Here, maximum and minimum EDI values are highlighted within the RMS or MNF measures for the unaffected and affected limbs across participants. SHR-G had the majority of maximum EDI values for 3 of the 4 measures of the unaffected limb and 2 of the 4 measures for the affected limb. In contrast, SHR-B had the majority of minimum EDI values for 2 of the 4 measures of the unaffected and affected limb, respectively. EDI values across limbs for measures of RMS and MNF are highlighted for each participant in Table 5-2.

To qualitatively visualize the differences across hand movements, the complete data set across trials (unsplit) was used to create the RDM for each limb. As previously mentioned, nonmetric MDS was used on each limb's RDM to reflect the higher dimensional distances across hand movements in a three-dimensional subspace. The MDS illustrated distinguishable differences between the various hand movements with few motions close and/or overlapping in the subspace as seen by the separation of points in the top panel of Figure 5-7a and b. Figure 5-7 shows both the median and IQR of RMS and MNF characteristics with the MDS (top) and corresponding RDM (bottom). Additionally, all MDS and RDM plots for participants can be seen in Appendix B. These results reveal, through a qualitative visualization, that the measures analyzed provide information to distinguish attempted hand movements by visual separation.

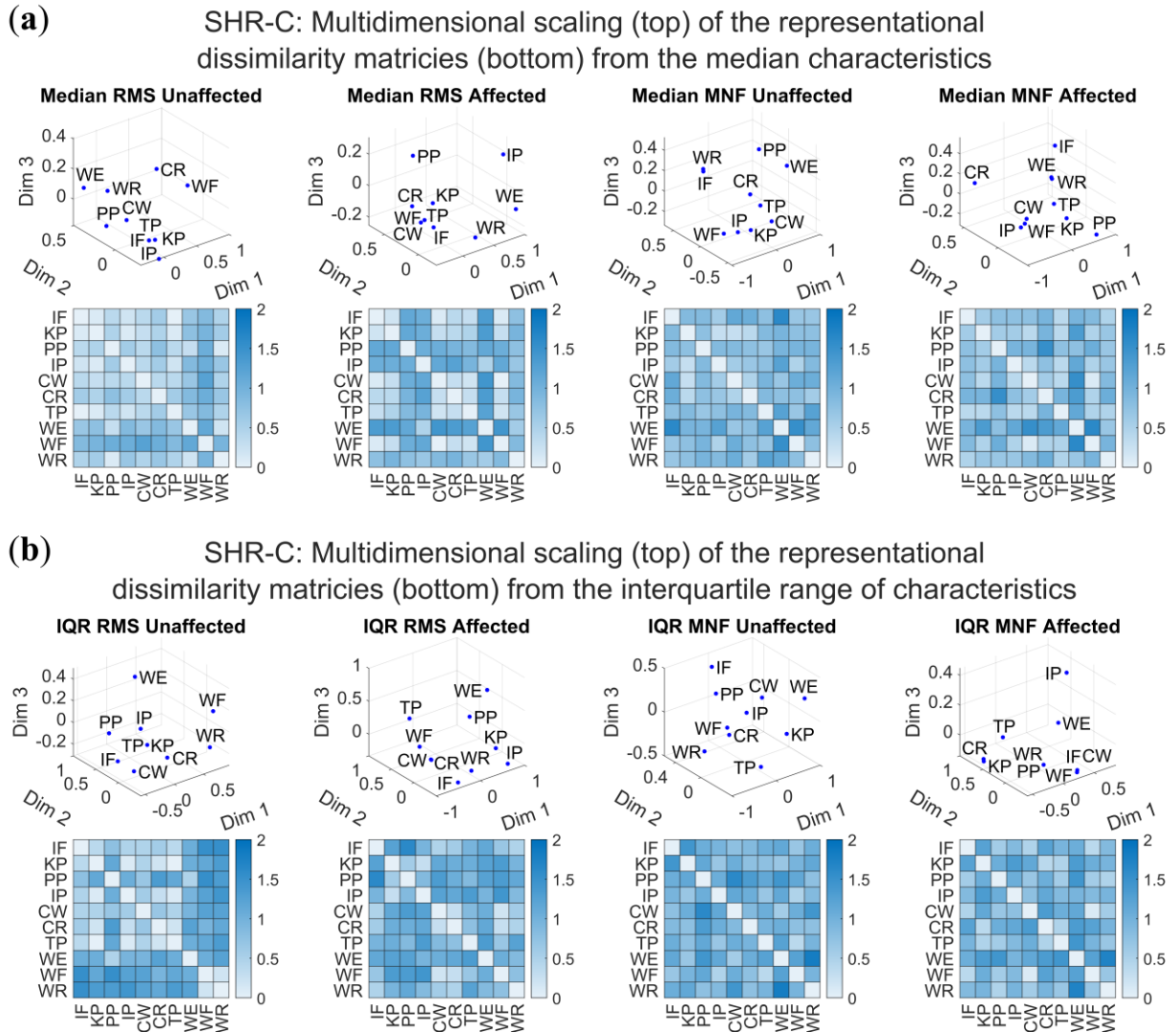


Figure 5-7. Visual representation of the correlation distances between hand movements for the amplitude and spread of measurement characteristics of SHR-C. The multidimensional scaling plots are provided in three dimensions corresponding to the representational dissimilarity matrices for **(a)** the median RMS and MNF characteristics and **(b)** the RMS and MNF interquartile range (IQR).

### 5.5.3. Differences across limbs

#### 5.5.3.1. Consistency across limbs

To get a better understanding of the differences in the participants' ability to attempt consistent hand movements with their affected limb, statistical comparisons were made to the consistency of their unaffected limb. We found RMS consistency in the affected limb to be statistically lower than the unaffected limb for participants SHR-A, C, D, E, and H. Alternatively for MNF,

participants SHR-C, SHR-E, and SHR-I had statistically lower consistency in the affected limb when compared to the unaffected limb. In each of the preceding cases, the unaffected limb had an overall higher median than the affected limb. The consistency for RMS and MNF across participants with highlighted statistical differences are shown in the top and bottom panels of Figure 5-8, respectively. The resulting consistencies in RMS and MNF across limbs (Figure 5-8) indicated that some participants had difficulty reproducing hand movements to a similar degree as that of their unaffected limb. This inability to reproduce movements, in turn, may hinder their potential to use multi-grasp prostheses.

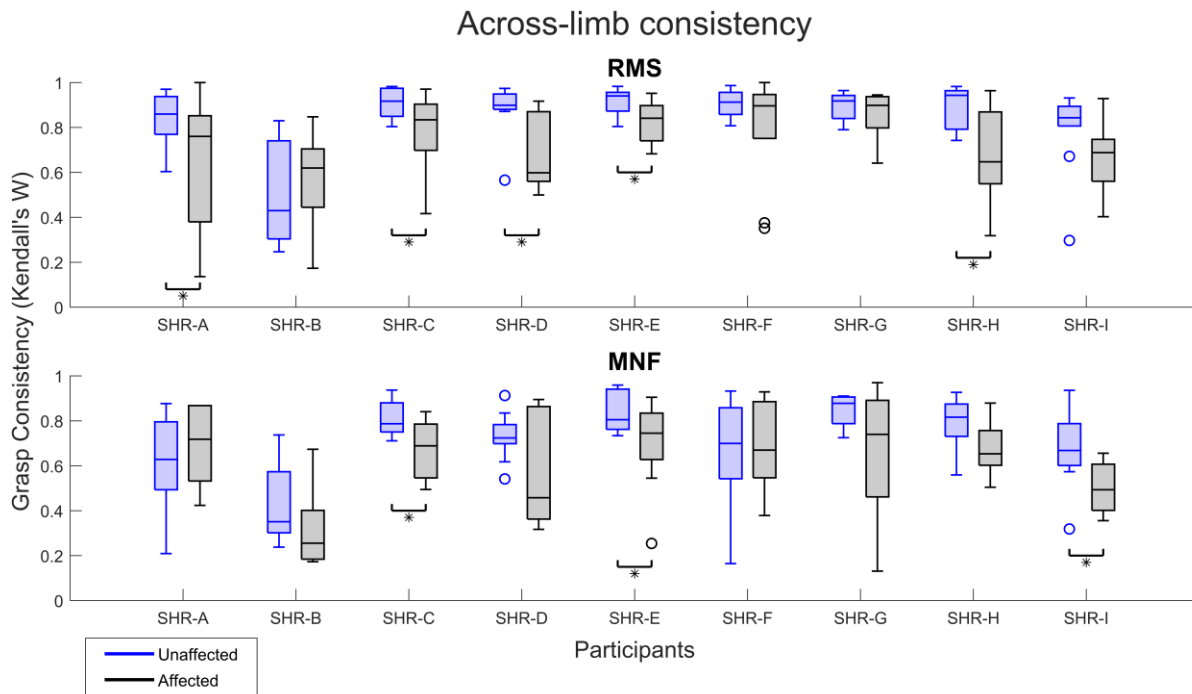


Figure 5-8. Comparison of across-limb consistency for the 10 hand movements. Participant comparisons are done with a Wilcoxon Signed Rank test given a significance level of  $\alpha = 0.05$ . Blue shading refers to the unaffected limb while black shading is for the affected limb. \*Represents those participants where the across-limb consistency was found to be in favor of the alternative hypothesis i.e., the difference in the median consistency across the two limbs was not zero.

### 5.5.3.2. Relatedness across limbs

To understand if the structure of the affected limb RDM was related to that of the unaffected limb, the non-parametric RDM label randomization test was used<sup>33</sup>. It was found that the majority of participants had some degree of shared information such that the pair-wise distances between hand movements for their affected limb were related to that of their unaffected limb. There was relatedness with the exception of the following participants: SHR-F ( $p = 0.060$ , RMS IQR), SHR-B ( $p = 0.055$ , median MNF), and SHR-F ( $p = 0.054$ , median MNF). Additionally, Table 5-3 shows the non-permuted Kendall's Tau-a ( $\tau_a$ ) correlations used for the RDM test with corresponding  $p$ -values. These results indicate that the majority of participants had related information across limbs for amplitude and spread of RMS and MNF characteristics.

Table 5-3. Relatedness of RDMs across limbs for each participant. The correlation and  $p$ -values for the amplitude and spread of RMS and MNF characteristics are provided. \*Red cells highlight values from the RDM label randomization test, which indicate there was not sufficient evidence for the relatedness across limbs (with a significance level of  $\alpha = 0.05$ ).

Participant	RDM Relatedness Across Limbs			
	RMS Correlation		MNF Correlation	
	Median	IQR	Median	IQR
SHR-A	0.219 $p = 0.002$	0.266 $p = 0.001$	0.234 $p = 0.002$	0.288 $p < 0.001$
SHR-B	0.401 $p < 0.001$	0.182 $p = 0.015$	0.119 $p = 0.055^*$	0.381 $p < 0.001$
SHR-C	0.255 $p = 0.005$	0.159 $p = 0.017$	0.318 $p < 0.001$	0.293 $p < 0.001$
SHR-D	0.272 $p < 0.001$	0.215 $p = 0.005$	0.180 $p = 0.008$	0.364 $p = 0.001$
SHR-E	0.465 $p < 0.001$	0.262 $p < 0.001$	0.298 $p = 0.001$	0.254 $p < 0.001$
SHR-F	0.200 $p = 0.005$	0.116 $p = 0.060^*$	0.123 $p = 0.054^*$	0.200 $p = 0.003$
SHR-G	0.439 $p < 0.001$	0.349 $p < 0.001$	0.204 $p = 0.002$	0.301 $p < 0.001$
SHR-H	0.224 $p = 0.014$	0.158 $p = 0.013$	0.423 $p < 0.001$	0.200 $p = 0.005$
SHR-I	0.179 $p = 0.007$	0.144 $p = 0.030$	0.202 $p = 0.011$	0.137 $p = 0.023$

## 5.6. Discussion

This chapter investigated the extent to which affected muscles respond when children with UCBED attempted to perform various hand movements. We have shown that even though these children were born with limb deficiency and have never used their affected muscles to actuate an intact limb there is still patterned, consistent, and distinguishable muscle activity in response to attempted missing hand movements.

### 5.6.1. Visible patterns of muscle excitation

Across most participants, different sEMG patterns of muscle excitation for both RMS and MNF characteristics were seen in the affected limb indicating their ability to excite coordinated muscle excitation as they attempted the various hand movements (Figure 5-4, Figure 5-5, and Appendix B). Furthermore, as expected in the unaffected limb, there were differences in muscle excitation as captured across sEMG channels. Although this was true for many participants' affected limbs, it was not true for all. For example, SHR-A had few visual patterns in their RMS muscle excitation across attempted hand movements, which can be seen in Appendix B Figure B-1. This finding is likely attributed to the affected limb circumference (15 cm) and length (13 cm), the smallest circumference out of the entire cohort. Therefore, due to the size, it is doubtful that the participant has developed similar muscular structure and mass to those participants with longer affected limbs. Additionally, participant SHR-B showed a large interquartile range in RMS muscle excitation in their affected limb and interestingly, similar results were also observed in their unaffected limb. This large spread in data across the hand movements and limbs was likely attributed to the child's age, as they were the youngest (8 years old) among our participants; their short attention span for the experimental task thereby affected movement reproducibility. Finally, when viewing participant SHR-D there was apparent muscle excitation, although few visual patterns emerged in

the affected limb for both RMS and MNF characteristics across the attempted hand movements. Although we believe that the limited observed patterns and large spread across data may have been attributed to a premature sensory-motor system in participants SHR-B and SHR-D, given their ages (8 and 9 years old, respectively) and the fact that their limbs have not fully developed, further investigation is required. This would involve larger cohorts spanning various ages and limb lengths to quantify these effects. Though it is clear that most participants can generate coordinated muscle activation in their affected side, it also appears that limb size may be a relevant factor in detecting muscle activity. Furthermore, age and cognitive factors such as attention spans may also be important in the reproducibility of muscle excitation and ultimately the efficacy of advanced prosthesis control systems.

#### 5.6.2. Reproducible attempted hand movements

The participants' ability to reproduce attempted hand movements was explored through measures of within-movement consistency. The unaffected limb exhibited quantitatively higher consistency than that of the affected limb. However, when comparing the median consistency across limbs for each participant, only a few measures were found to be significantly different (Figure 5-8). One exception was participant SHR-B who had the lowest consistency across both limbs for RMS and MNF characteristics, which aligns with the visualization of muscle excitation that depicted large interquartile ranges across sEMG channels (see Appendix B Figures B-3 and B-4). Additionally, the MNF consistency was quantitatively lower than that of the RMS across participants. This finding may be attributed to MNF itself because although it is a robust measure of muscle excitation, it is often used as an assessment of and is sensitive to muscle fatigue<sup>15,28</sup>. Even though participants were given multiple rest periods, it is possible they became fatigued at various stages which would explain our findings. Fatigue may be particularly relevant in this cohort given that



despite consistent patterns of movement-to-movement muscle excitation, the activity may be deemed as physically demanding because they have never contracted their affected muscles in these repeatable, distinct ways. However, MNF remains a relevant measure for investigating muscle excitation in this unique population, as it is commonly employed when assessing alternative measures of physiological muscle activity<sup>28</sup>. Additionally, participants' ability to produce repeatable patterns of muscle excitation in their affected limb suggests the potential for the use of multi-grasp prostheses. From this, it follows that given proper training, consistency is expected to approach that of their unaffected limb (i.e., nearing the consistency for 6-9 hand movements). Aside from training, an investigation into optimal sEMG characteristics, apart from RMS and MNF, should be explored for device control. The effects of physical conditioning, training, fatigue, and optimal sEMG characteristics are all important considerations for the use of advanced prostheses and muscle-based control systems in this population.

### 5.6.3. Distinguishable attempted hand movements

There was a distinguishable structure to the RMS and MNF characteristics in the affected limb for the majority of the participants (Table 5-2). Moreover, there was a degree of relatedness across limbs as children attempted missing hand movements (Table 5-3). However, this was not true for all participants. For example, participant SHR-B did not show a distinguishable structure for median RMS and relatedness for the median MNF across limbs, as previously shown in the results. This may support the large spread seen in the muscle excitation across sEMG channels and the lack of consistency in hand movements for this individual participant (see Appendix B Figures B-3 and B-4). As discussed previously, these findings are likely attributed to factors of age and limb size. For measures of spread, some participants did not demonstrate a distinguishable structure (i.e., SHR-D and SHR-I for RMS IQR, and SHR-F for MNF IQR). Moreover, for the latter (SHR-

F), we did not find that the pair-wise distances between hand movements for the RMS IQR measures were related across limbs. We found muscle excitation was conceivably both distinguishable across movements and related across limbs as a result of participants simultaneously mirroring hand movements. Accordingly, participants were trying to imagine performing the same movement to the same degree with every repetition. As a result, this still strongly indicates children's potential ability to actuate their affected muscles in distinguishable and consistent patterns, and with proper training may be able to effectively control dexterous prostheses.

The EDI values (Table 5-2) provided additional insight into the distinguishability of the muscle excitation structure. To note, participant SHR-G had the majority of maximum EDI values across all participants and limbs. This was likely attributed to a more mature sensory-motor system as the participant was 19 years old and uses a myoelectric prosthesis; that is, they control their device using the sEMG of their affected muscles. Although not a pattern recognition sEMG control system that necessitated contraction of their affected muscles in unique patterns, this participant still used 2-site control that required isolation and contraction of larger muscle groups in their affected limb. Presumably, this may have ameliorated their ability to generate consistent distinguishable muscle excitation patterns when prompted during the experiment. Participant SHR-B had a majority of the lowest EDI values across limbs, which parallels the previously discussed consistency and distinguishability results. Undoubtedly, these two participants can allow us to begin understanding the variability that may be present in this population of children and also provides a further appreciation for the improvements possible with regular prosthesis use and actuation of affected muscles through training.

The multidimensional scaling (MDS) plots are useful to visualize the distinguishability of the various hand movements. Although most participants showed a distinguishable structure across movements (see figures in Appendix B), there were a few exceptions. The RMS and MNF correlation distances between hand movements were determined by the median across repetitions. If a participant had low movement consistency the median would not be useful to define the motion, and the RDM and MDS plots would not demonstrate the distinguishability of hand movements. We can see this clearly demonstrated in participant SHR-B, who exhibited poor RMS and MNF consistency measures of muscle excitation for both the affected and unaffected limb.

## 5.7. Conclusions

We have shown in a limited cohort of children with UCBED that they possess a degree of biological control over their affected muscles with the ability to perform consistent and distinguishable hand movements. However, not all participants were able to achieve this degree of biological control over their affected muscles which may have been attributed to age and limb size, since cognitive demands and robust musculature are important to achieve meaningful muscle activation. A limitation of this study that could have affected the results was that we did not have a cohort of age- and sex-matched able-bodied participants to serve as a ground truth control for typical muscle excitation. Nevertheless, the participants underwent typical development and maturation, aside from their affected limb, allowing their unaffected limb to serve as an internal control for comparison. Our findings also suggest that children with UCBED may have the ability to use advanced prosthesis control systems. However, further work is needed to examine age and limb size with larger cohorts and more statistical power to effectively adapt, translate, and prescribe dexterous prostheses to the pediatric population. The bulk of literature for dexterous upper limb prosthetic devices is saturated in adult-based control systems using sEMG. Very

limited success has been found in prior studies with UCBED cohorts<sup>11,12</sup>. Moreover, these studies either did not investigate populations of children or simply applied commercially available control systems that were built on research and refinement in populations with acquired amputations. Our work shows distinguishable and consistent patterns of muscle excitation found in children with UCBED when they attempt to perform hand movements. We suggest that these findings warrant further investigation into techniques to best tune, adapt, and leverage existing advanced control techniques, such that they may be most effective in meeting the unique demand of children, most of whom will have a congenital upper limb absence<sup>2</sup>.

## 5.8. References

1. Giele, H., Giele, C., Bower, C. & Allison, M. The incidence and epidemiology of congenital upper limb anomalies: A total population study. *J. Hand Surg. Am.* **26**, 628–634 (2001).
2. Atkins, D. J., Heard, D. C. Y. & Donovan, W. H. Epidemiologic overview of individuals with upper-limb loss and their reported research priorities. *J. Prosthetics Orthot.* **8**, 2–11 (1996).
3. Biddiss, E. & Chau, T. Upper limb prosthesis use and abandonment: A survey of the last 25 years. *Prosthetics and Orthotics International* vol. 31 236–257 (2007).
4. James, M. A. *et al.* Impact of prostheses on function and quality of life for children with unilateral congenital below-the-elbow deficiency. *J. Bone Jt. Surg. - Ser. A* **88**, 2356–2365 (2006).
5. Battraw, M. A., Young, P. R., Joiner, W. M. & Schofield, J. S. A multiarticulate pediatric prosthetic hand for clinical and research applications. *Front. Robot. AI* **9**, 1–14 (2022).
6. Ten Kate, J., Smit, G. & Breedveld, P. 3D-printed upper limb prostheses: a review. *Disabil. Rehabil. Assist. Technol.* **12**, 300–314 (2017).
7. Dellacasa Bellingegni, A. *et al.* NLR, MLP, SVM, and LDA: A comparative analysis on EMG data from people with trans-radial amputation. *J. Neuroeng. Rehabil.* **14**, 1–16 (2017).
8. Kuiken, T. A., Miller, L. A., Turner, K. & Hargrove, L. J. A Comparison of Pattern Recognition Control and Direct Control of a Multiple Degree-of-Freedom Transradial Prosthesis. *IEEE J. Transl. Eng. Heal. Med.* **4**, (2016).
9. Resnik, L. *et al.* Evaluation of EMG pattern recognition for upper limb prosthesis control: A case study in comparison with direct myoelectric control. *J. Neuroeng. Rehabil.* **15**, 1–

- 13 (2018).
10. Scheme, E. & Englehart, K. Electromyogram pattern recognition for control of powered upper-limb prostheses: State of the art and challenges for clinical use. *J. Rehabil. Res. Dev.* **48**, 643–660 (2011).
  11. Kryger, M., Schultz, A. E. & Kuiken, T. Pattern recognition control of multifunction myoelectric prostheses by patients with congenital transradial limb defects: A preliminary study. *Prosthet. Orthot. Int.* **35**, 395–401 (2011).
  12. Kaluf, B., Gart, M. S., Loeffler, B. J. & Gaston, G. Evaluating the Ability of Congenital Upper Extremity Amputees to Control a Multi-Degree of Freedom Myoelectric Prosthesis. *J. Hand Surg. Am.* **47**, 1019.e1-1019.e9 (2022).
  13. Battraw, M. A. *et al.* A Review of Upper Limb Pediatric Prostheses and Perspectives on Future Advancements. *Prosthet. Orthot. Int.* **46**, 267–273 (2022).
  14. Roman-Liu, D. & Bartuzi, P. Influence of type of MVC test on electromyography measures of biceps brachii and triceps brachii. *Int. J. Occup. Saf. Ergon.* **24**, 200–206 (2018).
  15. Motion Lab System, EMG Analysis and EMG Graphing Software User Tutorial. <http://www.c3d.org-http://www.motion-labs.com> (2009).
  16. Farina, D., Merletti, R. & Enoka, R. M. The extraction of neural strategies from the surface EMG. *J. Appl. Physiol.* **96**, 1486–1495 (2004).
  17. Barak, Y., Ayalon, M. & Dvir, Z. Spectral EMG changes in vastus medialis muscle following short range of motion isokinetic training. *J. Electromyogr. Kinesiol.* **16**, 403–412 (2006).
  18. Englehart, K. & Hudgins, B. A Robust, Real-Time Control Scheme for Multifunction Myoelectric Control. *IEEE Trans. Biomed. Eng.* **50**, 848–854 (2003).
  19. Khushaba, R. N., Kodagoda, S., Takruri, M. & Dissanayake, G. Toward improved control of prosthetic fingers using surface electromyogram (EMG) signals. *Expert Syst. Appl.* **39**, 10731–10738 (2012).
  20. Simon, A. M., Lock, B. A. & Stubblefield, K. A. Patient training for functional use of pattern recognition-controlled prostheses. *J. Prosthetics Orthot.* **24**, 56–64 (2012).
  21. Hargrove, L. J., Li, G., Englehart, K. B. & Hudgins, B. S. Principal components analysis preprocessing for improved classification accuracies in pattern-recognition-based myoelectric control. *IEEE Trans. Biomed. Eng.* **56**, 1407–1414 (2009).
  22. Scheme, E. J., Englehart, K. B. & Hudgins, B. S. Selective classification for improved robustness of myoelectric control under nonideal conditions. *IEEE Trans. Biomed. Eng.* **58**, 1698–1705 (2011).
  23. Sensinger, J. W., Lock, B. A. & Kuiken, T. A. Adaptive Pattern Recognition of Myoelectric Signals: Exploration of Conceptual Framework and Practical Algorithms. *IEEE Trans Neural Syst Rehabil Eng.* **17**, 270–278 (2009).

24. Young, A. J., Hargrove, L. J. & Kuiken, T. A. Improving myoelectric pattern recognition robustness to electrode shift by changing interelectrode distance and electrode configuration. *IEEE Trans. Biomed. Eng.* **59**, 645–652 (2012).
25. Zheng, J. Z., De La Rosa, S. & Dollar, A. M. An Investigation of Grasp Type and Frequency in Daily Household and Machine Shop Tasks. in *IEEE International Conference on Robotics and Automation* (2011). doi:10.1109/TOH.2013.6.
26. Ortiz-Catalan, M., Brånemark, R. & Håkansson, B. BioPatRec: A modular research platform for the control of artificial limbs based on pattern recognition algorithms. *Source Code Biol. Med.* **8**, 1–18 (2013).
27. Asghari Oskoei, M., Member, S., Hu, H. & Member, S. Support Vector Machine-Based Classification Scheme for Myoelectric Control Applied to Upper Limb. *IEEE Trans. Biomed. Eng.* **55**, (2008).
28. Phinyomark, A., Thongpanja, S., Hu, H., Phukpattaranont, P. & Limsakul, C. The Usefulness of Mean and Median Frequencies in Electromyography Analysis. in *Computational Intelligence in Electromyography Analysis – A Perspective on Current Applications and Future Challenges* (ed. Naik, G. R.) 195–220 (In Tech, 2012). doi:10.5772/50639.
29. Abbaspour, S., Lindén, M., Gholamhosseini, H., Naber, A. & Ortiz-Catalan, M. Evaluation of surface EMG-based recognition algorithms for decoding hand movements. *Med. Biol. Eng. Comput.* **58**, 83–100 (2020).
30. Phinyomark, A., Phukpattaranont, P. & Limsakul, C. Feature reduction and selection for EMG signal classification. *Expert Syst. Appl.* **39**, 7420–7431 (2012).
31. Siegel, S. *Nonparametric Statistics for the Behavioral Sciences*. (McGraw-Hil, 1956).
32. Field, A. P. Kendall’s Coefficient of Concordance. *Encyclopedia of Statistics in Behavioral Science* vol. 2 1010–1011 (2005).
33. Kriegeskorte, N., Mur, M. & Bandettini, P. Representational similarity analysis - connecting the branches of systems neuroscience. *Front. Syst. Neurosci.* **2**, 1–28 (2008).
34. Ipek. Normality test package. *MATLAB Central File Exchange* <https://www.mathworks.com/matlabcentral/fileexchange/60147-normality-test-package> (2022).
35. O’Neill, T. A. An overview of interrater agreement on likert scales for researchers and practitioners. *Front. Psychol.* **8**, (2017).
36. Landis, J. R. & Koch, G. G. The Measurement of Observer Agreement for Categorical Data. *Biometrics* **33**, 159–174 (1977).
37. Krippendorff, K. *Content Analysis An Introduction to Its Methodology*. *Physical Review B* vol. 31 (SAGE Publications, Incorporated, 2004).
38. Kriegeskorte, N. & Kievit, R. A. Representational geometry: Integrating cognition, computation, and the brain. *Trends Cogn. Sci.* **17**, 401–412 (2013).

39. Sburlea, A. & Muller-Putz, G. Exploring representations of human grasping in neural, muscle and kinematic signals. *Sci. Rep.* **8**, (2018).
40. Nili, H., Walther, A., Alink, A. & Kriegeskorte, N. Inferring exemplar discriminability in brain representations. *PLoS One* **15**, (2020).
41. Kruskal, J. B. & Wish, M. Multidimensional Scaling. (1978).
42. Nili, H. *et al.* A Toolbox for Representational Similarity Analysis. *PLoS Comput. Biol.* **10**, (2014).
43. Kasman, G. & Wolf, S. *Surface emg made easy: A beginner's Guide for Rehabilitation Clinicians*. (Noraxon USA, Inc, 2002).
44. Feix, T., Romero, J., Schmiedmayer, H. B., Dollar, A. M. & Kragic, D. The GRASP Taxonomy of Human Grasp Types. *IEEE Trans. Human-Machine Syst.* **46**, 66–77 (2016).

## Chapter 6. Decoding hand motor intent in children with UCBD

The majority of this chapter has been submitted for review as:

Battraw MA, Fitzgerald J, Winslow E, James MA, Bagley AM, Joiner WM, Schofield JS. (2024). Surface electromyography evaluation for decoding motor intent in children with congenital upper limb deficiency. *Sci. Rep.* Under Review.

### 6.1. Chapter preface

The evaluation of surface electromyography (sEMG) to decode hand motor intent in children with unilateral congenital below-elbow deficiency (UCBED) is presented in this chapter. There are various sEMG signal characteristics (features) that can be extracted from the time domain, frequency domain, and time-frequency domain to enhance the decoding of hand motor intent. Common feature sets derived from sEMG data of able-bodied adults have been developed and employed to decode movements in adults with acquired limb loss. However, since children with UCBD were born with limb absence, it is unclear if these adult-based feature sets can be readily applied to provide optimal movement decoding. Additionally, the ability to decode with higher accuracy may come with the tradeoff of increased training and testing times. This poses relevant potential limitations, as time delays may promote user frustration and contribute to device rejection. Moreover, individuals using dexterous upper limb devices will typically employ a subset of grasp movements rather than wanting to use the full range of grasps offered by the device—a practical consideration for multi-grasp prostheses. To address these limitations, within this chapter, we systematically tuned classification algorithms with a large set of features to understand which sEMG signal characteristics maximized classification performance. Subsequently, we determined the training and testing times and assessed them in consideration of practical time limitations to avoid user frustration. Finally, we generated small subsets of grasp movements that provided optimal classification performance. The work presented within this chapter provides an essential



foundation for the next steps in real-time control of multi-grasp prostheses among children with UCBED.

## 6.2. Introduction

Unilateral congenital below-elbow deficiency (UCBED) is the absence of an upper limb that occurs at the anatomical region between the proximal to distal segments of the forearm<sup>1</sup>. To those afflicted, this condition can pose significant challenges in psychosocial and physical functioning while they interact within their daily environments<sup>2</sup>. The naturalistic motor control of advanced dexterous prosthesis utilizing surface electromyography (sEMG, the measurement of the residual muscle's electrical activity) has yet to be fully investigated for children with UCBED. As these children were born never having actuated a hand, and their muscles and limbs never fully developed, prosthesis control presents with a variety of considerations that are unique from adults or other children that acquired their limb absence later in life. For example, there has been very limited study on how the muscle activity of their affected limbs may manifest especially when attempting to move the missing hand for prosthetic control purposes. This presents a limitation in the effective implementation of dexterous upper limb devices and drives the need to explore, adapt, and leverage current adult-based technologies to improve the motor control possibilities for prostheses offered to children with UCBED.

Previous work has shown that children with UCBED have a degree of biological control over their affected musculature i.e., when they attempted various missing hand movements there was measurable consistency and distinguishability of sEMG muscle excitation<sup>3</sup>. Furthermore, through the use of an emerging prosthetic control modality, namely ultrasound, it has also been shown that children with UCBED generate distinct patterns of muscle deformation that can be classified to decode motor intent<sup>4</sup>. Although these results are exciting, ultrasound-based control technology is

not mature or commercially available and therefore lacks a translational component. Current state-of-the-art dexterous control uses sEMG classification algorithms to decode motor intent and therefore drive a prosthesis. However, little work has addressed how to effectively translate the currently available sEMG classification technologies to the pediatric UCBD population.

In contrast, much research has been conducted to understand what sEMG features and/or classifiers may be most effective in decoding hand motor intent from the activity of forearm muscles<sup>5-9</sup>, to name a few. However, most of this work was done with adult able-bodied individuals, and thus it is often assumed that top-performing feature sets and classifier combinations will translate effectively to those with acquired amputations<sup>10</sup>; however, these assumptions are often not tested rigorously in affected populations. In studies that do employ cohorts of adults with acquired amputations, classification of missing limb movements from sEMG data typically ranges from 81% to 97% depending on the hand movement, feature set, classifier, etc.,<sup>11</sup>. In a small cohort of adults with UCBD (N = 4), these values were significantly lower when simply applying a feature set developed for those with acquired limb loss (Hudgins set) with performance in the range of 52.1% ± 15.0% accuracy for 11 missing hand movements (including rest)<sup>12</sup>. Moreover, a small cohort of children (N = 4, less than 18 years old) and adults (N = 3) with UCBD have been studied utilizing a commercially available sEMG classification system, again developed for adults with acquired limb amputations<sup>13</sup>. The children achieved classification accuracies ranging from 80% ± 16.0% for 3 degrees of freedom<sup>13</sup>. As of our knowledge, only these two studies<sup>12,13</sup> have examined individuals with UCBD, with the notable distinction that one investigated pediatric participants<sup>13</sup>. Importantly, neither study systematically adjusted the feature sets and classifiers to address the unique conditions that UCBD affected muscles may present.

The aim of this chapter was to investigate feature sets and classification algorithm combinations tailored to children with UCBD. Furthermore, if implemented, how might sEMG classification techniques enhance prediction accuracy while maintaining low training and testing times. To accomplish this, we assessed individual features and feature set performance for 31 time domain features, 9 frequency domain features, and 9 time-frequency domain features. Top-performing feature sets were evaluated over five different classification algorithms (classifiers). We then proposed a new generalized feature set for this unique population and compared this to two feature sets commonly implemented for adults with acquired amputation; the Hudgins feature set (HDS)<sup>14,15</sup> and (2) a newly established efficient feature set (EFS)<sup>5</sup>. We hypothesized that a unique set of algorithmic parameters (i.e., features and classifiers) and attempted hand movements could be identified that would provide an effective balance between classification accuracy and computational time.

## 6.3. Methods

### 6.3.1. Participants

Nine participants with UCBD (8 male and 1 female, mean age of 14 years  $\pm$  4.4 years) completed the experimental protocol following relevant guidelines and regulations. Written informed consent and assent were obtained from participants and their legal guardians. This study received approval from the Institutional Review Board at Shriners Children's – Northern California. Participants had varying experiences of prosthesis use in addition to a wide range of affected limb lengths and circumferences, 8-18 cm and 15-23.5 cm, respectively (Table 6-1). All the children that participated in this study were clinically screened to ensure no other atypical development aside from UCBD.

Table 6-1. Participant demographics. PA = Passive, BP = Body-Powered, Myo = Myoelectric, †Activity specific device.

Subject ID	Age	Sex	Affected Limb	Length (cm)	Circumference (cm)	Type of Prosthesis Used
SHR-A	20	Male	Left	13	15	PA
SHR-B	8	Male	Right	14	20	PA
SHR-C	11	Male	Right	18	18	None
SHR-D	9	Male	Left	12.5	18.5	None
SHR-E	18	Male	Right	15	21	BP†
SHR-F	16	Female	Left	11.5	23.5	PA
SHR-G	19	Male	Left	13	21.5	Myo & PA
SHR-H	14	Male	Left	8	23	BP
SHR-I	12	Male	Right	10	21	BP

### 6.3.2. Experimental protocol

Participants were first introduced to the experiment which included an overview of the hand motions they would attempt, the equipment used, an explanation of sEMG, and general goals of the experiment. Then, seven wireless Trigno Mini sEMG electrodes from a Delsys Trigno EMG Research System (Delsys, USA) were adhered circumferentially<sup>16-18</sup> around the participants' affected forearm with double-sided adhesive (except for SHR-A who had only four sEMG electrodes due to limb size constraints). Given the unique anatomy of each child's limb difference, electrode placement was guided by palpation of the ventral side of the affected forearm to identify the region presenting with the most muscle bulk. Here the first electrode was placed with the remainder placed equidistant circumferentially from this location<sup>16</sup>.

Participants were situated in a chair with their affected and unaffected limbs in a comfortable position by their side. Afterward, they were instructed to perform a sequence of 10 repetitions for the same missing hand movement, divided into two groups of five. The order of hand movements was randomized to reduce any potential biases. A metronome was used to ensure consistency in

the repetition of movements by indicating when to execute each specified movement. Each movement was held for 3 seconds followed by a 4-second relax phase. A depiction of the sEMG data for the first five repetitions and a participant attempting the motion is shown in Figure 6-1a. The hand movements performed represented those most commonly used during activities of daily living<sup>19</sup>, wrist movements, and individual digit gestures. These motions are depicted in Figure 6-1b which included: index flexion (IF), key pinch (KP), pulp pinch (PP), index point (IP), cylindrical wrap (CW), cylindrical wrap wrist rotate (CR), tripod pinch (TP), wrist extension (WE), wrist flexion (WF), and wrist rotation (WR).

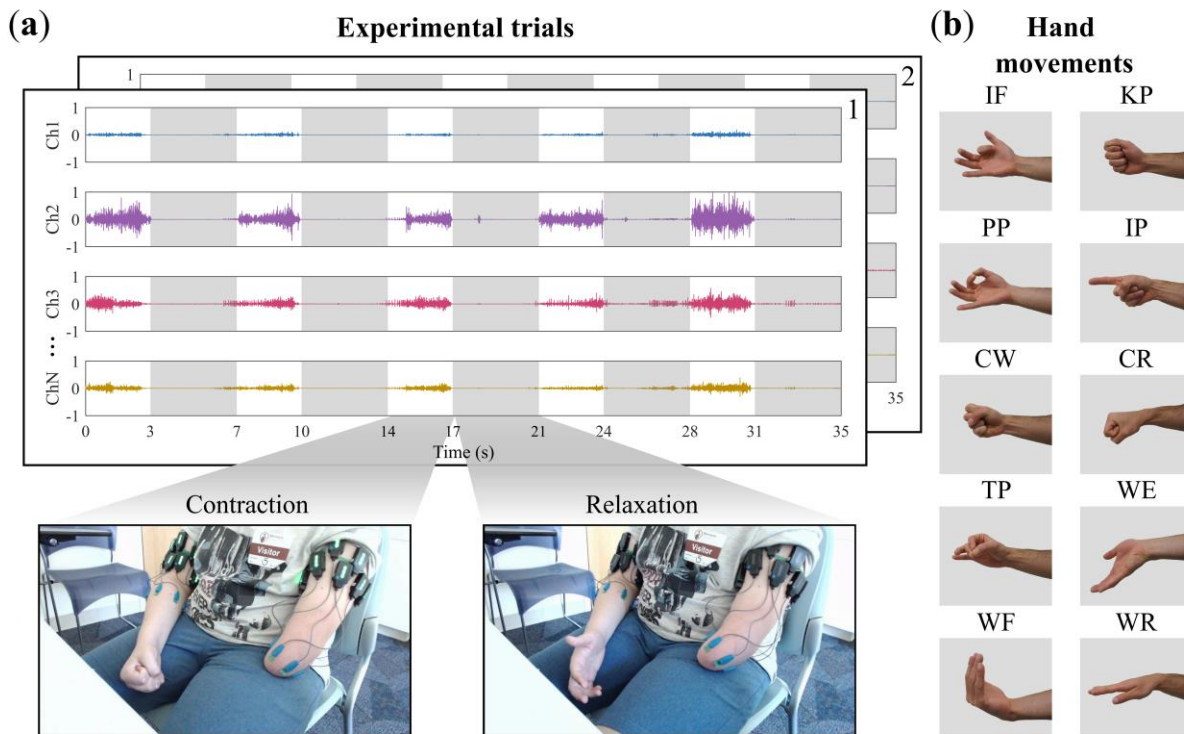


Figure 6-1. Experimental protocol. (a) Depicts a participant during a cylindrical wrap (CW) contraction and relaxation phase of the experiment along with the sEMG data across channels. (b) Displays the 10 different hand motions participants were instructed to attempt.

### 6.3.3. Data processing

As participants attempted the series of missing hand motions, the sEMG electrodes recorded the electrical activity and data were transmitted to the Delsys System where they were reconstructed,

band pass filtered from 20-450Hz<sup>20,21</sup>, and output as an analog signal. This analog signal was then read by a National Instruments USB 6210 data acquisition system through MATLAB (R2022a, MathWorks, Inc, USA) sampling at 6 kHz. After all data were collected, formatting and feature extraction were performed offline. Data was concatenated for each missing hand movement to create a single data set which consisted of all 10 repetitions. Then sEMG data were segmented (section 6.3.3.1), features were extracted (section 6.3.3.2), and classifiers were trained (section 6.3.3.3) to evaluate optimal feature sets (section 6.4). Evaluation was done with a custom MATLAB script that called functions in BioPatRec software<sup>22</sup>.

#### 6.3.3.1. Data segmentation

Data segmentation specifies a window and time increment in which sEMG data is separated for feature extraction and classification. The typical range for window lengths is 100 to 300 ms<sup>5,23</sup> and cannot exceed 300 ms as this threshold is perceived as a noticeable control delay if present in real-time prosthetic control applications<sup>24</sup>. Due to the large amount of data obtained, 300 ms windows and 150 ms time increments were used.

#### 6.3.3.2. Feature extraction

Feature extraction is the process of identifying relevant sEMG signal characteristics (features) to be classified<sup>25</sup>, which consists of discretized sEMG signals obtained from the time domain, frequency domain, or time-frequency domain. Here we used the features provided in BioPatRec and added additional ones to the software package after an extensive search of the literature. These included in total: 31 time domain features, 9 frequency domain features, and 9 time-frequency domain features, a summary of which are provided in Table 6-2.

Table 6-2. Extracted features from the time domain, frequency domain, and time-frequency domain. DWT: Discrete 4th order Coiflet Wavelet Transform, with 4th level decomposition.

Time Domain			
ID	Feature	Citation	
1	tmabs	Mean absolute value	5,7,8,12,22,26-31
2	tstd	Standard deviation	5,22,31
3	tvar	Variance	5,7,8,22,32-34
4	twl	Waveform length	5,7,8,12,22,26-31,34,35
5	trms	Root mean square	7,8,22,26,27,29,35,36
6	tzc	Zero-crossing	5,8,12,22,26-32,34
7	tpks	Number of peaks over the root mean square	5,22
8	tmpks	Peaks mean	5,22
9	tmvel	Mean velocity	5,22
10	tslpch	Slope changes	5,8,12,22,26,28-31,34
11	tpwr	Power	22
12	tdam	Difference absolute mean value	5,22
13	tmfl	Maximum fractal length	5,7,22,35,37
14	tfd	Fractal dimension	5,22
15	tfdh	Fractal dimension Higuchi	5,7,22,37
16	tren	Rough entropy	22
17	tcr	Correlation coefficient	5,22
18	tcv	Co-variance	22
19	tcard	Cardinality	22
20	tHmob	Hjorth mobility	5,33
21	tHcom	Hjorth complexity	5,33
22	tskw	Skewness (3 <sup>rd</sup> moment)	5
23	tdasdv	Difference absolute standard deviation value	5,8
24	tkurt	Kurtosis (4 <sup>th</sup> moment)	5
25	twam	Willison amplitude: threshold = 0.01	5,8,32,34,38
26	tmcer	Multi-channel energy ratio	5,39
27	tperc75	75 <sup>th</sup> Percentile	5
28	tiabs	Integrated absolute value	5,8,32,34
29	this	Histogram: min max voltage with 9 bins	5,8,32,34
30	tssi	Simple square integral	8
31	tlogd	Log detector	8,38
Frequency Domain			
1	fwl	Wavelength	5
2	fmn	Mean	5,26,34
3	fmd	Median	5,26
4	fpmn	Peak mean above the root mean square	5
5	fpm	Peak median above the root mean square	5
6	fpstd	Peak standard deviation above the root mean square	5
7	fmxp	Max peak	5
8	fr	Frequency ratio: 20-250 Hz & 251-450 Hz	5
9	fe	Frequency energy: 10 Hz bins	5,36
Time-Frequency Domain			
1	tfstd	Standard deviation – 4 <sup>th</sup> level wavelet coefficients (DWT)	5,40
2	tfvar	Variance – 4 <sup>th</sup> level wavelet coefficients (DWT)	5,40
3	tfwl	Waveform length – 4 <sup>th</sup> level wavelet coefficients (DWT)	5
4	tfe	Energy – 4 <sup>th</sup> level wavelet coefficients (DWT)	31,34
5	tfxabs1	Maximum absolute value – 4 <sup>th</sup> level wavelet coefficients (DWT)	5,41
6	tfxabs2	Maximum absolute value – tfxabs1 & all detail levels (DWT)	41
7	tfzc	Zero crossing – 4 <sup>th</sup> level wavelet coefficients (DWT)	34
8	tfmn	Mean – 4 <sup>th</sup> level wavelet coefficients (DWT)	5
9	tfxabs	Mean absolute value – 4 <sup>th</sup> level wavelet coefficients (DWT)	5

### 6.3.3.3. Pattern classification

Classification algorithms use sEMG features to identify patterns across the multiple sEMG electrode channels and predict the corresponding movement intent. Five classifiers were selected after a review of the literature, based on their performance and typical training and testing times, which are described as follows.

**Linear Discriminant Analysis (LDA)** is a common technique used to decode motor intent from muscle activity<sup>5,9,12,22,27–30,42,43</sup> in which the variance within a movement's feature space is minimized while the mean between movements is maximized, creating linear boundaries between each movement's feature space data. LDA was selected due to its simplicity of implementation, computational demands, and ease of training<sup>25</sup>. We updated LDA in BioPatRec using MATLAB's *fitdiscr* function with the discriminant type set to linear.

**K-Nearest Neighbor (KNN)** calculates the distance from a testing point to its k closest neighbors of the training data to predict the group a movement belongs to. This established method is another common classifier employed to decode hand movements from muscle activity<sup>5,21,28,30</sup>. We implemented KNN in BioPatRec with MATLAB's *fitcknn* function. Here the distance type was set to Euclidean with  $k = 1$  and the data were normalized with the norm-log in BioPatRec<sup>22</sup>.

**Regulatory Feedback Network (RFN)** is a classifier built into BioPatRec that utilizes a connectivity matrix or weights constructed from the average of all training feature vectors with predictions produced through outputs of a negative feedback system<sup>22</sup>. The training type was set to mean with the normalization set to unitary range<sup>28</sup>.

**Support Vector Machine (SVM)** is another commonly implemented classifier used to predict upper limb motor intent from muscle activity<sup>5,21,26–30,43</sup>. We implemented SVM in BioPatRec with



MATLAB's *fitcecoc* function. Here kernels are used to map data onto separable hyper-planes for classification<sup>5,28</sup>. The SVM had the kernel set to the radial basis function with a scale of 5.9, selected after empirical investigation, and a box constraint of 1. SVM normalization was set to 0-midrange with 2-range<sup>28</sup>.

**Design Tree (DT)** has been studied in the context of decoding hand movements from muscle activity<sup>5,28,30</sup> and we implemented this classifier into BioPatRec with MATLAB's *fitctree* function. The design tree uses predictors with greater than or less than criteria to transverse different branches of the tree and make a prediction. The maximum number of splits was set to 100 after empirical investigation and the split criterion was set to Gini's diversity index.

#### 6.4. Feature evaluation

To understand which features and classifier combinations provided the most effective classification performance in predicting attempted hand motions for children with UCBD, a detailed evaluation was performed. Data were collected, features were extracted, and evaluation was performed for each of the five classifiers for the following cases: individual features (49 in total) described in section 6.4.1, individual domains (time, frequency, and time-frequency), and combined domains, both described in section 6.4.2. During evaluation, the performance for each classifier was obtained by a 60-40 cross-validation, where 60% of the data was used for training and 40% was used for testing, this was repeated 100 times and averaged, where each iteration randomized the 60-40 training and testing datasets<sup>22</sup>. After the feature evaluation was performed, recommendations for a generalized congenital feature set (CFS) were provided (section 6.4.3). Data flow for the feature evaluation can be seen in Figure 6-2.

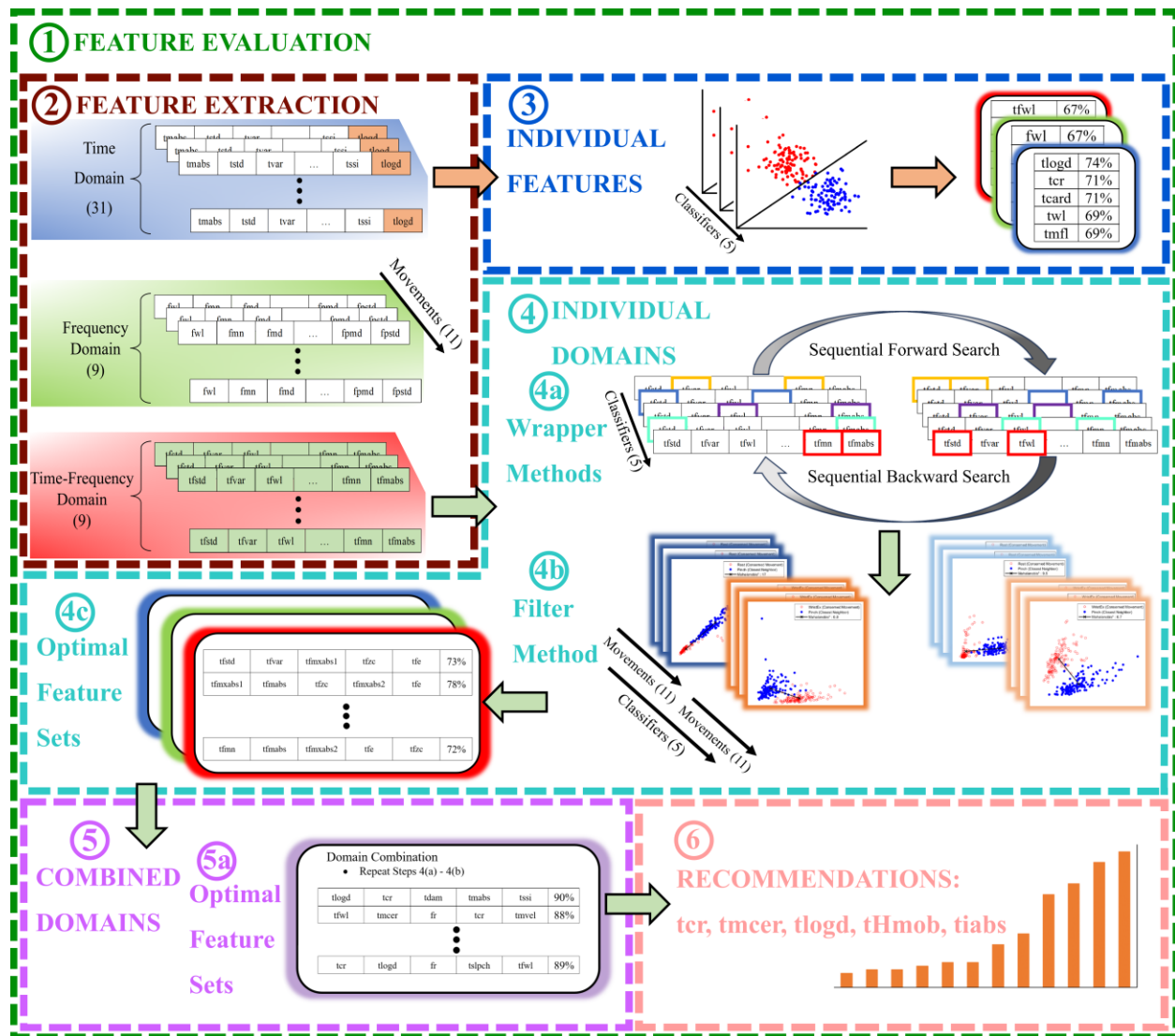


Figure 6-2. (1) Feature evaluation flow diagram. (2) Features were extracted for the time domain, frequency domain, and time-frequency domain. (3) Individual features were then evaluated across classifiers and the top five features were highlighted. (4) Feature sets within individual domains were evaluated via the two wrapper methods (4a) followed by the filter method (4b) to select the optimal feature set (4c). (5) The optimal feature sets produced from the individual domains were then combined and (4ab) were repeated to produce the optimal combined feature set (5a). (6) Recommendations for a generalized congenital feature set were then made.

### 6.4.1. Individual features

As an essential first step to help us ascertain the potential of decoding important motor information characterized by individual features, we trained and tested five classifiers. The individual features were split into three sets, one for each domain: time domain, frequency domain, and time-

frequency domain. The overall classification accuracy for each feature within the specified domain was determined through a 60-40 cross-validation, as previously described. In this procedure, the training and testing data were subject to 100 randomizations each time producing new movement classification accuracies. The classification accuracies from these randomizations were averaged together, and the correct individual movement accuracies were then averaged to produce the overall classification accuracy. A count of the top five highest-performing individual features for each classifier and participant was then obtained (shown in Figure 6-2 zone 3).

#### 6.4.2. Individual domains and combined domains

We evaluated sets of features for the individual and combined domains for each classifier in order to understand which sets of features may produce the most effective classification performance. The same methodology was used to evaluate individual and combined domains as shown in Figure 6-2 zones 4 and 5, respectively. The only difference between the two was that feature sets for individual domains were evaluated first to find their optimal sets. Upon evaluation, these optimal sets for the individual domains were combined and evaluated to produce the optimal combined-domain feature set. All feature evaluation was done on an individual participant basis.

We identified top-performing feature sets within the individual and combined domains using two wrapper methods (i.e., feature selection algorithms), namely sequential forward search and sequential backward search, as depicted in Figure 6-2 zone 4a<sup>6,44</sup>. The classification accuracies were produced as follows: the classification accuracy of every movement was computed for the 100 randomized datasets; then those 100 datasets were averaged together; and finally, the average across all the movements from that averaged dataset was determined. The sequential forward search method loops through all the features and selects the one that produces the average highest classification accuracy. It then loops through the remaining features, each time combining it with

the previously chosen feature, ultimately selecting the two features that produce the highest accuracy. This process is then repeated until all the features have been selected, thereby ordering the features based on their contribution to the prediction accuracy. Inversely, the sequential backward search starts with all the features and removes one at a time. Then, the feature that produces the highest classification accuracy when removed is discarded from the total feature set. This process is repeated with the remaining features until only one is left. After these methods were completed, two datasets were produced: one for sequential forward search and one for sequential backward search. Then for any given classifier and domain, we extracted the feature set containing the top five features produced from each of the two search methods for further analysis. It should be noted that the two feature sets produced from the forward and backward wrapper methods were not necessarily identical and required a filter method to determine the optimal feature set as depicted in Figure 6-2 zones 4b and 4c. Here, we employed the Mahalanobis distance, a typical feature space analysis method that provides a measure for the separability of attempted hand movements i.e., the separability index (SI)<sup>45-48</sup>. This process involved calculating the feature space Mahalanobis distance from one movement to all the remaining movements. The minimum distance among these was then tabulated. This procedure was repeated for each movement, and the average was taken as the SI. This was used as a measure of robustness for the feature sets. A larger SI indicates increased spatial distinction between motions while a smaller SI indicates a decreased spatial distinction<sup>45</sup>. In this way, the optimal set between the search methods was chosen as the one with a larger SI.

The modified SI was defined as the average minimum one-half Mahalanobis distance from the centroid  $\mu_j$  of the  $j^{\text{th}}$  class to the centroid  $\mu_i$  of the remaining  $i$  classes, where  $S_j$  is the covariance matrix of  $j^{\text{th}}$  class<sup>45</sup>. The inverse of the covariance matrix  $S_j$  was obtained with the Moore-Penrose

pseudoinverse to ensure its existence. This was done because some features were linear combinations of others, and threshold methods such as the Willison amplitude (*twam*) were defined with a single value for all participants, which could have caused sparse feature vectors. Taken together, linear combinations and sparse feature vectors could create noninvertible matrices, which could be addressed by using the pseudoinverse and calculating the magnitude. The modified SI is therefore defined by Equation 6-1.

$$SI = \frac{1}{11} \sum_{j=1}^{11} \left( \min_{i=1, \dots, j-1, j+1, \dots, 11} \frac{1}{2} \sqrt{(\mu_j - \mu_i)^T S_j^{-1} (\mu_j - \mu_i)} \right) \quad \text{Equation 6-1}$$

#### 6.4.3. Generalized congenital feature set

After the feature sets were produced for the individual domains, they were combined and reevaluated to produce an optimal feature set from the combined domains (Figure 6-2 zone 5). The optimal feature sets across classifiers and participants were aggregated to make a recommendation based on a count of the unique number of times each feature occurred (Figure 6-2 zone 6). The top five unique features that occurred most often were taken as the generalized congenital feature set (CFS): correlation coefficient (*ocr*), multi-channel energy ratio (*tmcer*), log detector (*tlogd*), Hjorth mobility parameter (*tHmob*), and integrated absolute value (*tiabs*).

### 6.5. Analysis

#### 6.5.1. Feature set comparisons

To determine which feature sets may be most suitable for children with UCBED, a comparison across domains and feature sets was performed on an individual participant basis to produce a unique feature set for each domain and classifier. The unique feature sets for each domain are referred to as the following: time domain feature set (TMS), frequency domain feature set (FQS), time-frequency domain feature set (TFS), and combined domain feature set (CDS). Additionally, generalized feature sets described previously in adult literature were also used for comparison.

There are a number of proposed feature sets that have been suggested to provide high classification accuracy in able-bodied individuals and adults with acquired limb loss. including ‘the Efficient Feature Set’ (EFS)<sup>5</sup> and ‘the Hudgins Set’ (HDS)<sup>14</sup>. The EFS consists of the following features: waveform length (*twl*), correlation coefficient (*ocr*), and the Hjorth parameters<sup>33</sup> (i.e., activity/variance (*tvar*), mobility (*tHmob*), and complexity (*tHcom*)<sup>5</sup>). Additionally, HDS contains the following features: mean absolute value (*tmabs*), waveform length (*twl*), slope sign changes (*tslpch*), zero crossing (*tzc*), and difference absolute mean value (*tdam*)<sup>14</sup>. Finally, our generalized CFS feature set, produced from an aggregate across participants in this work, was used for comparison.

We analyzed differences in prediction accuracy between the seven feature sets for each of the five classifiers using the non-parametric Friedman test<sup>49,50</sup>. Here, the improved Friedman statistic ( $F_F$ ) was then used as described by<sup>50</sup>. The null hypothesis,  $H_0$ , was that all feature sets had the same rank (i.e., the average classifier performance across movements will be the same regardless of the feature set). We selected a significance level of  $\alpha = 0.05$  and determined the critical value of  $F(6,60) = 2.25$  to evaluate statistical differences. If the improved Friedman statistic was greater than the critical value ( $F_F > 2.25$ ) then the null hypothesis was rejected. When this occurred, we proceeded with pairwise comparisons of the seven feature sets for a given classifier utilizing the post-hoc Nemenyi test<sup>51</sup>. The critical distance value of 2.72 was determined for the two-tailed Nemenyi test at a significance level of  $\alpha = 0.05$ , as described by Demšar *et al.*<sup>50</sup>. If the difference in ranked classification accuracy between any pair of feature sets exceeded the critical distance, it was deemed statistically significant.

### 6.5.2. Congenital feature set assessment

Our new congenital feature set was isolated in our analyses to further examine its efficacy as a generalized set for children with UCBED. This included comparisons of its performance across classifiers to understand which classifier may provide the highest performance (section 6.5.2.1). An investigation of training and testing times was also performed to understand the computational expense (section 6.5.2.2), an important aspect for future applications of real-time control. Additionally, we employed movement reduction techniques to identify a subset of high-performing missing hand motions (section 6.5.2.3); this is a practical consideration for prosthetic control in which identifying a subset of highly accurate hand movements may be most useful in executing activities of daily living.

#### 6.5.2.1. Classifier comparisons

Classifier comparisons were performed with the Friedman test as previously described in section 6.5.1. The null hypothesis,  $H_0$ , was that all classifiers have the same rank, that is, the performance across movements was the same regardless of the classifier algorithm. We selected a significance level of  $\alpha = 0.05$  and calculated the critical value of  $F(4,40) = 2.60$  to assess statistical differences. As before, if the improved Friedman statistic ( $F_F$ ) was greater than the critical value, then the null hypothesis was rejected, namely, that the rank-based classifier accuracies across movements were not the same for all classifiers. Subsequently, we performed pairwise classifier comparisons using the post-hoc two-tailed Nemenyi test at a significance level of  $\alpha = 0.05$ . The critical distance value of 1.84, calculated following Demšar *et al.*<sup>50</sup>, was used to determine statistical significance. This significance was defined as the difference in the ranked classification accuracies between any pair of classifiers that exceeded the critical distance.

### 6.5.2.2. Computational expense

The training and testing times for the generalized CFS were then obtained for each classifier and participant to understand the computational expense. These computational demands were assessed on a Lenovo PC with the following specifications: a 64-bit Windows 11 operating system with 32 GB of RAM and an Intel core i7-8550U at 1.80 GHz (Intel Corp, USA). The first computational demand, training time, is defined to be the duration to train a classifier and tune hyperparameters. The second computational demand is testing time, which is defined as the transitory period for the offline classifier to predict the labels (missing hand movements). The testing time was used as a metric to assess the potential for real-time control since any value exceeding the 300 ms threshold results in diminished prosthetic control<sup>24</sup>.

### 6.5.2.3. Movement reduction

Movement reduction was performed for each classifier on the CFS feature set. The reduction procedure involved training a classifier with all attempted hand movements and discarding the movement that produced the lowest classification performance. The remaining movements were then used to retrain the classifier, and this process was repeated until only two movements were left. In this way, we identified how the classification accuracy increased with a decrease in attempted hand movements. This is significant because individuals using multi-grasp prostheses will typically employ a limited subset of hand movements. Notably, research has shown that 6-9 hand movements can account for nearly 80% of daily activities<sup>19,52</sup>. Therefore, we propose investigating a subset of five movements for children with UCBED and identifying those subsets that surpass the minimum threshold of 85% classification accuracy needed to promote device usability<sup>25</sup>. It is important to note that the rest state was not considered part of the movements to be discarded because it is an essential state for prosthetic control. Consequently, with every



reduction, the rest state was always included, even when there were only two movements remaining, i.e., rest and one other movement were present at the end.

## 6.6. Results

### 6.6.1. Individual features

We identified and counted the top five performing individual features for a given participant and classifier. This process was performed for each feature domain and repeated for every participant and classification algorithm. The total possible occurrences for one feature across the five classifiers and nine participants was 45. Therefore, a higher count for an individual feature would indicate that it was more often among the top features for each participant (Figure 6-3). Here, we highlight four of the top-performing features for the time domain: *tmabs* (34/45), *tiabs* (32/45), *tlogd* (29/45), and *tcr* (26/45). Similarly, the top-performing features for the frequency domain were: *fwl* (45/45), *fpmn* (45/45), *fpstd* (45/45), *fpmd* (43/45). Finally, in the time-frequency domain, the top-performing features included: *tfwl* (45/45), *tfstd* (45/45), *tfmabs* (44/45), and *tfvar* (31/45). It is important to note that when examining classifiers, KNN demonstrated numerically higher classification accuracies for each participant's top-performing individual features, while RFN exhibited the lowest accuracies. Figure 6-3 illustrates the cumulative count of domain-specific features for each classifier, obtained by counting the top five high-performing features that occurred for each participant. Detailed tables showcasing the classification performance of all individual features for each participant are provided in Appendix C tables.

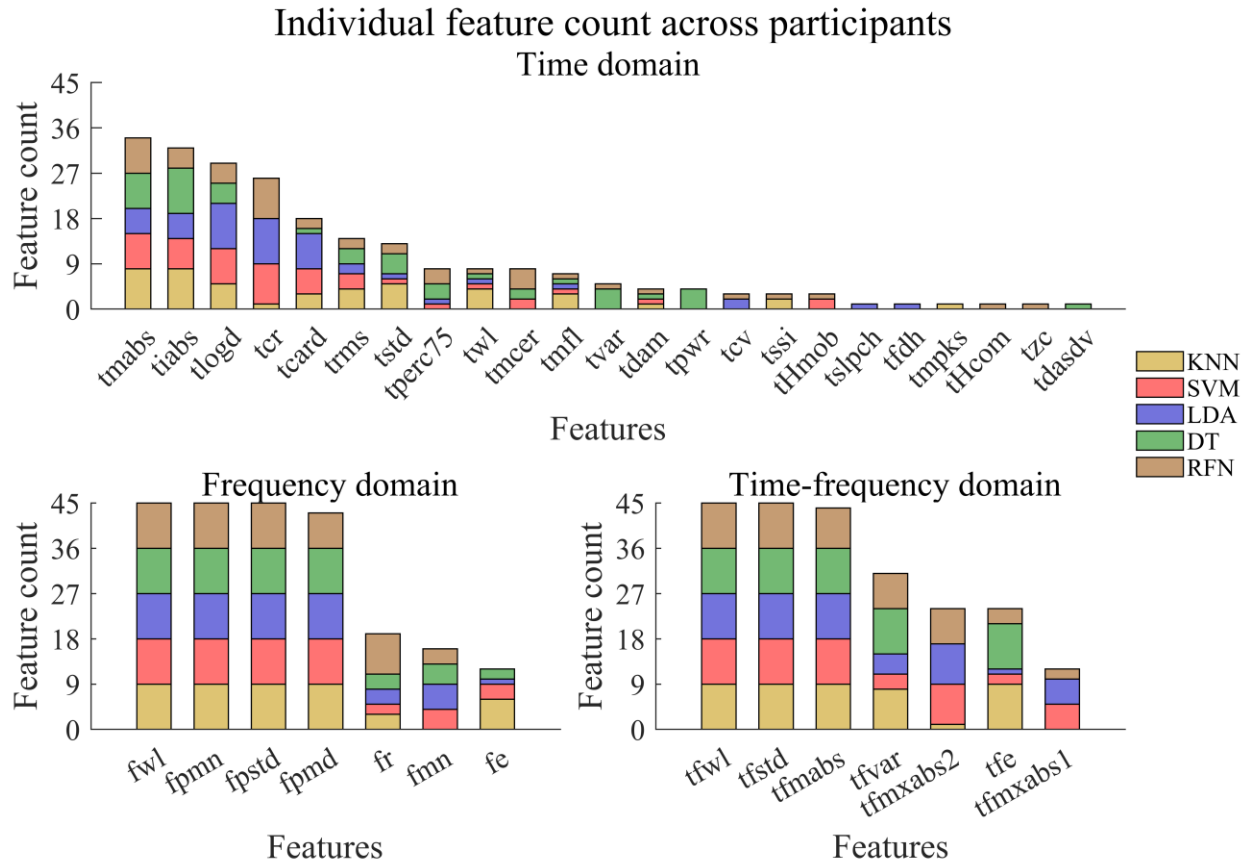


Figure 6-3. Cumulative count of domain-specific high-performing individual features. The top five high-performing features were identified and counted for a given participant and classifiers. This process was then repeated for every participant, with the results highlighted for the various classification algorithms. The top panel displays the count for the time domain, while the bottom left panel shows the frequency domain, and the bottom right panel shows the time-frequency domain. A count of 45 means that the given feature was in the top five for all nine participants and five classifiers.

### 6.6.2. Generalized congenital feature set

In the assessment of optimal combined domains, as detailed in section 6.4.2, distinct sets of five features were generated for each participant and classifier. Aggregating these results as displayed in Figure 6-4, we identified five features—*tcr*, *tmcer*, *tlogd*, *tHmob*, and *tiabs*—that occurred most frequently, forming the recommended generalized congenital feature set (CFS). Moreover, the CFS accounted for 60% of the total occurrences across participants, classifiers, and features. These results highlight the prevalent features present among the majority of participants, suggesting potential generalizability.

## Feature count across classifiers and participants

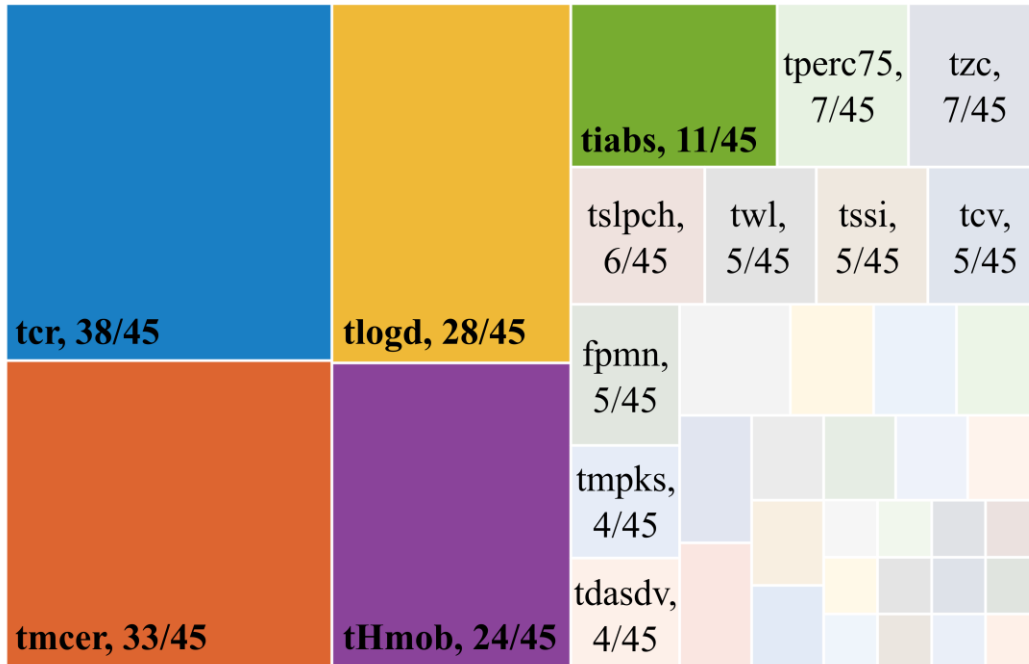


Figure 6-4. Feature count for recommending the generalized congenital feature set (CFS): correlation coefficient (tcr), multi-channel energy ratio (tmcer), log detector (tlogd), Hjorth mobility parameter (tHmob), and integrated absolute value (tiabs). The maximum occurrence for an individual feature within the combined domain feature sets was 45, indicating that a single feature could be present in the feature set for all five classifiers and nine participants. The CFS features accounted for 134 occurrences out of the possible 225, representing a total of 60%. In this context, the total possible occurrences result from the presence of the five features within the combined domain set for each of the five classifiers and all nine participants, totaling 225 occurrences.

### 6.6.3. Feature set comparisons

To identify the feature sets that have higher classification accuracy for children with UCBD, we performed feature set comparisons with the Friedman test, followed by the post-hoc Nemenyi test. For one participant and one classifier, we performed pairwise comparisons of the seven feature sets, this was then repeated for each of the classifiers, and then for every participant. Statistical significance between any pair of the seven feature sets is discernible when the displacement between the pair exceeds the critical distance of 2.72. As demonstrated in participant SHR-I (Figure 6-5), we found higher classification accuracies and few to no statistical differences in the

pairwise comparisons of TMS, CDS, CFS, and EFS feature sets for each classifier. Overall, TFS, FQS, and HDS feature sets had lower classification accuracies and exhibited the majority of statistical differences when compared to the remaining feature sets, with few exceptions. The detailed results for each participant can be found in Appendix C.

In general, the feature sets decreased in numerical accuracy in the following order: CDS, TMS, CFS, EFS, HDS, FQS, and TFS, as illustrated in Figure 6-5 and Appendix C. Upon further investigation, we found that the KNN, SVM, and LDA classifiers had numerically higher accuracies, while RFN had the lowest, followed by DT (see Figure 6-5 and Appendix C). Here, we highlight classification accuracies for the optimal combined domain feature set (CDS) which ranged from 63.87% – 95.37%, 62.61% – 92.86%, 57.33% – 92.87%, 50.79% – 83.19%, and 38.46% – 79.62% for KNN, SVM, LDA, DT, and RF, respectively. Participant SHR-F had the highest CDS feature set classification accuracy for all the classifiers. Participant SHR-B had the lowest values for LDA and RFN, while SHR-D had the lowest values for KNN, SVM, and DT. In this context, it's important to highlight that the chance accuracy for decoding the 11 movements is approximately 9%, and it's noteworthy that all accuracies recorded were above this threshold. Collectively, these results indicate that feature sets, in combination with key classifiers, can be tuned and generalized for children with UCBED to provide higher classification accuracy.

## SHR-I: Feature performance

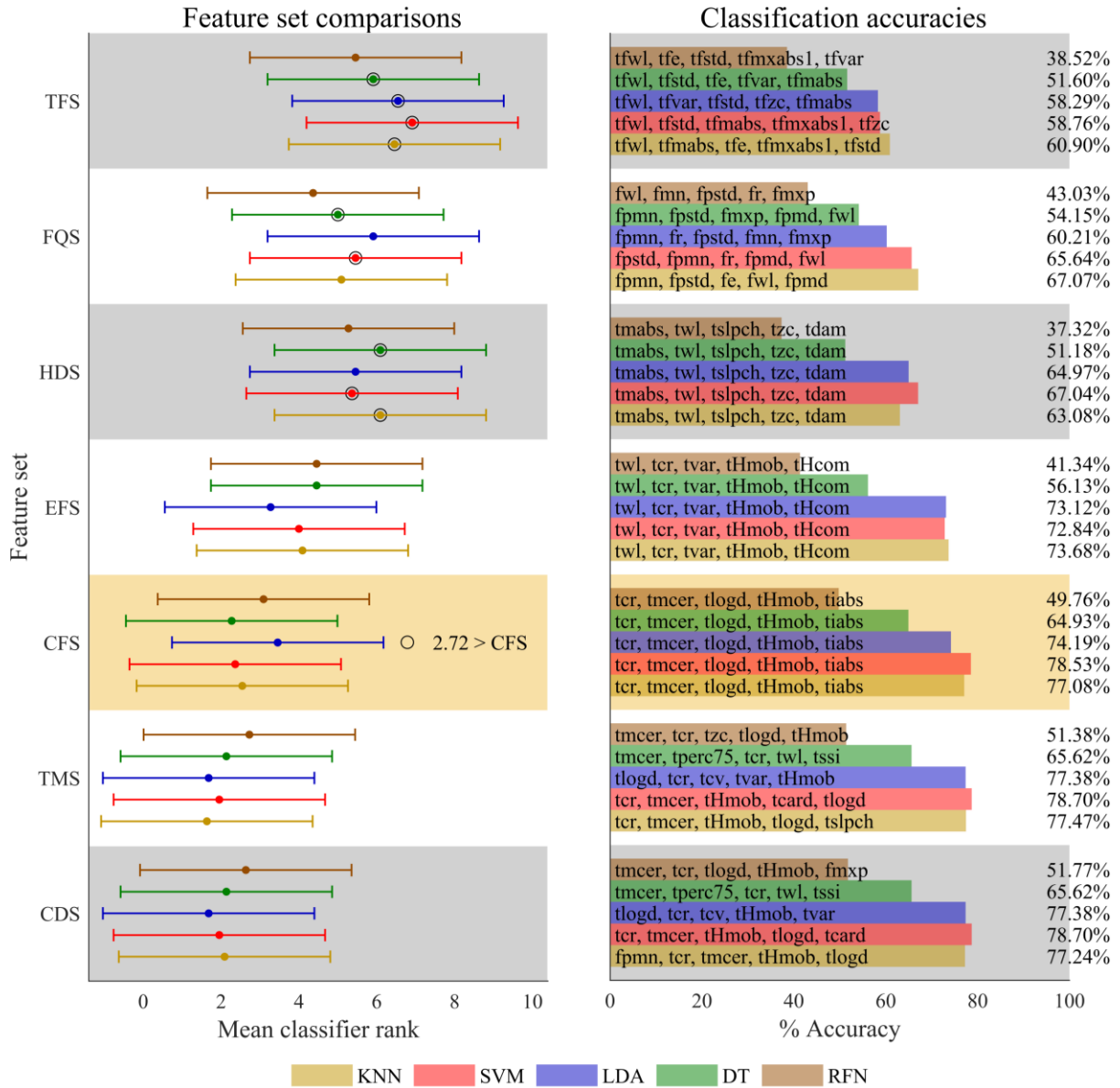


Figure 6-5. Investigation of feature set performance for participant SHR-I. The left panel shows the pairwise comparisons for the feature sets on an individual classifier basis. The Friedman test, with a critical value of  $F(6,60) = 2.25$  at  $\alpha = 0.05$ , was used to determine if average accuracy ranks significantly differed from the mean rank. Classifier F Statistics (KNN:  $F_F = 45.36$ , SVM:  $F_F = 51.99$ , LDA:  $F_F = 56.89$ , DT:  $F_F = 21.63$ , RFN:  $F_F = 4.3$ ) confirmed significant differences within each classifier's feature sets. A post-hoc Nemenyi test with a critical distance of 2.72 at  $\alpha = 0.05$  identified superior feature sets as indicated by pairs outside the critical distance marked by the interval bars. Each classifier is color-coded for easy comparison, with lower average ranks indicating better classification accuracy. Feature sets significantly different from the highlighted congenital feature set (CFS) were marked with an outer black ring. The right panel displays classification accuracies, which range from approximately 39% to 79%, alongside the corresponding feature sets, aligning them with the ranked performance shown in the left panel.

#### 6.6.4. Congenital feature set assessment

We further investigated the performance of the children-specific CFS feature set which included the comparison of accuracies across classifiers (section 6.6.4.1), the evaluation of computational expense (section 6.6.4.2), and how classification accuracy improves as we remove the lowest-performing hand movements (movement reduction, section 6.6.4.3).

##### 6.6.4.1. Classifier comparisons

All pairwise comparisons between SVM, LDA, and KNN classifiers showed no statistical differences in the average ranked classification accuracies and demonstrated consistently high classification performance (with the exception of participant SHR-B). In contrast, DT and RFN classifiers exhibited both lower classification performance and all other observed statistical differences when compared to KNN, SVM, and LDA. The range of classification accuracies for the CFS feature set were as follows: KNN (62.17% – 94.17%), SVM (62.01% – 93.11%), LDA (56.22% – 92.80%), DT (50.65% – 82.43%), and RFN (37.07% – 79.74%). Participant SHR-F exhibited the highest classification accuracy for each classifier, while SHR-B and SHR-D had the lowest. Friedman test statistics and a visual depiction of the post-hoc Nemenyi test are provided in Figure 6-6 for all participants. In these graphical depictions, pairwise comparisons between classifiers within the CFS are observed, and statistical differences were determined by those that exceeded the critical distance of 1.84. A lower rank denotes superior classifier performance while a higher rank denotes diminished performance. The results from pairwise classifier comparisons within the CFS suggest that KNN, SVM, and LDA classifiers provide a significant improvement over DT and RFN in their current states.

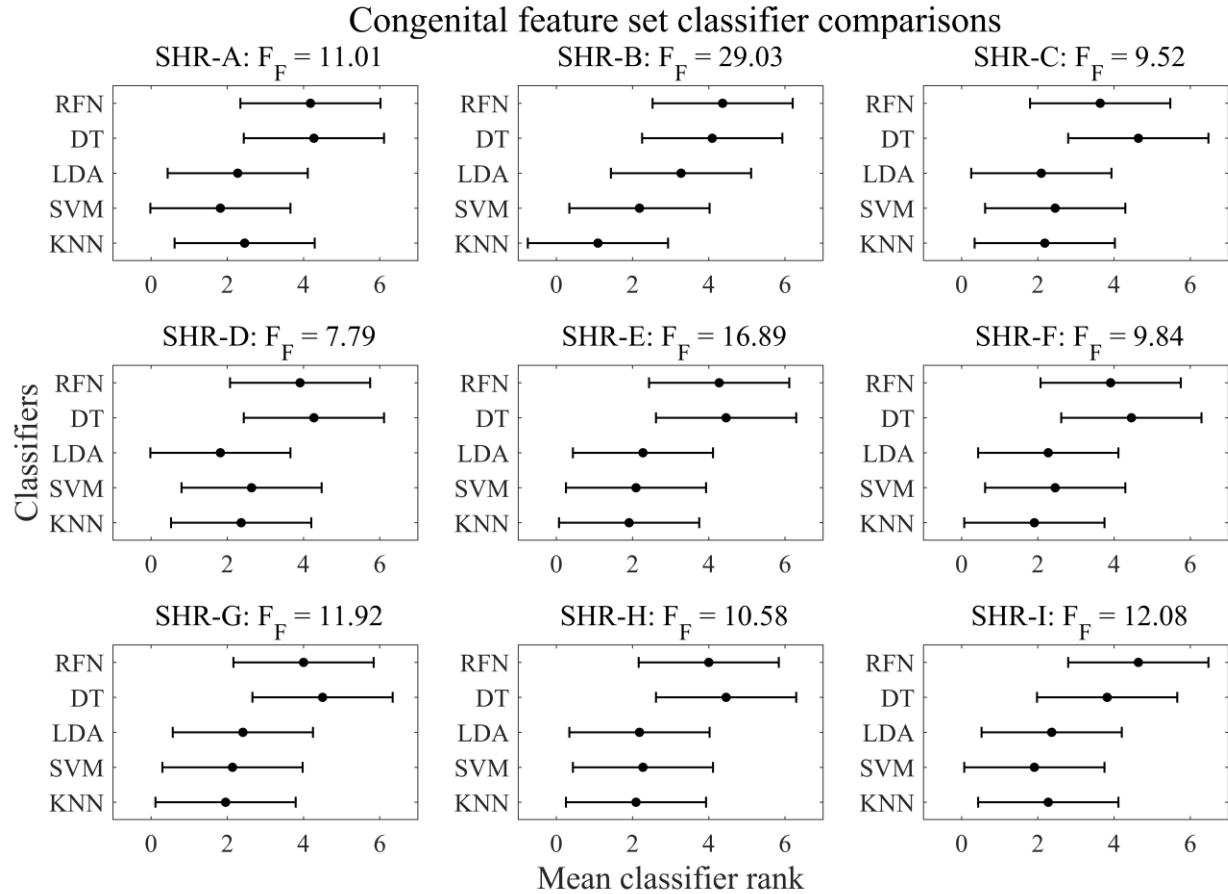


Figure 6-6. Congenital feature set classifier comparisons. The Friedman test, with a critical value of  $F(4,40) = 2.60$  at  $\alpha = 0.05$ , indicated all participants rejected the null hypothesis ( $F_F > 2.60$ ) in favor of the alternative, suggesting a difference across average rank-based classifier performance. A lower average rank indicates superior classifier performance. Pairwise comparisons were performed using the post-hoc Nemenyi test, with a critical distance of 1.84 at  $\alpha = 0.05$ . Statistical significance for a specific classifier is denoted by classifiers positioned outside the critical distance, as indicated by the interval bars.

#### 6.6.4.2. Computational expense

To understand the associated computational expense for the CFS feature set, we obtained the average training and testing times for each participant and classifier algorithm. On average, we see the RFN classifier had the largest training times ranging from 421 ms – 758 ms, followed by SVM with 560 ms – 637 ms. LDA, KNN, and DT had relatively similar training times, all falling within the LDA range of 243 ms – 362 ms. Additionally, all testing times fell under the 300 ms threshold for usable real-time control<sup>24</sup>, and the range of time values are provided are follows: SVM (18.61

– 19.45 ms), KNN (3.59 – 3.93 ms), DT (2.03 ms – 2.38 ms), RFN (0.32 ms – 0.44 ms), and LDA (0.12 ms – 0.15 ms). Training and testing times for the CFS of each participant and classifier are shown in Table 6-3. The low training and testing time results suggest effective employment of the CFS across classifiers for future real-time control.

Table 6-3. Computational expense of the congenital feature set (CFS) across classifiers.

Participants	Training Time (ms)					Testing Time (ms)				
	LDA	KNN	RFN	SVM	DT	LDA	KNN	RFN	SVM	DT
SHR-A	276	258	421	589	249	0.12	3.65	0.32	18.61	2.38
SHR-B	290	329	752	574	279	0.12	3.84	0.44	18.94	2.28
SHR-C	243	300	644	592	306	0.12	3.59	0.37	19.45	2.08
SHR-D	362	333	758	605	352	0.12	3.89	0.42	19.18	2.35
SHR-E	349	317	640	564	280	0.12	3.73	0.41	18.80	2.14
SHR-F	345	310	587	560	351	0.13	3.92	0.37	18.66	2.21
SHR-G	323	296	560	591	305	0.13	3.65	0.36	18.76	2.19
SHR-H	349	315	657	599	318	0.15	3.91	0.44	18.85	2.03
SHR-I	344	321	661	637	335	0.12	3.93	0.43	19.25	2.31

#### 6.6.4.3. Movement reduction

We eliminated attempted hand movements one at a time, based on the lowest classification accuracy; to examine the relationship between the number of movements and classification accuracy. Although we reduced the number of movements to two (rest and one other motion), our point of interest was a reduced state of five (rest state and four other motions). This was done primarily because prosthesis wearers generally use a smaller selection of hand movements to assist in activities of daily living. The other point of interest was a minimum 85% classification accuracy threshold, which is needed to mitigate wearer frustration and promote device usability<sup>25</sup>.



The majority of participants across classifiers had accuracies greater than the 85% threshold for the reduced set of five movements. For the LDA classifier, participants had accuracies ranging from 91.38% – 99.45% except for SHR-B, who had a classification accuracy of 84.49% (less than the 85% threshold). All participants had KNN classification accuracies greater than the threshold, ranging from 87.64% – 99.74%. With the exceptions of SHR-B (71.86%), SHR-D (81.08%), and SHR-I (81.72%), all other participants had RFN classification accuracies greater than 85%, ranging from 93.00% – 98.09%. For the SVM classifier, all accuracies were above the threshold and ranged from 87.73% – 98.38%. Finally, for the DT classifier, SHR-B and SHR-D had classification accuracies of 77.23% and 83.31%, respectively, while all other participants ranged from 92.95% – 98.45%. Movement reduction radar plots for all participants are provided in Figure 6-7.

### Impact of movement reduction on average classification performance

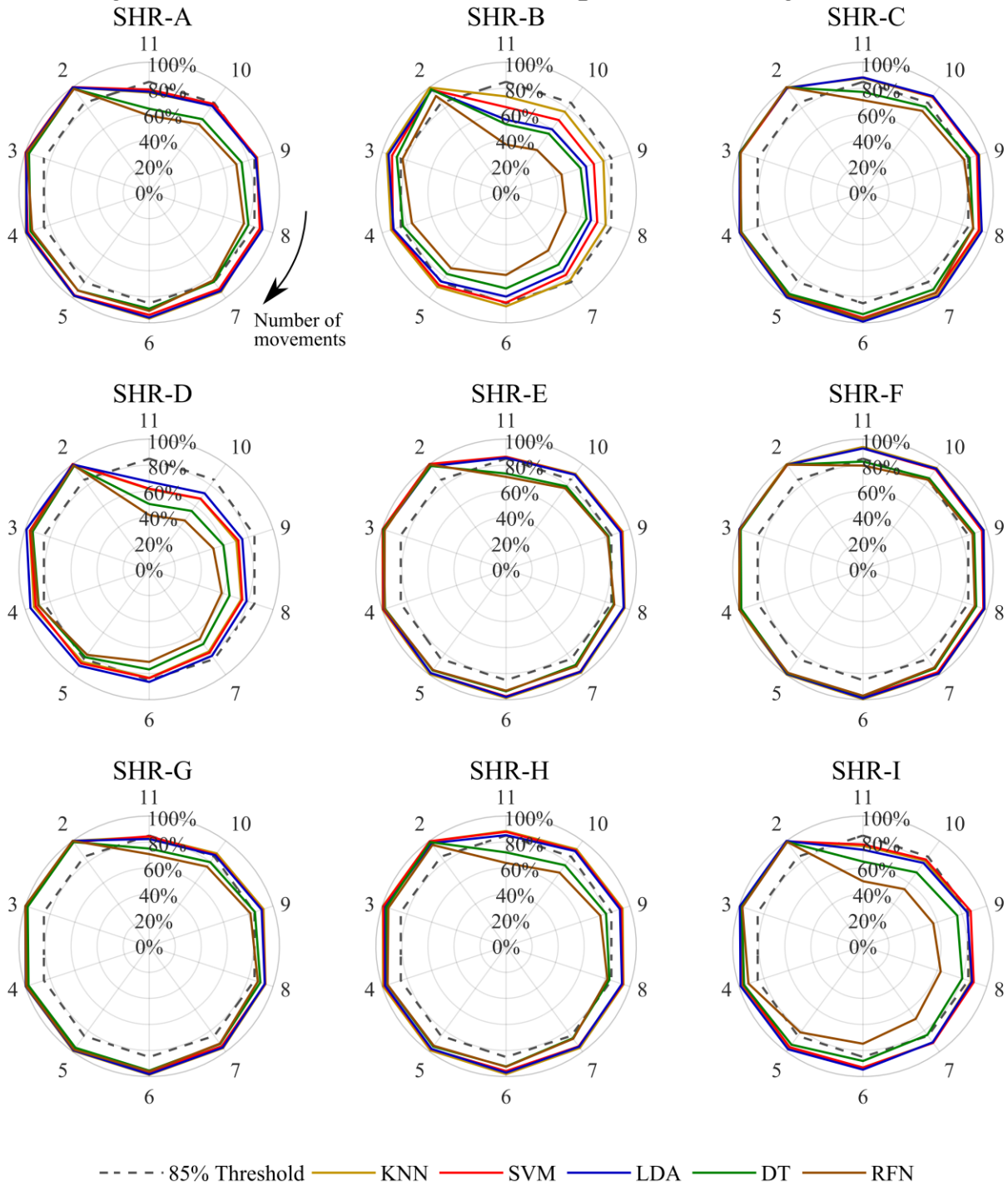


Figure 6-7. Impact of movement reduction. Movements were reduced from all 11 to a set of 2, as annotated on the radar plot. Note that the rest state was not removed during this reduction process. The movement with the lowest classification accuracy was omitted, and the remaining movements were used to retain the given classifier. This process was repeated until only two movements remained: rest and one other. The dashed line indicates the suggested threshold for usability device control at 85% accuracy<sup>25</sup>.

To identify common movements within the reduced set of five across participants, we first counted the frequency of each movement's occurrence across the five classifiers for a single participant. Consequently, a single movement could appear in each of the five classifiers. This process was repeated for all nine participants, potentially resulting in a total occurrence of one movement 45 times and for five movements 225 times. The rest state, which was kept fixed and not removed to establish a foundation for predicting motor intent, retained a total occurrence of 45. Figure 6-8 depicts a count of the reduced set of five movements for each participant and aggregated across all participants. Here, we observed that wrist extension (WE) and wrist flexion (WF) accounted for 34 out of 45 (76%) and 24 out of 45 (53%) of the top single-movement occurrences, respectively. Aggregating rest, WE, WF, CW, and IF accounted for 148 out of 225 total occurrences (66%). These results highlight that some movements may be easier for all participants to envision and attempt.

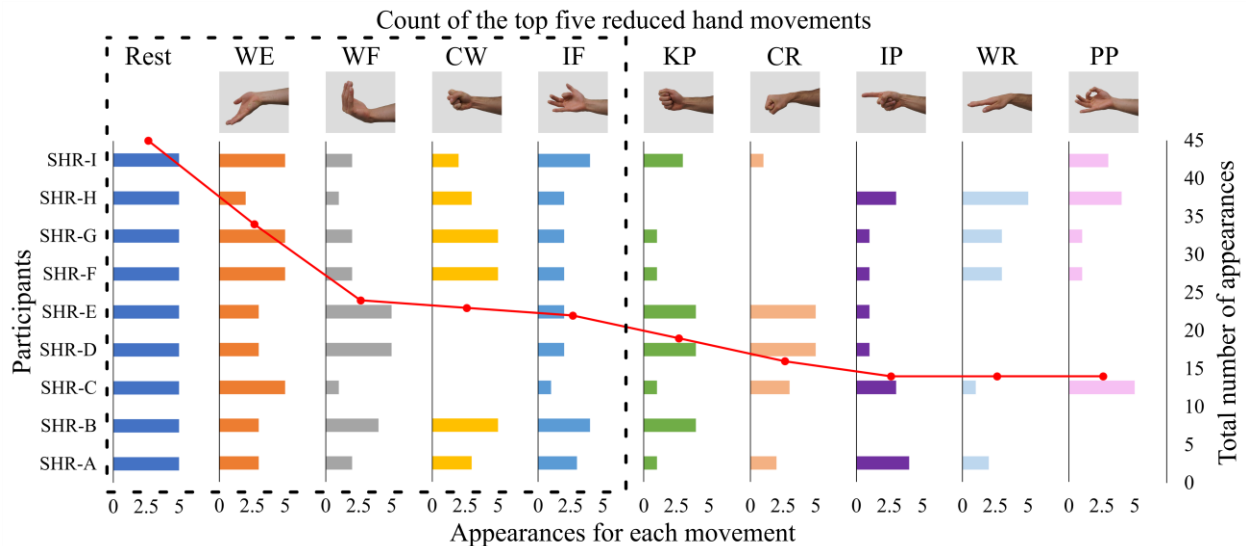


Figure 6-8. Count of the top five reduced hand movements. In a given column, the individual participant's numerical bar value indicates the cumulative occurrence of the movement across all five classifiers. Notably, rest was not removed during reduction and thus occurs in every participant and classifier. The superimposed red scatter plot illustrates the overall occurrence of a specific movement across all nine participants and five classifiers; therefore, the maximum possible occurrence was 45 (as seen on rest).

## 6.7. Discussion

### 6.7.1. Unique features can be identified for children with UCBED

When we analyzed the individual features and feature sets, unique features were identified for children with UCBED. The top-performing individual features identified across classifiers and participants for the time domain were: *tmabs*, *tiabs*, *tlogd*, and *tcr* (Figure 6-3). It is interesting to note that three of these top-performing individual features (*tcr*, *tlogd*, and *tiabs*) were also observed frequently within the tuned feature sets for the time and combined domains across every classifier (see Figure 6-4, Figure 6-5, and Appendix C). These three features showed up in the generalized congenital feature set (CFS) which consisted of *tcr*, *tmcer*, *tlogd*, *tHmob*, and *tiabs*.

### 6.7.2. Children with UCBED benefit from certain feature sets

Numerous feature sets and classification algorithms have been tuned for adult able-bodied individuals, with the common assumption that they will seamlessly translate to those with acquired amputation<sup>10</sup>. Nevertheless, these assumptions are not rigorously tested in affected populations. Unlike individuals with traumatic amputation, the unique population studied here presents more uncertainty as they were born with limb absence and, consequently, have never actuated an intact hand. Interestingly, the efficient feature set (EFS) developed on able-bodied individuals<sup>5</sup> performed well for those with congenital limb deficiency. Although not statistically significant relative to the EFS, the newly developed generalized congenital feature set (CFS) provided numerically higher classification accuracies and was comparable to each participant's tuned time-domain and combined-domain feature sets.

When we analyzed the feature sets for each classifier and participant, very few statistical differences were obtained for the following feature sets: TMS, CDS, EFS, and CFS (see Figure 6-5 and Appendix C). The majority of pairwise statistical differences that were observed occurred

between the previously mentioned feature sets and the TFS, FQS, and HDS sets (which had lower classification accuracies). This suggests that pure frequency, time-frequency, or even the commonly implemented generalized Hudgins set do not provide sufficient information for optimal classification in children with UCBED. Moreover, although the CDS feature set was produced from the optimal set of each domain on an individual participant basis, we found that the majority of features within the CDS sets ended up being from the time domain. Evidently so, these results are in line with previous research that attributes the best performance to time domain features<sup>20</sup>, which is also the case here for children with UCBED.

Interestingly, participant SHR-F had the highest classification accuracy for the CDS feature set of each classifier (LDA: 92.87%, KNN: 95.37%, RFN: 79.62%, SVM: 92.86%, and DT: 83.19%). It is important to note that this participant exhibited seemingly unlikely factors that would merit good classification performance: (1) they only reported the use of a passive device as opposed to a myoelectric prosthesis; (2) they were not the oldest, but rather in the upper middle age range at 16 years old; (3) neither did they have the largest limb length (11.5 cm) or circumference (23.5 cm). Despite these demographics, the only difference between this participant and the others was their sex (female). In contrast, the two lowest accuracies for the CDS feature set of each classifier were attributed to SHR-B (8 years old) and SHR-D (9 years old), the two youngest participants of the cohort. Moreover, the oldest participant SHR-A (20 years old) had the smallest residual limb circumference (15 cm) and had the third lowest scores for LDA, KNN, and DT. It follows that a composite effect of limb size with sex- and age-related cognitive demands may impact the ability to decode motor intent.

### 6.7.3. The congenital feature set is an effective generalized set

The CFS feature set demonstrated generalizability and efficacy in decoding motor intent for our cohort of children with UCBEED. Comparative analysis from the CFS revealed no statistical differences in classification accuracy when compared to the individually tuned feature sets TMS and CDS, as well as the generalized EFS feature set (with the exception of SHR-B). It is important to note that, in general, the CFS exhibited numerically higher accuracy than the generalized EFS. Furthermore, while tuning feature sets (TMS and CDS) on an individual participant basis has the potential to improve classification accuracy, the observed numerical gains are negligible when contrasted with the generalized CFS. Therefore, we recommend the adoption of the CFS feature set for participants with UCBEED.

Therefore, in revisiting participant SHR-F, we found they also exhibited the highest classification accuracy for each classifier relative to all other participants, while SHR-B and SHR-D displayed the lowest. Moreover, we found that when attempted hand movements were reduced to a set of five (including rest state) the majority of participants across classifiers had average accuracies greater than the 85% threshold (Figure 6-7). The participants that did not meet this threshold in totality were nonetheless able to meet it for at least two classifiers (SVM and KNN). For example, participants SHR-B and SHR-D did not meet this threshold and held the following values: SHR-B (LDA 84.49%, RFN 71.86%, and DT 77.23%) and SHR-D (RFN 81.08%, DT 83.31%). These results further confirm the effects of age and sex in decoding motor intent, given that SHR-B and SHR-D were the youngest two participants. Collectively, these findings reveal the efficacy of the generalized CFS feature set considering that all participants were able to perform 5 hand movements above the 85% threshold.

What's more, we found that within the top five reduced hand movements that were aggregated across participants, the following gross motor movements emerged (Figure 6-8): wrist extension (WE), wrist flexion (WF), and cylindrical wrap (CW). This is likely attributed to the fact that participants were born with limb deficiency and conceivably did not fully develop fine motor skills, hence why intricate hand movements may have proved challenging. It is astounding that the only digit movement, index flexion (IF), emerged following the bulk-movement sequence (WE, WF, and CW). This discovery comes into view in light of the fact that index flexion is unlike any other movement that participants were prompted to attempt, despite being a fine motor skill. Perceivably, this muscle activity is uniquely distinguishable from the other movements which can be seen by its presence in the top five reduced hand movements. Finally, since the tripod pinch (TP) did not occur in any of the five reduced movements observed across participants, we inferred that it shares similarities with the pulp pinch, a comparison frequently made by participants during testing. Comprehensively, we can glean that notwithstanding the dominance of gross movements, participants had the capacity to actuate unique motions, which can thereby be improved with regular prosthesis use and proper training.

We found no statistical differences in the average ranked classification accuracies for the CFS feature set when we made pairwise comparisons between SVM, LDA, and KNN classifiers, with the exception of SHR-B (Figure 6-6). However, the majority of statistical differences were observed from the previously mentioned classifiers to DT and RFN. Although the DT exhibited lower classification accuracies, in previous work, it has indicated similar performance to the other classifiers<sup>5,28</sup>. This may suggest that the DT classifier requires additional tuning. In general, RFN also produced the lowest classification accuracy across participants, which aligns with other comparisons made to this classifier<sup>22,28</sup>. Additionally, when examining the computational expense

of the CFS, we found minimal time delays within classifiers across participants (Table 6-3). Furthermore, all classifier training times were within a reasonable range of less than 758 ms. Similarly, the testing time was also within a range suitable for future implementation of real-time control, with all values less than 19.45 ms. From these performance results, we deduce that SVM, LDA, and KNN are ideal classifiers for future investigations as currently implemented in MATLAB since they produced high accuracies and relatively low training and testing times.

## 6.8. Conclusions

To date, we have not found any other studies involving children with UCBD that investigate sEMG classification algorithms and tuned feature sets. Our work suggests three crucial points: (1) unique features arise for these children, (2) certain feature sets are beneficial for optimal classification, and (3) the newly developed generalized congenital feature set (CFS) effectively decodes motor intent. In tandem with these three points, we suggest that cognitive demands related to age, sex, and limb size seemingly play a critical role in determining motor intent. We suggest further examination of these factors with larger cohorts. In general, we found that the range of accuracies obtained for the CFS across all movements and classifiers was  $73.8\% \pm 13.8\%$ . However, these results were impacted by the difficulty children experienced in attempting repeated hand movements to the same degree. Therefore, we suggest that with physical conditioning and training, children may be able to effectively control multiple movements of dexterous upper limb prostheses. Moreover, when the 11 movements were reduced to a subset of 5, we found that all participants were able to reach the ideal threshold (85%) with accuracies of  $96.5\% \pm 6.6\%$ . This is an encouraging discovery since multi-grasp prosthesis wearers generally use only a small subset of movements and reaching the ideal threshold would thereby mitigate wearer frustration and ensure device useability<sup>25</sup>. We have found that the limited number of studies that investigate



UCBED cohorts do not adapt tuned classifiers and feature sets for this unique population. Generally, these studies only apply commercially available sEMG control systems or the Hudgins feature set, both of which are tailored to adults with acquired amputations<sup>12,13</sup>. Our work has shown that the Hudgins set often performs statistically worse when compared to the generalized CFS feature set or the individually tuned time-domain and combined-domain feature sets for each participant. Since the CFS shows promising results as a generalized feature set, further endeavors should be undertaken to determine its robustness on both a feature space level and in larger cohorts. In conclusion, the results indicate that children with UCBED have the ability to actuate their muscles in ways that classifier algorithms can decode and use for control of dexterous upper limb prostheses. Ultimately, there is a need to bridge the gap between our offline work performed on pre-recorded datasets and that of real-time control. Bridging this gap would enable us to develop effective devices for the unique clinical population.

## 6.9. References

1. Davids, J. R., Wagner, L. V., Meyer, L. C. & Blackhurst, D. W. Prosthetic management of children with unilateral congenital below-elbow deficiency. *J. Bone Jt. Surg. - Ser. A* **88**, 1294–1300 (2006).
2. Battraw, M. A. *et al.* A Review of Upper Limb Pediatric Prostheses and Perspectives on Future Advancements. *Prosthet. Orthot. Int.* **46**, 267–273 (2022).
3. Battraw, M. A. *et al.* Understanding the capacity of children with congenital unilateral below - elbow deficiency to actuate their affected muscles. *Sci. Rep.* 1–16 (2024) doi:10.1038/s41598-024-54952-7.
4. Fitzgerald, J. J. *et al.* Moving a missing hand : children born with below elbow deficiency can enact hand grasp patterns with their residual muscles. *J. Neuroeng. Rehabil.* **21**, 1–15 (2024).
5. Abbaspour, S., Lindén, M., Gholamhosseini, H., Naber, A. & Ortiz-Catalan, M. Evaluation of surface EMG-based recognition algorithms for decoding hand movements. *Med. Biol. Eng. Comput.* **58**, 83–100 (2020).
6. Adewuyi, A. A., Hargrove, L. J. & Kuiken, T. A. Evaluating EMG Feature and Classifier Selection for Application to Partial-Hand Prosthesis Control. *Front. Neurorobot.* **10**, (2016).

7. Arjunan, S. P. & Kumar, D. K. Decoding subtle forearm flexions using fractal features of surface electromyogram from single and multiple sensors. *J. Neuroeng. Rehabil.* **7**, (2010).
8. Phinyomark, A., Phukpattaranont, P. & Limsakul, C. Feature reduction and selection for EMG signal classification. *Expert Syst. Appl.* **39**, 7420–7431 (2012).
9. Ortiz-Catalan, M., Håkansson, B. & Brånemark, R. Real-time and simultaneous control of artificial limbs based on pattern recognition algorithms. *IEEE Trans. Neural Syst. Rehabil. Eng.* **22**, 756–764 (2014).
10. Atzori, M., Gijssberts, A., Muller, H. & Caputo, B. Classification of hand movements in amputated subjects by sEMG and accelerometers. in *2014 36th Annual International Conference of the IEEE Engineering in Medicine and Biology Society* (2014). doi:10.1109/EMBC.2014.6944388.
11. Parajuli, N. *et al.* Real-Time EMG Based Pattern Recognition Control Challenges: A Review on Existing Methods, Challenges and Future Implementation. *Sensors* **19**, 4596 (2019).
12. Kryger, M., Schultz, A. E. & Kuiken, T. Pattern recognition control of multifunction myoelectric prostheses by patients with congenital transradial limb defects: A preliminary study. *Prosthet. Orthot. Int.* **35**, 395–401 (2011).
13. Kaluf, B., Gart, M. S., Loeffler, B. J. & Gaston, G. Evaluating the Ability of Congenital Upper Extremity Amputees to Control a Multi-Degree of Freedom Myoelectric Prosthesis. *J. Hand Surg. Am.* **47**, 1019.e1-1019.e9 (2022).
14. Hudgins, B., Parker, P. & Scott, R. The Recognition of Myoelectric Patterns for Prosthetic Limb Control. in *Annual International Conference of the IEEE Engineering in Medicine and Biology Society* 2040–2041 (1991).
15. Hudgins, B., Parker, P. & Scott, R. N. A New Strategy for Multifunction Myoelectric Control. *IEEE Trans. Biomed. Eng.* **40**, 82–94 (1993).
16. Hargrove, L. J., Li, G., Englehart, K. B. & Hudgins, B. S. Principal components analysis preprocessing for improved classification accuracies in pattern-recognition-based myoelectric control. *IEEE Trans. Biomed. Eng.* **56**, 1407–1414 (2009).
17. Scheme, E. J., Englehart, K. B. & Hudgins, B. S. Selective classification for improved robustness of myoelectric control under nonideal conditions. *IEEE Trans. Biomed. Eng.* **58**, 1698–1705 (2011).
18. Sensinger, J. W., Lock, B. A. & Kuiken, T. A. Adaptive Pattern Recognition of Myoelectric Signals: Exploration of Conceptual Framework and Practical Algorithms. *IEEE Trans Neural Syst Rehabil Eng.* **17**, 270–278 (2009).
19. Zheng, J. Z., De La Rosa, S. & Dollar, A. M. An Investigation of Grasp Type and Frequency in Daily Household and Machine Shop Tasks. in *IEEE International Conference on Robotics and Automation* (2011). doi:10.1109/TOH.2013.6.
20. Englehart, K. & Hudgins, B. A Robust, Real-Time Control Scheme for Multifunction

- Myoelectric Control. *IEEE Trans. Biomed. Eng.* **50**, 848–854 (2003).
21. Khushaba, R. N., Kodagoda, S., Takruri, M. & Dissanayake, G. Toward improved control of prosthetic fingers using surface electromyogram (EMG) signals. *Expert Syst. Appl.* **39**, 10731–10738 (2012).
  22. Ortiz-Catalan, M., Brånemark, R. & Håkansson, B. BioPatRec: A modular research platform for the control of artificial limbs based on pattern recognition algorithms. *Source Code Biol. Med.* **8**, 1–18 (2013).
  23. Smith, L. H., Hargrove, L. J., Lock, B. A. & Kuiken, T. A. Determining the optimal window length for pattern recognition-based myoelectric control: Balancing the competing effects of classification error and controller delay. *IEEE Trans. Neural Syst. Rehabil. Eng.* **19**, 186–192 (2011).
  24. Asghari Oskoei, M. & Hu, H. Myoelectric control systems-A survey. *Biomed. Signal Process. Control* **2**, 275–294 (2007).
  25. Scheme, E. & Englehart, K. Electromyogram pattern recognition for control of powered upper-limb prostheses: State of the art and challenges for clinical use. *J. Rehabil. Res. Dev.* **48**, 643–660 (2011).
  26. Tsai, A. C., Hsieh, T. H., Luh, J. J. & Lin, T. Te. A comparison of upper-limb motion pattern recognition using EMG signals during dynamic and isometric muscle contractions. *Biomed. Signal Process. Control* **11**, 17–26 (2014).
  27. Asghari Oskoei, M., Member, S., Hu, H. & Member, S. Support Vector Machine-Based Classification Scheme for Myoelectric Control Applied to Upper Limb. *IEEE Trans. Biomed. Eng.* **55**, (2008).
  28. Abbaspour, S., Naber, A., Ortiz-catalan, M., Gholamhosseini, H. & Lindén, M. Real-time and offline evaluation of myoelectric pattern recognition for the decoding of hand movements. *Sensors* **21**, (2021).
  29. Stango, A., Negro, F. & Farina, D. Spatial Correlation of High Density EMG Signals Provides Features Robust to Electrode Number and Shift in Pattern Recognition for Myocontrol. *IEEE Trans. Neural Syst. Rehabil. Eng.* **23**, 189–198 (2015).
  30. Shin, S., Tafreshi, R. & Langari, R. A performance comparison of hand motion EMG classification. in *Middle East Conference on Biomedical Engineering, MECBME* 353–356 (IEEE Computer Society, 2014). doi:10.1109/MECBME.2014.6783276.
  31. Al-Angari, H. M., Kanitz, G., Tarantino, S. & Cipriani, C. Distance and mutual information methods for EMG feature and channel subset selection for classification of hand movements. *Biomed. Signal Process. Control* **27**, 24–31 (2016).
  32. Zardoshti-Kermani, M., Wheeler, B. C., Badie, K. & Hashemi, R. M. EMG Feature Evaluation for Movement Control of Upper Extremity Prostheses. *IEEE Trans. Rehabil. Eng.* **3**, 324–333 (1995).
  33. Hjorth, B. EEG analysis based on time domain properties. *Electroencephalogr. Clin. Neurophysiol.* **29**, 306–310 (1970).

34. Boostani, R. & Moradi, M. H. Evaluation of the forearm EMG signal features for the control of a prosthetic hand. *Physiol. Meas.* **24**, 309–319 (2003).
35. Phinyomark, A., Phukpattaranont, P. & Limsakul, C. Fractal analysis features for weak and single-channel upper-limb EMG signals. *Expert Syst. Appl.* **39**, 11156–11163 (2012).
36. Saponas, T. S., Tan, D. S., Morris, D. & Balakrishnan, R. Demonstrating the feasibility of using forearm electromyography for muscle-computer interfaces. *Conf. Hum. Factors Comput. Syst. - Proc.* (2008) doi:10.1145/1357054.1357138.
37. Iqbal, N. V., Subramaniam, K. & Asmi P., S. Robust feature sets for contraction level invariant control of upper limb myoelectric prosthesis. *Biomed. Signal Process. Control* **51**, 90–96 (2019).
38. Tkach, D., Huang, H. & Kuiken, T. A. Study of stability of time-domain features for electromyographic pattern recognition. 1–13 (2010).
39. Tang, X., Liu, Y., Lv, C. & Sun, D. Hand motion classification using a multi-channel surface electromyography sensor. *Sensors* **12**, 1130–1147 (2012).
40. Rafiee, J., Rafiee, M. A., Yavari, F. & Schoen, M. P. Feature extraction of forearm EMG signals for prosthetics. *Expert Syst. Appl.* **38**, 4058–4067 (2011).
41. Duan, F. *et al.* SEMG-Based Identification of Hand Motion Commands Using Wavelet Neural Network Combined with Discrete Wavelet Transform. *IEEE Trans. Ind. Electron.* **63**, 1923–1934 (2016).
42. Zhang, D., Zhao, X., Han, J. & Zhao, Y. A comparative study on PCA and LDA based EMG pattern recognition for anthropomorphic robotic hand. in *Proceedings - IEEE International Conference on Robotics and Automation* 4850–4855 (Institute of Electrical and Electronics Engineers Inc., 2014). doi:10.1109/ICRA.2014.6907569.
43. Dellacasa Bellingegni, A. *et al.* NLR, MLP, SVM, and LDA: A comparative analysis on EMG data from people with trans-radial amputation. *J. Neuroeng. Rehabil.* **14**, 1–16 (2017).
44. John, G. H., Kohavi, R. & Pfleger, K. Irrelevant Features and the Subset Selection Problem. in *Machine Learning: Proceedings of the Eleventh International Conference* 121–129 (Morgan Kaufmann Publishers, 1994). doi:10.1016/b978-1-55860-335-6.50023-4.
45. Bunderson, N. E. & Kuiken, T. A. Quantification of feature space changes with experience during electromyogram pattern recognition control. *IEEE Trans. Neural Syst. Rehabil. Eng.* **20**, 239–246 (2012).
46. Kristoffersen, M. B., Franzke, A. W., Sluis, C. K. Van Der, Murgia, A. & Bongers, R. M. The Effect of Feedback During Training Sessions on Learning Pattern-Recognition-Based Prosthesis Control. *IEEE Trans. Neural Syst. Rehabil. Eng.* **27**, 2087–2096 (2019).
47. Kristoffersen, M. B., Franzke, A. W., van der Sluis, C. K., Murgia, A. & Bongers, R. M. Serious gaming to generate separated and consistent EMG patterns in pattern-recognition prosthesis control. *Biomed. Signal Process. Control* **62**, 102140 (2020).

48. Powell, M. A., Kaliki, R. R. & Thakor, N. V. User training for pattern recognition-based myoelectric prostheses: Improving phantom limb movement consistency and distinguishability. *IEEE Trans. Neural Syst. Rehabil. Eng.* **22**, 522–532 (2014).
49. Friedman, M. The Use of Ranks to Avoid the Assumption of Normality Implicit in the Analysis of Variance. *J. Am. Stat. Assoc.* **32**, 675–701 (1937).
50. Demšar, J. Statistical comparisons of classifiers over multiple data sets. *J. Mach. Learn. Res.* **7**, 1–30 (2006).
51. Nemenyi, P. B. Distribution-free multiple comparisons. (Princeton University, 1963).
52. Feix, T., Romero, J., Schmiedmayer, H. B., Dollar, A. M. & Kragic, D. The GRASP Taxonomy of Human Grasp Types. *IEEE Trans. Human-Machine Syst.* **46**, 66–77 (2016).

## Chapter 7. Real-time control of multiple grasp patterns for children with UCBED

The majority of this chapter is a draft for publication as:

Battraw MA, Fitzgerald J, James MA, Bagley AM, Joiner WM, Schofield JS. Real-time control of multiple movement patterns for children with unilateral congenital below-elbow deficiency: A Case Series

### 7.1. Chapter preface

This chapter presents a case series study focusing on the real-time control of a child-sized dexterous prosthetic hand among children with unilateral congenital below-elbow deficiency (UCBED). Chapters 5 and 6 have laid the groundwork for understanding the degree to which children with UCBED can actuate their affected musculature, and how to appropriately tune classification algorithms to decode their motor intent. While we have provided the initial steps towards translating dexterous control interfaces to children with UCBED, our previous work in decoding motor intent from attempted hand movements was conducted in offline settings (Chapter 6). Real-time control presents additional challenges that require investigation. Therefore, in this chapter, we examined the robustness, responsiveness, stability, separability, consistency, and variability of real-time control for children with UCBED as they attempted missing hand movements using a child-sized dexterous prosthetic hand. These metrics are used to benchmark their ability to perform missing hand movements in real-time.

### 7.2. Introduction

Pediatric upper limb prosthesis users typically demonstrate device abandonment rates that far surpass adults, ranging from 35-45%, when compared to 23-26% in adults<sup>1</sup>. This phenomenon has been attributed to a large number of device-specific factors such as limited functionality, inadequate comfort, bulky weight, challenges with consistent control, etc<sup>1-3</sup>. Moreover, adults who

use upper limb prostheses are more likely to have acquired their limb loss later in life, as opposed to the majority of children who were born with limb deficiency, adding another level of complexity to prosthesis abandonment. These children have never operated a fully formed hand and their musculature and limbs will have never reached full maturation, marking a clear distinction from most adults with upper limb amputation who will use a prosthesis. However, current state-of-the-art techniques for controlling upper limb prostheses were developed and tested for adult amputee populations; these techniques employ surface electromyography (sEMG), which measures muscle electrical activity from the surface of the skin. Consequently, it remains unknown how real-time control of advanced dexterous devices may be used by this unique population. While child-sized multi-grasp devices are emerging, there has been limited investigation into the extent to which the pediatric population can effectively control this newly available dexterity<sup>4</sup>.

There have been few studies examining the motor control abilities of individuals born with upper limb absence to coordinate multiple movements for prosthesis use. Two studies, published 11 years apart, both employed systems established on adult amputee populations with limited success<sup>5,6</sup>. Kryger *et al.* demonstrated the ability to decode motor intent for 11 missing hand movements with a prediction accuracy of  $52.1\% \pm 15.0\%$  in a group of ( $N = 4$ ) adults with congenital upper limb absence<sup>5</sup>. Additionally, Kaluf *et al.* showed an  $80\% \pm 16.0\%$  prediction accuracy when only 3 degrees of freedom were investigated for ( $N = 4$ ) children with congenital upper limb absence<sup>6</sup>. In our previous work with sEMG, we demonstrated that children with unilateral congenital below-elbow deficiency (UCBED) exhibit a large degree of consistent and distinguishable control over their affected musculature<sup>7</sup>. Additionally, in Chapter 6, we explored classifier and feature set combinations to maximize multi-movement decoding accuracy. We proposed the time domain congenital feature set (CFS) which consisted of the following features: correlation coefficient (*tc*),

multi-channel energy ratio (*tmcer*), log detector (*tlogd*), Hjorth mobility parameter (*tHmob*), and integrated absolute value (*tiabs*). These results revealed that when (N = 9) participants attempted to move their missing hand for a subset of 5 movements, the classification accuracy was (96.5% ± 6.6%) (see Chapter 6). Furthermore, we investigated a promising measurement modality for prosthetic control among children with UCBED—ultrasound imaging to measure muscle displacement and deformation—which provides a complementary measure to sEMG for attempted missing hand movements<sup>8</sup>. However, before evaluating techniques for prosthetic control that are not commercially available, it is important to assess the current standard of care. Therefore, within this chapter, we investigated how the current state-of-the-art for sEMG dexterous real-time control translates to children with UCBED.

The aim of this chapter was to explore the capability of UCBED children to control multiple hand movement patterns in real-time with a robotic prosthetic hand. To achieve this, we employed the Motion Test, which allows for the extraction and analysis of real-time performance metrics, which include robustness, responsiveness, and stability of attempted movements<sup>9</sup>. Additionally, we investigated feature space quality metrics such as separability, consistency, and variability<sup>10-12</sup> of real-time sEMG data. We hypothesized that children with UCBED would exhibit control over multiple missing hand movements with their affected limb, and this may be to a lesser degree than their unaffected limb, as reflected by real-time performance and feature space quality. Altogether, this work represents a significant step in understanding how children use dexterous prostheses and how to begin the effective development and translation of such devices and control techniques to the pediatric UCBED population.






### 7.3. Methods

#### 7.3.1. Participants

Three male participants, aged 14, 13, and 10 years, all diagnosed with right unilateral congenital below-elbow deficiency, were enrolled in this study. Participants had a different history of prosthesis use, which included body-powered, activity-specific, passive, or none. Participant demographics and experimental setup are provided in Table 7-1. Prior to participation, informed consent was obtained from participants and/or their legally authorized representatives. The research protocols were approved by the Institutional Review Board at Shriners Children’s – Northern California, and all research methods were performed in accordance with relevant guidelines and regulations.

Table 7-1. Participant demographics for children with unilateral congenital below-elbow deficiency. Values in brackets represent measurements for the unaffected limb. The elbow range of motion is defined as extension/flexion. †Participant is currently not wearing the device.

<b>Participant ID</b>	<b>PAR1</b>	<b>PAR2</b>	<b>PAR3</b>
<b>Participant Setup</b>			
<b>Age</b>	14 (y/o)	13 (y/o)	10 (y/o)
<b>Sex</b>	Male	Male	Male
<b>Affected Limb</b>	Right	Right	Right
<b>Limb Length (cm)</b>	11.0 (29.5)	21.5 (23.0)	13.0 (23.5)
<b>Limb Circumference (cm)</b>	22.5 (26.0)	19.0 (21.5)	14.0 (18.5)
<b>Elbow Range of Motion (deg)</b>	180/50 (180/35)	180/35 (180/40)	195/40 (180/45)
<b>Prosthesis Use</b>	Body-powered† Activity-specific	None	Passive†

### 7.3.2. Data collection

Seven non-invasive sEMG Mini Trigno electrodes were placed over the forearm muscles of each limb using double-sided adhesive. These electrodes are part of the 16-Channel Delsys Trigno sEMG research platform (Delsys, Natick, USA). Electrodes were adhered circumferentially on the participants' affected limb, located where the bulk muscle belly was palpated, and on the unaffected limb approximately two-thirds of the forearm length as measured from the distal end<sup>7</sup>.

Before real-time testing, sEMG data were collected from participants' affected and unaffected forearm muscles in an offline algorithm-training phase. Participants were instructed to imagine and attempt a series of muscle contractions necessary to perform five common hand movements. Four of these movements are defined in adult hand grasp taxonomy<sup>13</sup> and our previous work in Chapter 3 on pediatric hand grasp taxonomy: Key, Pinch, Power, and Tripod. Additionally, we selected the fifth hand movement, Open, for practical application in controlling multi-grasp prostheses, as users will require the ability to return the hand to a neutral position. During this offline algorithm-training phase, participants mirrored these movements with the unaffected side to help promote the activation of their affected limb. For each hand movement, participants performed two trials of three repetitions with 3 seconds of contraction followed by 4 seconds of relaxation. These movements were recorded using the wireless sEMG Mini Trigno electrodes. The data were transmitted to the Delsys research platform, where it was reconstructed and output as an analog signal to a National Instruments USB 6210 Data Acquisition System (National Instruments Corp., Austin, USA), sampling at 6 kHz. A custom MATLAB script (R2022a, MathWorks, Inc., Natick, USA) was employed to collect and store the sEMG data for offline algorithm training. All data collection, processing, and real-time control were conducted on a Lenovo PC with a 64-bit

Windows 11 operating system, 32 GB of RAM, and an Intel core i7-8550U at 1.80 GHz (Intel Corp., Santa Clara, USA).

The collected data were then structured for use with BioPatRec, an sEMG pattern recognition software that operates in MATLAB<sup>14</sup>. Using this software, the sEMG data were processed with the following settings for offline algorithm training and real-time control. Segmentation was conducted with 200 ms windows and 50 ms time increments, and the features extracted were defined by the congenital feature set (CFS): *tcr*, *tmcer*, *tlogd*, *tHmob*, *tiabs* (see Chapter 6). During offline preprocessing, data were cleaned to remove latencies in participant reaction times by extracting 70% of the 3-second contraction time (2.1 seconds in total). Offline algorithm training was performed with a linear discriminant analysis (LDA) classifier, as our previous work indicated that this classifier/feature set combination offers low computational time and good performance for children with UCBD (see Chapter 6). However, the classifier topology was set to one-vs-one (OVO) because it has been demonstrated to improve individual movement classification accuracy<sup>15,16</sup>. This topology trains all possible combinations of paired movements from  $M$  total movements, producing  $C$  classifiers ( $C=M*(M-1)/2$ )<sup>15</sup>. Within this topological scheme, the movement that occurs most often across the  $C$  classifiers is the predicted output<sup>15</sup>.

### 7.3.3. Motion Test

To evaluate real-time classification performance in children with UCBD, we conducted the Motion Test<sup>9</sup>. This test required participants to perform the previously trained hand movements while their actions were predicted in real-time using BioPatRec. Real-time control was achieved using the LDA-OVO classifier through the *Real-time PatRec Mov2Mov* graphical interface within BioPatRec. Each trial of the Motion Test consisted of three randomized repetitions for each of the five movements. This procedure was repeated for five trials, resulting in a total of 75 attempted

movements. The timeout period, which indicated the total time allotted to complete each movement, was set to 6 seconds, with a 6-second preparation interval between randomized movements. The BioPatRec graphical interface displayed the movements for participants to follow and indicated the predicted movement in real-time. Verbal cues and movement actions were provided to assist participants in following the displayed movement. Additionally, as the children attempted the movements, the predictions were simultaneously mapped in real time to the BEAR PAW, a research-based multi-articulate pediatric prosthetic hand<sup>17</sup>. This allowed for the visualization of prosthetic control throughout the Motion Test.

Furthermore, this test facilitated the capture of real-time performance metrics during attempted missing hand movements<sup>9,14</sup>. These metrics were calculated based on real-time predictions, with a new prediction generated every 50 ms, equating to 20 predictions per second. The following metrics facilitate the evaluation of how robust, responsive, and stable the control of multiple hand movements is within our cohort of UCBED children.

***Selection Time*** served as an indicator of the responsiveness of real-time classification and is defined as the time to the first correct prediction<sup>9</sup>. This metric is calculated starting from movement onset, which is identified as the first prediction during the experimental trial that is different from the rest prediction<sup>9</sup>. In this context, a lower selection time indicates faster responsiveness, meaning participants may initiate the movement for control of a device sooner, while a higher value signifies decreased responsiveness<sup>9</sup>.

***Completion Time*** reflects the stability of real-time classification and is defined as the time taken to produce the first 20 correct predictions, calculated from movement onset<sup>9</sup>. A faster completion time indicates better control stability, which signifies the participants were able to attain the

intended missing hand movement early on during attempted muscle actuation (speed of use stability), whereas a longer completion time indicates poorer control stability<sup>9</sup>.

**Completion Rate** is an indicator of robustness, which is defined as the ratio of movements during the experimental trials that reached the completion time within the 6-second timeout period to the 75 total attempted movements<sup>9</sup>. The higher rate suggests that participants were able to achieve more of their attempted missing hand movements, while a smaller value indicates fewer movements were achieved<sup>9</sup>.

**Real-Time Accuracy** was an additional indicator of real-time classification stability, as introduced by Ortiz-Catalan *et al*<sup>14</sup>. It is defined as the accuracy obtained within the completion time, i.e., the ratio of 20 correct predictions to the total number of predictions made within the completion time<sup>14</sup>.

**Binned Accuracy** is a supplementary metric similar to real-time accuracy, providing insight into the temporal classification stability. It is defined as the total number of correctly predicted movements calculated within time intervals (10 bins) throughout the entire timeout period. Given the 6-second timeout period and that 20 predictions were made per second, each of the 10 bins would include 120/10 individual predictions of the missing hand movements. This provides a metric to understand if the participants were able to sustain the desired missing hand movement at some time interval throughout the timeout period.

#### 7.3.4. Feature space quality

During the Motion Test, raw sEMG signals were collected to investigate the feature space quality of real-time data. Recall that participants were instructed to maintain the desired movement for the entire 6-second timeout period during the Motion Test. The raw sEMG signals acquired during the test underwent preprocessing using the same parameters as the offline data: they were segmented

into 200 ms time windows with 50 ms time increments, and the CFS features were extracted following the procedures outlined in section 7.3.2. Common feature space quality metrics, including separability, consistency, and variability,<sup>10-12</sup> were calculated over 2.1-second intervals of the feature space data with 50 ms time steps, producing temporal feature space trajectories. It is noteworthy that we chose a 2.1-second interval to align with offline data processing, as participant latencies for the 3-second offline contractions were accounted for by extracting 70% of the 3-second contraction (equivalent to 2.1 seconds). An illustration of the feature space metrics separability, consistency, and variability is provided in Figure 7-1.

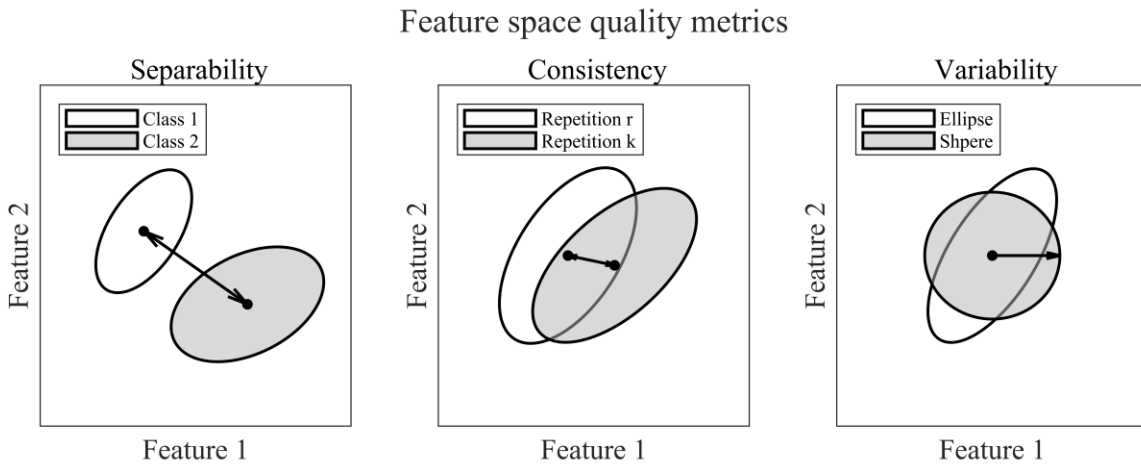


Figure 7-1. Illustration of the feature space metrics employed for analysis. Separability represents the minimum distance from one class (grasp) to the remaining classes<sup>12</sup>. Consistency signifies the distance between repetitions of the same class<sup>12</sup>. Variability indicates the spread of the feature space for a given class. It is estimated as the radius of a hypersphere with the same volume as a hyper-ellipsoid, under the assumption that the feature space data conforms to a hyper-ellipsoid distribution<sup>12</sup>.

#### 7.3.4.1. Separability

Separability defines a conflicting distance between movements within feature space. The average real-time separability index (RSI) across the movement classes was defined and adapted following Franzke *et al.*<sup>11</sup>. Here, the inter-class distance to the nearest neighbor separability index provided the average distance of the nearest neighbor<sup>10-12</sup> across the  $m = 5$  movement classes. The distance

to the nearest neighbor in feature space for each movement serves as a metric of conflict, with the average distance defining the “overall” separability of the movements.

We calculated the RSI given by Equation 7-1, defined as the minimum one-half Mahalanobis distance of the real-time feature space data between movements  $i$  and  $j$ . Here,  $\mu_{Ri}$  and  $\mu_{Rj}$  represent the feature space centroids of the real-time data for the  $i$  and  $j$  movements, respectively. Equation 7-2 represents the real-time covariance matrix ( $S_R$ ), considering both movement classes, as described by Nilsson *et al.*<sup>18</sup>. Furthermore,  $S_{Ri}$  and  $S_{Rj}$  denote the covariance matrices for the real-time feature space data for the  $i$  and  $j$  movements, respectively. Finally, it is important to note that when taking the inverse of the covariance matrix, the Moore-Penrose inverse was used to ensure its existence.

$$RSI = \frac{1}{m} \sum_{j=1}^m \left( \min_{i=1, \dots, j-1, j+1, \dots, m} \frac{1}{2} \sqrt{(\mu_{Ri} - \mu_{Rj})^T * S_R^{-1} * (\mu_{Ri} - \mu_{Rj})} \right) \quad \text{Equation 7-1}$$

$$S_R = \frac{S_{Ri} + S_{Rj}}{2} \quad \text{Equation 7-2}$$

#### 7.3.4.2. Consistency

The consistency of repetitions within a given movement represents the ability for participants to perform repeatable patterns of muscle excitation, as assessed by determining the proximity of repetitions in feature space<sup>10-12</sup>. Consistency between the  $n = 3$  movement repetitions for the real-time trials is defined by the average within-class distance from each pair-wise repetition ( $p = 2$ ). The consistency metric for the repetitions in feature space, represented by real-time within-class distance (RWD), is provided below in Equation 7-3, calculated as the average of the  $m$  movements, as modified from Franzke *et al.*<sup>11</sup>.

$$RWD = \frac{p!(n-p)!}{m * n!} \sum_{i=1}^m \left( \sum_{\substack{r=1, k=1 \\ k > r}}^n \left( \frac{1}{2} \sqrt{(\mu_{Rri} - \mu_{Rki})^T * S_R^{-1} * (\mu_{Rri} - \mu_{Rki})} \right) \right) \quad \text{Equation 7-3}$$

$$S_R = \frac{S_{Rri} + S_{Rki}}{2} \quad \text{Equation 7-4}$$

The RWD was calculated in the same manner as the previously discussed separability metric but is defined as the one-half Mahalanobis distance for a single movement  $i$  of the real-time feature space data between repetitions  $r$  and  $k$ . Here,  $\mu_{Rri}$ , and  $\mu_{Rki}$  indicate the feature space centroids of the real-time data for the  $r$  and  $k$  repetitions of the  $i^{\text{th}}$  movement, respectively. Equation 7-4 represents the real-time covariance matrix ( $S_R$ ) for the repetitions, where both repetitions  $r$  and  $k$  were taken into consideration, as described by Nilsson *et al.*<sup>18</sup>. The  $S_{Rri}$  and  $S_{Rki}$  are the covariance matrices for the real-time feature space data of the  $r$  and  $k$  repetitions for a given movement  $i$ , respectively.

#### 7.3.4.3. Variability

Variability quantifies the spread of data within feature space for a particular movement. Here, the mean semi-principal axis serves as a metric for the average variability of the feature space across the  $m$  movements<sup>10-12</sup>. The real-time mean semi-principal axis (RMSA) is formulated as the radius of a hypersphere with the same volume as a hyper-ellipsoid, reflecting the assumption that the feature space data conforms to a hyper-ellipsoid<sup>12</sup>. Here,  $a_{Rik}$  represents the real-time semi-principal axes for the  $i^{\text{th}}$  of  $m$  movements, respectively. The semi-principal axes of the hyper-ellipsoid were approximated from singular value decomposition<sup>11</sup> for the  $k^{\text{th}}$  of  $d$  dimensions (where  $d = 57$  dimensions as given by the feature set and sEMG channel combination). The RMSA is calculated by Equation 7-5, as defined by Bunderson *et al.*<sup>12</sup>.

$$RMSA = \frac{1}{m} \sum_{i=1}^m \left( \left( \prod_{k=1}^d a_{Rik} \right)^{\frac{1}{d}} \right) \quad \text{Equation 7-5}$$



## 7.4. Analysis

### 7.4.1. Offline evaluation

To evaluate the LDA-OVO offline classification performance for attempted hand movements, we employed a 60-40 cross-validation method. This method entails allocating 60% of the data for training and 40% for testing. We then conduct 100 randomizations of the training and testing sets, recalculating the classifier performance with each iteration. The average performance was then derived from these 100 randomizations. Furthermore, we measured the computational time by determining the average training time required to train the  $C$  classifiers and the average testing time needed for the  $C$  classifiers to predict the movement for the one-vs-one topology.

### 7.4.2. Motion Test

The Motion Test allowed us to understand the real-time classification performance metrics as participants attempted movements. Selection time, completion time, completion rate, real-time accuracy, and binned accuracy are compared across limbs to determine if the affected limb performs similar to the unaffected limb. These metrics aid in our understanding of the robustness, responsiveness, and stability, and are visualized using box and whisker plots. Statistical comparisons across limbs for each movement were performed with the nonparametric Mann-Whitney U test at a significance level of  $\alpha = 0.05$ . However, the completion rate comparison across limbs was performed by aggregating all movements due to the metric definition. The null hypothesis  $H_0$  states that there is no difference in the central tendency between the affected and unaffected limbs for the real-time classification performance metrics. Additionally, to contextualize the Motion Test data an ideal metrics range was obtained from adult able-bodied literature following a similar classification approach, utilizing LDA-OVO<sup>20</sup>. It is worth noting that the ideal metric range for binned accuracy was adapted to match that of the real-time accuracy, while all others were directly used.

### 7.4.3. Feature space quality

In order to assess whether the real-time feature space quality metrics of the affected limb were comparable to those of the unaffected limb, a comparative analysis was conducted. To facilitate inter-limb comparisons, the trajectories of the feature space quality metrics were normalized using min-max normalization as determined across the five trials for each limb. These normalized data were then discretized into ten bins and represented using box and whisker plots to visualize temporal changes across limbs and the timeout period. Statistical comparisons between limbs for each bin were conducted with the nonparametric Mann-Whitney U test at a significance level of  $\alpha = 0.05$ . The null hypothesis  $H_0$  was defined as there being no difference in the central tendency between the affected and unaffected limb for the observed feature space metric. Furthermore, in order to highlight differences in the trajectory of feature space quality metrics, trial-to-trial relatedness was quantified as the area enclosed by any two normalized trajectories for separability, consistency, and variability. This area was calculated by computing the integral of the absolute difference between two trajectories in MATLAB using the *trapz* function. Within this context, a larger area between any two trials suggests a greater deviation, while a smaller value indicates closer consistency between trials.

## 7.5. Results

### 7.5.1. Offline evaluation

To understand the ability to classify six movements, the five selected missing hand movements, and rest, we evaluated offline classification accuracy and computational time using the LDA-OVO classifier for each participant. We selected a target offline threshold value of 85% classification accuracy since it has been suggested as the minimum for usable real-time control, where values lower than this can lead to user frustration due to inadequate device control<sup>19</sup>. All participants exhibited average classification accuracies exceeding this threshold, ranging from 91.47% to

99.63% across the affected and unaffected limbs. Notably, all unaffected limb average classification accuracies fell within the range observed in able-bodied adults<sup>20</sup>, while only participant 2 achieved this range with their affected limb. Classification accuracies indicating individual movement performance for each participant are discussed in detail in the following sections. In addition to the classification accuracy, computational time is a critical factor that was explored. Extended classifier training times pose a practical hurdle for everyday use of dexterous prostheses, since users will not want to endure extensive waiting periods for classifier training. Additionally, testing times exceeding 300 (ms) can lead to noticeable controller delays and thereby user frustration<sup>21</sup>. Training times across the participants and limbs ranged from 0.682 (s) to 0.800 (s), approximately twice as long as those reported in able-bodied adults<sup>20</sup>. Moreover, testing times ranged from 0.145 (s) to 0.161 (s), slightly faster than those reported in able-bodied adults<sup>20</sup>. A summary of average offline performance metrics are presented in Table 7-2. These findings highlight the potential for effectively decoding the attempted missing hand movements from the affected musculature in children with UCBED and how that relates to their unaffected limb.

Table 7-2. Average offline performance metrics.

<b>Participants</b>	<b>Limb</b>	<b>Accuracy (%)</b>	<b>Training time (s)</b>	<b>Testing time (ms)</b>
Participant 1	Affected	91.47	0.760	0.145
	Unaffected	99.11	0.682	0.146
Participant 2	Affected	97.10	0.776	0.148
	Unaffected	99.63	0.764	0.147
Participant 3	Affected	92.21	0.800	0.156
	Unaffected	99.31	0.703	0.161
Adult able-bodied N=15 <sup>18</sup>	Dominant	97.9 ± 2.69	0.342 ± 0.058	2.20 ± 0.090

#### 7.5.1.1. Participant 1

For the affected limb, five of the six movements were above the real-time control performance threshold of 85%. Here, Tripod achieved 84.60%, and Power slightly surpassed the threshold at 85.90%. Notably, Tripod tended to misclassify as Pinch with a rate of 5.70%, while Power commonly misclassified as Key with a rate of 6.80%. In contrast, their unaffected limb exhibited high classification accuracy with all movements surpassing the 85% threshold, while the lowest-performing movement, Pinch, achieved an accuracy of 96.20%. The confusion matrices, depicting individual movement classification accuracy and their misclassifications, are presented in the first column of Figure 7-2.

#### 7.5.1.2. Participant 2

All six attempted missing hand movements for their affected limb exceeded the 85% threshold. The lowest-performing movement, Power, achieved a classification accuracy of 92.50%, with a misclassification rate of 4.50% as Key. Similarly, for the unaffected limb, all movements exceeded the 85% threshold, with Power having the lowest classification accuracy of 99.30%. Detailed classification accuracies are provided in the confusion matrices within the middle column of Figure 7-2.

#### 7.5.1.3. Participant 3

For the affected limb, five out of the six missing hand movements were above the 85% threshold. Pinch, however, fell below the threshold of usable real-time control, with a classification accuracy of 84.20%. Interestingly, this movement was frequently misclassified as both Open and Tripod, with misclassification rates of 7.80% and 6.00%, respectively. All six movements for the unaffected limb surpassed the suggested threshold, with the lowest-performing movement, Power,

having an accuracy of 98.00%. Detailed classification accuracies for individual movements are presented in the last column of Figure 7-2.

## Offline confusion matrices

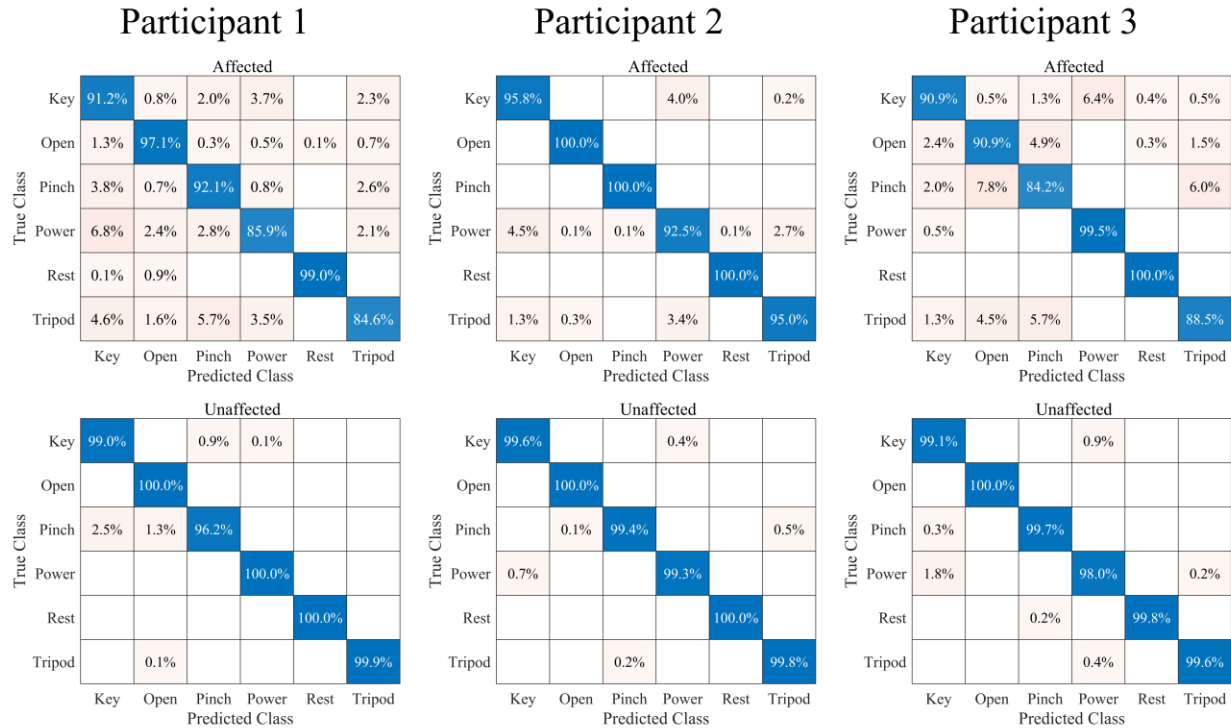


Figure 7-2. Offline confusion matrices. Within each given participant column, two confusion matrices are displayed: affected limb (top) and unaffected limb (bottom). These matrices illustrate the ability to classify each hand movement, with the average of the diagonal indicating the overall classification accuracy. Across all five movements, and rest, participants exhibited an average classification accuracy which exceeded approximately 91% for their affected limb and about 99% for their unaffected limb.

### 7.5.2. Motion Test

The Motion Test was conducted to assess participants' ability to control a multi-grasp prosthetic hand in real-time with their affected limb and to determine if their performance was comparable to that of their unaffected limb. An illustration of the Motion Test setup is provided in Figure 7-3. Across both limbs, participants exhibited average real-time accuracy, selection time, and completion time which ranged from 38.10% to 56.83%, 0.74 (s) to 1.43 (s), and 2.28 (s) to 3.10 (s), respectively. In comparison, literature on able-bodied adults suggests ideal metrics with real-

time accuracy ranging from  $69.3 \pm 10.8\%$ , selection time ranging from  $0.659 \pm 0.238$  (s), and completion time ranging from  $4.79 \pm 0.815$  (s)<sup>20</sup>. Notably, the ideal range for completion time, although slower than that reported in other adult literature,<sup>9,14</sup> was selected since the experimental setup described by Abbaspour *et al.*<sup>20</sup> closely matched ours.

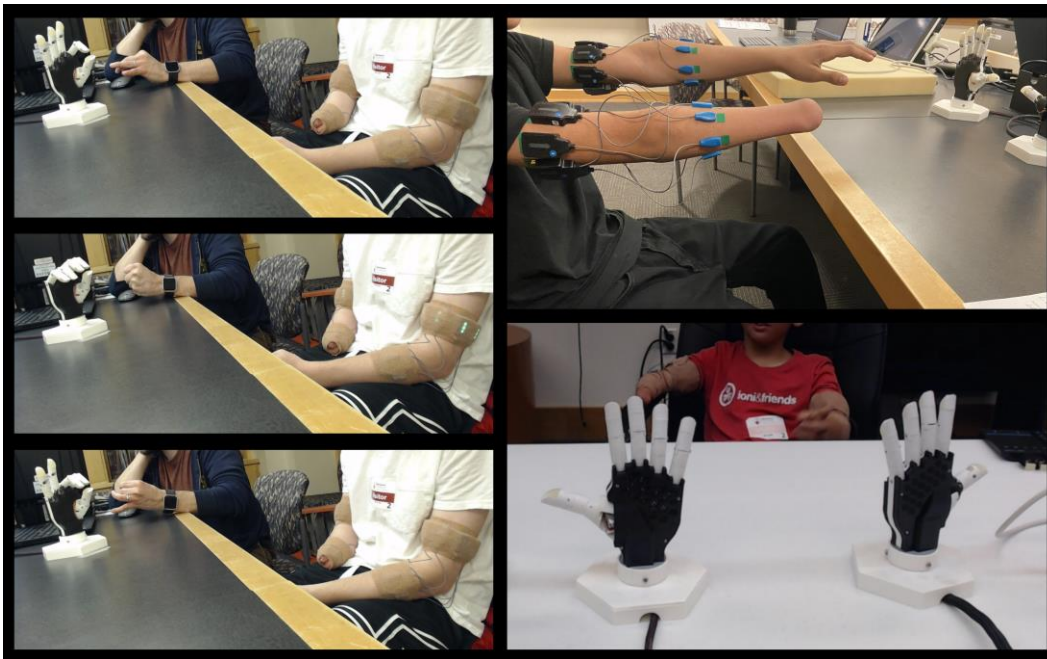


Figure 7-3. Participant examples for the Motion Test and setup. The various panels in this figure depict participants performing the Motion Test using different hand movements, the surface electromyography (sEMG) setup for both affected and unaffected limbs, and an overview of the general device setup.

Detailed statistical analyses for the Motion Test metrics, organized on an individual movement basis, are provided in the participant-specific sections below. The completion rate serves as an overall metric generated across the movements; therefore, statistical analysis was not conducted on an individual movement basis. Across participants, the completion rate for the affected limb ranged from 48.00% to 80.00%, while for the unaffected limb, it ranged from 68.00% to 92.00%. In comparison, the ideal completion rate metric for adult able-bodied individuals ranged from  $71.3 \pm 14.4\%$ <sup>20</sup>. It is important to highlight that participant 2 achieved an 80.00% completion rate for their affected limb, within the ideal completion rate range of  $71.3 \pm 14.4\%$ <sup>20</sup>. This indicates that they

were able to successfully perform the majority of their attempted missing hand movements. A single statistical difference was observed in the completion rate, which occurred for participant 3, where the unaffected limb exhibited a statistically higher performance than the affected limb. A summary of the average data for these metrics, along with the ideal adult able-bodied range, is presented in Table 7-3.

Table 7-3. Average real-time performance metrics. †This value was higher than found in other adult able-bodied literature but was used since the classification technique closely matched our setup. ‡Indicates there was a statistical difference in completion rate across limbs, with a significance level of  $\alpha = 0.05$ .

Participants	Limb	Accuracy (%)	Selection time (s)	Completion time (s)	Completion rate (%)
Participant 1	Affected	38.10	1.4289	3.0953	56.00
	Unaffected	49.52	1.1600	2.4268	68.00
Participant 2	Affected	53.77	1.0870	2.4231	80.00
	Unaffected	51.38	1.2298	2.4883	85.33
Participant 3	Affected	56.83	1.1873	2.2829	48.00‡
	Unaffected	55.86	0.7424	2.3592	92.00‡
Adult able-bodied N=15 <sup>20</sup>	Dominant	69.3 ± 10.8	0.659 ± 0.238	4.79 ± 0.815†	71.3 ± 14.4

#### 7.5.2.1. Participant 1

The median selection times for three movements in the affected limb —Key, Power, and Tripod— were within the ideal range for adult able-bodied individuals. Additionally, for the unaffected limb, the median selection times for Key, Open, and Pinch also fell within the ideal range. Statistical significance was observed in the selection time for the Tripod movement, wherein the affected limb surprisingly outperformed the unaffected limb with a quicker selection time, indicating heightened responsiveness. Furthermore, the affected limb exhibited median completion times for all movements faster than the ideal range, while the unaffected limb had only one movement, Tripod, within the range. Note that faster completion times indicate that the participant had a better speed of use stability, as they were able to achieve the intended missing hand movement sooner<sup>9</sup>.

Moreover, both the affected and unaffected limbs showed median real-time accuracies that were below the ideal range. Analyzing completion time and real-time accuracy revealed significant differences between the affected and unaffected limbs for two movements: Key and Open. Specifically, the affected limb displayed statistically higher completion times, indicating decreased speed of use stability, which means it took longer to achieve 20 correct predictions and, consequently, longer to perform the intended hand movement. Additionally, the affected limb exhibited statistically lower real-time accuracy. Finally, although all median values for the binned accuracy were numerically higher for the unaffected limb compared to the affected limb, no statistical differences were observed. Detailed Motion Test data for participant 1 can be found in the first column of Figure 7-4.

#### 7.5.2.2. Participant 2

The median selection times for four movements—Open, Pinch, Power, and Tripod—were within the ideal range for the affected limb. Among the movements for the unaffected limb, Pinch and Power fell within the selection time ideal range, while Key and Open were borderline. Statistically, only Power differed between limbs in selection time, with the affected limb performing better than the unaffected limb. All movements across both limbs, except Tripod, had faster median completion times compared to the ideal range, which indicates attempted missing hand movements were achieved faster<sup>9</sup>. However, no statistical differences were found between the affected and unaffected limbs for the completion time. Regarding real-time accuracy, the median values for three movements—Open, Pinch, and Power—were within the ideal range for the affected limb, while for the unaffected limb, only Open and Pinch met this criterion. No statistical differences for real-time accuracy were found for any of the movements across limbs. In terms of the binned accuracy, nine bins for the affected limb were within the ideal range, compared to only five for the



unaffected limb. Recall that the ideal range for the binned accuracy was defined to match that of real-time accuracy. No statistical differences were found across limbs for the binned accuracies. The Motion Test data for participant 2 is provided in the middle column of Figure 7-4.

#### 7.5.2.3. Participant 3

In the affected limb, the median selection time for the Open hand movement fell within the ideal range, while Key exhibited a faster responsiveness. Conversely, all movements for the unaffected limb demonstrated either ideal or faster responsiveness. Two movements, Open and Tripod, showed a statistically significant difference across limbs for the selection time, with the affected limb performing worse. For the completion time, median values for all movements across both limbs had faster times than the ideal range. However, there was a statistical difference observed in the Open hand movement across limbs, which indicated that the affected limb took longer to achieve the intended missing hand movement<sup>9</sup>. In terms of real-time accuracy, only the median of Power from the affected limb was within the ideal range, while Open and Pinch from the unaffected limb had medians above and within the ideal ranges, respectively. A statistical difference was observed across limbs for the Open hand movement, with the affected limb performing statistically worse. It is important to note that both completion time and real-time accuracy for the affected limb had exceptions. More specifically, only one out of 15 repetitions of Pinch completed 20 correct predictions within the 6-second timeout period, affecting the completion time and real-time accuracy, while Tripod had none. Additionally, for the binned accuracy not a single bin for the affected limb achieved a median accuracy within the ideal range, contrasted with the unaffected limb, where the last 5 bins fell within this range. Only one statistical difference emerged across limbs in bin 9, indicating the affected limb performed statistically worse. All Motion Test data for participant 3 is depicted in the last column of Figure 7-4.

## Real-time performance metrics

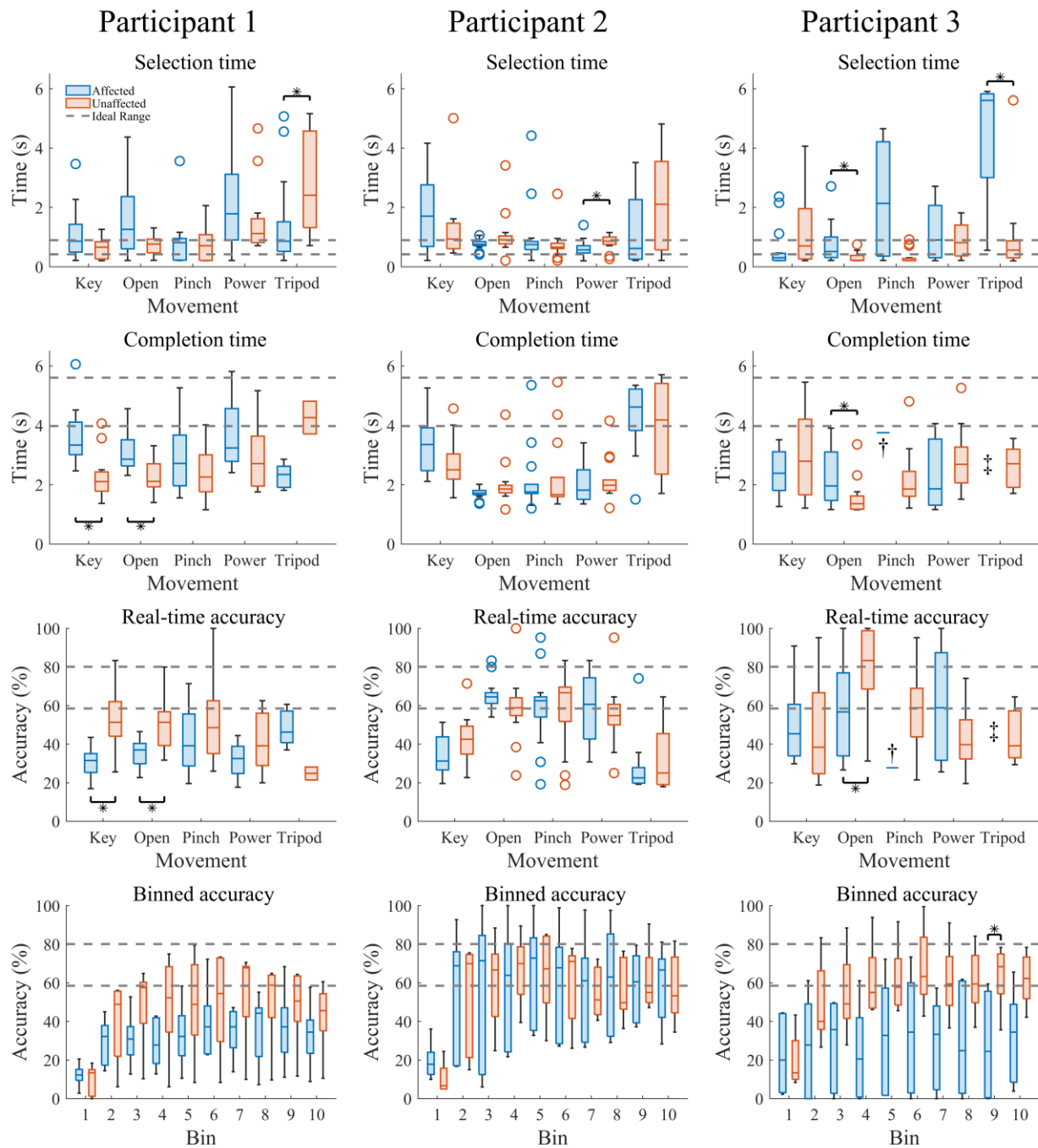


Figure 7-4. Real-time performance metrics. Within each given participant column, four metrics are displayed from top to bottom: selection time, completion time, real-time accuracy, and binned accuracy. Blue shading represents the affected limb, while red shading represents the unaffected limb. \*Signifies a statistical difference between the limbs. †Denotes that only a single value was achieved out of the 15 affected limb movement repetitions. ‡Indicates the participant was unable to achieve the desired metric for the affected limb. Additionally, dashed lines represent the ideal range obtained from adult able-bodied literature for the Motion Test using a similar classification approach, LDA-OVO<sup>20</sup>.

### 7.5.3. Feature space quality

The feature space quality metrics—separability, consistency, and variability—provided a framework for examining temporal changes across limbs and trial-to-trial relatedness. Values for these metrics were averaged across movements within limbs to obtain overall metrics. Comparisons between the affected and unaffected limbs were made using the binned data as discussed in sections 7.3.4 and 7.4.3. Additionally, trial-to-trial relatedness was defined as the area between pair-wise trials within a given feature space quality metric. These metrics collectively offer insight into the dynamic nature of motor performance and the interplay between temporal changes and trial-to-trial consistency across limbs.

#### 7.5.3.1. Separability

Across all participants, we observed a notable pattern in the separability for their unaffected limb, characterized by a sharp increase followed by a plateau. A similar trend was evident in the affected limb of participant 1, although the central tendency of participant 2 showed a slight decline from bin 7 to bin 10 (3.6 (s) to 6.0 (s)). Additionally, participant 3 exhibited an initial increase up to bin 3, followed by a steady decline, representing a distinct departure from the patterns observed in the previous participants. Moreover, participant 3 demonstrated statistically significant differences in separability for bins 4 through 10 (1.8 (s) to 6.0 (s)) across limbs, with the affected limb showing a significant decrease compared to the unaffected limb. The trajectory of separability for all participants is illustrated in the first row of Figure 7-5. These findings may suggest that, for some participants, the temporal trajectory of separability in the feature space of muscle excitation for the affected limb resembles that of the unaffected limb.

#### 7.5.3.2. Consistency

Similar to separability, the consistency exhibited an initial numerical increase followed by a plateau. This upward trend suggests an initial decrease in consistency between repeated repetitions, followed by stabilization at a relatively steady level of consistency. However, this pattern was observed only for participants 1 and 2, as participant 3 showed a trend in the central tendency that lacked clear visual distinction. For participants 2 and 3, the affected limb showed statistically significant differences from the unaffected limb in bin 1 of the consistency metric, with the affected limb demonstrating a larger consistency value, indicating greater inconsistency at the onset of movement contraction. The participant consistency trajectories are shown in the middle row of Figure 7-5. These results indicate that, in some participants, the ability to consistently repeat movements with the affected limb over a specific time period mirrors that of their unaffected limb.

#### 7.5.3.3. Variability

The variability initially showed a large spread as each movement transitioned from the rest state to an active movement state, traversing the feature space which resulted in high variability at the onset. However, the variability gradually stabilized at a lower value over time. This consistent trend in the variability trajectory was observed across all participants, except for participant 3, who displayed an exceptionally high spread in their variability across the trials. The trajectories of variability for each participant are depicted in the last row of Figure 7-5. The similar variability observed across limbs for some participants may suggest a potential common underlying pattern of muscle variability between affected and unaffected limbs.

## Feature space quality metrics

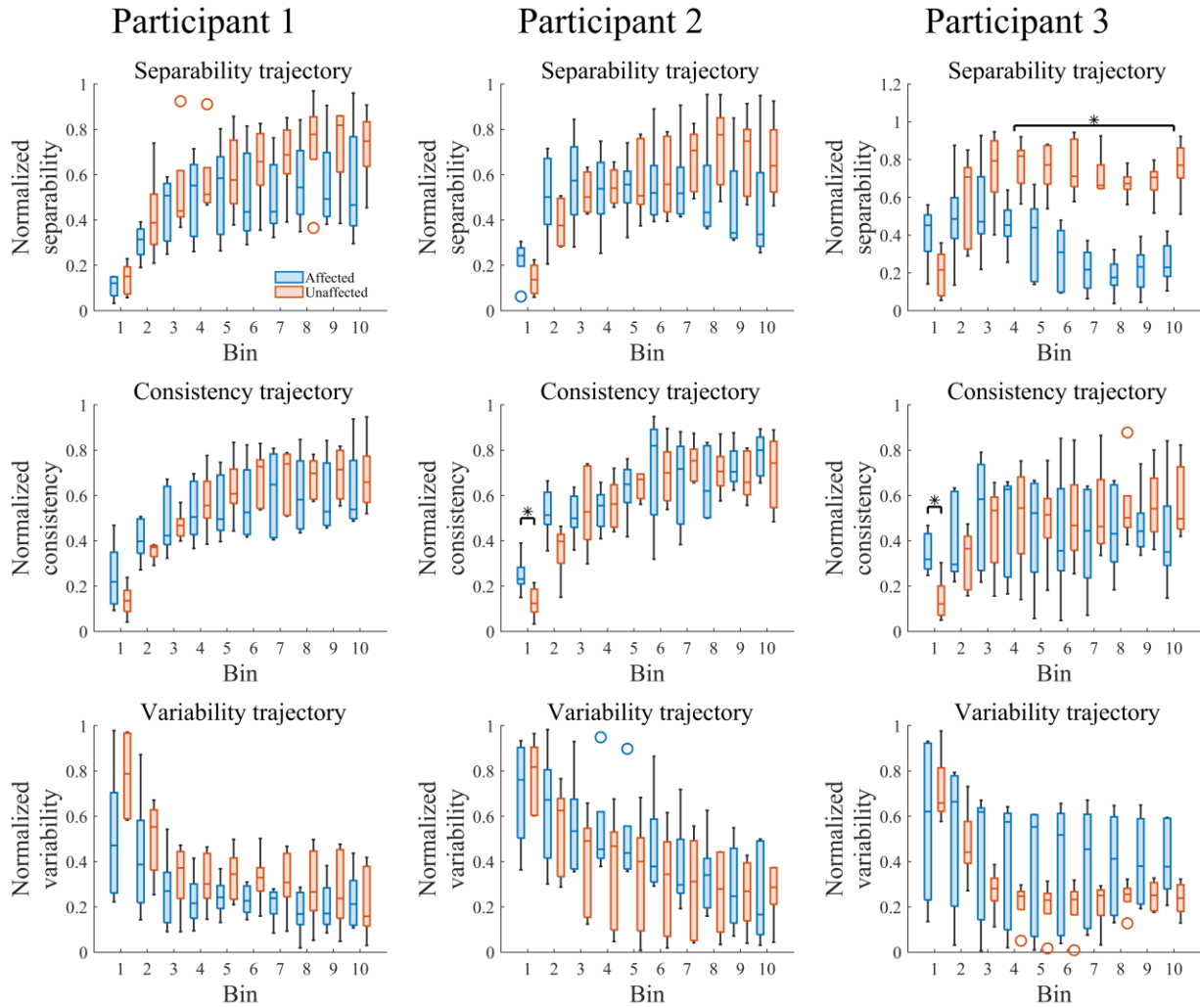


Figure 7-5. Feature space quality metric trajectories. Within each given participant column, three normalized trajectory metrics are illustrated from top to bottom: separability, consistency, and variability. Blue shading represents the affected limb, while red indicates the unaffected limb. \*Signifies a statistical difference between the limbs for the given bin(s).

### 7.5.3.4. Trial-to-trial relatedness

The trial-to-trial area provided insight into the relationship between trials throughout the Motion Test. A larger area is an indication of a greater deviation and therefore inconsistency among trial trajectories. Generally, the trial-to-trial area for the separability trajectories of the affected limb showed an increase from trial 1 to subsequent trials, with minor exceptions (refer to Figure 7-6). No discernible trends were observed for the separability of the unaffected limb. Furthermore, there

were few if any observable trends for the trial-to-trial area in consistency and variability across all participants and limbs, as detailed in Appendix D. This increase in the separability area is likely attributed to an increase in sEMG amplitude, which may suggest effects of fatigue, which warrant further investigation.

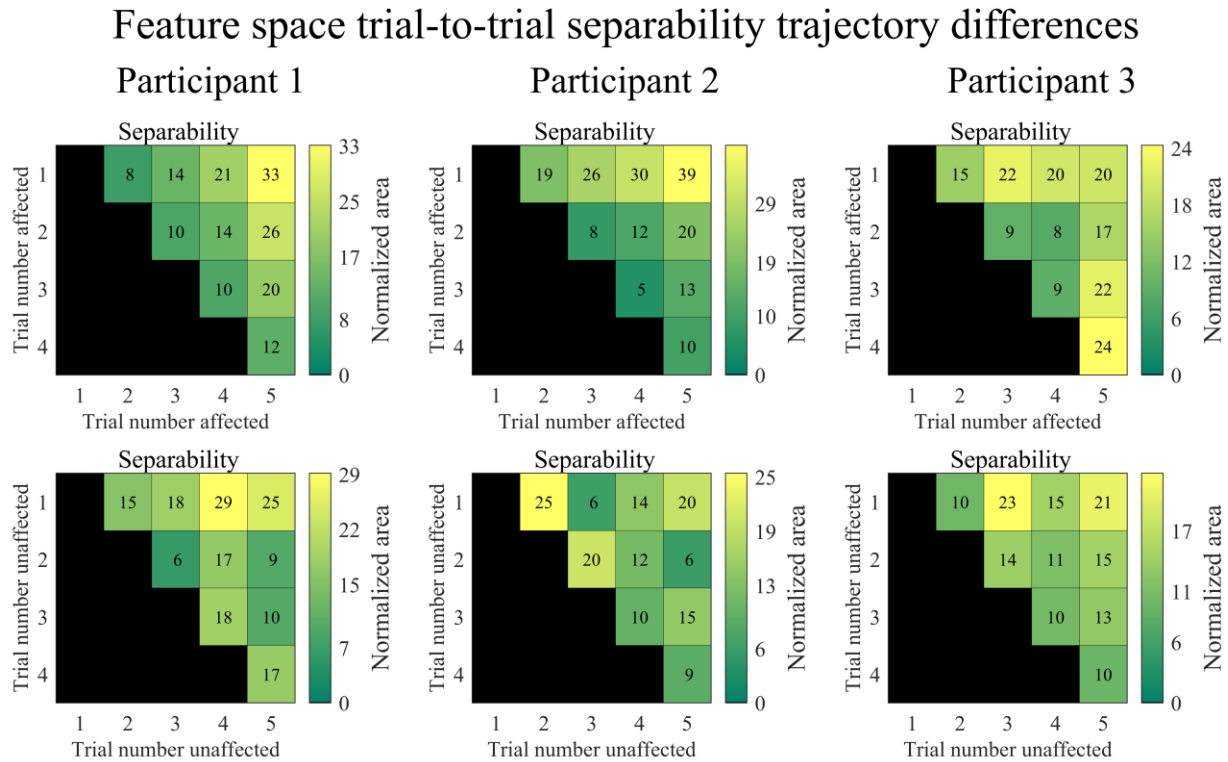


Figure 7-6. Feature space trial-to-trial separability trajectory differences. Each column represents the trial-to-trial area of the normalized separability trajectory for the affected limb (top) and unaffected limb (bottom). Lighter yellow coloring indicates a larger area between two normalized trajectories. The affected limb consistently exhibits an increase in area from trial 1 to trial 5 across all participants, whereas the unaffected limb shows indiscernible behavior. Note that the area is rounded to the nearest whole number.

## 7.6. Discussion

We examined the real-time performance and feature space quality metrics of three children with UCBD as they controlled multiple movements of a dexterous prosthetic hand. Our findings reveal minimal differences across limbs in real-time performance metrics, which approach those observed in adult able-bodied individuals<sup>20</sup>. Moreover, we demonstrated in a by-case example that

the feature space metric trajectories of the affected limb closely parallel those of the unaffected limb, with few exceptions. Collectively, these results indicate that despite being born with upper limb deficiency, as children with UCBD attempt to perform missing hand movements they possess the real-time capacity to control a dexterous prosthesis in a reproducible manner.

#### 7.6.1 Children with UCBD can control dexterous prostheses

Children with UCBD exhibit muscle activity linked to attempted missing hand movements, which demonstrate behavior comparable to their unaffected limb and approaching that of adult able-bodied individuals. Our analysis, conducted offline using LDA-OVO for movement decoding, revealed that participants achieved average classification accuracies exceeding 91% for their affected limb, reaching as high as approximately 97% for participant 2 who was consistent with those observed in adult able-bodied individuals<sup>20</sup>. Additionally, all average classification accuracies for the unaffected limb of each participant were approximately 99%, aligning with reported values for adult able-bodied individuals<sup>20</sup>. The results for the affected limb are consistent with our previous research on decoding attempted missing hand movements in children with UCBD, which showed high classification performance ( $96.5 \pm 6.6\%$ ) when the number of movements was reduced from 11 to a subset that contained only 5 (see Chapter 6). When assessing offline classification accuracies for each participant, all participants exceeded the suggested 85% threshold for usable real-time control<sup>19</sup>, with only two exceptions: participants 1 and 3, whose classification accuracies for Tripod and Pinch fell just below this threshold, at 84.60% and 84.20%, respectively. Interestingly, all participants displayed movement misclassification behavior for their affected limb that would resemble typical misclassification of the unaffected limb. For instance, participant 1 commonly misclassified Tripod as Pinch and Power as Key; participant 2 more frequently misclassified Power as Key; participant 3 often misclassified Pinch as Tripod.

These misclassifications within the affected limb share similarities: Tripod and Pinch differ by only one finger, with the introduction of the middle finger for Tripod, while Power and Key involve similar movements, differing primarily in thumb abduction versus adduction, respectively. Overall, these results suggest that children with UCBD can achieve a high level of motor control over their affected muscles that approaches that of able-bodied individuals, when muscle activity and classification performance is assessed offline.

Furthermore, we investigated the real-time performance of children with UCBD using the Motion Test and compared the performance between their affected and unaffected limbs. Overall, we observed mixed findings in the selection times (responsiveness), completion times (stability), and completion rate (robustness) across participants, with few statistical differences observed for individual movements between limbs. Some affected limb movements exhibited selection times within the ideal adult able-bodied range of  $0.659 \pm 0.238$  (s)<sup>20</sup>, indicating an ideal responsiveness to initiate certain movements for device control<sup>9</sup>, while other movements showed decreased responsiveness. Additionally, the majority of movements for both limbs were performed with a faster completion time than that presented in adult able-bodied literature<sup>20</sup>, suggesting potentially better speed of use stability in achieving the desired movement more rapidly<sup>9</sup>. It is important to note that the ideal completion time range of  $4.79 \pm 0.815$  (s) was obtained from adult able-bodied literature<sup>20</sup>, as it was consistent with our current experimental protocol, providing contextualization for our results. However, the ideal completion time was larger than other adult literature, with minor differences in setup<sup>9,14</sup>. When assessing the completion rate, a measure of robustness that indicates the success of performing the attempted missing hand movements<sup>9</sup>, we found that participant 2 had an 80.0% completion rate for their affected limb, well within the adult able-bodied range of  $71.3 \pm 14.4\%$ <sup>20</sup>. When examining average real-time accuracy across



participants, the affected limb demonstrated numerically higher accuracy for participants 2 and 3 compared to their unaffected limb, although this trend was not consistent for participant 1. Moreover, few statistical differences were found between the affected and unaffected limbs when assessing real-time accuracy for individual movements, where all movements approached the real-time accuracy of adult able-bodied individuals<sup>20</sup>. To further investigate real-time accuracy, we implemented the binned accuracy to assess the temporal performance throughout the Motion Test. While variations were observed between participants, the binned accuracy generally favored the unaffected limb, with more bins within or approaching the ideal range<sup>20</sup>. In summary, these findings underscore variability in motor control capabilities among children with UCBD, with some demonstrating comparable performance between affected and unaffected limbs in certain metrics, while others exhibited significant differences for specific movements. This highlights the importance of future research in evaluating the effects of motor learning on these performance metrics.

#### 7.6.2 Feature space metrics follow similar behavior across limbs

As the participants with UCBD actuated their affected musculature, the trajectories of feature space metrics resembled those of their unaffected limb, with few exceptions. This suggests that the activation patterns of affected muscles mirror those of the unaffected limb, enabling the execution of separable movements with consistency across repeated repetitions and similar variability. These findings further support claims that there is a degree of relatedness in muscle excitation across limbs for children with UCBD<sup>7</sup>. However, a notable exception was observed in participant 3, where the temporal separability of the affected limb exhibited a drastic decline from bins 4 through 10 (1.8 (s) to 6.0 (s)), statistically differing from that of the unaffected limb (see Figure 7-5). Furthermore, participant 3 also displayed a significant spread in the variability

metrics. These results for participant 3 are likely attributed to their age (10 years old), as they were the youngest in our cohort and showed signs of difficulty in maintaining attention during data collection. Further investigations should be conducted to assess age-related real-time feature space metrics for children with UCBD, aiming to enhance our understanding of their separability, consistency, and variability in performing multiple hand movements and how these may be related to typical motor control.

When assessing the trial-to-trial differences, determined by the area between pair-wise trial trajectories, only qualitative observations were noted for the separability. In general, the separability increased with each proceeding trial for the affected limb. However, due to the absence of a trend in the consistency and variability for the trial-to-trial area, it is challenging to determine whether participants enhanced separability by improving repetition consistency or reduced movement variability across trials. The likely explanation for these results is participant fatigue throughout the trials, as it has been demonstrated that sEMG amplitude increases with fatigue<sup>22,23</sup>. Therefore, it is highly likely that the increased separability was a result of elevated sEMG activity due to fatigue. Further, investigation is needed to understand how children with UCBD perform consistent, separable, movements with minimal variability, particularly regarding the effects of fatigue and the evolution of feature space metrics with active training and regular prosthesis use.

## 7.7. Conclusions

Our finding suggests that children with UCBD have the potential to control a dexterous prosthesis in real-time with their affected limb, approaching the proficiency level of typical adult able-bodied individuals. Statistical analysis revealed minimal differences in performance metrics across limbs for the Motion Test. The feature space trajectory metrics of the affected limb resembled those of the unaffected limb, with few exceptions, further supporting the notion that children with UCBD

actuate their affected musculature similarly to typically developed muscles<sup>7</sup>. Furthermore, examination of feature space differences between trials indicated an increase in separability, likely attributed to muscle fatigue. However, our study had some limitations. The calculation method for the Motion Test completion time and real-time accuracy may have introduced biases into our results, since any movement repetition that did not achieve 20 correct predictions would not receive a completion time or real-time accuracy and thus were discarded. To overcome this, we reported the completion rate as a metric to indicate the total percentage of successfully completed movements. Additionally, the nonparametric test used for statistical analysis had limited power, reducing our ability to detect true effects between limbs. Moreover, the latency (delay) in the BEAR PAW actuation system, including both the time it took for the movement prediction to reach the BEAR PAW and the time the BEAR PAW took to move, might have affected how quickly participants recognized incorrect movements. This delay could have caused a lag in adjusting the intended missing hand movement, potentially impacting the accuracy or timing of their movements. Future research for children with UCBD should consider using additional sEMG sensors. Recent evidence suggests that employing 16 sEMG channels improves real-time control capabilities compared to only 8 channels, with some functional test metric error rates improving by more than a factor of three<sup>24</sup>. Finally, there have been a number of tests to assess hand functionality in both clinical and experimental settings for individuals with hand impairments<sup>9,25-32</sup>, and a comprehensive functional test should be implemented to understand the ability for children with UCBD to control a dexterous prosthesis in real-time daily activities. Taken together, our study provides evidence that children with UCBD demonstrate the ability to perform multiple movements during real-time control of a dexterous prosthesis, emphasizing the

need for further investigation into how these children may learn and enhance their control over such devices.

## 7.8. References

1. Biddiss, E. & Chau, T. Upper limb prosthesis use and abandonment: A survey of the last 25 years. *Prosthetics and Orthotics International* vol. 31 236–257 (2007).
2. Postema, K., Van Der Donk, V., Van Limbeek, J., Rijken, R. & Poelma, M. J. Prosthesis rejection in children with a unilateral congenital arm defect. *Clin. Rehabil.* **13**, 243–249 (1999).
3. Egermann, M., Kasten, P. & Thomsen, M. Myoelectric hand prostheses in very young children. *Int. Orthop.* **33**, 1101–1105 (2009).
4. Battraw, M. A. *et al.* A Review of Upper Limb Pediatric Prostheses and Perspectives on Future Advancements. *Prosthet. Orthot. Int.* **46**, 267–273 (2022).
5. Kryger, M., Schultz, A. E. & Kuiken, T. Pattern recognition control of multifunction myoelectric prostheses by patients with congenital transradial limb defects: A preliminary study. *Prosthet. Orthot. Int.* **35**, 395–401 (2011).
6. Kaluf, B., Gart, M. S., Loeffler, B. J. & Gaston, G. Evaluating the Ability of Congenital Upper Extremity Amputees to Control a Multi-Degree of Freedom Myoelectric Prosthesis. *J. Hand Surg. Am.* **47**, 1019.e1-1019.e9 (2022).
7. Battraw, M. A. *et al.* Understanding the capacity of children with congenital unilateral below - elbow deficiency to actuate their affected muscles. *Sci. Rep.* 1–16 (2024) doi:10.1038/s41598-024-54952-7.
8. Fitzgerald, J. J. *et al.* Moving a missing hand : children born with below elbow deficiency can enact hand grasp patterns with their residual muscles. *J. Neuroeng. Rehabil.* **21**, 1–15 (2024).
9. Kuiken, T. A. *et al.* Targeted muscle reinnervation for real-time myoelectric control of multifunction artificial arms. *JAMA - J. Am. Med. Assoc.* **301**, 619–628 (2009).
10. Kristoffersen, M. B., Franzke, A. W., Sluis, C. K. Van Der, Murgia, A. & Bongers, R. M. The Effect of Feedback During Training Sessions on Learning Pattern-Recognition-Based Prosthesis Control. *IEEE Trans. Neural Syst. Rehabil. Eng.* **27**, 2087–2096 (2019).
11. Franzke, A. W. *et al.* Exploring the Relationship between EMG Feature Space Characteristics and Control Performance in Machine Learning Myoelectric Control. *IEEE Trans. Neural Syst. Rehabil. Eng.* **29**, 21–30 (2021).
12. Bunderson, N. E. & Kuiken, T. A. Quantification of feature space changes with experience during electromyogram pattern recognition control. *IEEE Trans. Neural Syst. Rehabil. Eng.* **20**, 239–246 (2012).
13. Feix, T., Romero, J., Schmiedmayer, H. B., Dollar, A. M. & Kragic, D. The GRASP

- Taxonomy of Human Grasp Types. *IEEE Trans. Human-Machine Syst.* **46**, 66–77 (2016).
14. Ortiz-Catalan, M., Brånemark, R. & Håkansson, B. BioPatRec: A modular research platform for the control of artificial limbs based on pattern recognition algorithms. *Source Code Biol. Med.* **8**, 1–18 (2013).
  15. Scheme, E. J., Englehart, K. B. & Hudgins, B. S. Selective classification for improved robustness of myoelectric control under nonideal conditions. *IEEE Trans. Biomed. Eng.* **58**, 1698–1705 (2011).
  16. Ortiz-Catalan, M., Håkansson, B. & Brånemark, R. Real-time and simultaneous control of artificial limbs based on pattern recognition algorithms. *IEEE Trans. Neural Syst. Rehabil. Eng.* **22**, 756–764 (2014).
  17. Battraw, M. A., Young, P. R., Joiner, W. M. & Schofield, J. S. A multiarticulate pediatric prosthetic hand for clinical and research applications. *Front. Robot. AI* **9**, 1–14 (2022).
  18. Nilsson, N. & Ortiz-Catalan, M. Estimates of Classification Complexity for Myoelectric Pattern Recognition. in *Proceedings - International Conference on Pattern Recognition* 2682–2687 (2016). doi:10.1109/ICPR.2016.7900040.
  19. Scheme, E. & Englehart, K. Electromyogram pattern recognition for control of powered upper-limb prostheses: State of the art and challenges for clinical use. *J. Rehabil. Res. Dev.* **48**, 643–660 (2011).
  20. Abbaspour, S., Naber, A., Ortiz-Catalan, M., Gholamhosseini, H. & Lindén, M. Real-time and offline evaluation of myoelectric pattern recognition for the decoding of hand movements. *Sensors* **21**, (2021).
  21. Englehart, K. & Hudgins, B. A Robust, Real-Time Control Scheme for Multifunction Myoelectric Control. *IEEE Trans. Biomed. Eng.* **50**, 848–854 (2003).
  22. Kallenberg, L. A. C., Schulte, E., Disselhorst-Klug, C. & Hermens, H. J. Myoelectric manifestations of fatigue at low contraction levels in subjects with and without chronic pain. *J. Electromyogr. Kinesiol.* **17**, 264–274 (2007).
  23. Enoka, R. M. & Duchateau, J. Muscle fatigue: What, why and how it influences muscle function. *J. Physiol.* **586**, 11–23 (2008).
  24. Simon, A. M. *et al.* Implications of EMG channel count: enhancing pattern recognition online prosthetic testing. *Front. Rehabil. Sci.* **5**, 2–11 (2024).
  25. Mathiowetz, V. & Weber, K. Adult Norms for the Box and Block. *Am. J. Occupational Ther.* **39**, 387–391 (1985).
  26. Hebert, J. S., Lewicke, J., Williams, T. R. & Vette, A. H. Normative data for modified box and blocks test measuring upper-limb function via motion capture. *J. Rehabil. Res. Dev.* **51**, 919–931 (2014).
  27. Jebsen, R., Taylor, N., Trieschmann, R., Trotter, M. & Howard, L. An objective and standardized test of hand function. *Arch. Phys. Med. Rehabil.* **50**, 311–319 (1969).
  28. Kyberd, P., Hussaini, A. & Maillet, G. Characterisation of the Clothespin Relocation Test

- as a functional assessment tool. *J. Rehabil. Assist. Technol. Eng.* **5**, 1–7 (2018).
29. Light, C. M., Chappell, P. H. & Kyberd, P. J. Establishing a standardized clinical assessment tool of pathologic and prosthetic hand function: Normative data, reliability, and validity. *Arch. Phys. Med. Rehabil.* **83**, 776–783 (2002).
  30. Vasluian, E., Bongers, R. M., Reinders-Messelink, H. A., Dijkstra, P. U. & Van Der Sluis, C. K. Preliminary study of the Southampton Hand Assessment Procedure for Children and its reliability. *BMC Musculoskelet. Disord.* **15**, (2014).
  31. Davids, J. R. *et al.* Validation of the Shriners Hospital for Children Upper Extremity Evaluation (SHUEE) for children with hemiplegic cerebral palsy. *J. Bone Jt. Surg.* **88**, 326–333 (2006).
  32. Bagley, A. M., Molitor, F., Wagner, L. V., Tomhave, W. & James, M. A. The Unilateral Below Elbow Test: A function test for children with unilateral congenital below elbow deficiency. *Dev. Med. Child Neurol.* **48**, 569–575 (2006).

## Chapter 8. Conclusions and future directions

Prosthesis abandonment significantly impacts children at a higher rate than their adult counterparts, ranging from 35-45%, compared to 23-26%, respectively<sup>1</sup>. There are a number of factors that contribute to whether a child prescribed a prosthesis will continue to wear their device, including weight, comfort, and aesthetics<sup>2-5</sup>. However, a leading cause for prosthesis rejection remains, that these devices do not offer sufficient functional benefit to warrant their use<sup>2-4,6,7</sup>. This lack of functional benefit may stem from a limited understanding of the extent to which children can effectively use the newly available adult-based dexterous systems. Furthermore, the majority of children who may be prescribed an upper limb prosthesis are born with limb deficiency<sup>8</sup>, a stark contrast from the adult population, which typically experiences limb loss later in life. This distinction underscores the need to investigate the extent to which children born with upper limb deficiency can actuate their affected muscles and utilize this actuation to drive dexterous prostheses. This gap in knowledge has remained a significant barrier to the translation of dexterous devices into the pediatric arena.

In this dissertation, we investigate the motor control of attempted missing hand movements in children with unilateral congenital below-elbow deficiency (UCBED), laying the foundation for translating adult-based dexterous prosthesis technology to these children. Our investigation begins with an overview in Chapter 2 of the current standard of care for children utilizing upper limb prostheses and the inherent challenges within this domain. Moving forward, Chapter 3 examines how typically developed able-bodied children employ their hands in daily activities, offering insight to inform device development. Chapter 4 details the development of a child-sized multiarticulate prosthetic hand, tailored for use within research settings. Subsequently, Chapter 5 explores muscle response when children with UCBED attempt to move their missing hand,

assessing the consistency and distinguishability of affected muscle actuation, as this is important for modern prosthetic control systems. With a comprehensive understanding of these children's muscular capabilities, Chapter 6 focuses on tuning machine learning algorithms to predict their motor intent, culminating in the development of a generalized congenital feature set. Finally, in Chapter 7 we evaluate the real-time capability of these children to control the dexterous device developed in Chapter 4.

The extent to which children born with upper limb absence can actuate their affected musculature has remained unstudied. However, in Chapter 5, we demonstrated that children with UCBED exhibit a degree of biological control over their affected muscles. This control manifested as consistent and distinguishable patterns of muscle excitation, with some shared information observed across affected and unaffected limbs as participants attempted the various missing hand movements. Our findings establish the case that children born with upper limb absence can produce distinguishable hand movements with their affected musculature, thereby promoting further investigation into how machine learning algorithms could be employed.

To initiate the effective translation of dexterous devices to children with UCBED, it was necessary to tune machine learning algorithms for decoding their hand motor intent. Previous studies investigating individuals with UCBED have primarily leveraged machine learning algorithms and commercially available pattern recognition systems designed for adult-amputee populations<sup>9,10</sup>. As a result, the prediction accuracy for UCBED adults (N = 4) ranged from 52.1% ± 15.0% for 11 attempted hand movements<sup>9</sup>, while for UCBED children (N = 4), it was 80% ± 16.0% for 3 degrees of freedom<sup>10</sup>. Unlike adults with acquired limb loss, individuals born with upper limb absence have never actuated an intact hand. Despite this distinction, machine learning algorithms designed for adult amputee populations have been applied with little success and without rigorous testing.



In Chapter 6, we explored five different machine learning algorithms and 49 feature combinations to determine what characteristics (features) of muscle activity may be most important to decode hand motor intent. This investigation led to the development of the congenital feature set, which demonstrated robust generalization across our UCBD participant cohort. Furthermore, we achieved high offline classification accuracy with a reduced set of five movements, a significant finding given our previous research in Chapter 3, which revealed that typically developed children use a subset of movements for activities of daily living. Ultimately, these findings lay the necessary foundation for transitioning from offline analysis of pre-recorded datasets to evaluating real-time control, as detailed in Chapter 7.

Finally, this work culminates in the assessment of real-time control of the BEAR PAW, a research-based pediatric prosthetic hand developed in Chapter 4. It is essential to examine how children with UCBD can operate a dexterous device in real time, as offline analysis serves only as a proxy for real-time control. In fact, performance during real-time control often decreases when compared to offline analysis<sup>11-13</sup>. Our study provides encouraging results, although in a small cohort, indicating that children with UCBD have the potential to control dexterous prostheses in real-time with their affected limb, achieving performance levels that resemble their unaffected limb. This finding further supports the argument outlined in Chapter 5, which suggests that children demonstrate a degree of shared information across limbs as they attempt missing hand movements.

Moving forward, it is imperative to consider larger cohorts of participants with UCBD to comprehensively understand the impact age, sex, and limb size have on decoding hand motor intent and the ability of these children to actuate their affected musculature. This is essential to establishing clinical guidelines for prosthesis prescription and effectively translating this research to the child population. Additionally, exploring the effects of motor learning for children with

UCBED as they acquire proficiency in using and controlling multiple hand movements in real-time settings is important for the successful translation of advanced prostheses. A thorough functional assessment should be implemented to begin understanding how children operate dexterous devices within daily environments. Furthermore, investigating how children with UCBED currently use their affected limb to assist in daily activities is warranted, as this can further inform which prosthesis movements may be beneficial to provide for improved functionality. These endeavors are significant but have the potential to change clinical practices and improve the quality of life for children with UCBED.

## 8.1. References

1. Biddiss, E. & Chau, T. Upper limb prosthesis use and abandonment: A survey of the last 25 years. *Prosthetics and Orthotics International* vol. 31 236–257 (2007).
2. Vasluian, E. *et al.* Opinions of Youngsters with Congenital Below-Elbow Deficiency, and Those of Their Parents and Professionals Concerning Prosthetic Use and Rehabilitation Treatment. *PLoS One* **8**, (2013).
3. Postema, K., Van Der Donk, V., Van Limbeek, J., Rijken, R. & Poelma, M. J. Prosthesis rejection in children with a unilateral congenital arm defect. *Clin. Rehabil.* **13**, 243–249 (1999).
4. Wagner, L. V., Bagley, A. M. & James, M. A. Reasons for Prosthetic Rejection by Children With Unilateral Congenital Transverse Forearm Total Deficiency. *J. Prosthetics Orthot.* **19**, 51–54 (2007).
5. Egermann, M., Kasten, P. & Thomsen, M. Myoelectric hand prostheses in very young children. *Int. Orthop.* **33**, 1101–1105 (2009).
6. James, M. A. *et al.* Impact of prostheses on function and quality of life for children with unilateral congenital below-the-elbow deficiency. *J. Bone Jt. Surg. - Ser. A* **88**, 2356–2365 (2006).
7. Battraw, M. A. *et al.* A Review of Upper Limb Pediatric Prostheses and Perspectives on Future Advancements. *Prosthet. Orthot. Int.* **46**, 267–273 (2022).
8. Atkins, D. J., Heard, D. C. Y. & Donovan, W. H. Epidemiologic overview of individuals with upper-limb loss and their reported research priorities. *J. Prosthetics Orthot.* **8**, 2–11 (1996).
9. Kryger, M., Schultz, A. E. & Kuiken, T. Pattern recognition control of multifunction myoelectric prostheses by patients with congenital transradial limb defects: A preliminary

- study. *Prosthet. Orthot. Int.* **35**, 395–401 (2011).
10. Kaluf, B., Gart, M. S., Loeffler, B. J. & Gaston, G. Evaluating the Ability of Congenital Upper Extremity Amputees to Control a Multi-Degree of Freedom Myoelectric Prosthesis. *J. Hand Surg. Am.* **47**, 1019.e1-1019.e9 (2022).
  11. Ortiz-Catalan, M., Brånemark, R. & Håkansson, B. BioPatRec: A modular research platform for the control of artificial limbs based on pattern recognition algorithms. *Source Code Biol. Med.* **8**, 1–18 (2013).
  12. Ortiz-Catalan, M., Håkansson, B. & Brånemark, R. Real-time classification of simultaneous hand and wrist motions using Artificial Neural Networks with variable threshold outputs. in *Proceedings of the XXXIV International Conference on Artificial Neural Networks (ICANN)* 1159–1164 (2013).
  13. Abbaspour, S., Naber, A., Ortiz-Catalan, M., Gholamhosseini, H. & Lindén, M. Real-time and offline evaluation of myoelectric pattern recognition for the decoding of hand movements. *Sensors* **21**, (2021).

## References

### Chapter 1

1. Giele, H., Giele, C., Bower, C. & Allison, M. The incidence and epidemiology of congenital upper limb anomalies: A total population study. *J. Hand Surg. Am.* **26**, 628–634 (2001).
2. Ekblom, A. G., Laurell, T. & Arner, M. Epidemiology of congenital upper limb anomalies in 562 children born in 1997 to 2007: A total population study from Stockholm, Sweden. *J. Hand Surg. Am.* **35**, 1742–1754 (2010).
3. Davids, J. R., Wagner, L. V., Meyer, L. C. & Blackhurst, D. W. Prosthetic management of children with unilateral congenital below-elbow deficiency. *J. Bone Jt. Surg. - Ser. A* **88**, 1294–1300 (2006).
4. Biddiss, E. & Chau, T. Upper limb prosthesis use and abandonment: A survey of the last 25 years. *Prosthetics and Orthotics International* vol. 31 236–257 (2007).
5. Battraw, M. A. *et al.* A Review of Upper Limb Pediatric Prostheses and Perspectives on Future Advancements. *Prosthet. Orthot. Int.* **46**, 267–273 (2022).
6. Kuiken, T. A. *et al.* Targeted muscle reinnervation for real-time myoelectric control of multifunction artificial arms. *JAMA - J. Am. Med. Assoc.* **301**, 619–628 (2009).
7. Kristoffersen, M. B., Franzke, A. W., Sluis, C. K. Van Der, Murgia, A. & Bongers, R. M. The Effect of Feedback During Training Sessions on Learning Pattern-Recognition-Based Prosthesis Control. *IEEE Trans. Neural Syst. Rehabil. Eng.* **27**, 2087–2096 (2019).
8. Franzke, A. W. *et al.* Exploring the Relationship between EMG Feature Space Characteristics and Control Performance in Machine Learning Myoelectric Control. *IEEE Trans. Neural Syst. Rehabil. Eng.* **29**, 21–30 (2021).
9. Bunderson, N. E. & Kuiken, T. A. Quantification of feature space changes with experience during electromyogram pattern recognition control. *IEEE Trans. Neural Syst. Rehabil. Eng.* **20**, 239–246 (2012).

### Chapter 2

1. Parker, S. E. *et al.* Updated national birth prevalence estimates for selected birth defects in the United States, 2004-2006. *Birth Defects Res. Part A - Clin. Mol. Teratol.* **88**, 1008–1016 (2010).
2. Ekblom, A. G., Laurell, T. & Arner, M. Epidemiology of congenital upper limb anomalies in 562 children born in 1997 to 2007: A total population study from Stockholm, Sweden. *J. Hand Surg. Am.* **35**, 1742–1754 (2010).
3. Shaperman, J., Landsberger, S. & Setoguchi, Y. Early Upper Limb Prosthesis Fitting: When and What Do We Fit. *Prosthet. ORTHOTIC Sci.* **15**, 11–17 (2003).
4. Davids, J. R., Wagner, L. V., Meyer, L. C. & Blackhurst, D. W. Prosthetic management of children with unilateral congenital below-elbow deficiency. *J. Bone Jt. Surg. - Ser. A* **88**,

- 1294–1300 (2006).
5. Vasluian, E. *et al.* Opinions of Youngsters with Congenital Below-Elbow Deficiency, and Those of Their Parents and Professionals Concerning Prosthetic Use and Rehabilitation Treatment. *PLoS One* **8**, (2013).
  6. Postema, K. *et al.* *Prosthesis rejection in children with a unilateral congenital arm defect. Clinical Rehabilitation* vol. 13 (1999).
  7. Biddiss, E. & Chau, T. Upper limb prosthesis use and abandonment: A survey of the last 25 years. *Prosthetics and Orthotics International* vol. 31 236–257 (2007).
  8. Franzblau, L. E. *et al.* Coping with congenital hand differences. *Plast. Reconstr. Surg.* **135**, 1067–1075 (2015).
  9. Valevicius, A. M. *et al.* Compensatory strategies of body-powered prosthesis users reveal primary reliance on trunk motion and relation to skill level. *Clin. Biomech.* **72**, 122–129 (2020).
  10. Egermann, M., Kasten, P. & Thomsen, M. Myoelectric hand prostheses in very young children. *Int. Orthop.* **33**, 1101–1105 (2009).
  11. Englehart, K. & Hudgins, B. A Robust, Real-Time Control Scheme for Multifunction Myoelectric Control. *IEEE Trans. Biomed. Eng.* **50**, 848–854 (2003).
  12. Castellini, C. *et al.* Proceedings of the first workshop on peripheral machine interfaces: Going beyond traditional surface electromyography. *Front. Neurobot.* **8**, 1–17 (2014).
  13. Chowdhury, R. H. *et al.* Surface electromyography signal processing and classification techniques. *Sensors (Switzerland)* **13**, 12431–12466 (2013).
  14. Young, A. J., Hargrove, L. J. & Kuiken, T. A. Improving myoelectric pattern recognition robustness to electrode shift by changing interelectrode distance and electrode configuration. *IEEE Trans. Biomed. Eng.* **59**, 645–652 (2012).
  15. Castellini, C. & Van Der Smagt, P. Surface EMG in advanced hand prosthetics. *Biol. Cybern.* **100**, 35–47 (2009).
  16. James, M. A. *et al.* Impact of Prostheses on Function and Quality of Life for Children With Unilateral Congenital Below- the-Elbow Deficiency. *J. Bone Jt. Surgery-American* Vol. **88**, 2356–2365 (2006).
  17. Johansen, H., Dammann, B., Øinæs Andersen, L. & Andresen, I. L. Children with congenital limb deficiency in Norway: issues related to school life and health-related quality of life. A cross-sectional study. *Disabil. Rehabil.* **38**, 1803–1810 (2016).
  18. Ardon, M. S., Janssen, W. G., Hovius, S. E., Stam, H. J. & Selles, R. W. Low impact of congenital hand differences on health-related quality of life. *Arch. Phys. Med. Rehabil.* **93**, 351–357 (2012).
  19. Varni, J., Burwinkle, T., Seid, M. & Skarr, D. The PedsQL 4.0 as a Pediatric Population Health Measure: Feasibility, Reliability, and Validity. *Ambulatory. Ambul. Pediatr.* **3**, 329–341 (2003).

20. Johansen, H., Dammann, B., Andresen, I. L. & Fagerland, M. W. Health-related quality of life for children with rare diagnoses, their parents' satisfaction with life and the association between the two. *Health Qual. Life Outcomes* **11**, 1 (2013).
21. Engelen, V., Haentjens, M. M., Detmar, S. B., Koopman, H. M. & Grootenhuis, M. A. Health related quality of life of Dutch children: Psychometric properties of the PedsQL in the Netherlands. *BMC Pediatr.* **9**, 68 (2009).
22. Varni, J. W. The PedsQL Measurement Model for the Pediatric Quality of Life Inventory. <https://www.pedsqol.org/> (1998).
23. Ylimäinen, K., Nachemson, A., Sommerstein, K., Stocksélius, A. & Norling Hermansson, L. Health-related quality of life in Swedish children and adolescents with limb reduction deficiency. *Acta Paediatr. Int. J. Paediatr.* **99**, 1550–1555 (2010).
24. Schmidt, S. & The DISABKIDS group. *The DISABKIDS questionnaires: quality of life questionnaires for children with chronic conditions. Handbook.* (Lengerich: Pabst Science Publishers, 2006).
25. Bowker, J. & American Academy of Orthopaedic Surgeons. *Atlas of Limb Prosthetics: Surgical, Prosthetic, and Rehabilitation Principles.* (Mosby Year Book, 1992).
26. Lumsdaine, S. & Thurston, M. Growing up in a Mainstream World: A Retrospective Enquiry into the Childhood Experiences of Young Adults with a Physical Disability. *Int. J. Disabil. Dev. Educ.* **64**, 182–197 (2017).
27. Kerr, S. M. & McIntosh, J. B. Disclosure of disability: Exploring the perspective of parents. *Midwifery* **14**, 225–232 (1998).
28. Oliver, J., Dixon, C. & Murray, C. D. Being the parent of a child with limb difference who has been provided with an artificial limb: an interpretative phenomenological analysis. *Disabil. Rehabil.* **0**, 1–8 (2018).
29. Andrews, E. E., Williams, J. L., VandeCreek, L. & Allen, J. B. Experiences of Parents of Children with Congenital Limb Differences With Health Care Providers: A Qualitative Study. *Rehabil. Psychol.* **54**, 217–221 (2009).
30. De Jong, I. G. M. *et al.* Activity and Participation of children and adolescents with Unilateral Congenital Below Elbow Deficiency : An online focus group study. *J. Rehabil. Med.* **44**, 885–892 (2012).
31. Crandall, R. C. & Tomhave, W. Pediatric unilateral below-elbow amputees: Retrospective analysis of 34 patients given multiple prosthetic options. *J. Pediatr. Orthop.* **22**, 380–383 (2002).
32. Huizing, K., Reinders-Messelink, H., Maathuis, C., Hadders-Algra, M. & Van Der Sluis, C. K. Age at first prosthetic fitting and later functional outcome in children and young adults with unilateral congenital below-elbow deficiency: A cross-sectional study. *Prosthet. Orthot. Int.* **34**, 166–174 (2010).
33. Wagner, L. V., Bagley, A. M. & James, M. A. Reasons for Prosthetic Rejection by Children With Unilateral Congenital Transverse Forearm Total Deficiency. *Am. Acad.*

- Orthotists Prosthetists* **19**, 51–54 (2007).
34. Routhier, F., Vincent, C., Morissette, M. J. & Desaulniers, L. Clinical results of an investigation of paediatric upper limb myoelectric prosthesis fitting at the Quebec Rehabilitation Institute. *Prosthet. Orthot. Int.* **25**, 119–131 (2001).
  35. Pylatiuk, C., Schulz, S. & Döderlein, L. Results of an internet survey of myoelectric prosthetic hand users. *Prosthet. Orthot. Int.* **31**, 362–370 (2007).
  36. Jain, S. Rehabilitation in limb deficiency. 2. The pediatric amputee. *Arch. Phys. Med. Rehabil.* **77**, (1996).
  37. Agur, A. M. R. & Lee, M. J. *Grant's Atlas of Anatomy*. (Lippincott Williams and Wilkins, 1999).
  38. Feix, T., Romero, J., Schmiedmayer, H. B., Dollar, A. M. & Kragic, D. The GRASP Taxonomy of Human Grasp Types. *IEEE Trans. Human-Machine Syst.* **46**, 66–77 (2016).
  39. Zheng, J. Z., De La Rosa, S. & Dollar, A. M. An Investigation of Grasp Type and Frequency in Daily Household and Machine Shop Tasks. in *IEEE International Conference on Robotics and Automation* (2011). doi:10.1109/TOH.2013.6.
  40. Vujaklija, I., Farina, D. & Aszmann, O. New developments in prosthetic arm systems. *Orthop. Res. Rev.* **8**, 31–39 (2016).
  41. IBT. Sense. <https://www.i-biomed.com> (2020).
  42. Ottobock. Myo Plus. <https://www.ottobockus.com> (2020).
  43. COAPT. CoApt Complete Control. <https://coaptengineering.com> (2020).
  44. LTI. MYOTRAINER. <https://liberatingtech.com/> (2020).
  45. Ortiz-Catalan, M., Brånemark, R. & Håkansson, B. BioPatRec: A modular research platform for the control of artificial limbs based on pattern recognition algorithms. *Source Code Biol. Med.* **8**, 1–18 (2013).
  46. Toledo, C. *et al.* A comparison of direct and pattern recognition control for a two degree-of-freedom above elbow virtual prosthesis. *Proc. Annu. Int. Conf. IEEE Eng. Med. Biol. Soc. EMBS* 4332–4335 (2012) doi:10.1109/EMBC.2012.6346925.
  47. Franzke, A. W. *et al.* Users' and therapists' perceptions of myoelectric multi-function upper limb prostheses with conventional and pattern recognition control. 1–13 (2019) doi:10.5281/zenodo.2585639.
  48. Resnik, L. J., Acluche, F. & Klinger, S. L. *User experience of controlling the DEKA Arm with EMG pattern recognition*. *PLoS ONE* vol. 13 (2018).
  49. Fougner, A., Scheme, E., Chan, A. D. C., Englehart, K. & Staudahl, Ø. Resolving the limb position effect in myoelectric pattern recognition. *IEEE Trans. Neural Syst. Rehabil. Eng.* **19**, 644–651 (2011).
  50. Beaulieu, R. J. *et al.* Multi-position Training Improves Robustness of Pattern Recognition and Reduces Limb-Position Effect in Prosthetic Control. *J. Prosthetics Orthot.* **29**, 54–62

- (2017).
51. Betthausen, J. L. *et al.* Limb Position Tolerant Pattern Recognition for Myoelectric Prosthesis Control with Adaptive Sparse Representations from Extreme Learning. *IEEE Trans. Biomed. Eng.* **65**, 770–778 (2018).
  52. Akhlaghi, N. *et al.* Real-Time Classification of Hand Motions Using Ultrasound Imaging of Forearm Muscles. *IEEE Trans. Biomed. Eng.* **63**, 1687–1698 (2016).
  53. Dhawan, A. S. *et al.* Proprioceptive Sonomyographic Control: A novel method for intuitive and proportional control of multiple degrees-of-freedom for individuals with upper extremity limb loss. *Sci. Rep.* **9**, 1–15 (2019).
  54. Kuiken, T. A., Dumanian, G. A., Lipschutz, R. D., Miller, L. A. & Stubblefield, K. A. The use of targeted muscle reinnervation for improved myoelectric prosthesis control in a bilateral shoulder disarticulation amputee. *Prosthet. Orthot. Int.* **28**, 245–253 (2004).
  55. Hebert, J. S. *et al.* Novel targeted sensory reinnervation technique to restore functional hand sensation after transhumeral amputation. *IEEE Trans. Neural Syst. Rehabil. Eng.* **22**, 765–773 (2014).
  56. Kuiken, T. A., Marasco, P. D., Lock, B. A., Harden, R. N. & Dewald, J. P. A. Redirection of cutaneous sensation from the hand to the chest skin of human amputees with targeted reinnervation. *Proc. Natl. Acad. Sci. U. S. A.* **104**, 20061–20066 (2007).
  57. Marasco, P. D. *et al.* Illusory movement perception improves motor control for prosthetic hands. *Sci. Transl. Med.* **10**, (2018).
  58. Yildiz, K. A., Shin, A. Y. & Kaufman, K. R. Interfaces with the peripheral nervous system for the control of a neuroprosthetic limb: A review. *J. Neuroeng. Rehabil.* **17**, (2020).
  59. Svensson, P., Wijk, U., Björkman, A. & Antfolk, C. A review of invasive and non-invasive sensory feedback in upper limb prostheses. *Expert Rev. Med. Devices* **14**, 439–447 (2017).

### **Chapter 3**

1. Kim, E. S. *et al.* Longitudinal Impact of Depression on Quality of Life in Stroke Patients. *Psychiatry Investig.* **15**, 141–146 (2018).
2. Maciejasz, P., Eschweiler, J., Gerlach-Hahn, K., Jansen-Troy, A. & Leonhardt, S. A survey on robotic devices for upper limb rehabilitation. *J. NeuroEngineering Rehabil.* **2014 111** **11**, 1–29 (2014).
3. Plessis, T., Djouani, K. & Oosthuizen, C. A Review of Active Hand Exoskeletons for Rehabilitation and Assistance. *Robot. 2021, Vol. 10, Page 40* **10**, 40 (2021).
4. Heo, P., Gu, G. M., Lee, S. jin, Rhee, K. & Kim, J. Current hand exoskeleton technologies for rehabilitation and assistive engineering. *Int. J. Precis. Eng. Manuf.* **2012 135** **13**, 807–824 (2012).
5. Mendez, V., Iberite, F., Shokur, S. & Micera, S. Current Solutions and Future Trends for



- Robotic Prosthetic Hands. *Annu. Rev. of Control, Robot. Auton. Syst.* **4**, 595–627 (2021).
6. Belter, J. T., Segil, J. L., Dollar, A. M. & Weir, R. F. Mechanical design and performance specifications of anthropomorphic prosthetic hands: A review. *J. Rehabil. Res. Dev.* **50**, 599–618 (2013).
  7. Falzarano, V., Marini, F., Morasso, P. & Zenzeri, J. Devices and protocols for upper limb robot-assisted rehabilitation of children with neuromotor disorders. *Appl. Sci.* **9**, 1–22 (2019).
  8. Simon-Martinez, C. *et al.* Age-related changes in upper limb motion during typical development. *PLoS One* **13**, 1–15 (2018).
  9. Franzblau, L. E. *et al.* Coping with Congenital Hand Differences. *Plast Reconstr Surg.* **135**, 1067–1075 (2015).
  10. Bassini, L. & Patel, M. *Fundamentals of Hand Therapy: Clinical reasoning and Treatment Guidelines for Common Diagnoses of the Upper Extremity.* (Mosby, 2007).
  11. Charles, J. & Gordon, A. M. Development of hand-arm bimanual intensive training (HABIT) for improving bimanual coordination in children with hemiplegic cerebral palsy. *Dev. Med. Child Neurol.* **48**, 931–936 (2006).
  12. Peck-Murray, J. A. Utilizing everyday items in play to facilitate hand therapy for pediatric patients. *J. Hand Ther.* **28**, 228–232 (2015).
  13. Agur, A. M. R. & Lee, M. J. *Grant's Atlas of Anatomy.* (Lippincott Williams and Wilkins, 1999).
  14. Ritter, H. & Haschke, R. *Humanoid Robotics and Neuroscience: Science, Engineering and Society.* (Taylor & Francis, 2015).
  15. Feix, T., Romero, J., Schmiedmayer, H. B., Dollar, A. M. & Kragic, D. The GRASP Taxonomy of Human Grasp Types. *IEEE Trans. Human-Machine Syst.* **46**, 66–77 (2016).
  16. Zheng, J. Z., De La Rosa, S. & Dollar, A. M. An Investigation of Grasp Type and Frequency in Daily Household and Machine Shop Tasks. in *IEEE International Conference on Robotics and Automation* (2011). doi:10.1109/TOH.2013.6.
  17. Oldfield, R. C. The Assessment and Analysis of Handedness the Edinburgh Inventory. *Neuropsychologia* **9**, 97–113 (1971).
  18. Liu, J., Feng, F., Nakamura, Y. C. & Pollard, N. S. A Taxonomy of Everyday Grasps in Action. *IEEE-RAS Int. Conf. Humanoid Robot.* (2014).
  19. Bullock, I. M., Zheng, J. Z., De La Rosa, S., Guertler, C. & Dollar, A. M. Grasp frequency and usage in daily household and machine shop tasks. *IEEE Trans. Haptics* **6**, 296–308 (2013).

#### **Chapter 4**

1. Giele, H., Giele, C., Bower, C. & Allison, M. The incidence and epidemiology of congenital upper limb anomalies: A total population study. *J. Hand Surg. Am.* **26**, 628–

- 634 (2001).
2. Davids, J. R., Wagner, L. V., Meyer, L. C. & Blackhurst, D. W. Prosthetic management of children with unilateral congenital below-elbow deficiency. *J. Bone Jt. Surg. - Ser. A* **88**, 1294–1300 (2006).
  3. Krebs, D. E. & Fishman, S. Characteristics of the child amputee population. *J. Pediatr. Orthop.* **4**, 89–95 (1984).
  4. Edmonds, L. D. *et al.* Congenital malformations surveillance: two American systems. *Int. J. Epidemiol.* **10**, 247–252 (1981).
  5. Biddiss, E. & Chau, T. Upper limb prosthesis use and abandonment: A survey of the last 25 years. *Prosthetics and Orthotics International* vol. 31 236–257 (2007).
  6. Vasluian, E. *et al.* Opinions of Youngsters with Congenital Below-Elbow Deficiency, and Those of Their Parents and Professionals Concerning Prosthetic Use and Rehabilitation Treatment. *PLoS One* **8**, (2013).
  7. Postema, K., Van Der Donk, V., Van Limbeek, J., Rijken, R. & Poelma, M. J. Prosthesis rejection in children with a unilateral congenital arm defect. *Clin. Rehabil.* **13**, 243–249 (1999).
  8. Wagner, L. V., Bagley, A. M. & James, M. A. Reasons for Prosthetic Rejection by Children With Unilateral Congenital Transverse Forearm Total Deficiency. *J. Prosthetics Orthot.* **19**, 51–54 (2007).
  9. Egermann, M., Kasten, P. & Thomsen, M. Myoelectric hand prostheses in very young children. *Int. Orthop.* **33**, 1101–1105 (2009).
  10. Oliver, J., Dixon, C. & Murray, C. D. Being the parent of a child with limb difference who has been provided with an artificial limb: an interpretative phenomenological analysis. *Disabil. Rehabil.* **0**, 1–8 (2018).
  11. Franzblau, L. E. *et al.* Coping with Congenital Hand Differences. *Plast Reconstr Surg.* **135**, 1067–1075 (2015).
  12. Agur, A. M. R. & Lee, M. J. *Grant's Atlas of Anatomy*. (Lippincott Williams and Wilkins, 1999).
  13. Feix, T., Romero, J., Schmiedmayer, H. B., Dollar, A. M. & Kragic, D. The GRASP Taxonomy of Human Grasp Types. *IEEE Trans. Human-Machine Syst.* **46**, 66–77 (2016).
  14. Zheng, J. Z., De La Rosa, S. & Dollar, A. M. An Investigation of Grasp Type and Frequency in Daily Household and Machine Shop Tasks. in *IEEE International Conference on Robotics and Automation* (2011). doi:10.1109/TOH.2013.6.
  15. Belter, J. T., Segil, J. L., Dollar, A. M. & Weir, R. F. Mechanical design and performance

- specifications of anthropomorphic prosthetic hands: A review. *J. Rehabil. Res. Dev.* **50**, 599–618 (2013).
16. Battraw, M. A. *et al.* A Review of Upper Limb Pediatric Prostheses and Perspectives on Future Advancements. *Prosthet. Orthot. Int.* **46**, 267–273 (2022).
  17. Kryger, M., Schultz, A. E. & Kuiken, T. Pattern recognition control of multifunction myoelectric prostheses by patients with congenital transradial limb defects: A preliminary study. *Prosthet. Orthot. Int.* **35**, 395–401 (2011).
  18. Copeland, C., Mukherjee, M., Wang, Y., Fraser, K. & Zuniga, J. M. Changes in Sensorimotor Cortical Activation in Children Using Prostheses and Prosthetic Simulators. *Brain Sci.* **11**, (2021).
  19. Da Paz, A. C. & Braga, L. W. Brain activation in a myoelectric prosthetic hand: The role of the brain in the rehabilitation of amputees. *J. Pediatr. Orthop.* **27**, 947–951 (2007).
  20. Ten Kate, J., Smit, G. & Breedveld, P. 3D-printed upper limb prostheses: a review. *Disabil. Rehabil. Assist. Technol.* **12**, 300–314 (2017).
  21. Llop-Harillo, I., Pérez-González, A., Starke, J. & Asfour, T. The Anthropomorphic Hand Assessment Protocol (AHAP). *Rob. Auton. Syst.* **121**, 103259 (2019).
  22. Vujaklija, I., Farina, D. & Aszmann, O. New developments in prosthetic arm systems. *Orthop. Res. Rev.* (2016) doi:10.2147/ORR.S71468.
  23. *ANSI/ISA Process Instrumentation Terminology, ANSI/ISA Standard 51.1.* (1979).
  24. User Manual: SingleTact Miniature Force Sensors. [https://www.singletact.com/SingleTact\\_Manual.pdf](https://www.singletact.com/SingleTact_Manual.pdf) (2017).
  25. High Accuracy, Galvanically Isolated Current Sensor IC With Small Footprint SOIC8 Package. <https://download.mikroe.com/documents/datasheets/ACS723.pdf> (2018).
  26. Llop-Harillo, I., Pérez-González, A. & Andrés-Esperanza, J. Grasping Ability and Motion Synergies in Affordable Tendon-Driven Prosthetic Hands Controlled by Able-Bodied Subjects. *Front. Neurobot.* **14**, 1–15 (2020).
  27. Cheng, I. F., Kuo, L. C., Lin, C. J., Chieh, H. F. & Su, F. C. Anthropometric Database of the Preschool Children from 2 to 6 Years in Taiwan. *J. Med. Biol. Eng.* **39**, 552–568 (2019).
  28. Snyder, R. G. *et al.* *Anthropometry of Infants, Children, and Youths to Age 18.* (1977).
  29. Brenneis, D. J. A., Dawson, M. R. & Pilarski, P. M. Development of the Handi Hand : an Inexpensive , Multi-Articulating , Sensorized Hand for Machine Learning Research in Myoelectric Control. in *Myoelectric Controls Symposium* (2017).

30. Featured Technology: Open Bionics Hero Arm. <https://hangerclinic.com/blog/featured-technology/open-bionics-hero-arm/#:~:text=The Hero Arm weighs less,the lightest bionic hand available.&text=Up to six easy-to,provide outstanding versatility and control> (2019).
31. Battraw, M. A., Young, P. R., Welner, M. E., Joiner, W. M. & Schofield, J. S. Characterizing Pediatric Hand Grasps During Activities of Daily Living to Inform Robotic Rehabilitation and Assistive Technologies. in *IEEE International Conference on Rehabilitation Robotics* (2022).
32. Hebert, J. S., Lewicke, J., Williams, T. R. & Vette, A. H. Normative data for modified box and blocks test measuring upper-limb function via motion capture. *J. Rehabil. Res. Dev.* **51**, 919–931 (2014).
33. Mathiowetz, V. & Weber, K. Adult Norms for the Box and Block. *Am. J. Occupational Ther.* **39**, 387–391 (1985).
34. Jepsen, R., Taylor, N., Trieschmann, R., Trotter, M. & Howard, L. An objective and standardized test of hand function. *Arch. Phys. Med. Rehabil.* **50**, 311–319 (1969).
35. Kyberd, P., Hussaini, A. & Maillet, G. Characterisation of the Clothespin Relocation Test as a functional assessment tool. *J. Rehabil. Assist. Technol. Eng.* **5**, 1–7 (2018).
36. Light, C. M., Chappell, P. H. & Kyberd, P. J. Establishing a standardized clinical assessment tool of pathologic and prosthetic hand function: Normative data, reliability, and validity. *Arch. Phys. Med. Rehabil.* **83**, 776–783 (2002).

## **Chapter 5**

1. Giele, H., Giele, C., Bower, C. & Allison, M. The incidence and epidemiology of congenital upper limb anomalies: A total population study. *J. Hand Surg. Am.* **26**, 628–634 (2001).
2. Atkins, D. J., Heard, D. C. Y. & Donovan, W. H. Epidemiologic overview of individuals with upper-limb loss and their reported research priorities. *J. Prosthetics Orthot.* **8**, 2–11 (1996).
3. Biddiss, E. & Chau, T. Upper limb prosthesis use and abandonment: A survey of the last 25 years. *Prosthetics and Orthotics International* vol. 31 236–257 (2007).
4. James, M. A. *et al.* Impact of prostheses on function and quality of life for children with unilateral congenital below-the-elbow deficiency. *J. Bone Jt. Surg. - Ser. A* **88**, 2356–2365 (2006).
5. Battraw, M. A., Young, P. R., Joiner, W. M. & Schofield, J. S. A multiarticulate pediatric prosthetic hand for clinical and research applications. *Front. Robot. AI* **9**, 1–14 (2022).
6. Ten Kate, J., Smit, G. & Breedveld, P. 3D-printed upper limb prostheses: a review. *Disabil. Rehabil. Assist. Technol.* **12**, 300–314 (2017).
7. Dellacasa Bellingegni, A. *et al.* NLR, MLP, SVM, and LDA: A comparative analysis on

- EMG data from people with trans-radial amputation. *J. Neuroeng. Rehabil.* **14**, 1–16 (2017).
8. Kuiken, T. A., Miller, L. A., Turner, K. & Hargrove, L. J. A Comparison of Pattern Recognition Control and Direct Control of a Multiple Degree-of-Freedom Transradial Prosthesis. *IEEE J. Transl. Eng. Heal. Med.* **4**, (2016).
  9. Resnik, L. *et al.* Evaluation of EMG pattern recognition for upper limb prosthesis control: A case study in comparison with direct myoelectric control. *J. Neuroeng. Rehabil.* **15**, 1–13 (2018).
  10. Scheme, E. & Englehart, K. Electromyogram pattern recognition for control of powered upper-limb prostheses: State of the art and challenges for clinical use. *J. Rehabil. Res. Dev.* **48**, 643–660 (2011).
  11. Kryger, M., Schultz, A. E. & Kuiken, T. Pattern recognition control of multifunction myoelectric prostheses by patients with congenital transradial limb defects: A preliminary study. *Prosthet. Orthot. Int.* **35**, 395–401 (2011).
  12. Kaluf, B., Gart, M. S., Loeffler, B. J. & Gaston, G. Evaluating the Ability of Congenital Upper Extremity Amputees to Control a Multi-Degree of Freedom Myoelectric Prosthesis. *J. Hand Surg. Am.* **47**, 1019.e1-1019.e9 (2022).
  13. Battraw, M. A. *et al.* A Review of Upper Limb Pediatric Prostheses and Perspectives on Future Advancements. *Prosthet. Orthot. Int.* **46**, 267–273 (2022).
  14. Roman-Liu, D. & Bartuzi, P. Influence of type of MVC test on electromyography measures of biceps brachii and triceps brachii. *Int. J. Occup. Saf. Ergon.* **24**, 200–206 (2018).
  15. Motion Lab System, EMG Analysis and EMG Graphing Software User Tutorial. <http://www.c3d.org-http://www.motion-labs.com> (2009).
  16. Farina, D., Merletti, R. & Enoka, R. M. The extraction of neural strategies from the surface EMG. *J. Appl. Physiol.* **96**, 1486–1495 (2004).
  17. Barak, Y., Ayalon, M. & Dvir, Z. Spectral EMG changes in vastus medialis muscle following short range of motion isokinetic training. *J. Electromyogr. Kinesiol.* **16**, 403–412 (2006).
  18. Englehart, K. & Hudgins, B. A Robust, Real-Time Control Scheme for Multifunction Myoelectric Control. *IEEE Trans. Biomed. Eng.* **50**, 848–854 (2003).
  19. Khushaba, R. N., Kodagoda, S., Takruri, M. & Dissanayake, G. Toward improved control of prosthetic fingers using surface electromyogram (EMG) signals. *Expert Syst. Appl.* **39**, 10731–10738 (2012).
  20. Simon, A. M., Lock, B. A. & Stubblefield, K. A. Patient training for functional use of pattern recognition-controlled prostheses. *J. Prosthetics Orthot.* **24**, 56–64 (2012).
  21. Hargrove, L. J., Li, G., Englehart, K. B. & Hudgins, B. S. Principal components analysis preprocessing for improved classification accuracies in pattern-recognition-based

- myoelectric control. *IEEE Trans. Biomed. Eng.* **56**, 1407–1414 (2009).
22. Scheme, E. J., Englehart, K. B. & Hudgins, B. S. Selective classification for improved robustness of myoelectric control under nonideal conditions. *IEEE Trans. Biomed. Eng.* **58**, 1698–1705 (2011).
  23. Sensinger, J. W., Lock, B. A. & Kuiken, T. A. Adaptive Pattern Recognition of Myoelectric Signals: Exploration of Conceptual Framework and Practical Algorithms. *IEEE Trans Neural Syst Rehabil Eng.* **17**, 270–278 (2009).
  24. Young, A. J., Hargrove, L. J. & Kuiken, T. A. Improving myoelectric pattern recognition robustness to electrode shift by changing interelectrode distance and electrode configuration. *IEEE Trans. Biomed. Eng.* **59**, 645–652 (2012).
  25. Zheng, J. Z., De La Rosa, S. & Dollar, A. M. An Investigation of Grasp Type and Frequency in Daily Household and Machine Shop Tasks. in *IEEE International Conference on Robotics and Automation* (2011). doi:10.1109/TOH.2013.6.
  26. Ortiz-Catalan, M., Brånemark, R. & Håkansson, B. BioPatRec: A modular research platform for the control of artificial limbs based on pattern recognition algorithms. *Source Code Biol. Med.* **8**, 1–18 (2013).
  27. Asghari Oskoei, M., Member, S., Hu, H. & Member, S. Support Vector Machine-Based Classification Scheme for Myoelectric Control Applied to Upper Limb. *IEEE Trans. Biomed. Eng.* **55**, (2008).
  28. Phinyomark, A., Thongpanja, S., Hu, H., Phukpattaranont, P. & Limsakul, C. The Usefulness of Mean and Median Frequencies in Electromyography Analysis. in *Computational Intelligence in Electromyography Analysis – A Perspective on Current Applications and Future Challenges* (ed. Naik, G. R.) 195–220 (In Tech, 2012). doi:10.5772/50639.
  29. Abbaspour, S., Lindén, M., Gholamhosseini, H., Naber, A. & Ortiz-Catalan, M. Evaluation of surface EMG-based recognition algorithms for decoding hand movements. *Med. Biol. Eng. Comput.* **58**, 83–100 (2020).
  30. Phinyomark, A., Phukpattaranont, P. & Limsakul, C. Feature reduction and selection for EMG signal classification. *Expert Syst. Appl.* **39**, 7420–7431 (2012).
  31. Siegel, S. *Nonparametric Statistics for the Behavioral Sciences*. (McGraw-Hil, 1956).
  32. Field, A. P. Kendall’s Coefficient of Concordance. *Encyclopedia of Statistics in Behavioral Science* vol. 2 1010–1011 (2005).
  33. Kriegeskorte, N., Mur, M. & Bandettini, P. Representational similarity analysis - connecting the branches of systems neuroscience. *Front. Syst. Neurosci.* **2**, 1–28 (2008).
  34. Ipek. Normality test package. *MATLAB Central File Exchange* <https://www.mathworks.com/matlabcentral/fileexchange/60147-normality-test-package> (2022).
  35. O’Neill, T. A. An overview of interrater agreement on likert scales for researchers and

- practitioners. *Front. Psychol.* **8**, (2017).
36. Landis, J. R. & Koch, G. G. The Measurement of Observer Agreement for Categorical Data. *Biometrics* **33**, 159–174 (1977).
  37. Krippendorff, K. *Content Analysis An Introduction to Its Methodology. Physical Review B* vol. 31 (SAGE Publications, Incorporated, 2004).
  38. Kriegeskorte, N. & Kievit, R. A. Representational geometry: Integrating cognition, computation, and the brain. *Trends Cogn. Sci.* **17**, 401–412 (2013).
  39. Sburlea, A. & Muller-Putz, G. Exploring representations of human grasping in neural, muscle and kinematic signals. *Sci. Rep.* **8**, (2018).
  40. Nili, H., Walther, A., Alink, A. & Kriegeskorte, N. Inferring exemplar discriminability in brain representations. *PLoS One* **15**, (2020).
  41. Kruskal, J. B. & Wish, M. *Multidimensional Scaling.* (1978).
  42. Nili, H. *et al.* A Toolbox for Representational Similarity Analysis. *PLoS Comput. Biol.* **10**, (2014).
  43. Kasman, G. & Wolf, S. *Surface emg made easy: A beginner's Guide for Rehabilitation Clinicians.* (Noraxon USA, Inc, 2002).
  44. Feix, T., Romero, J., Schmiedmayer, H. B., Dollar, A. M. & Kragic, D. The GRASP Taxonomy of Human Grasp Types. *IEEE Trans. Human-Machine Syst.* **46**, 66–77 (2016).

## **Chapter 6**

1. Davids, J. R., Wagner, L. V., Meyer, L. C. & Blackhurst, D. W. Prosthetic management of children with unilateral congenital below-elbow deficiency. *J. Bone Jt. Surg. - Ser. A* **88**, 1294–1300 (2006).
2. Battraw, M. A. *et al.* A Review of Upper Limb Pediatric Protheses and Perspectives on Future Advancements. *Prosthet. Orthot. Int.* **46**, 267–273 (2022).
3. Battraw, M. A. *et al.* Understanding the capacity of children with congenital unilateral below - elbow deficiency to actuate their affected muscles. *Sci. Rep.* 1–16 (2024) doi:10.1038/s41598-024-54952-7.
4. Fitzgerald, J. J. *et al.* Moving a missing hand : children born with below elbow deficiency can enact hand grasp patterns with their residual muscles. *J. Neuroeng. Rehabil.* **21**, 1–15 (2024).
5. Abbaspour, S., Lindén, M., Gholamhosseini, H., Naber, A. & Ortiz-Catalan, M. Evaluation of surface EMG-based recognition algorithms for decoding hand movements. *Med. Biol. Eng. Comput.* **58**, 83–100 (2020).
6. Adewuyi, A. A., Hargrove, L. J. & Kuiken, T. A. Evaluating EMG Feature and Classifier Selection for Application to Partial-Hand Prosthesis Control. *Front. Neurorobot.* **10**, (2016).

7. Arjunan, S. P. & Kumar, D. K. Decoding subtle forearm flexions using fractal features of surface electromyogram from single and multiple sensors. *J. Neuroeng. Rehabil.* **7**, (2010).
8. Phinyomark, A., Phukpattaranont, P. & Limsakul, C. Feature reduction and selection for EMG signal classification. *Expert Syst. Appl.* **39**, 7420–7431 (2012).
9. Ortiz-Catalan, M., Håkansson, B. & Brånemark, R. Real-time and simultaneous control of artificial limbs based on pattern recognition algorithms. *IEEE Trans. Neural Syst. Rehabil. Eng.* **22**, 756–764 (2014).
10. Atzori, M., Gijssberts, A., Muller, H. & Caputo, B. Classification of hand movements in amputated subjects by sEMG and accelerometers. in *2014 36th Annual International Conference of the IEEE Engineering in Medicine and Biology Society* (2014). doi:10.1109/EMBC.2014.6944388.
11. Parajuli, N. *et al.* Real-Time EMG Based Pattern Recognition Control Challenges: A Review on Existing Methods, Challenges and Future Implementation. *Sensors* **19**, 4596 (2019).
12. Kryger, M., Schultz, A. E. & Kuiken, T. Pattern recognition control of multifunction myoelectric prostheses by patients with congenital transradial limb defects: A preliminary study. *Prosthet. Orthot. Int.* **35**, 395–401 (2011).
13. Kaluf, B., Gart, M. S., Loeffler, B. J. & Gaston, G. Evaluating the Ability of Congenital Upper Extremity Amputees to Control a Multi-Degree of Freedom Myoelectric Prosthesis. *J. Hand Surg. Am.* **47**, 1019.e1-1019.e9 (2022).
14. Hudgins, B., Parker, P. & Scott, R. The Recognition of Myoelectric Patterns for Prosthetic Limb Control. in *Annual International Conference of the IEEE Engineering in Medicine and Biology Society* 2040–2041 (1991).
15. Hudgins, B., Parker, P. & Scott, R. N. A New Strategy for Multifunction Myoelectric Control. *IEEE Trans. Biomed. Eng.* **40**, 82–94 (1993).
16. Hargrove, L. J., Li, G., Englehart, K. B. & Hudgins, B. S. Principal components analysis preprocessing for improved classification accuracies in pattern-recognition-based myoelectric control. *IEEE Trans. Biomed. Eng.* **56**, 1407–1414 (2009).
17. Scheme, E. J., Englehart, K. B. & Hudgins, B. S. Selective classification for improved robustness of myoelectric control under nonideal conditions. *IEEE Trans. Biomed. Eng.* **58**, 1698–1705 (2011).
18. Sensinger, J. W., Lock, B. A. & Kuiken, T. A. Adaptive Pattern Recognition of Myoelectric Signals: Exploration of Conceptual Framework and Practical Algorithms. *IEEE Trans Neural Syst Rehabil Eng.* **17**, 270–278 (2009).
19. Zheng, J. Z., De La Rosa, S. & Dollar, A. M. An Investigation of Grasp Type and Frequency in Daily Household and Machine Shop Tasks. in *IEEE International Conference on Robotics and Automation* (2011). doi:10.1109/TOH.2013.6.
20. Englehart, K. & Hudgins, B. A Robust, Real-Time Control Scheme for Multifunction



- Myoelectric Control. *IEEE Trans. Biomed. Eng.* **50**, 848–854 (2003).
21. Khushaba, R. N., Kodagoda, S., Takruri, M. & Dissanayake, G. Toward improved control of prosthetic fingers using surface electromyogram (EMG) signals. *Expert Syst. Appl.* **39**, 10731–10738 (2012).
  22. Ortiz-Catalan, M., Brånemark, R. & Håkansson, B. BioPatRec: A modular research platform for the control of artificial limbs based on pattern recognition algorithms. *Source Code Biol. Med.* **8**, 1–18 (2013).
  23. Smith, L. H., Hargrove, L. J., Lock, B. A. & Kuiken, T. A. Determining the optimal window length for pattern recognition-based myoelectric control: Balancing the competing effects of classification error and controller delay. *IEEE Trans. Neural Syst. Rehabil. Eng.* **19**, 186–192 (2011).
  24. Asghari Oskoei, M. & Hu, H. Myoelectric control systems-A survey. *Biomed. Signal Process. Control* **2**, 275–294 (2007).
  25. Scheme, E. & Englehart, K. Electromyogram pattern recognition for control of powered upper-limb prostheses: State of the art and challenges for clinical use. *J. Rehabil. Res. Dev.* **48**, 643–660 (2011).
  26. Tsai, A. C., Hsieh, T. H., Luh, J. J. & Lin, T. Te. A comparison of upper-limb motion pattern recognition using EMG signals during dynamic and isometric muscle contractions. *Biomed. Signal Process. Control* **11**, 17–26 (2014).
  27. Asghari Oskoei, M., Member, S., Hu, H. & Member, S. Support Vector Machine-Based Classification Scheme for Myoelectric Control Applied to Upper Limb. *IEEE Trans. Biomed. Eng.* **55**, (2008).
  28. Abbaspour, S., Naber, A., Ortiz-catalan, M., Gholamhosseini, H. & Lindén, M. Real-time and offline evaluation of myoelectric pattern recognition for the decoding of hand movements. *Sensors* **21**, (2021).
  29. Stango, A., Negro, F. & Farina, D. Spatial Correlation of High Density EMG Signals Provides Features Robust to Electrode Number and Shift in Pattern Recognition for Myocontrol. *IEEE Trans. Neural Syst. Rehabil. Eng.* **23**, 189–198 (2015).
  30. Shin, S., Tafreshi, R. & Langari, R. A performance comparison of hand motion EMG classification. in *Middle East Conference on Biomedical Engineering, MECBME* 353–356 (IEEE Computer Society, 2014). doi:10.1109/MECBME.2014.6783276.
  31. Al-Angari, H. M., Kanitz, G., Tarantino, S. & Cipriani, C. Distance and mutual information methods for EMG feature and channel subset selection for classification of hand movements. *Biomed. Signal Process. Control* **27**, 24–31 (2016).
  32. Zardoshti-Kermani, M., Wheeler, B. C., Badie, K. & Hashemi, R. M. EMG Feature Evaluation for Movement Control of Upper Extremity Prostheses. *IEEE Trans. Rehabil. Eng.* **3**, 324–333 (1995).
  33. Hjorth, B. EEG analysis based on time domain properties. *Electroencephalogr. Clin. Neurophysiol.* **29**, 306–310 (1970).

34. Boostani, R. & Moradi, M. H. Evaluation of the forearm EMG signal features for the control of a prosthetic hand. *Physiol. Meas.* **24**, 309–319 (2003).
35. Phinyomark, A., Phukpattaranont, P. & Limsakul, C. Fractal analysis features for weak and single-channel upper-limb EMG signals. *Expert Syst. Appl.* **39**, 11156–11163 (2012).
36. Saponas, T. S., Tan, D. S., Morris, D. & Balakrishnan, R. Demonstrating the feasibility of using forearm electromyography for muscle-computer interfaces. *Conf. Hum. Factors Comput. Syst. - Proc.* (2008) doi:10.1145/1357054.1357138.
37. Iqbal, N. V., Subramaniam, K. & Asmi P., S. Robust feature sets for contraction level invariant control of upper limb myoelectric prosthesis. *Biomed. Signal Process. Control* **51**, 90–96 (2019).
38. Tkach, D., Huang, H. & Kuiken, T. A. Study of stability of time-domain features for electromyographic pattern recognition. 1–13 (2010).
39. Tang, X., Liu, Y., Lv, C. & Sun, D. Hand motion classification using a multi-channel surface electromyography sensor. *Sensors* **12**, 1130–1147 (2012).
40. Rafiee, J., Rafiee, M. A., Yavari, F. & Schoen, M. P. Feature extraction of forearm EMG signals for prosthetics. *Expert Syst. Appl.* **38**, 4058–4067 (2011).
41. Duan, F. *et al.* SEMG-Based Identification of Hand Motion Commands Using Wavelet Neural Network Combined with Discrete Wavelet Transform. *IEEE Trans. Ind. Electron.* **63**, 1923–1934 (2016).
42. Zhang, D., Zhao, X., Han, J. & Zhao, Y. A comparative study on PCA and LDA based EMG pattern recognition for anthropomorphic robotic hand. in *Proceedings - IEEE International Conference on Robotics and Automation* 4850–4855 (Institute of Electrical and Electronics Engineers Inc., 2014). doi:10.1109/ICRA.2014.6907569.
43. Dellacasa Bellingegni, A. *et al.* NLR, MLP, SVM, and LDA: A comparative analysis on EMG data from people with trans-radial amputation. *J. Neuroeng. Rehabil.* **14**, 1–16 (2017).
44. John, G. H., Kohavi, R. & Pflieger, K. Irrelevant Features and the Subset Selection Problem. in *Machine Learning: Proceedings of the Eleventh International Conference* 121–129 (Morgan Kaufmann Publishers, 1994). doi:10.1016/b978-1-55860-335-6.50023-4.
45. Bunderson, N. E. & Kuiken, T. A. Quantification of feature space changes with experience during electromyogram pattern recognition control. *IEEE Trans. Neural Syst. Rehabil. Eng.* **20**, 239–246 (2012).
46. Kristoffersen, M. B., Franzke, A. W., Sluis, C. K. Van Der, Murgia, A. & Bongers, R. M. The Effect of Feedback During Training Sessions on Learning Pattern-Recognition-Based Prosthesis Control. *IEEE Trans. Neural Syst. Rehabil. Eng.* **27**, 2087–2096 (2019).
47. Kristoffersen, M. B., Franzke, A. W., van der Sluis, C. K., Murgia, A. & Bongers, R. M. Serious gaming to generate separated and consistent EMG patterns in pattern-recognition prosthesis control. *Biomed. Signal Process. Control* **62**, 102140 (2020).

48. Powell, M. A., Kaliki, R. R. & Thakor, N. V. User training for pattern recognition-based myoelectric prostheses: Improving phantom limb movement consistency and distinguishability. *IEEE Trans. Neural Syst. Rehabil. Eng.* **22**, 522–532 (2014).
49. Friedman, M. The Use of Ranks to Avoid the Assumption of Normality Implicit in the Analysis of Variance. *J. Am. Stat. Assoc.* **32**, 675–701 (1937).
50. Demšar, J. Statistical comparisons of classifiers over multiple data sets. *J. Mach. Learn. Res.* **7**, 1–30 (2006).
51. Nemenyi, P. B. Distribution-free multiple comparisons. (Princeton University, 1963).
52. Feix, T., Romero, J., Schmiedmayer, H. B., Dollar, A. M. & Kragic, D. The GRASP Taxonomy of Human Grasp Types. *IEEE Trans. Human-Machine Syst.* **46**, 66–77 (2016).

## **Chapter 7**

1. Biddiss, E. & Chau, T. Upper limb prosthesis use and abandonment: A survey of the last 25 years. *Prosthetics and Orthotics International* vol. 31 236–257 (2007).
2. Postema, K., Van Der Donk, V., Van Limbeek, J., Rijken, R. & Poelma, M. J. Prosthesis rejection in children with a unilateral congenital arm defect. *Clin. Rehabil.* **13**, 243–249 (1999).
3. Egermann, M., Kasten, P. & Thomsen, M. Myoelectric hand prostheses in very young children. *Int. Orthop.* **33**, 1101–1105 (2009).
4. Battraw, M. A. *et al.* A Review of Upper Limb Pediatric Prostheses and Perspectives on Future Advancements. *Prosthet. Orthot. Int.* **46**, 267–273 (2022).
5. Kryger, M., Schultz, A. E. & Kuiken, T. Pattern recognition control of multifunction myoelectric prostheses by patients with congenital transradial limb defects: A preliminary study. *Prosthet. Orthot. Int.* **35**, 395–401 (2011).
6. Kaluf, B., Gart, M. S., Loeffler, B. J. & Gaston, G. Evaluating the Ability of Congenital Upper Extremity Amputees to Control a Multi-Degree of Freedom Myoelectric Prosthesis. *J. Hand Surg. Am.* **47**, 1019.e1-1019.e9 (2022).
7. Battraw, M. A. *et al.* Understanding the capacity of children with congenital unilateral below - elbow deficiency to actuate their affected muscles. *Sci. Rep.* 1–16 (2024) doi:10.1038/s41598-024-54952-7.
8. Fitzgerald, J. J. *et al.* Moving a missing hand : children born with below elbow deficiency can enact hand grasp patterns with their residual muscles. *J. Neuroeng. Rehabil.* **21**, 1–15 (2024).
9. Kuiken, T. A. *et al.* Targeted muscle reinnervation for real-time myoelectric control of multifunction artificial arms. *JAMA - J. Am. Med. Assoc.* **301**, 619–628 (2009).
10. Kristoffersen, M. B., Franzke, A. W., Sluis, C. K. Van Der, Murgia, A. & Bongers, R. M. The Effect of Feedback During Training Sessions on Learning Pattern-Recognition-Based Prosthesis Control. *IEEE Trans. Neural Syst. Rehabil. Eng.* **27**, 2087–2096 (2019).

11. Franzke, A. W. *et al.* Exploring the Relationship between EMG Feature Space Characteristics and Control Performance in Machine Learning Myoelectric Control. *IEEE Trans. Neural Syst. Rehabil. Eng.* **29**, 21–30 (2021).
12. Bunderson, N. E. & Kuiken, T. A. Quantification of feature space changes with experience during electromyogram pattern recognition control. *IEEE Trans. Neural Syst. Rehabil. Eng.* **20**, 239–246 (2012).
13. Feix, T., Romero, J., Schmiedmayer, H. B., Dollar, A. M. & Kragic, D. The GRASP Taxonomy of Human Grasp Types. *IEEE Trans. Human-Machine Syst.* **46**, 66–77 (2016).
14. Ortiz-Catalan, M., Brånemark, R. & Håkansson, B. BioPatRec: A modular research platform for the control of artificial limbs based on pattern recognition algorithms. *Source Code Biol. Med.* **8**, 1–18 (2013).
15. Scheme, E. J., Englehart, K. B. & Hudgins, B. S. Selective classification for improved robustness of myoelectric control under nonideal conditions. *IEEE Trans. Biomed. Eng.* **58**, 1698–1705 (2011).
16. Ortiz-Catalan, M., Håkansson, B. & Brånemark, R. Real-time and simultaneous control of artificial limbs based on pattern recognition algorithms. *IEEE Trans. Neural Syst. Rehabil. Eng.* **22**, 756–764 (2014).
17. Batraw, M. A., Young, P. R., Joiner, W. M. & Schofield, J. S. A multiarticulate pediatric prosthetic hand for clinical and research applications. *Front. Robot. AI* **9**, 1–14 (2022).
18. Nilsson, N. & Ortiz-Catalan, M. Estimates of Classification Complexity for Myoelectric Pattern Recognition. in *Proceedings - International Conference on Pattern Recognition* 2682–2687 (2016). doi:10.1109/ICPR.2016.7900040.
19. Scheme, E. & Englehart, K. Electromyogram pattern recognition for control of powered upper-limb prostheses: State of the art and challenges for clinical use. *J. Rehabil. Res. Dev.* **48**, 643–660 (2011).
20. Abbaspour, S., Naber, A., Ortiz-Catalan, M., Gholamhosseini, H. & Lindén, M. Real-time and offline evaluation of myoelectric pattern recognition for the decoding of hand movements. *Sensors* **21**, (2021).
21. Englehart, K. & Hudgins, B. A Robust, Real-Time Control Scheme for Multifunction Myoelectric Control. *IEEE Trans. Biomed. Eng.* **50**, 848–854 (2003).
22. Kallenberg, L. A. C., Schulte, E., Disselhorst-Klug, C. & Hermens, H. J. Myoelectric manifestations of fatigue at low contraction levels in subjects with and without chronic pain. *J. Electromyogr. Kinesiol.* **17**, 264–274 (2007).
23. Enoka, R. M. & Duchateau, J. Muscle fatigue: What, why and how it influences muscle function. *J. Physiol.* **586**, 11–23 (2008).
24. Simon, A. M. *et al.* Implications of EMG channel count: enhancing pattern recognition online prosthetic testing. *Front. Rehabil. Sci.* **5**, 2–11 (2024).
25. Mathiowetz, V. & Weber, K. Adult Norms for the Box and Block. *Am. J. Occupational*

- Ther.* **39**, 387–391 (1985).
26. Hebert, J. S., Lewicke, J., Williams, T. R. & Vette, A. H. Normative data for modified box and blocks test measuring upper-limb function via motion capture. *J. Rehabil. Res. Dev.* **51**, 919–931 (2014).
  27. Jebsen, R., Taylor, N., Trieschmann, R., Trotter, M. & Howard, L. An objective and standardized test of hand function. *Arch. Phys. Med. Rehabil.* **50**, 311–319 (1969).
  28. Kyberd, P., Hussaini, A. & Maillet, G. Characterisation of the Clothespin Relocation Test as a functional assessment tool. *J. Rehabil. Assist. Technol. Eng.* **5**, 1–7 (2018).
  29. Light, C. M., Chappell, P. H. & Kyberd, P. J. Establishing a standardized clinical assessment tool of pathologic and prosthetic hand function: Normative data, reliability, and validity. *Arch. Phys. Med. Rehabil.* **83**, 776–783 (2002).
  30. Vasluian, E., Bongers, R. M., Reinders-Messelink, H. A., Dijkstra, P. U. & Van Der Sluis, C. K. Preliminary study of the Southampton Hand Assessment Procedure for Children and its reliability. *BMC Musculoskelet. Disord.* **15**, (2014).
  31. Davids, J. R. *et al.* Validation of the Shriners Hospital for Children Upper Extremity Evaluation (SHUEE) for children with hemiplegic cerebral palsy. *J. Bone Jt. Surg.* **88**, 326–333 (2006).
  32. Bagley, A. M., Molitor, F., Wagner, L. V., Tomhave, W. & James, M. A. The Unilateral Below Elbow Test: A function test for children with unilateral congenital below elbow deficiency. *Dev. Med. Child Neurol.* **48**, 569–575 (2006).

## **Chapter 8**

1. Biddiss, E. & Chau, T. Upper limb prosthesis use and abandonment: A survey of the last 25 years. *Prosthetics and Orthotics International* vol. 31 236–257 (2007).
2. Vasluian, E. *et al.* Opinions of Youngsters with Congenital Below-Elbow Deficiency, and Those of Their Parents and Professionals Concerning Prosthetic Use and Rehabilitation Treatment. *PLoS One* **8**, (2013).
3. Postema, K., Van Der Donk, V., Van Limbeek, J., Rijken, R. & Poelma, M. J. Prosthesis rejection in children with a unilateral congenital arm defect. *Clin. Rehabil.* **13**, 243–249 (1999).
4. Wagner, L. V., Bagley, A. M. & James, M. A. Reasons for Prosthetic Rejection by Children With Unilateral Congenital Transverse Forearm Total Deficiency. *J. Prosthetics Orthot.* **19**, 51–54 (2007).
5. Egermann, M., Kasten, P. & Thomsen, M. Myoelectric hand prostheses in very young children. *Int. Orthop.* **33**, 1101–1105 (2009).
6. James, M. A. *et al.* Impact of prostheses on function and quality of life for children with unilateral congenital below-the-elbow deficiency. *J. Bone Jt. Surg. - Ser. A* **88**, 2356–2365 (2006).

7. Batraw, M. A. *et al.* A Review of Upper Limb Pediatric Prostheses and Perspectives on Future Advancements. *Prosthet. Orthot. Int.* **46**, 267–273 (2022).
8. Atkins, D. J., Heard, D. C. Y. & Donovan, W. H. Epidemiologic overview of individuals with upper-limb loss and their reported research priorities. *J. Prosthetics Orthot.* **8**, 2–11 (1996).
9. Kryger, M., Schultz, A. E. & Kuiken, T. Pattern recognition control of multifunction myoelectric prostheses by patients with congenital transradial limb defects: A preliminary study. *Prosthet. Orthot. Int.* **35**, 395–401 (2011).
10. Kaluf, B., Gart, M. S., Loeffler, B. J. & Gaston, G. Evaluating the Ability of Congenital Upper Extremity Amputees to Control a Multi-Degree of Freedom Myoelectric Prosthesis. *J. Hand Surg. Am.* **47**, 1019.e1-1019.e9 (2022).
11. Ortiz-Catalan, M., Brånemark, R. & Håkansson, B. BioPatRec: A modular research platform for the control of artificial limbs based on pattern recognition algorithms. *Source Code Biol. Med.* **8**, 1–18 (2013).
12. Ortiz-Catalan, M., Håkansson, B. & Brånemark, R. Real-time classification of simultaneous hand and wrist motions using Artificial Neural Networks with variable threshold outputs. in *Proceedings of the XXXIV International Conference on Artificial Neural Networks (ICANN)* 1159–1164 (2013).
13. Abbaspour, S., Naber, A., Ortiz-Catalan, M., Gholamhosseini, H. & Lindén, M. Real-time and offline evaluation of myoelectric pattern recognition for the decoding of hand movements. *Sensors* **21**, (2021).

## Appendix A: BEAR PAW movement assessment

Table A-1. Anthropomorphic Hand Assessment Protocol scores from each of the three test investigators for all grasp types/postures over each trial for grasping and maintaining obtained for the BEAR PAW.

Test Investigator	Trial	Grasp Type/Posture	Object	Grasping			Maintaining		
				Trial 1	Trial 2	Trial 3	Trial 1	Trial 2	Trial 3
1	1	Hook	Skillet lid	0.5	0.5	0.5	0.5	0.5	0.5
	2	Spherical grip	Plastic apple	0.5	0.5	0.5	1	1	1
	3	Tripod pinch	Large marker	1	0.5	0.5	1	0.5	1
	4	Extension grip	Plate	1	1	1	0	0	0
	5	Cylindrical grip	Chips can	1	1	1	1	1	1
	6	Diagonal volar grip	Phillips screwdriver	0.5	0.5	0.5	1	1	1
	7	Lateral pinch	Bowl	0.5	0.5	0.5	1	1	1
	8	Pulp pinch	Small marker	1	0.5	1	0	1	1
	9	Index pointing/pressing	Timer	1	1	1	1	1	1
	10	Hook	Pitcher base	0.5	0.5	0.5	0.5	0.5	0.5
	11	Spherical grip	Softball	1	0.5	1	1	1	1
	12	Tripod pinch	Tuna can	1	1	1	0.5	0.5	0.5
	13	Extension grip	Cracker box	0.5	0.5	0.5	0	0	0
	14	Cylindrical grip	Coffee can	0.5	0.5	0.5	0	0	0
	15	Diagonal volar grip	Spatula	0.5	0.5	0.5	0.5	0.5	0.5
	16	Lateral pinch	XS Clamp	1	1	1	1	0.5	1
	17	Pulp pinch	Plastic pear	1	1	1	0	0.5	0
	18	Platform	Plate	1	1	1	-	-	-
	19	Hook	Wood blocks with rope	0.5	0.5	0.5	0.5	0.5	0.5
	20	Spherical grip	Mini soccer ball	0.5	0.5	0.5	0	0	0
	21	Tripod pinch	Golf ball	1	1	1	1	0.5	1
	22	Extension grip	Pudding box	1	1	1	0	0	0
	23	Cylindrical grip	Power drill	1	1	1	1	1	1
	24	Diagonal volar grip	Skillet	0	0	0	0	0	0

	25	Lateral pinch	Key	0.5	0.5	0.5	0.5	0.5	0.5
	26	Pulp pinch	Washer 10mm	1	1	1	1	1	0.5
2	1	Hook	Skillet lid	0.5	0.5	0.5	0.5	0	0
	2	Spherical grip	Plastic apple	0.5	0.5	0.5	1	1	1
	3	Tripod pinch	Large marker	0.5	1	0.5	0.5	0.5	0.5
	4	Extension grip	Plate	1	1	1	0	0	0
	5	Cylindrical grip	Chips can	1	1	1	1	1	1
	6	Diagonal volar grip	Phillips screwdriver	0.5	0.5	0.5	1	1	1
	7	Lateral pinch	Bowl	0.5	0.5	0.5	1	1	1
	8	Pulp pinch	Small marker	1	1	1	0.5	1	0
	9	Index pointing/pressing	Timer	1	1	1	1	1	1
	10	Hook	Pitcher base	0.5	0.5	0.5	0.5	0.5	0.5
	11	Spherical grip	Softball	1	1	1	0.5	0.5	0.5
	12	Tripod pinch	Tuna can	1	1	1	0	0	0.5
	13	Extension grip	Cracker box	0.5	0.5	0.5	0	0	0
	14	Cylindrical grip	Coffee can	0.5	0.5	0.5	0	0	0
	15	Diagonal volar grip	Spatula	0.5	0.5	0.5	0.5	0.5	0.5
	16	Lateral pinch	XS Clamp	1	1	1	1	1	1
	17	Pulp pinch	Plastic pear	1	1	1	0	1	1
	18	Platform	Plate	1	1	1	-	-	-
	19	Hook	Wood blocks with rope	0.5	0.5	0.5	0.5	0.5	0.5
	20	Spherical grip	Mini soccer ball	0.5	0.5	0.5	0	0	0
21	Tripod pinch	Golf ball	1	1	0.5	1	1	1	
22	Extension grip	Pudding box	1	1	1	0	0	0	
23	Cylindrical grip	Power drill	1	1	1	0.5	1	1	
24	Diagonal volar grip	Skillet	0	0	0	0	0	0	
	25	Lateral pinch	Key	0.5	0.5	0.5	0.5	0.5	0.5
	26	Pulp pinch	Washer 10mm	1	1	1	1	1	1
3	1	Hook	Skillet lid	0.5	0.5	0.5	0	0	0.5
	2	Spherical grip	Plastic apple	1	0.5	1	1	0	1
	3	Tripod pinch	Large marker	0.5	0.5	0.5	0.5	0.5	0.5
	4	Extension grip	Plate	1	1	1	0	0	0



5	Cylindrical grip	Chips can	1	1	1	1	0	0
6	Diagonal volar grip	Phillips screwdriver	0.5	0.5	0.5	0.5	1	1
7	Lateral pinch	Bowl	0.5	0.5	0.5	1	1	1
8	Pulp pinch	Small marker	1	1	1	1	0.5	1
9	Index pointing/pressing	Timer	1	1	1	1	1	1
10	Hook	Pitcher base	0.5	0.5	0.5	0.5	0.5	0.5
11	Spherical grip	Softball	1	1	1	0.5	0.5	0.5
12	Tripod pinch	Tuna can	1	1	1	0	0.5	0.5
13	Extension grip	Cracker box	0.5	0.5	0.5	0	0	0
14	Cylindrical grip	Coffee can	0.5	0.5	0.5	0	0	0
15	Diagonal volar grip	Spatula	0.5	0.5	0.5	0.5	0.5	0.5
16	Lateral pinch	XS Clamp	1	1	1	1	1	1
17	Pulp pinch	Plastic pear	1	1	1	1	1	1
18	Platform	Plate	1	1	1	-	-	-
19	Hook	Wood blocks with rope	0.5	0.5	0.5	0.5	0.5	0.5
20	Spherical grip	Mini soccer ball	0.5	0.5	0.5	0	0	0
21	Tripod pinch	Golf ball	1	1	1	1	0.5	1
22	Extension grip	Pudding box	1	1	1	0	0	0
23	Cylindrical grip	Power drill	1	1	1	1	1	1
24	Diagonal volar grip	Skillet	0	0	0	0	0	0
25	Lateral pinch	Key	0.5	0.5	0.5	0.5	0.5	1
26	Pulp pinch	Washer 10mm	1	1	1	1	0	1

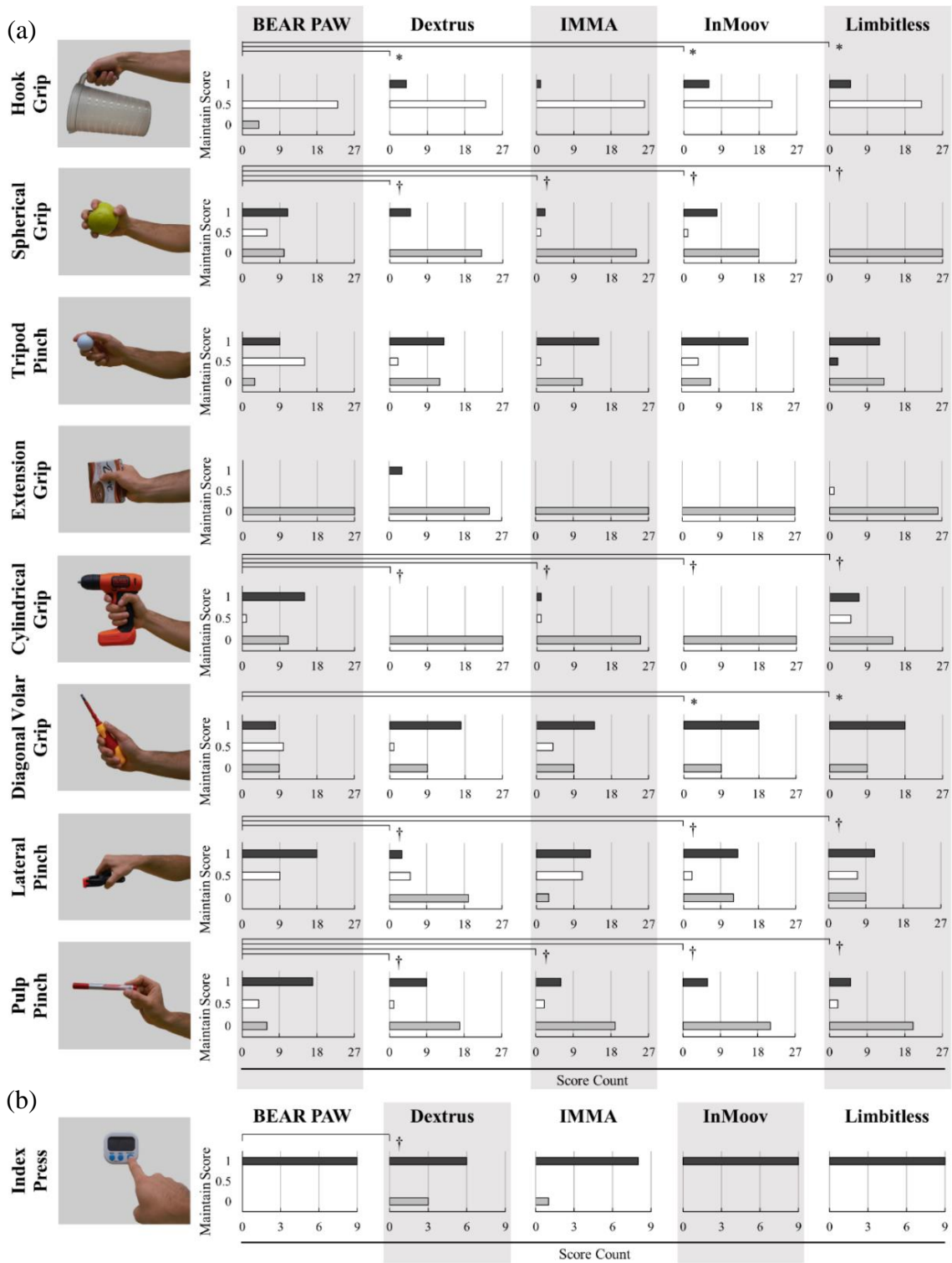


Figure A-1. BEAR PAW maintaining comparison scores for the (a) 8 grasp types and (b) 1 posture across the 4 adult hands. For each grasp type/posture, the number of times each hand scored a 1, 0.5, or 0 was plotted. \*Represents when the BEAR PAW performed statistically worse. †Represents when the BEAR PAW performed statistically better.

# Appendix B: Muscle excitation and visualization

## RMS and MNF muscle excitation

Participant: SHR-A

SHR-A: Normalized RMS across channels and movements

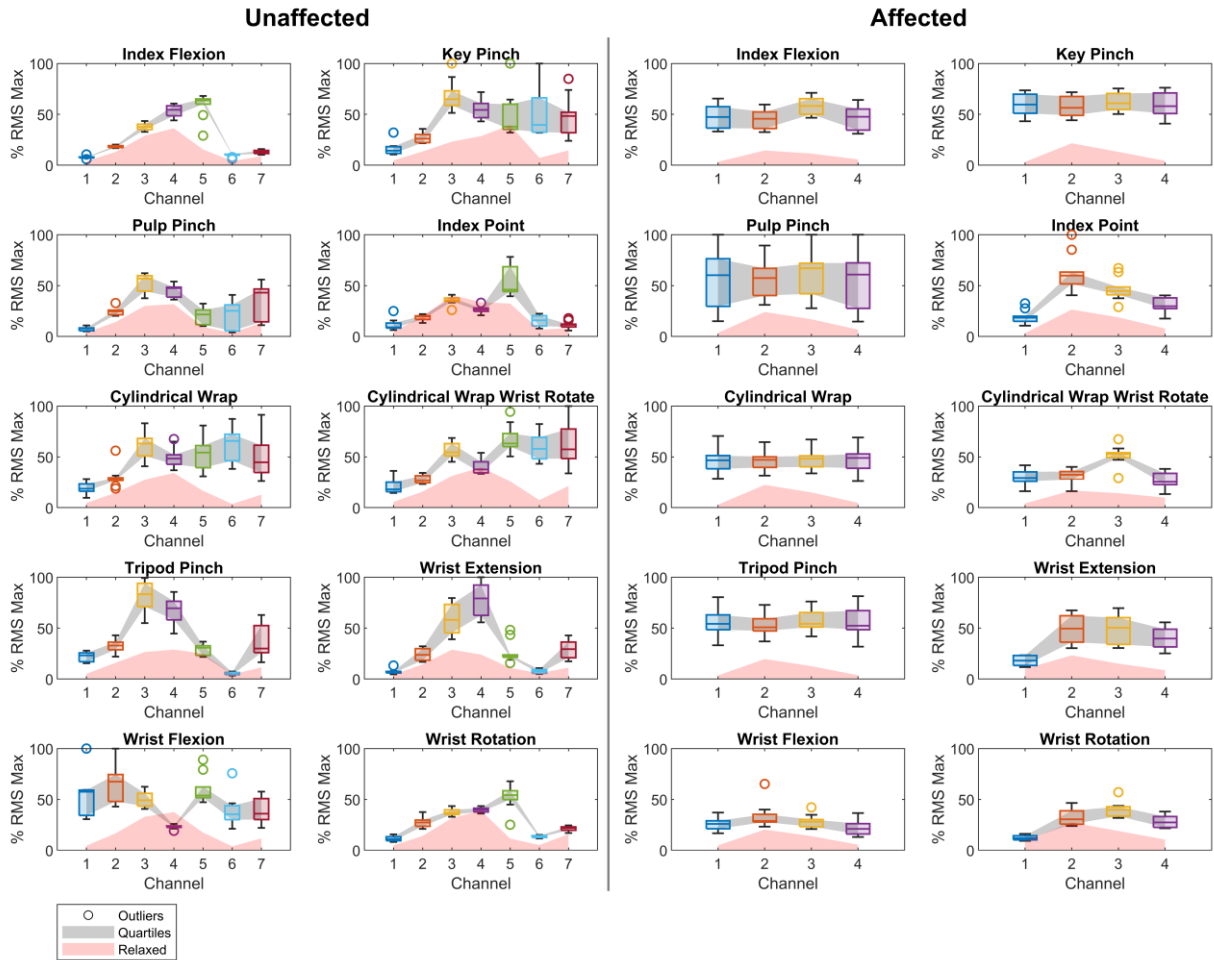


Figure B-1. The box and whisker plots provide a visualization of the RMS muscle excitation patterns and relaxed states seen for the various hand movements across the unaffected and affected limbs for participant SHR-A.

SHR-A: Normalized MNF across channels and movements

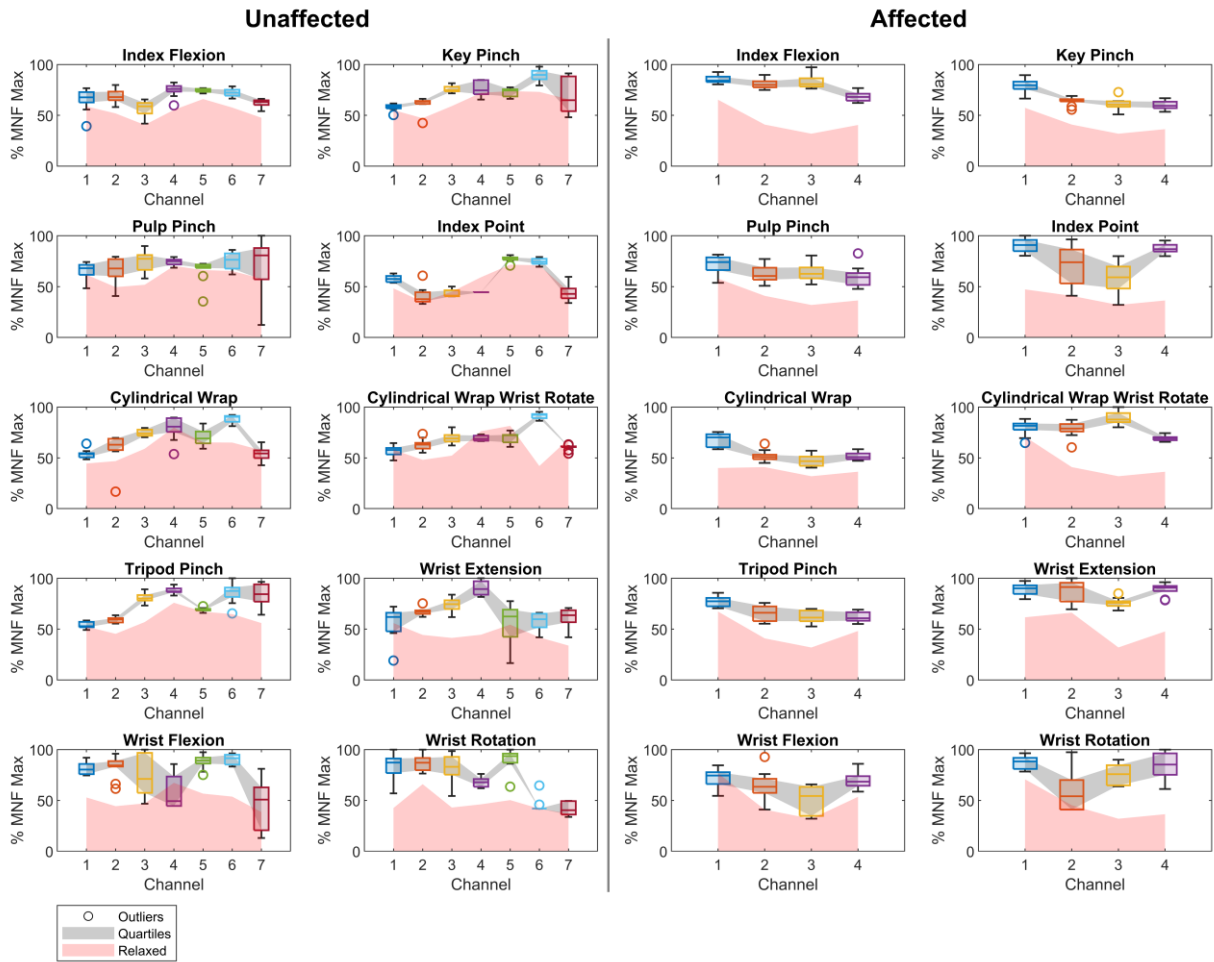


Figure B-2. The box and whisker plots provide a visualization of the MNF muscle excitation patterns and relaxed states seen for the various hand movements across the unaffected and affected limbs for participant SHR-A.

# Participant: SHR-B

## SHR-B: Normalized RMS across channels and movements

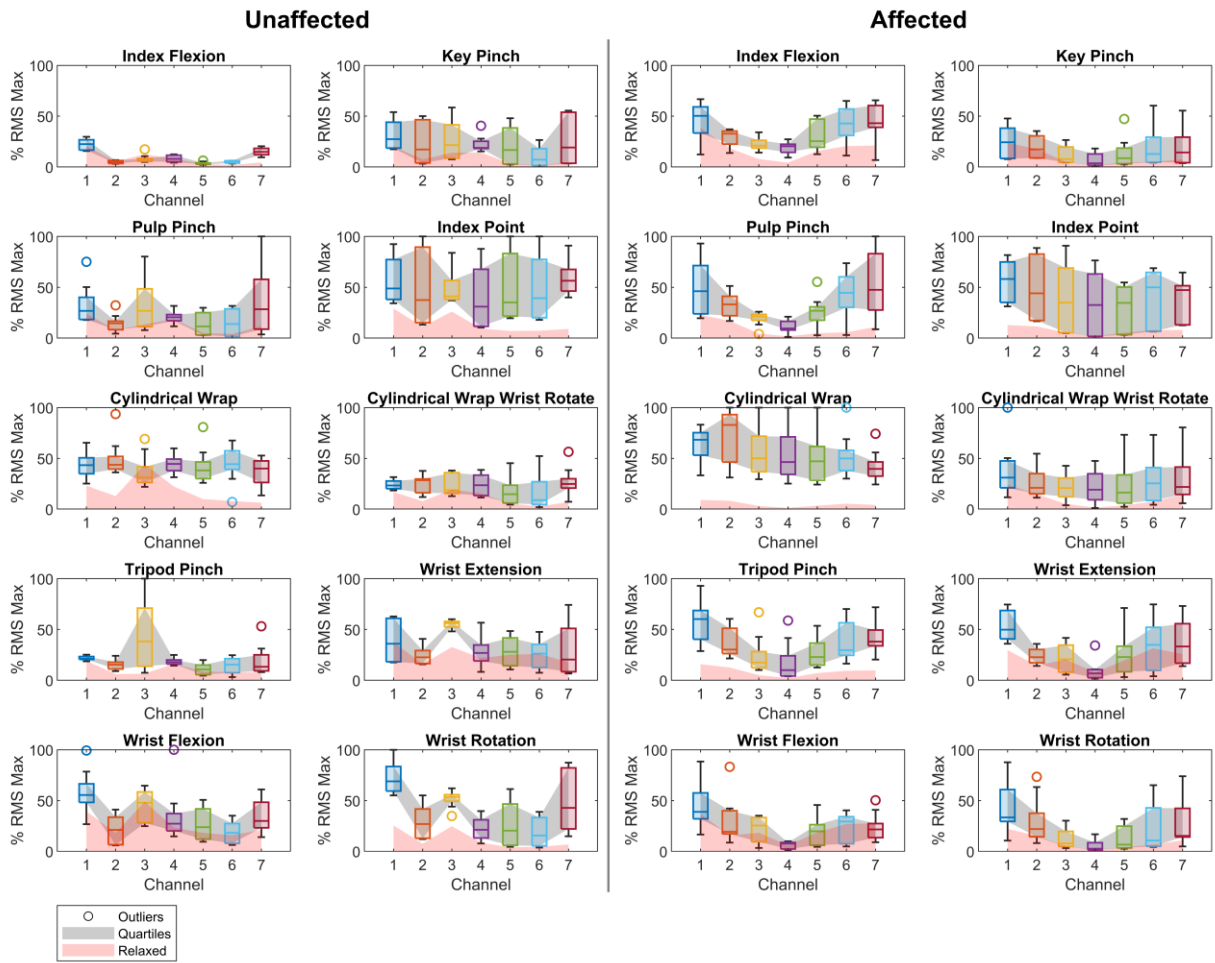


Figure B-3. The box and whisker plots provide a visualization of the RMS muscle excitation patterns and relaxed states seen for the various hand movements across the unaffected and affected limbs for participant SHR-B.

SHR-B: Normalized MNF across channels and movements

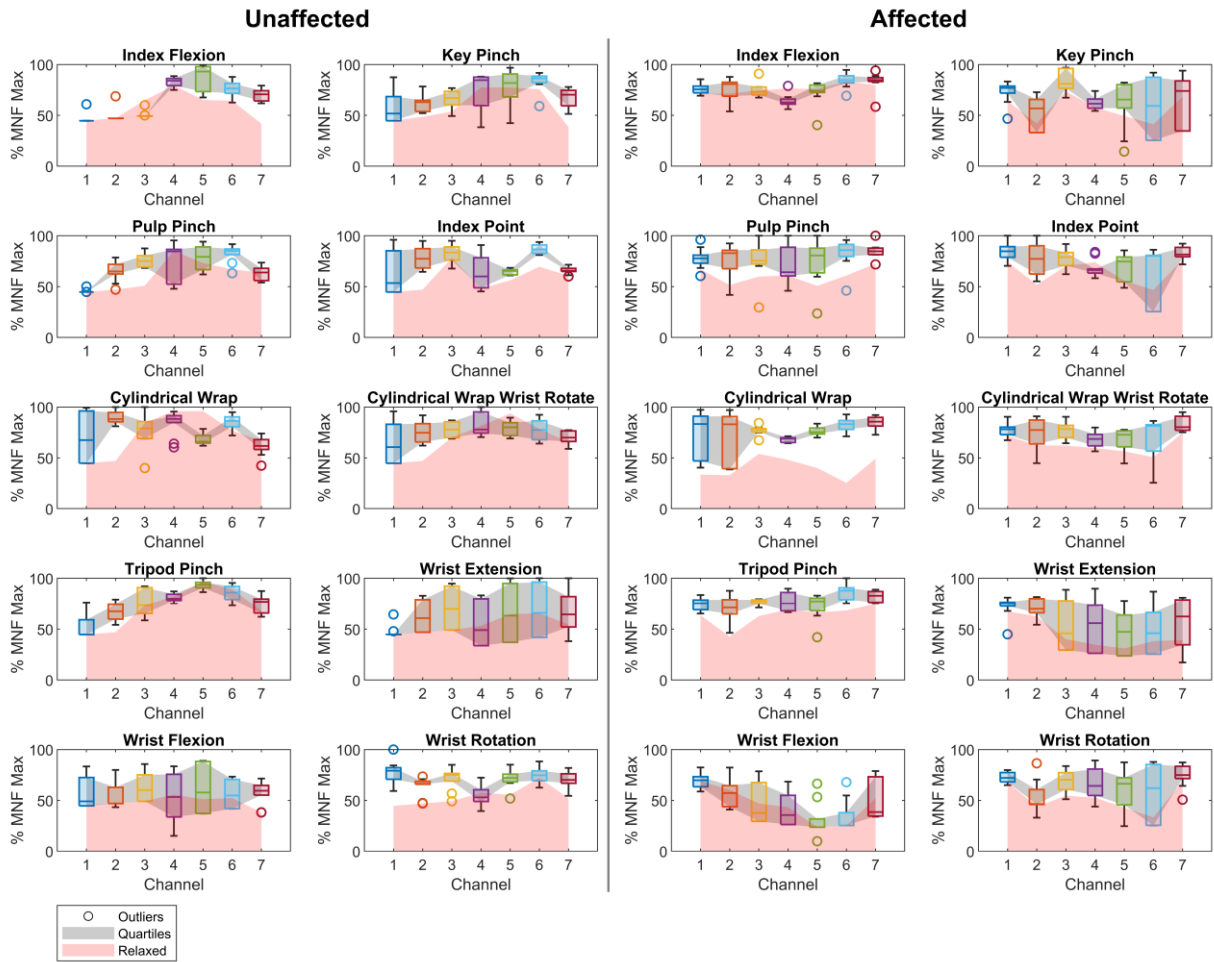


Figure B-4. The box and whisker plots provide a visualization of the MNF muscle excitation patterns and relaxed states seen for the various hand movements across the unaffected and affected limbs for participant SHR-B.

# Participant: SHR-C

## SHR-C: Normalized RMS across channels and movements

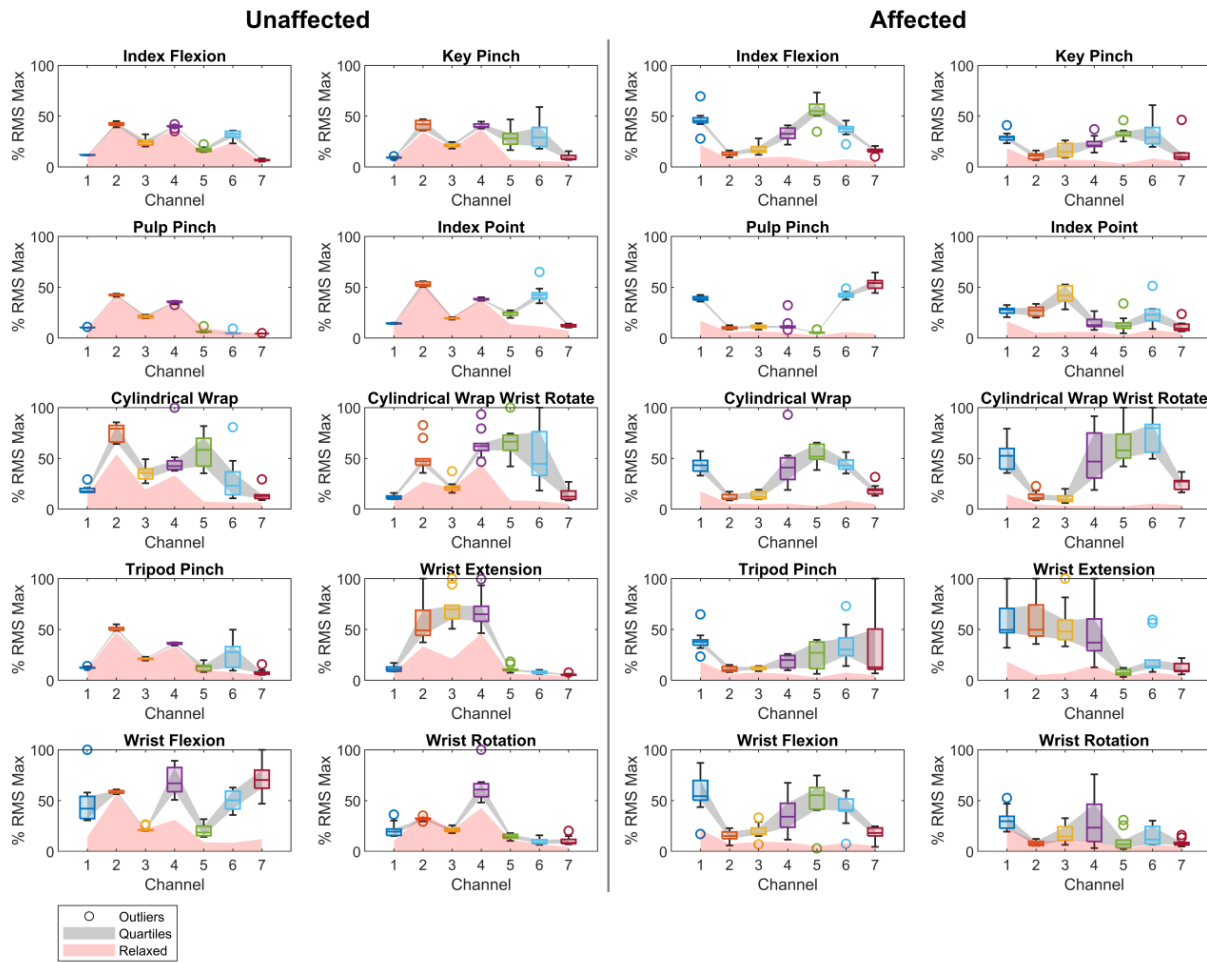


Figure B-5. The box and whisker plots provide a visualization of the RMS muscle excitation patterns and relaxed states seen for the various hand movements across the unaffected and affected limbs for participant SHR-C.

SHR-C: Normalized MNF across channels and movements

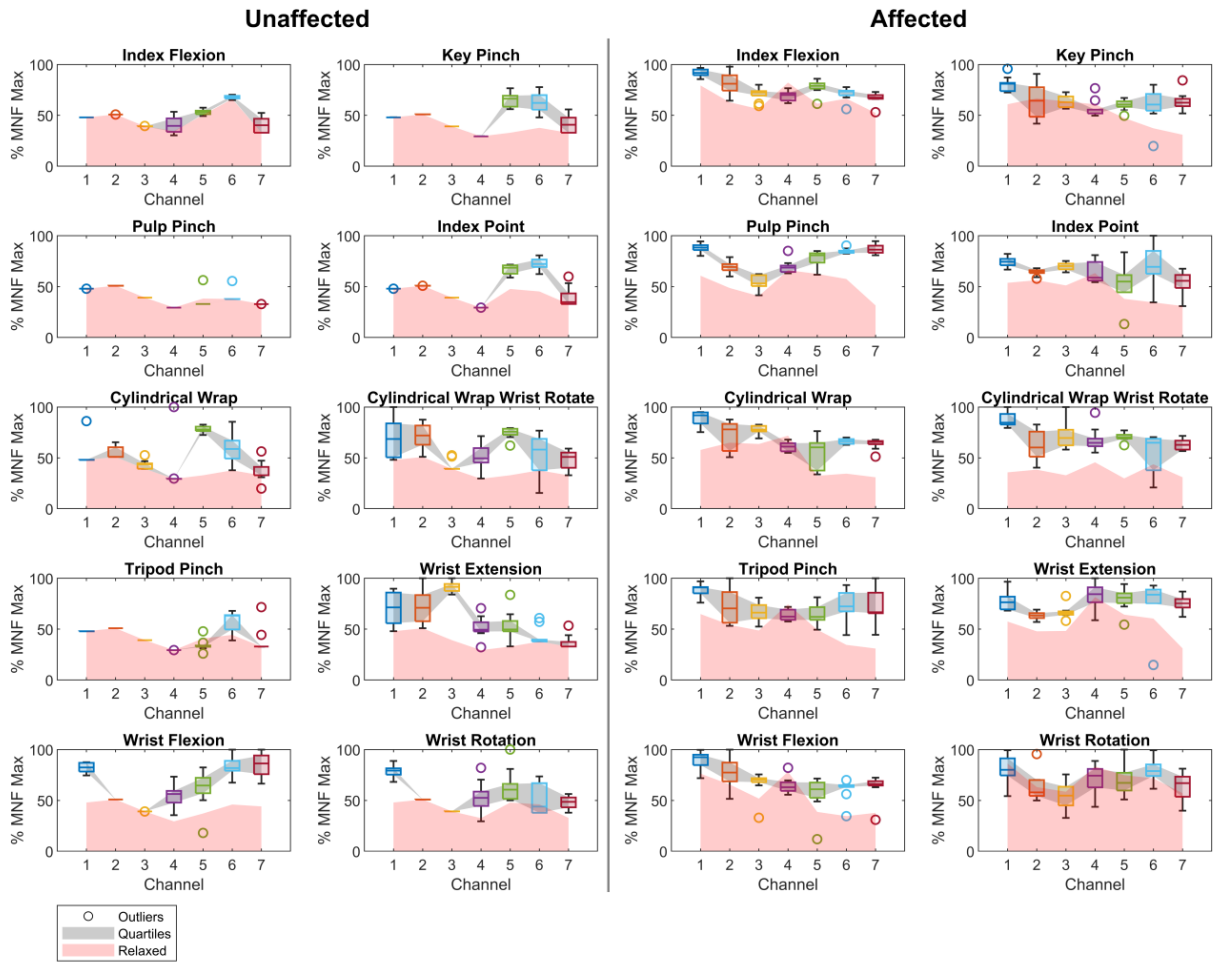


Figure B-6. The box and whisker plots provide a visualization of the MNF muscle excitation patterns and relaxed states seen for the various hand movements across the unaffected and affected limbs for participant SHR-C.



# Participant: SHR-D

## SHR-D: Normalized RMS across channels and movements

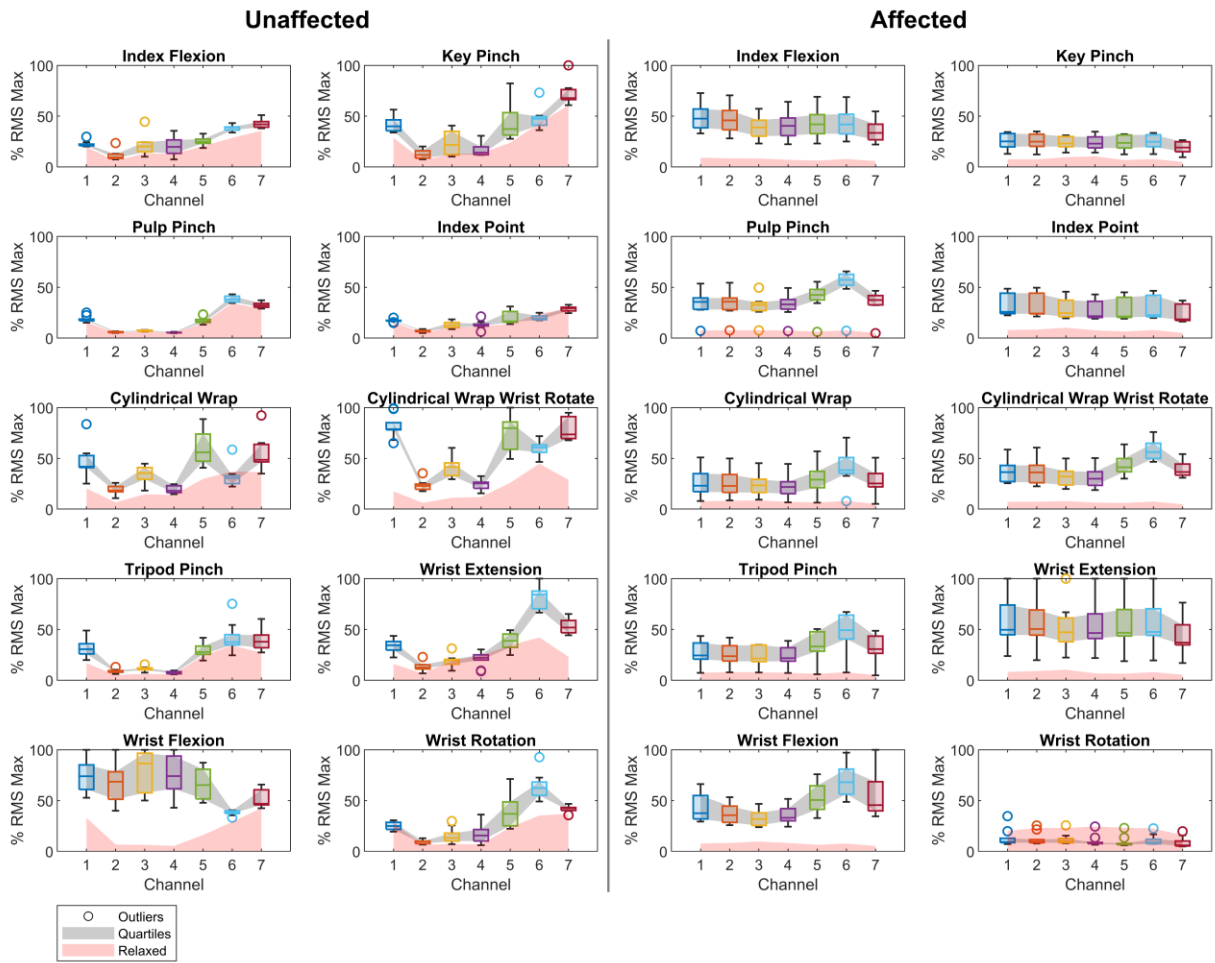


Figure B-7. The box and whisker plots provide a visualization of the RMS muscle excitation patterns and relaxed states seen for the various hand movements across the unaffected and affected limbs for participant SHR-D.

SHR-D: Normalized MNF across channels and movements

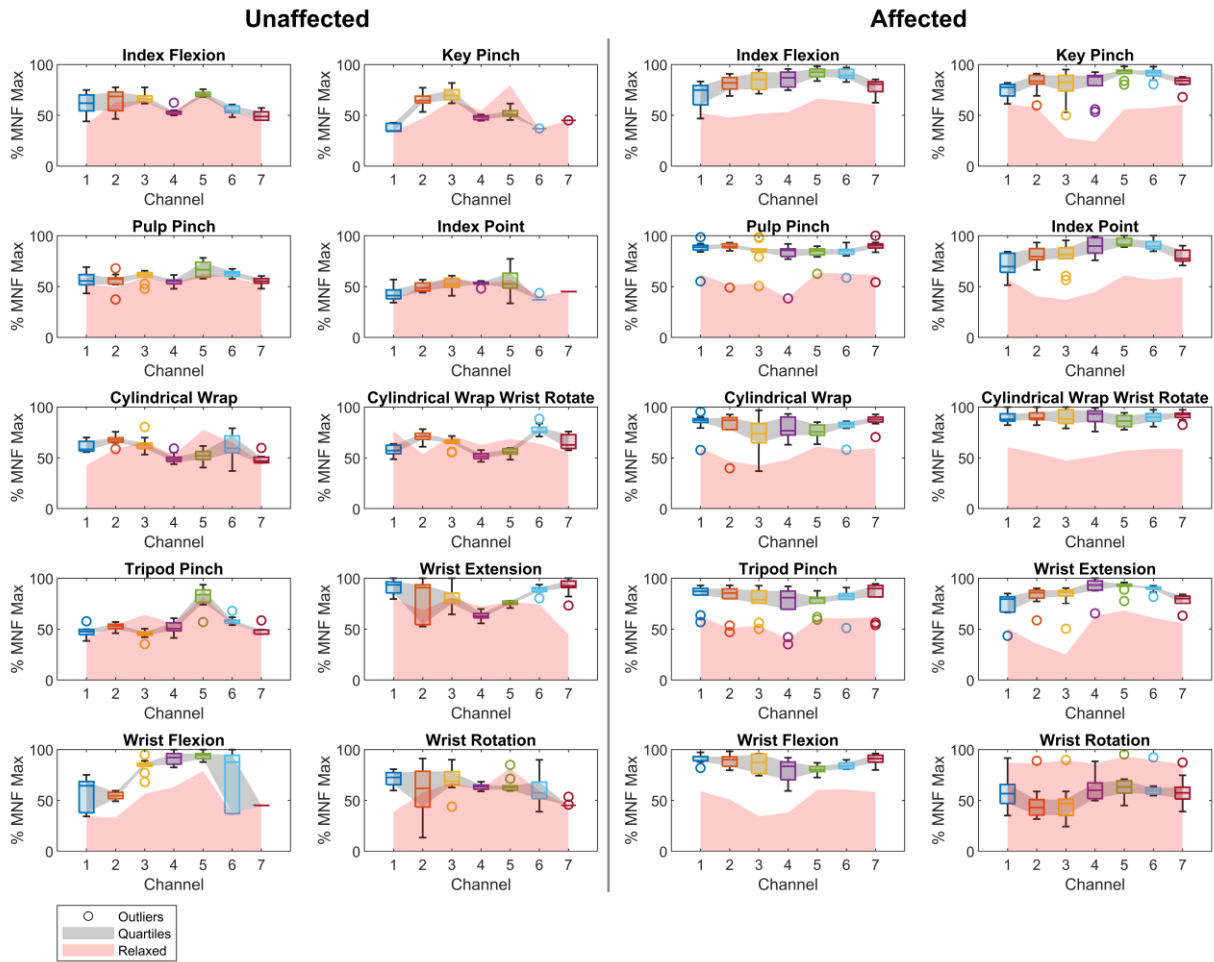


Figure B-8. The box and whisker plots provide a visualization of the MNF muscle excitation patterns and relaxed states seen for the various hand movements across the unaffected and affected limbs for participant SHR-D.

# Participant: SHR-E

## SHR-E: Normalized RMS across channels and movements

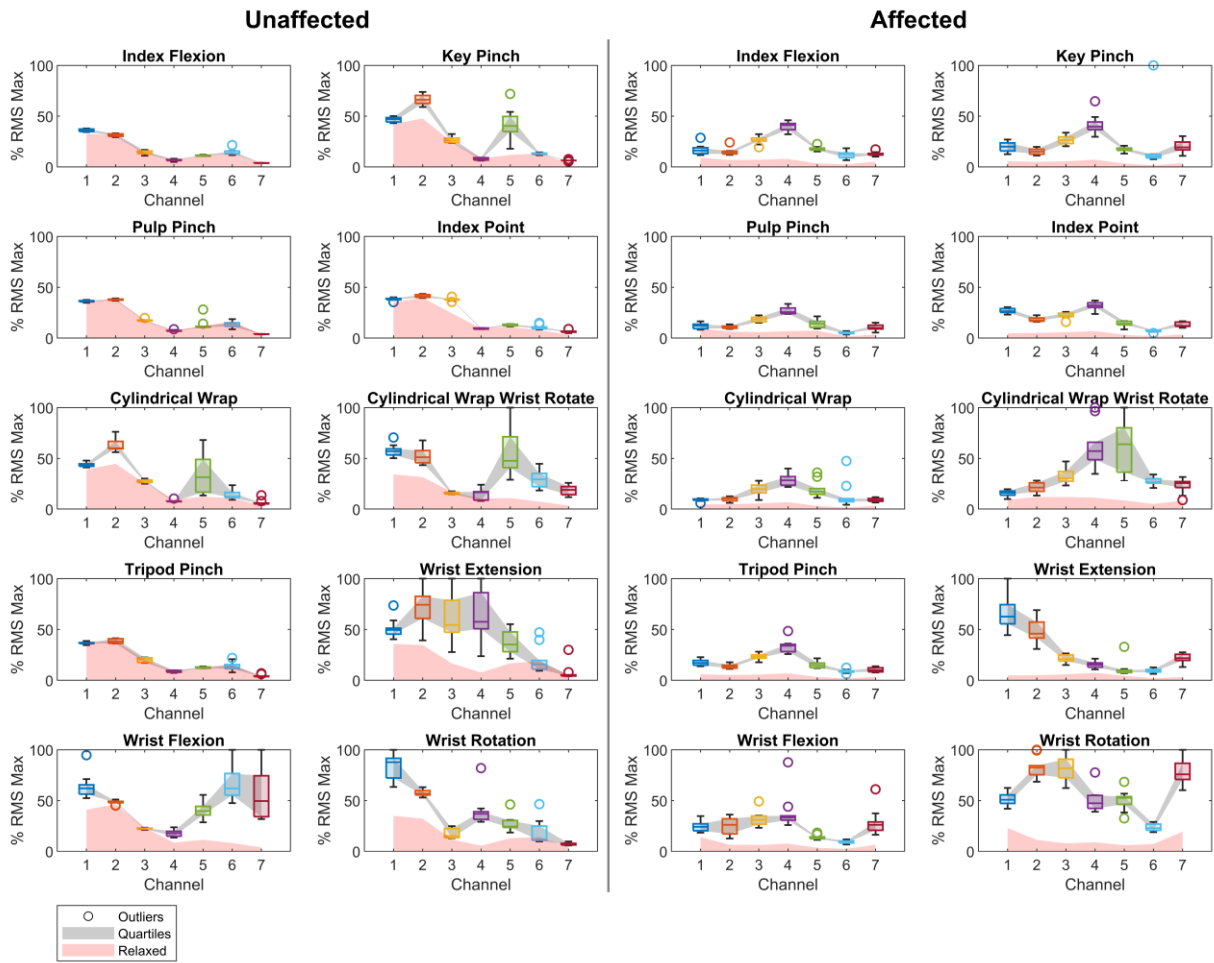


Figure B-9. The box and whisker plots provide a visualization of the RMS muscle excitation patterns and relaxed states seen for the various hand movements across the unaffected and affected limbs for participant SHR-E.

SHR-E: Normalized MNF across channels and movements

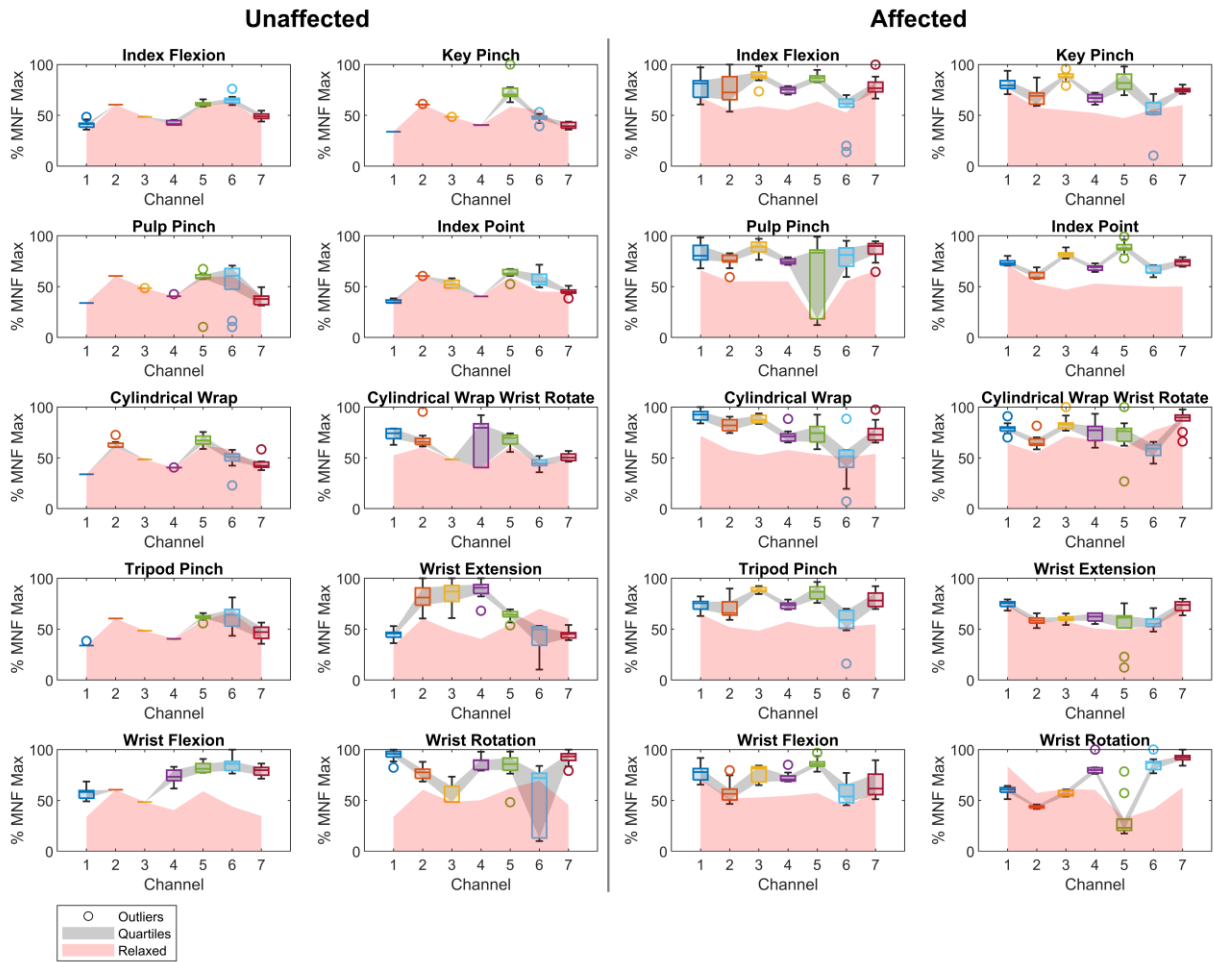


Figure B-10. The box and whisker plots provide a visualization of the MNF muscle excitation patterns and relaxed states seen for the various hand movements across the unaffected and affected limbs for participant SHR-E.

**Participant: SHR-F**

**SHR-F: Normalized RMS across channels and movements**

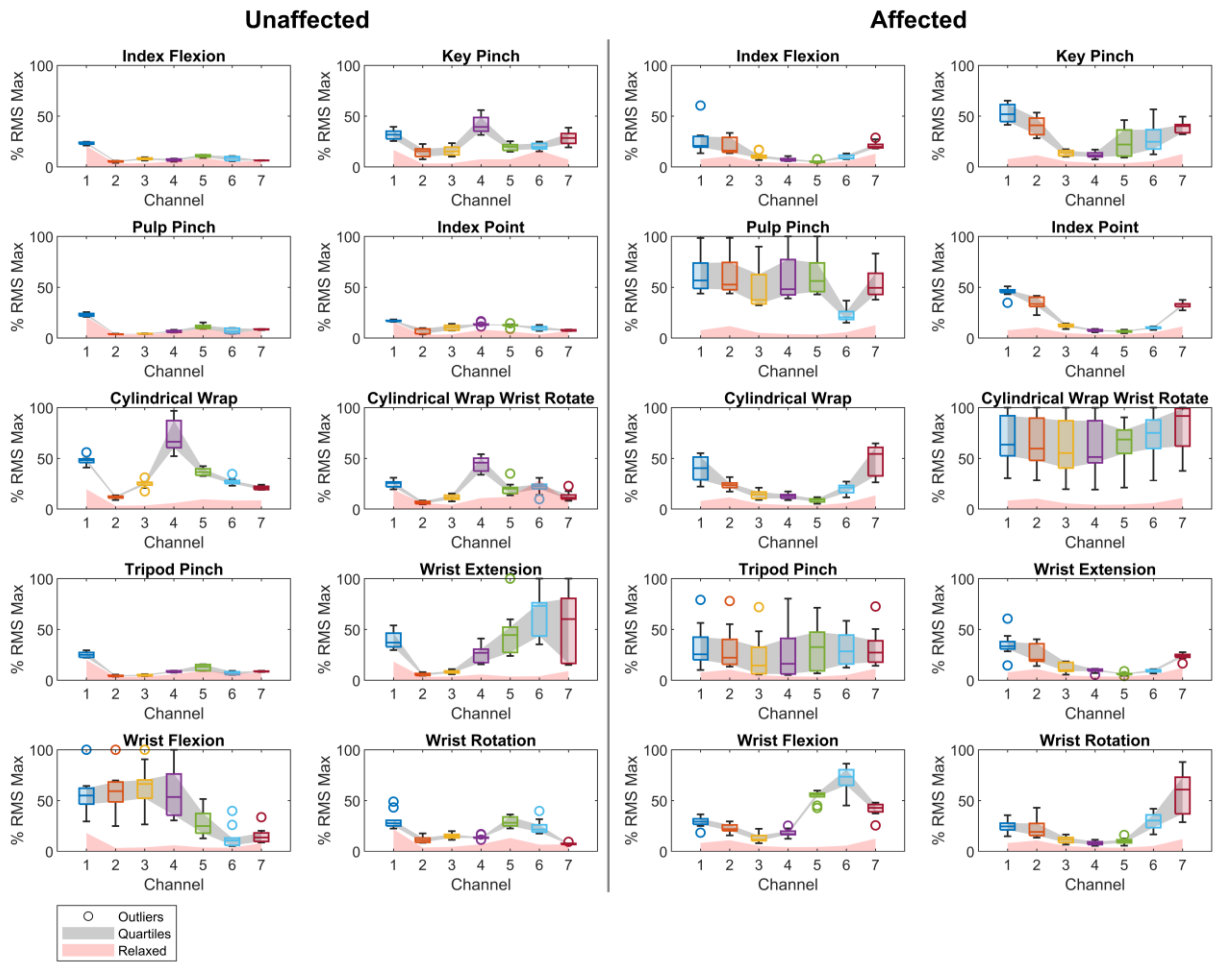


Figure B-11. The box and whisker plots provide a visualization of the RMS muscle excitation patterns and relaxed states seen for the various hand movements across the unaffected and affected limbs for participant SHR-F.

SHR-F: Normalized MNF across channels and movements

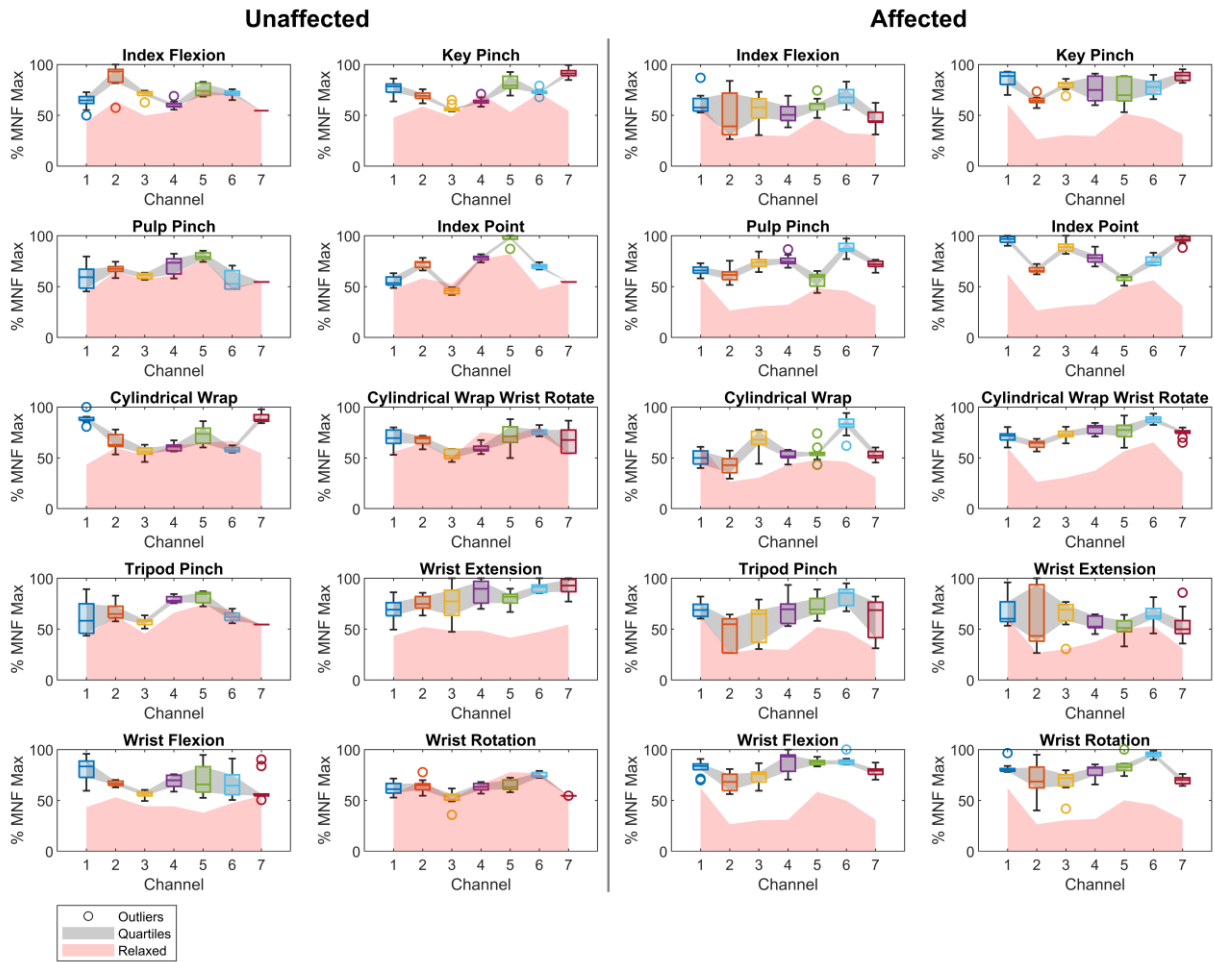


Figure B-12. The box and whisker plots provide a visualization of the MNF muscle excitation patterns and relaxed states seen for the various hand movements across the unaffected and affected limbs for participant SHR-F.

# Participant: SHR-G

## SHR-G: Normalized RMS across channels and movements

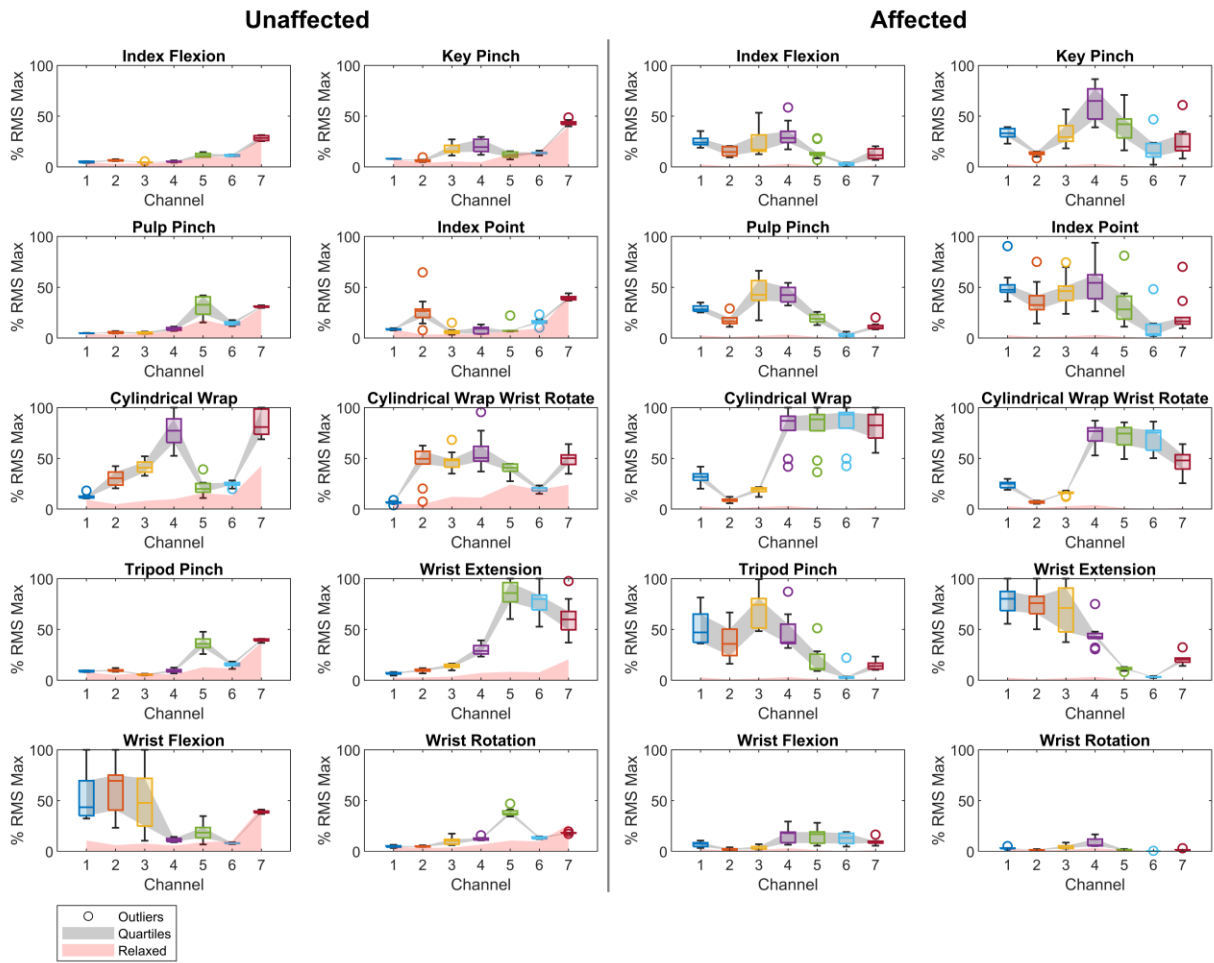


Figure B-13. The box and whisker plots provide a visualization of the RMS muscle excitation patterns and relaxed states seen for the various hand movements across the unaffected and affected limbs for participant SHR-G.

SHR-G: Normalized MNF across channels and movements

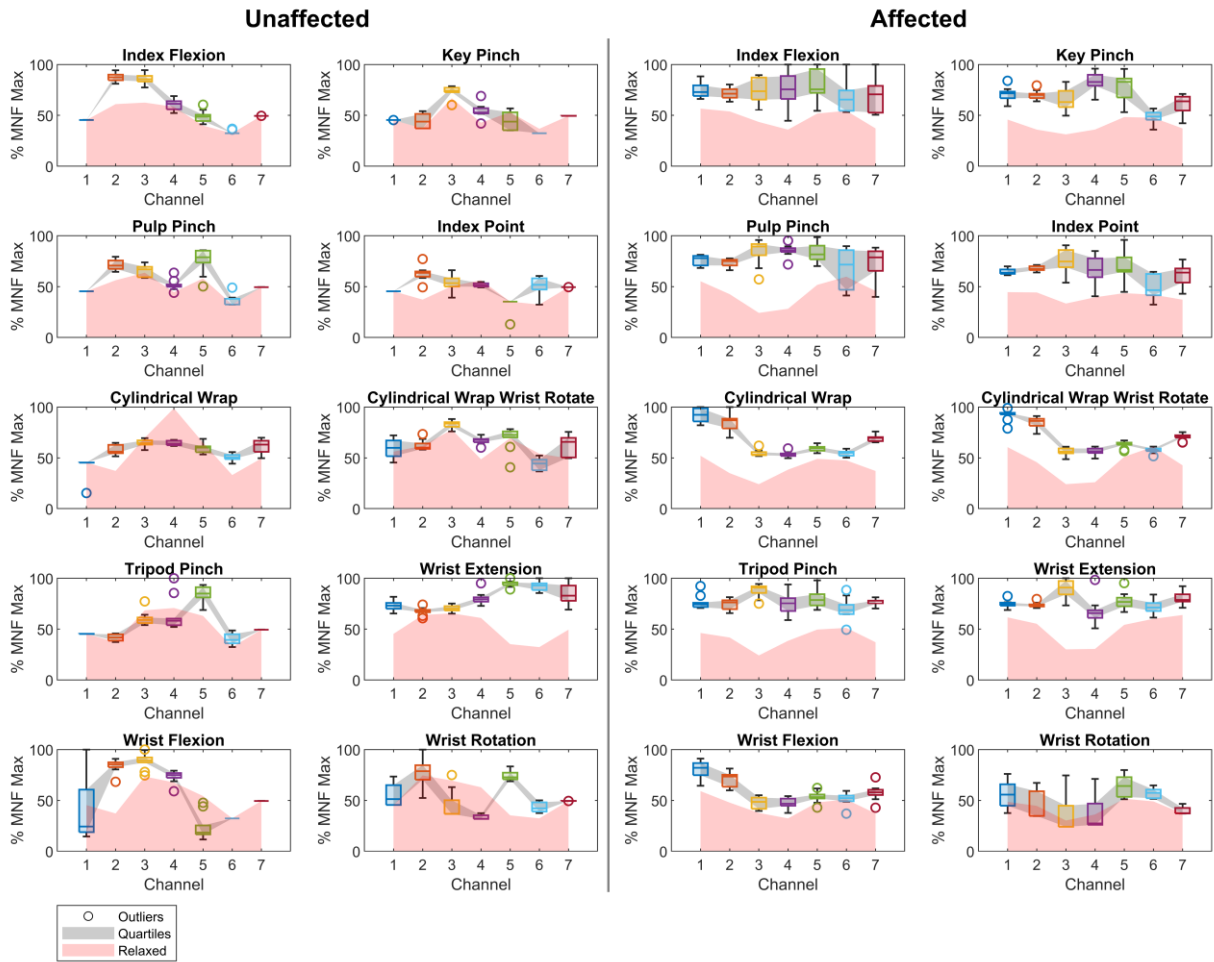


Figure B-14. The box and whisker plots provide a visualization of the MNF muscle excitation patterns and relaxed states seen for the various hand movements across the unaffected and affected limbs for participant SHR-G.



# Participant: SHR-H

## SHR-H: Normalized RMS across channels and movements

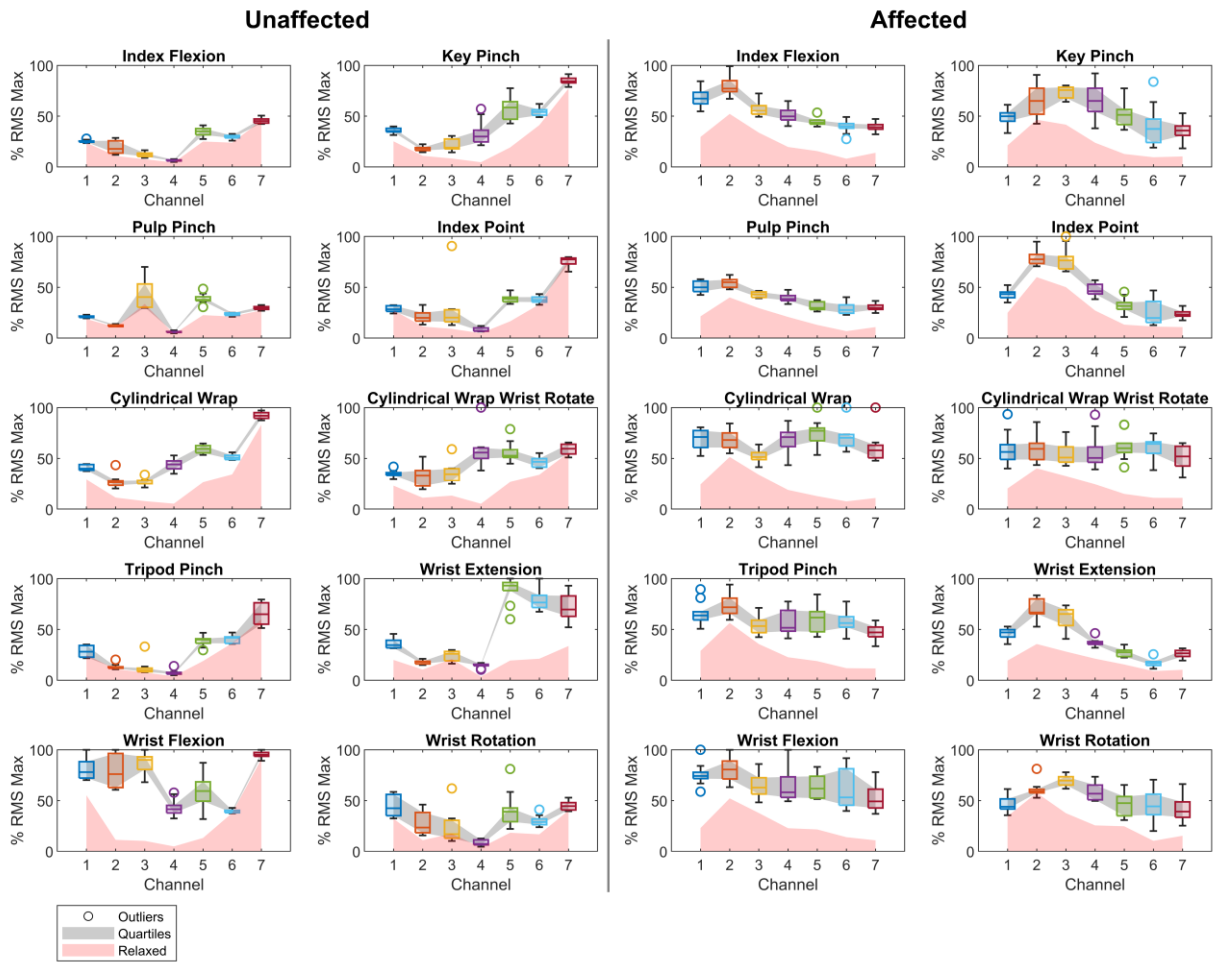


Figure B-15. The box and whisker plots provide a visualization of the RMS muscle excitation patterns and relaxed states seen for the various hand movements across the unaffected and affected limbs for participant SHR-H.

SHR-H: Normalized MNF across channels and movements

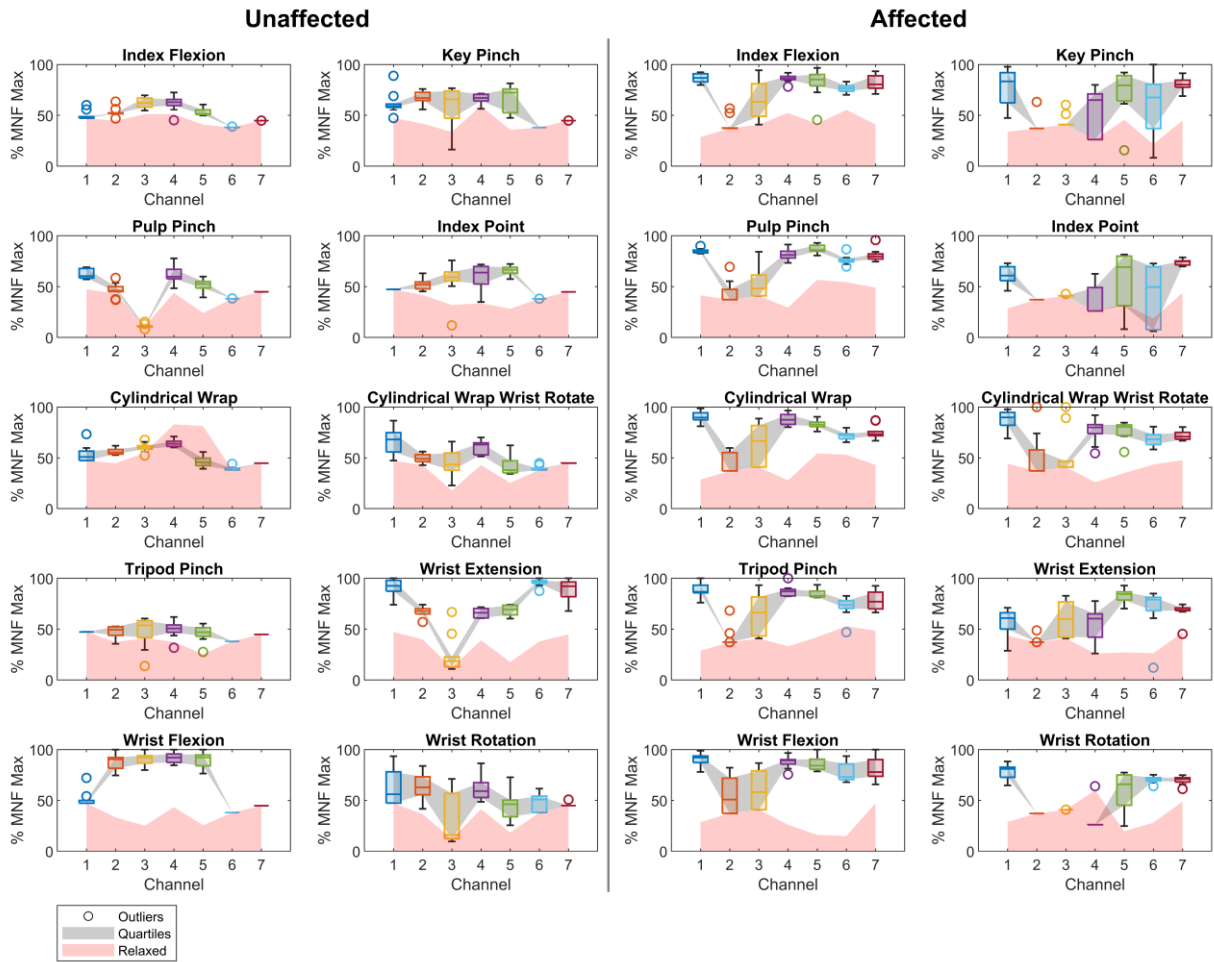


Figure B-16. The box and whisker plots provide a visualization of the MNF muscle excitation patterns and relaxed states seen for the various hand movements across the unaffected and affected limbs for participant SHR-H.

# Participant: SHR-I

## SHR-I: Normalized RMS across channels and movements

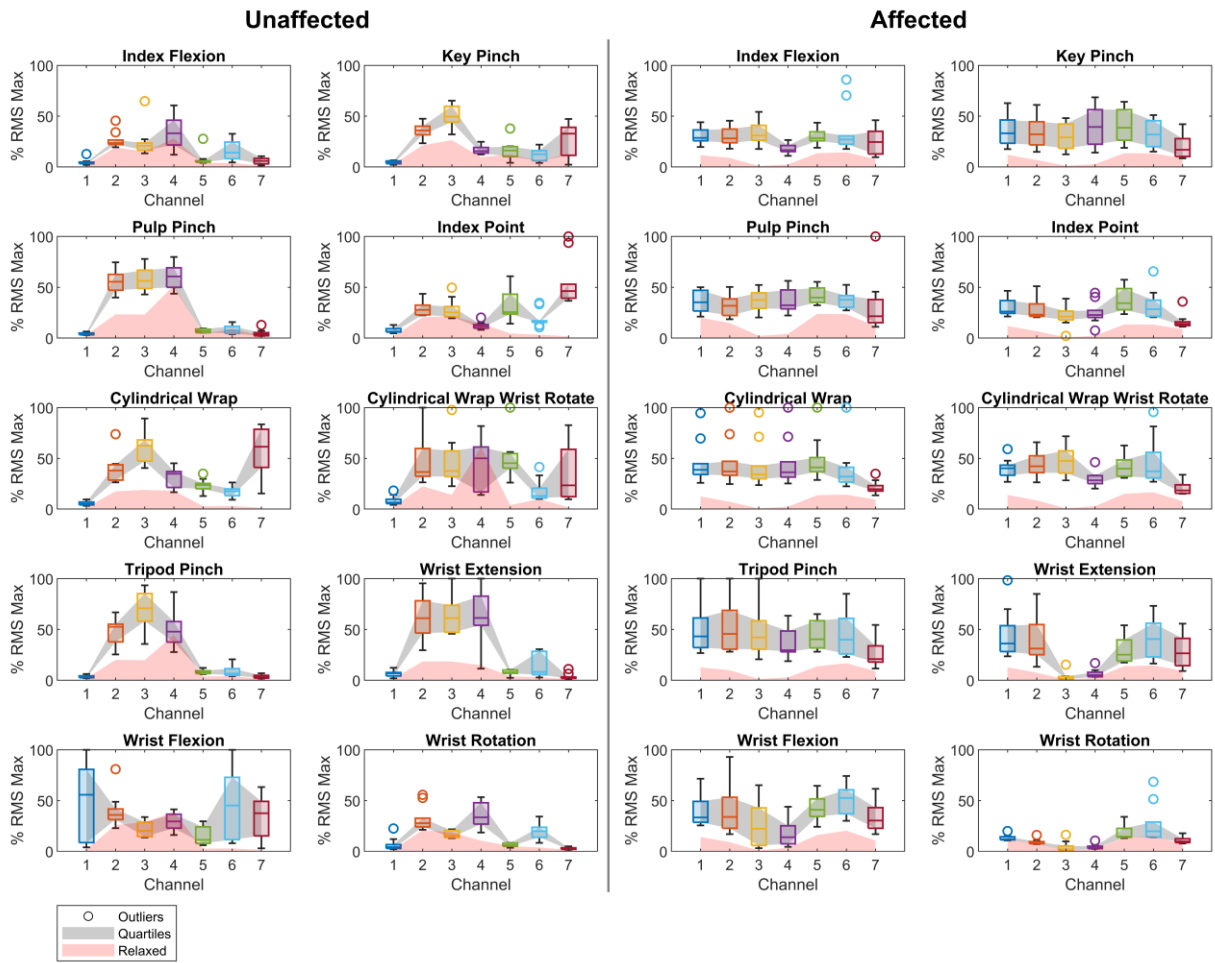


Figure B-17. The box and whisker plots provide a visualization of the RMS muscle excitation patterns and relaxed states seen for the various hand movements across the unaffected and affected limbs for participant SHR-I.

SHR-I: Normalized MNF across channels and movements

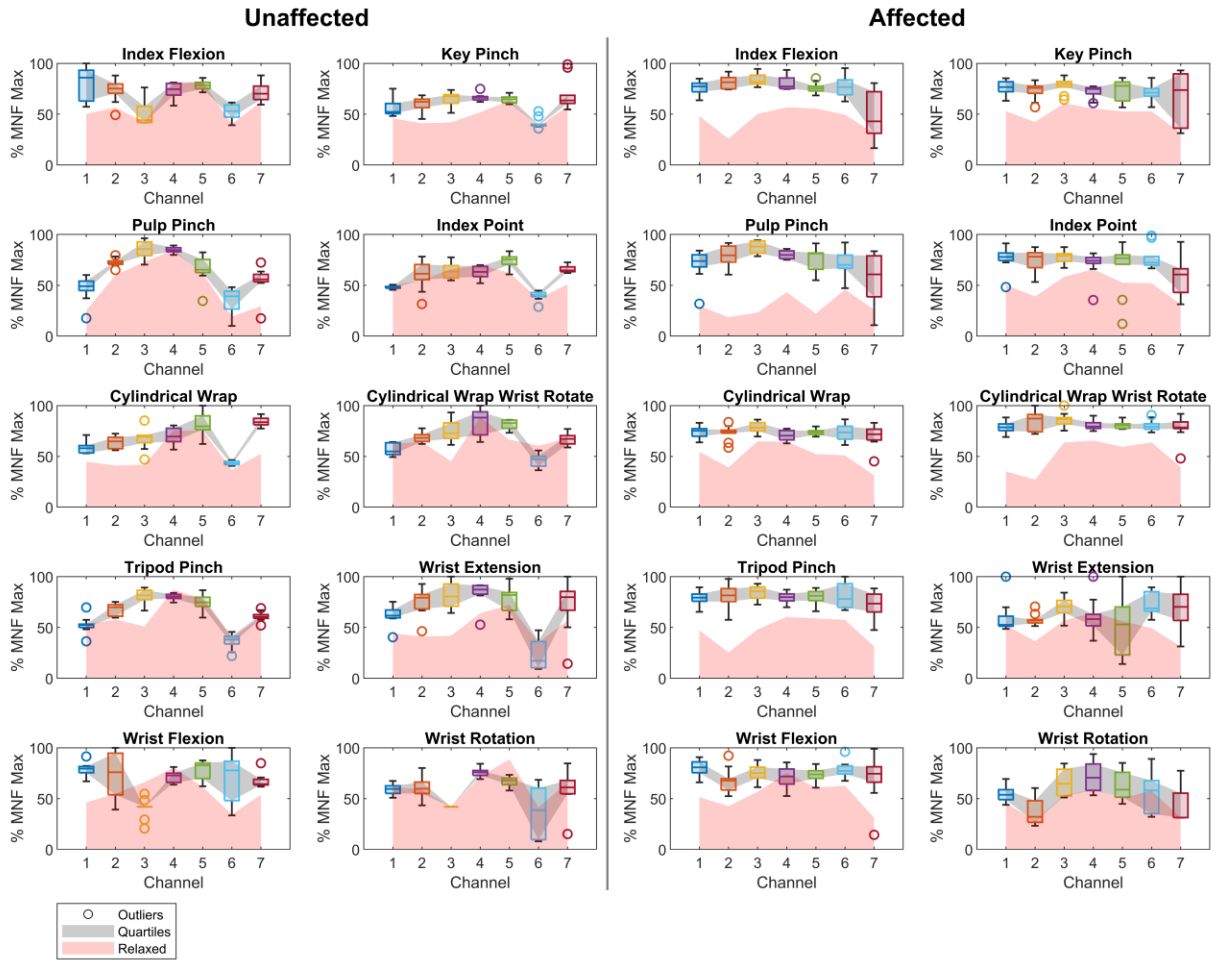


Figure B-18. The box and whisker plots provide a visualization of the MNF muscle excitation patterns and relaxed states seen for the various hand movements across the unaffected and affected limbs for participant SHR-I.

# Multidimensional scaling and representational dissimilarity matrices

Participant: SHR-A

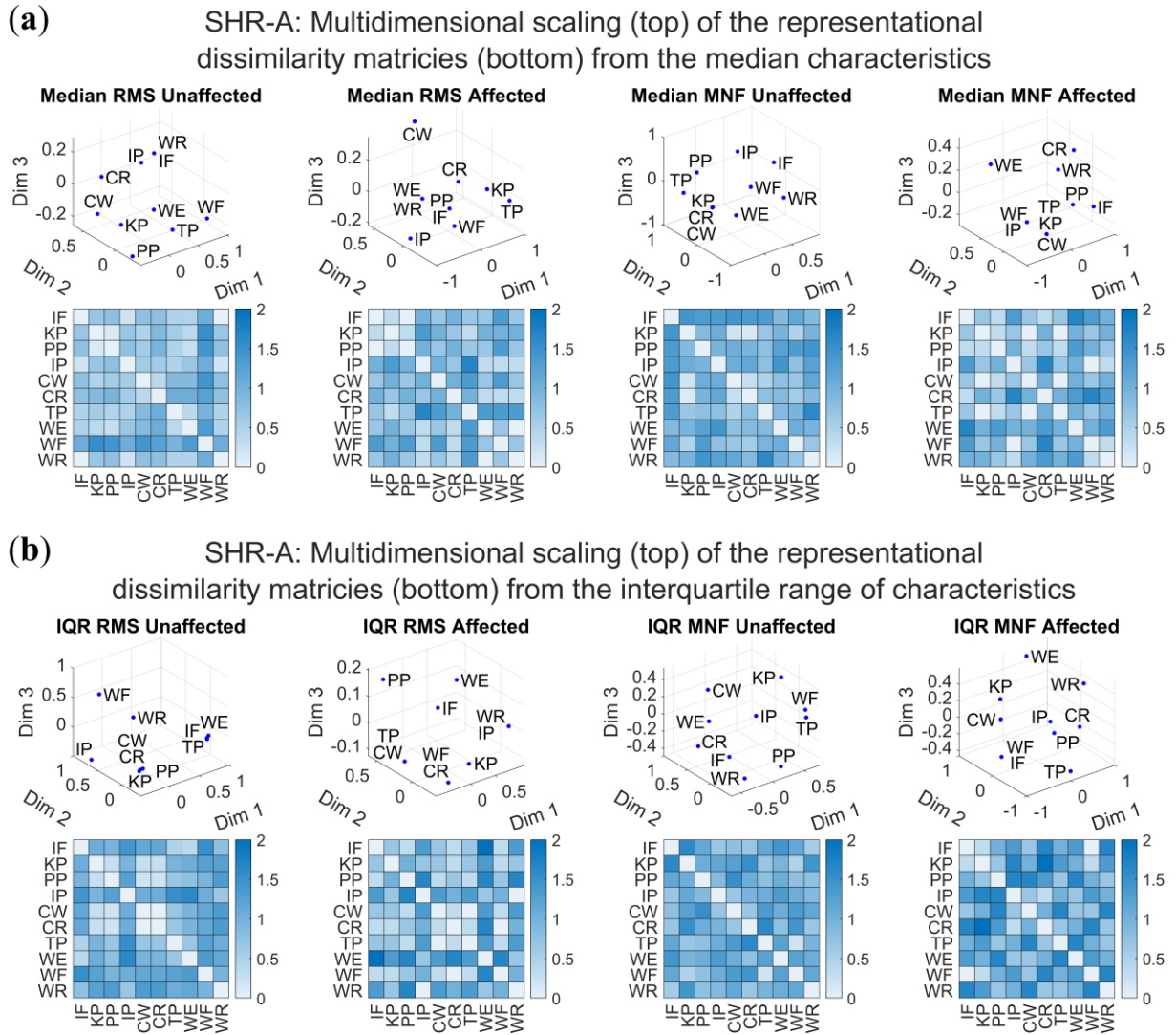
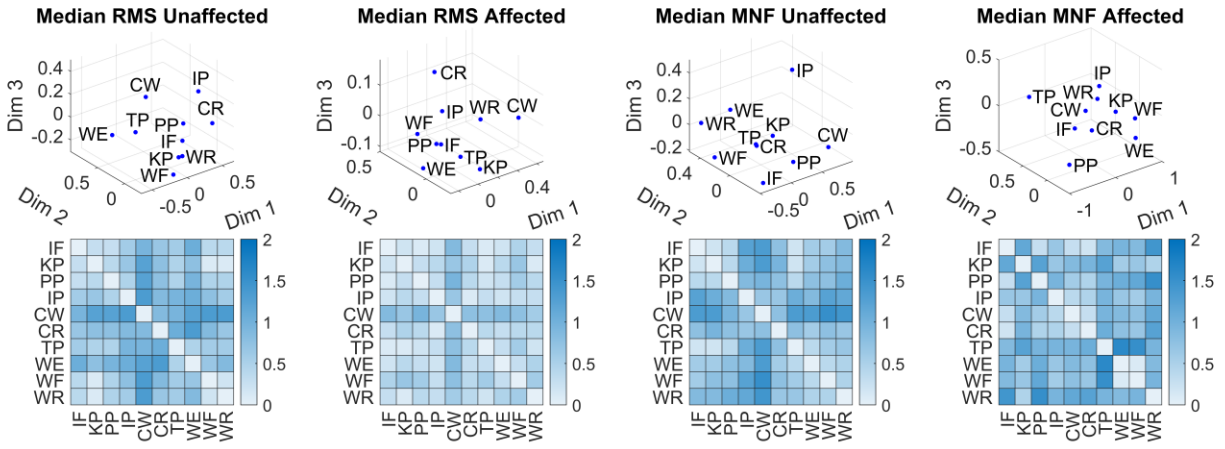


Figure B-19. Visual representation of the correlation distances between hand movements for the amplitude and spread of measurement characteristics of SHR-A. The multidimensional scaling plots are provided in three dimensions corresponding to the representational dissimilarity matrices for (a) the median RMS and MNF characteristics and (b) the RMS and MNF interquartile range (IQR).

**Participant: SHR-B**

**(a)** SHR-B: Multidimensional scaling (top) of the representational dissimilarity matrices (bottom) from the median characteristics



**(b)** SHR-B: Multidimensional scaling (top) of the representational dissimilarity matrices (bottom) from the interquartile range of characteristics

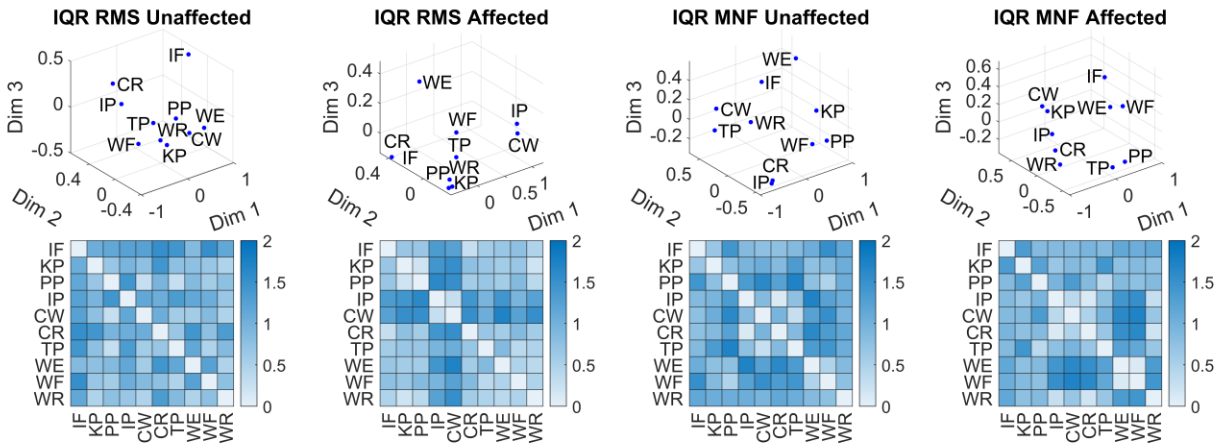
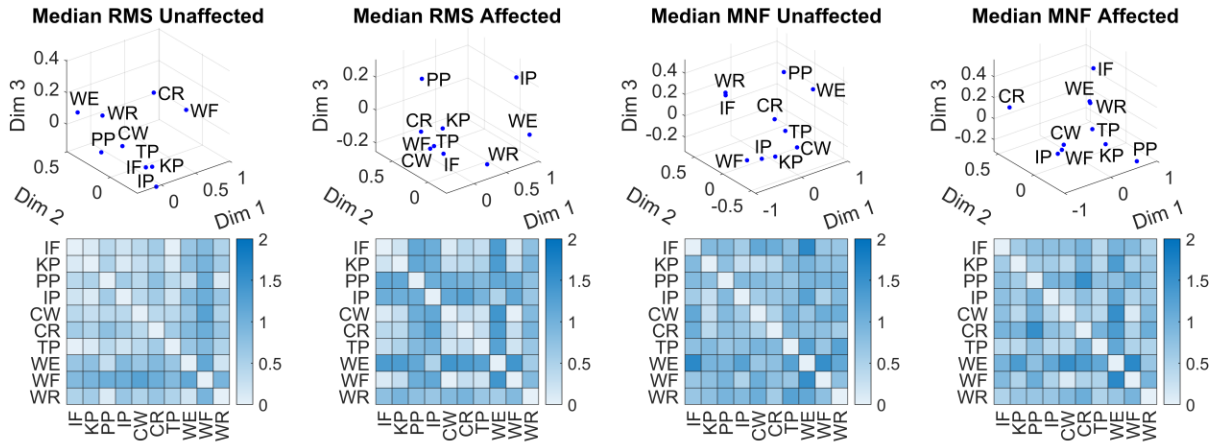


Figure B-20. Visual representation of the correlation distances between hand movements for the amplitude and spread of measurement characteristics of SHR-B. The multidimensional scaling plots are provided in three dimensions corresponding to the representational dissimilarity matrices for **(a)** the median RMS and MNF characteristics and **(b)** the RMS and MNF interquartile range (IQR).

**Participant: SHR-C**

**(a)** SHR-C: Multidimensional scaling (top) of the representational dissimilarity matrices (bottom) from the median characteristics



**(b)** SHR-C: Multidimensional scaling (top) of the representational dissimilarity matrices (bottom) from the interquartile range of characteristics

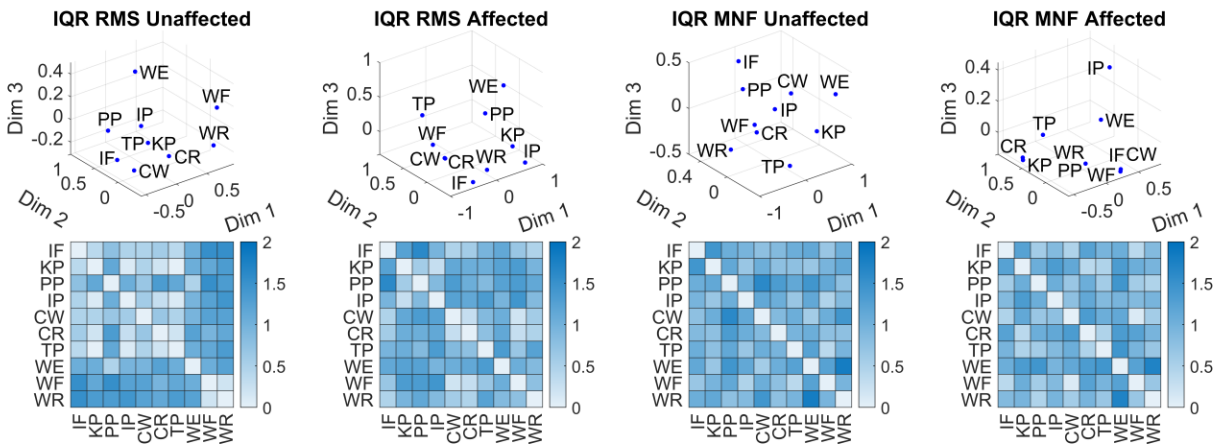
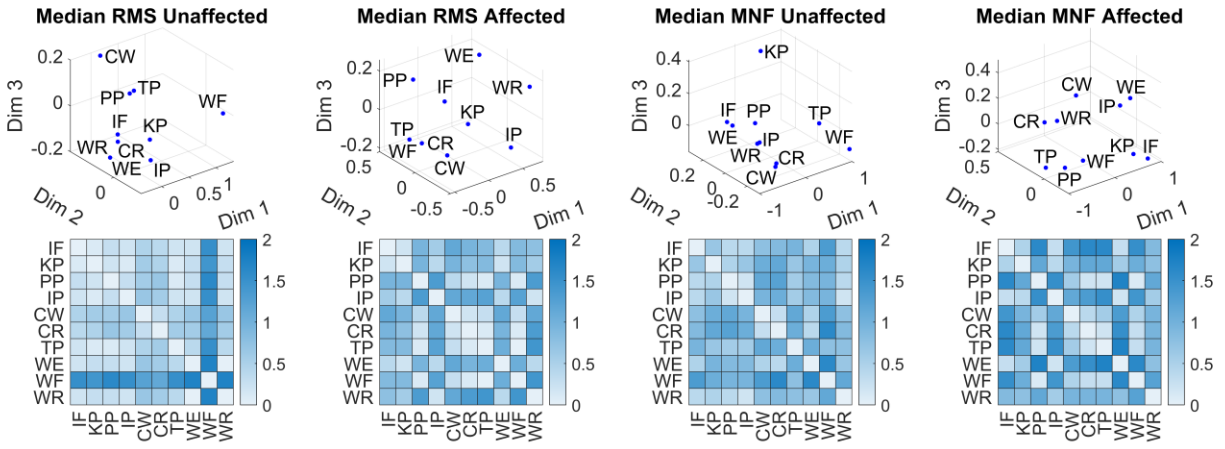


Figure B-21. Visual representation of the correlation distances between hand movements for the amplitude and spread of measurement characteristics of SHR-C. The multidimensional scaling plots are provided in three dimensions corresponding to the representational dissimilarity matrices for **(a)** the median RMS and MNF characteristics and **(b)** the RMS and MNF interquartile range (IQR).

**Participant: SHR-D**

**(a)** SHR-D: Multidimensional scaling (top) of the representational dissimilarity matrices (bottom) from the median characteristics



**(b)** SHR-D: Multidimensional scaling (top) of the representational dissimilarity matrices (bottom) from the interquartile range of characteristics

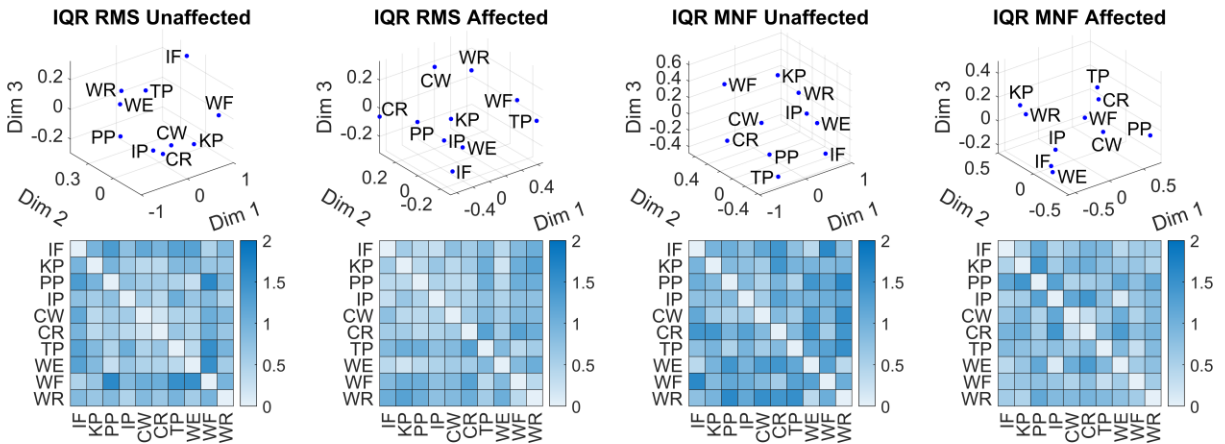
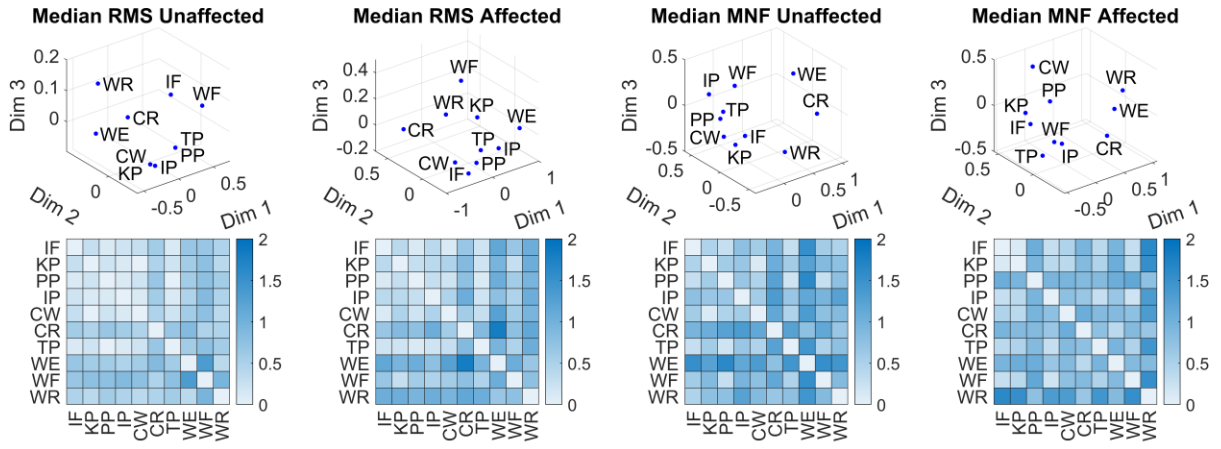


Figure B-22. Visual representation of the correlation distances between hand movements for the amplitude and spread of measurement characteristics of SHR-D. The multidimensional scaling plots are provided in three dimensions corresponding to the representational dissimilarity matrices for **(a)** the median RMS and MNF characteristics and **(b)** the RMS and MNF interquartile range (IQR).



**Participant: SHR-E**

**(a)** SHR-E: Multidimensional scaling (top) of the representational dissimilarity matrices (bottom) from the median characteristics



**(b)** SHR-E: Multidimensional scaling (top) of the representational dissimilarity matrices (bottom) from the interquartile range of characteristics

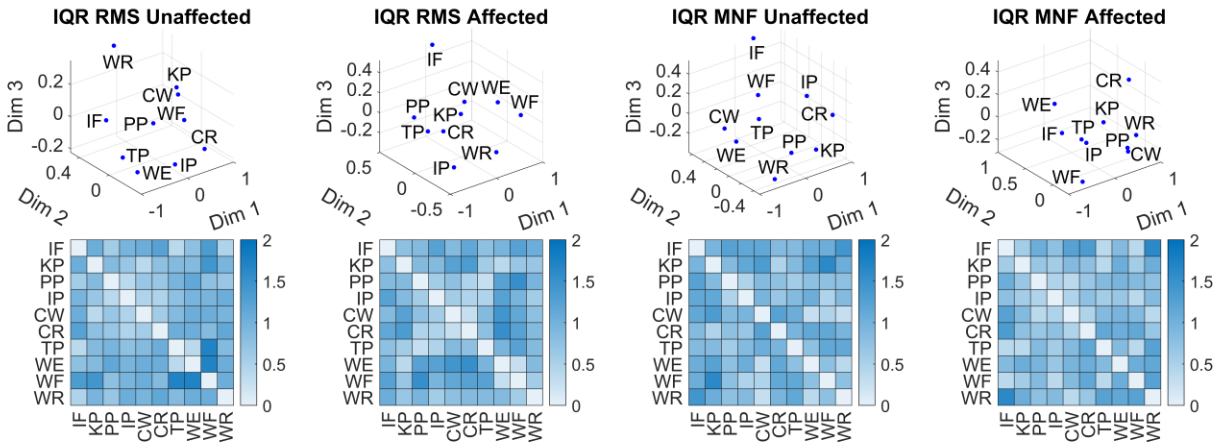
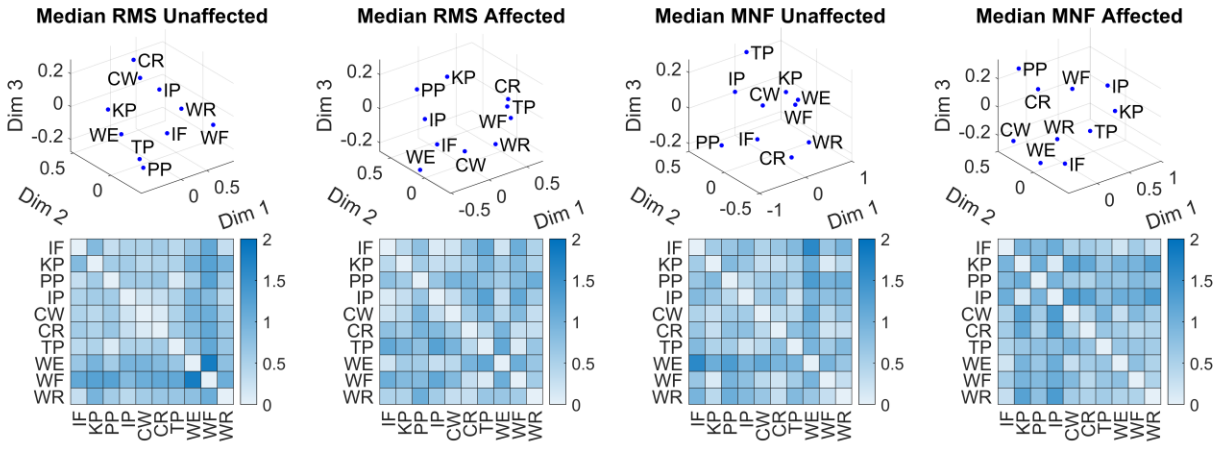


Figure B-23. Visual representation of the correlation distances between hand movements for the amplitude and spread of measurement characteristics of SHR-E. The multidimensional scaling plots are provided in three dimensions corresponding to the representational dissimilarity matrices for **(a)** the median RMS and MNF characteristics and **(b)** the RMS and MNF interquartile range (IQR).

**Participant: SHR-F**

**(a)** SHR-F: Multidimensional scaling (top) of the representational dissimilarity matrices (bottom) from the median characteristics



**(b)** SHR-F: Multidimensional scaling (top) of the representational dissimilarity matrices (bottom) from the interquartile range of characteristics

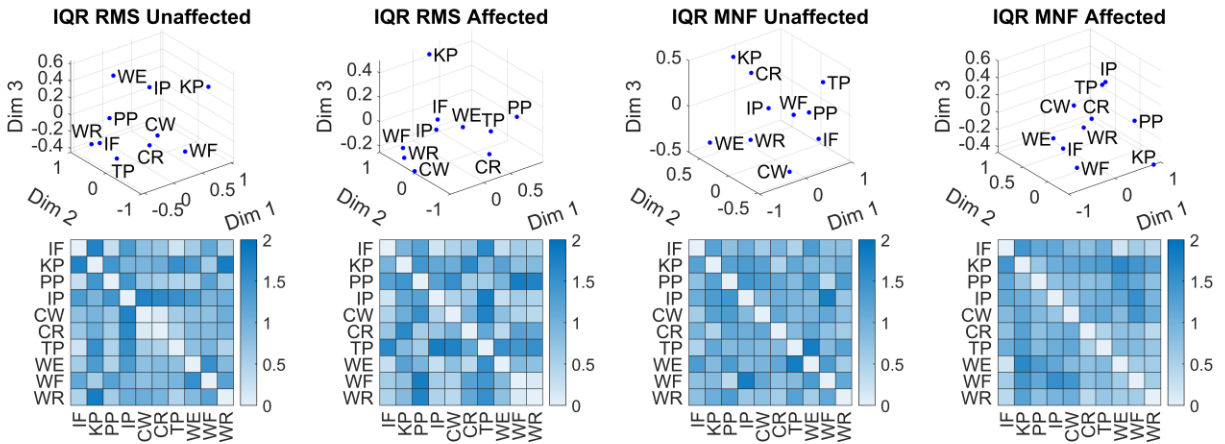
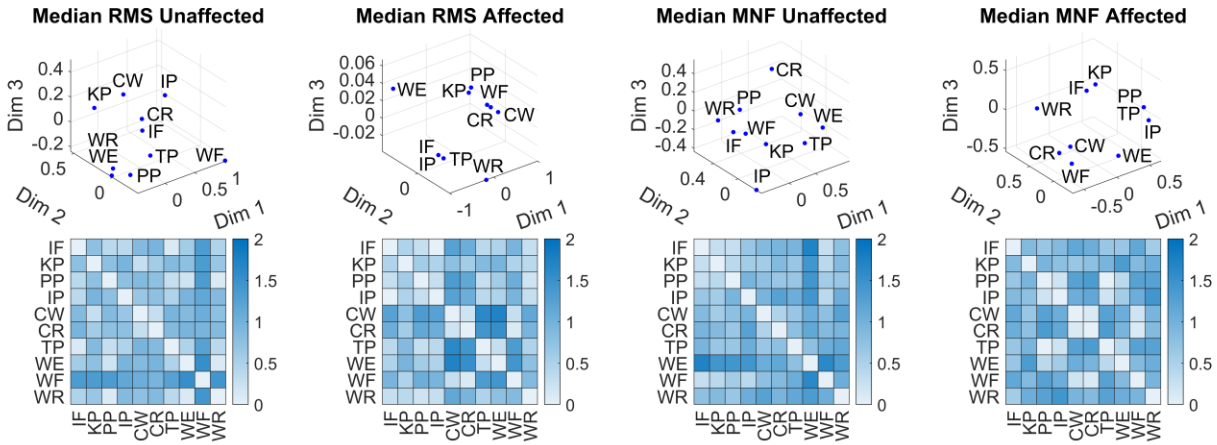


Figure B-24. Visual representation of the correlation distances between hand movements for the amplitude and spread of measurement characteristics of SHR-F. The multidimensional scaling plots are provided in three dimensions corresponding to the representational dissimilarity matrices for **(a)** the median RMS and MNF characteristics and **(b)** the RMS and MNF interquartile range (IQR).

**Participant: SHR-G**

**(a)** SHR-G: Multidimensional scaling (top) of the representational dissimilarity matrices (bottom) from the median characteristics



**(b)** SHR-G: Multidimensional scaling (top) of the representational dissimilarity matrices (bottom) from the interquartile range of characteristics

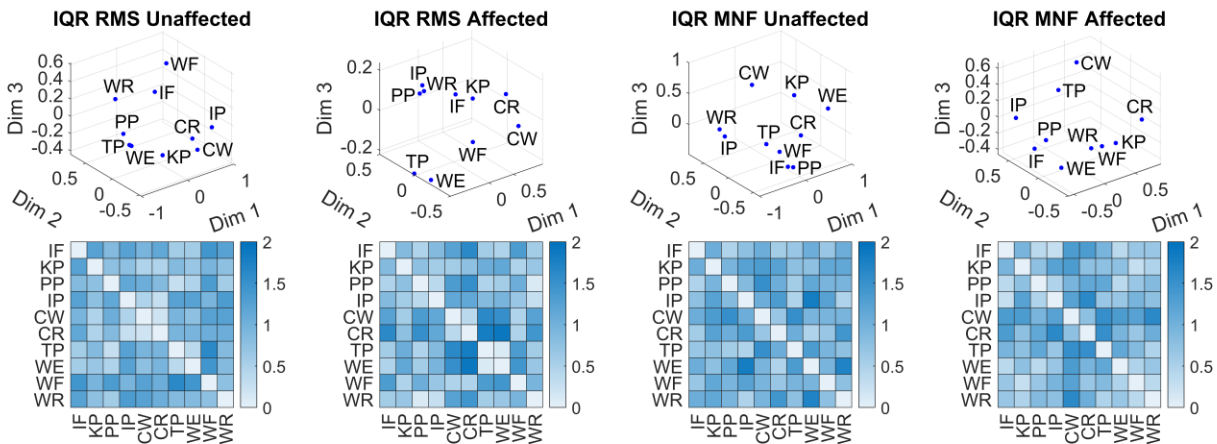
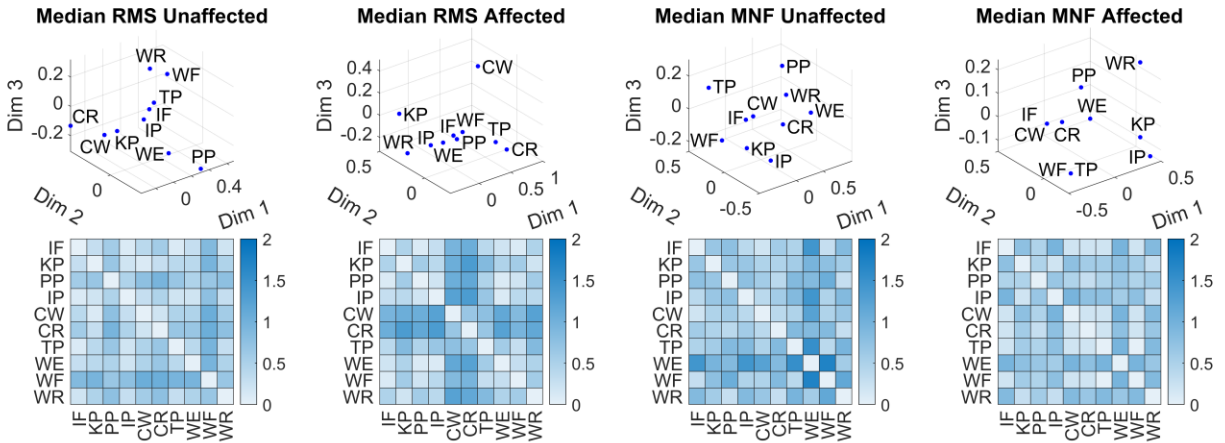


Figure B-25. Visual representation of the correlation distances between hand movements for the amplitude and spread of measurement characteristics of SHR-G. The multidimensional scaling plots are provided in three dimensions corresponding to the representational dissimilarity matrices for **(a)** the median RMS and MNF characteristics and **(b)** the RMS and MNF interquartile range (IQR).

**Participant: SHR-H**

**(a)** SHR-H: Multidimensional scaling (top) of the representational dissimilarity matrices (bottom) from the median characteristics



**(b)** SHR-H: Multidimensional scaling (top) of the representational dissimilarity matrices (bottom) from the interquartile range of characteristics

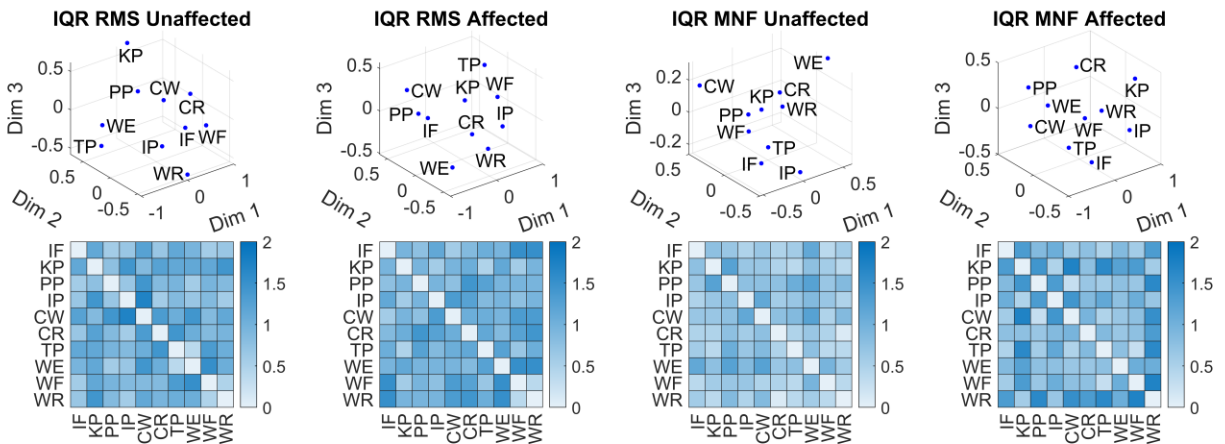
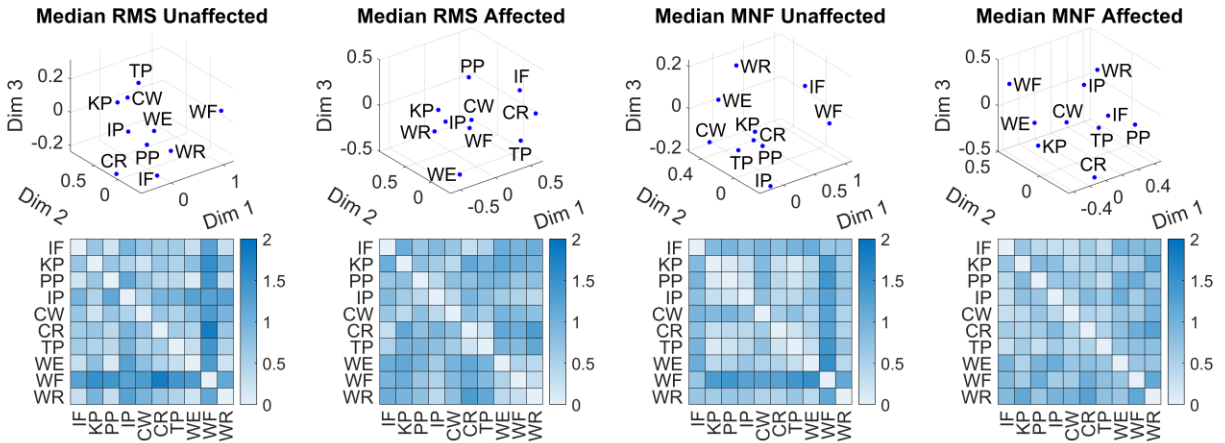


Figure B-26. Visual representation of the correlation distances between hand movements for the amplitude and spread of measurement characteristics of SHR-H. The multidimensional scaling plots are provided in three dimensions corresponding to the representational dissimilarity matrices for **(a)** the median RMS and MNF characteristics and **(b)** the RMS and MNF interquartile range (IQR).

**Participant: SHR-I**

**(a)** SHR-I: Multidimensional scaling (top) of the representational dissimilarity matrices (bottom) from the median characteristics



**(b)** SHR-I: Multidimensional scaling (top) of the representational dissimilarity matrices (bottom) from the interquartile range of characteristics

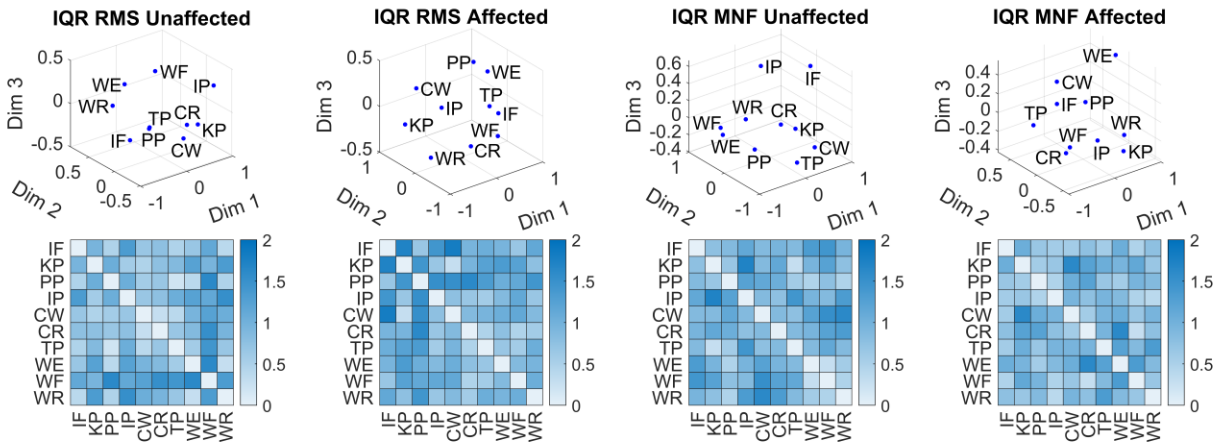


Figure B-27. Visual representation of the correlation distances between hand movements for the amplitude and spread of measurement characteristics of SHR-I. The multidimensional scaling plots are provided in three dimensions corresponding to the representational dissimilarity matrices for **(a)** the median RMS and MNF characteristics and **(b)** the RMS and MNF interquartile range (IQR).

## Appendix C: Classification tables and analysis

### Individual feature performance accuracy

**Participant: SHR-A**

Table C-1. SHR-A individual time domain feature performance. Red shading highlights the top five performing features within a given classifier (column).

Time Domain		Classifier Accuracy				
Feature		LDA	KNN	RFN	SVM	DT
1	tmabs	58.82	63.28	38.08	36.39	57.53
2	tstd	55.62	63.63	37.44	37.68	56.26
3	tvar	48.12	62.29	37.89	27.04	56.50
4	twl	51.64	62.71	34.65	37.47	53.58
5	trms	55.85	63.37	37.17	37.60	56.18
6	tzc	39.87	31.96	25.54	33.09	34.25
7	tpks	29.80	25.37	19.97	21.69	26.16
8	tmpks	52.20	60.12	35.45	39.35	53.81
9	tmvel	47.82	50.62	33.69	32.48	45.25
10	tslpch	40.11	35.80	26.90	28.39	35.47
11	tpwr	48.02	62.49	37.89	26.96	56.61
12	tdam	51.80	61.74	34.41	37.30	53.39
13	tmfl	51.99	62.53	34.32	36.75	53.71
14	tfd	28.25	24.21	21.70	23.95	24.25
15	tfdh	38.58	32.21	29.00	30.80	32.05
16	tren	54.92	52.85	35.53	35.51	49.66
17	tcr	60.13	59.20	37.94	39.81	52.31
18	tcv	44.93	54.75	30.80	23.55	47.03
19	tcard	58.55	59.49	32.39	39.40	52.65
20	tHmob	51.20	50.94	31.28	38.17	47.13
21	tHcom	43.57	47.44	33.61	22.65	41.62
22	tskw	31.17	34.66	18.50	14.15	32.22
23	tdasdv	51.71	61.03	33.77	38.52	54.66
24	tkurt	29.99	30.42	24.93	17.88	29.25
25	twam	49.19	51.03	28.14	30.20	47.87
26	tmcer	45.53	53.15	28.84	27.99	51.88
27	tperc75	47.41	52.92	32.08	29.30	50.68
28	tiabs	59.25	63.91	38.26	36.40	57.66
29	thist	34.39	36.17	30.19	29.89	28.06
30	tssi	47.89	63.55	37.96	27.39	56.22
31	tlogd	58.37	58.80	33.60	37.06	53.93

Table C-2. SHR-A individual frequency domain feature performance. Red shading highlights the top five performing features within a given classifier (column).

Frequency Domain		Classifier Accuracy				
Feature		LDA	KNN	RFN	SVM	DT
1	fwl	54.20	57.11	35.00	38.53	53.13
2	fmn	44.66	39.99	27.16	33.27	39.93
3	fmd	41.68	33.75	25.52	33.36	35.62
4	fpmn	52.59	53.80	30.33	26.18	46.59
5	fpmd	47.41	49.46	28.83	27.35	43.81
6	fpstd	38.48	39.48	21.19	21.15	33.53
7	fmxp	21.42	17.57	16.08	13.51	24.21
8	fr	46.79	43.27	34.18	33.62	41.54
9	fe	38.73	56.91	28.65	38.81	39.16

Table C-3. SHR-A individual time-frequency domain feature performance. Red shading highlights the top five performing features within a given classifier (column).

Time-Frequency Domain		Classifier Accuracy				
Feature		LDA	KNN	RFN	SVM	DT
1	tfstd	54.52	57.58	36.26	34.35	52.38
2	tfvar	45.15	55.85	36.23	24.26	52.41
3	tfwl	54.82	59.13	36.13	34.34	53.44
4	tfe	44.86	57.39	36.24	24.28	52.60
5	tfxabs1	43.33	43.68	30.56	31.85	40.90
6	tfxabs2	48.09	47.89	37.86	43.80	43.11
7	tfzc	24.75	20.30	18.30	22.01	20.98
8	tfmn	14.20	22.92	10.98	11.86	20.43
9	tfmabs	54.63	56.67	35.84	33.83	51.87

**Participant: SHR-B**

Table C-4. SHR-B individual time domain feature performance. Red shading highlights the top five performing features within a given classifier (column).

Time Domain		Classifier Accuracy				
Feature		LDA	KNN	RFN	SVM	DT
1	tmabs	34.41	62.53	28.05	21.73	51.05
2	tstd	34.77	62.80	25.40	22.85	51.06
3	tvar	30.43	56.48	22.33	19.26	50.94
4	twl	32.91	61.29	22.88	20.61	47.35
5	trms	35.10	63.22	25.25	22.80	50.93
6	tzc	30.69	35.45	21.87	23.52	30.71
7	tpks	28.26	38.56	20.19	22.67	31.20
8	tmpks	34.78	62.13	24.51	22.81	50.88
9	tmvel	32.94	52.72	23.15	19.60	42.74
10	tslpch	33.45	43.88	26.34	22.30	37.83
11	tpwr	30.21	57.22	22.50	19.35	51.04
12	tdam	33.04	59.74	23.21	20.46	47.48
13	tmfl	32.79	61.71	22.95	20.56	47.43
14	tfd	26.39	23.91	18.26	20.65	21.97
15	tfdh	28.99	40.01	23.05	22.07	31.45
16	tren	30.51	38.31	23.00	21.60	33.32
17	tcr	39.70	61.74	27.63	32.42	40.77
18	tcv	34.48	55.90	28.52	24.15	44.72
19	tcard	37.52	62.68	25.52	23.06	48.88
20	tHmob	33.90	54.60	23.05	26.83	40.55
21	tHcom	34.73	52.61	26.26	24.81	40.36
22	tskw	22.52	40.13	21.13	15.75	33.23
23	tdasdv	33.97	60.68	22.55	21.17	47.20
24	tkurt	18.63	35.95	18.77	13.53	26.79
25	twam	26.70	41.77	22.33	18.06	35.20
26	tmcer	28.97	55.83	25.16	19.91	45.53
27	tperc75	35.92	55.94	28.70	20.44	49.67
28	tiabs	34.37	64.48	27.55	21.88	51.30
29	thist	28.39	36.99	25.08	26.92	23.21
30	tssi	30.59	61.04	22.24	19.37	50.87
31	tlogd	39.88	61.47	28.42	21.22	49.44



Table C-5. SHR-B individual frequency domain feature performance. Red shading highlights the top five performing features within a given classifier (column).

Frequency Domain		Classifier Accuracy				
Feature		LDA	KNN	RFN	SVM	DT
1	fwl	34.90	55.18	22.38	21.00	44.32
2	fmn	31.23	41.79	19.84	24.33	34.52
3	fmd	29.61	27.65	21.13	24.69	27.65
4	fpmn	29.43	52.82	19.67	19.04	37.58
5	fpmd	26.79	51.07	19.41	18.94	38.10
6	fpstd	25.63	37.22	20.31	15.20	29.79
7	fmxp	22.67	24.81	18.67	18.47	24.96
8	fr	32.34	43.21	25.57	25.98	32.00
9	fe	24.19	53.43	20.05	20.81	33.59

Table C-6. SHR-B individual time-frequency domain feature performance. Red shading highlights the top five performing features within a given classifier (column).

Time-Frequency Domain		Classifier Accuracy				
Feature		LDA	KNN	RFN	SVM	DT
1	tfstd	34.70	57.62	26.66	22.86	47.71
2	tfvar	30.01	50.80	23.38	20.41	47.97
3	tfwl	34.38	61.08	25.59	22.59	48.05
4	tfe	29.86	55.27	23.27	20.28	47.49
5	tfxabs1	29.58	47.88	21.67	20.96	40.32
6	tfxabs2	33.37	50.15	24.38	26.58	39.84
7	tfzc	25.04	24.17	20.47	24.30	25.24
8	tfmn	14.91	20.28	11.78	14.16	20.20
9	tfmabs	35.46	54.66	27.61	21.85	45.88

**Participant: SHR-C**

Table C-7. SHR-C individual time domain feature performance. Red shading highlights the top five performing features within a given classifier (column).

Time Domain		Classifier Accuracy				
Feature		LDA	KNN	RFN	SVM	DT
1	tmabs	67.37	80.89	57.11	46.00	72.38
2	tstd	67.01	80.88	56.08	45.44	71.73
3	tvar	51.81	74.64	49.69	30.46	71.40
4	twl	68.71	85.21	55.26	44.01	72.98
5	trms	67.18	81.36	56.40	45.36	71.70
6	tzc	51.21	45.51	39.60	41.03	42.40
7	tpks	50.78	55.33	39.77	41.68	48.67
8	tmpks	65.38	79.46	55.18	43.77	69.77
9	tmvel	62.52	74.88	52.15	42.74	66.44
10	tslpch	61.10	64.64	48.34	44.44	59.34
11	tpwr	52.02	74.72	49.40	29.96	71.83
12	tdam	68.54	82.62	55.33	44.15	73.15
13	tmfl	68.58	85.11	55.23	44.53	72.91
14	tfd	33.54	27.06	23.14	27.24	25.17
15	tfdh	54.08	51.19	44.41	42.42	48.18
16	tren	56.71	53.02	43.72	44.68	52.48
17	tcr	70.93	70.25	53.86	60.00	54.66
18	tcv	53.74	67.67	44.22	40.11	63.76
19	tcard	70.64	81.45	56.18	50.97	70.30
20	tHmob	55.71	61.46	41.27	43.23	49.24
21	tHcom	57.53	73.26	42.78	46.27	60.39
22	tskw	37.48	53.96	23.82	19.53	52.32
23	tdasdv	67.86	82.15	55.68	44.05	72.46
24	tkurt	25.65	35.65	22.21	15.89	27.72
25	twam	47.06	53.39	42.58	22.13	58.79
26	tmcer	52.91	74.39	50.12	41.05	69.78
27	tperc75	63.96	74.71	56.52	45.78	71.02
28	tiabs	67.42	84.31	57.11	46.02	72.39
29	thist	36.31	37.66	35.77	37.29	27.21
30	tssi	52.44	77.82	49.67	29.89	71.76
31	tlogd	73.96	83.20	56.75	51.49	71.99

Table C-8. SHR-C individual frequency domain feature performance. Red shading highlights the top five performing features within a given classifier (column).

Frequency Domain		Classifier Accuracy				
Feature		LDA	KNN	RFN	SVM	DT
1	fwl	66.85	77.43	55.01	45.56	70.14
2	fmn	52.82	49.17	37.57	40.41	45.00
3	fmd	44.18	34.54	35.48	39.34	33.83
4	fpmn	38.21	69.81	42.85	42.08	45.08
5	fpmd	37.92	68.25	43.56	44.66	46.09
6	fpstd	35.27	55.06	38.04	35.13	35.50
7	fmxp	29.33	28.69	22.47	27.14	30.41
8	fr	52.62	52.35	43.52	39.46	44.95
9	fe	29.65	50.95	29.01	36.85	32.55

Table C-9. SHR-C individual time-frequency domain feature performance. Red shading highlights the top five performing features within a given classifier (column).

Time-Frequency Domain		Classifier Accuracy				
Feature		LDA	KNN	RFN	SVM	DT
1	tfstd	61.81	73.04	55.28	45.12	66.78
2	tfvar	48.88	66.56	46.83	29.26	66.63
3	tfwl	67.40	81.24	57.88	47.64	69.53
4	tfe	48.72	68.48	46.93	28.98	66.70
5	tfxabs1	55.38	66.15	49.17	40.02	59.69
6	tfxabs2	60.61	67.43	55.57	52.69	61.47
7	tfzc	30.78	22.88	23.11	29.62	23.74
8	tfmn	15.78	27.25	11.40	13.07	26.27
9	tfmabs	62.70	70.60	56.31	45.65	66.62

**Participant: SHR-D**

Table C-10. SHR-D individual time domain feature performance. Red shading highlights the top five performing features within a given classifier (column).

Time Domain		Classifier Accuracy				
Feature		LDA	KNN	RFN	SVM	DT
1	tmabs	44.43	49.19	22.81	39.61	43.75
2	tstd	42.71	49.15	21.70	39.50	42.58
3	tvar	39.36	48.19	22.22	36.91	42.87
4	twl	43.49	45.22	23.63	38.56	40.95
5	trms	42.66	48.73	21.82	39.00	42.96
6	tzc	34.05	28.38	26.61	36.35	27.88
7	tpks	24.56	25.26	20.39	27.10	24.40
8	tmpks	41.12	49.31	21.74	38.59	41.73
9	tmvel	41.58	42.35	23.34	33.35	37.50
10	tslpch	30.82	31.71	19.95	35.64	30.27
11	tpwr	39.70	47.93	22.19	36.51	42.65
12	tdam	43.58	45.01	23.86	38.89	40.80
13	tmfl	43.04	44.64	23.74	38.88	40.85
14	tfd	24.62	19.89	16.84	25.93	20.30
15	tfdh	28.10	26.16	20.22	28.99	23.85
16	tren	25.81	24.69	17.96	28.87	24.29
17	tcr	49.20	50.56	30.21	46.43	42.29
18	tcv	45.47	49.06	25.92	35.25	39.65
19	tcard	42.10	45.73	21.60	38.89	40.33
20	tHmob	38.85	38.30	27.81	40.30	33.86
21	tHcom	39.60	41.88	26.72	36.92	36.85
22	tskw	30.96	36.39	21.98	31.30	29.71
23	tdasdv	43.37	44.74	23.25	39.02	39.67
24	tkurt	20.44	24.58	15.83	23.04	20.27
25	twam	26.01	22.82	18.18	22.67	27.63
26	tmcer	40.76	41.74	31.93	42.55	37.84
27	tperc75	43.65	48.57	23.64	39.66	46.93
28	tiabs	44.65	49.13	22.29	40.03	43.78
29	thist	25.50	31.55	23.34	30.93	19.49
30	tssi	39.68	48.11	21.90	36.65	42.78
31	tlogd	50.66	52.45	24.66	43.08	45.39

Table C-11. SHR-D individual frequency domain feature performance. Red shading highlights the top five performing features within a given classifier (column).

Frequency Domain		Classifier Accuracy				
Feature		LDA	KNN	RFN	SVM	DT
1	fwl	40.51	41.50	21.33	38.07	38.36
2	fmn	33.47	31.71	23.72	35.28	27.86
3	fmd	26.48	18.96	20.92	26.00	19.83
4	fpmn	41.78	47.40	20.98	38.98	41.62
5	fpmd	40.22	42.96	20.87	38.72	38.83
6	fpstd	42.05	45.54	23.50	42.99	40.83
7	fmxp	28.05	25.06	19.89	29.12	25.48
8	fr	33.15	29.67	25.34	33.92	26.46
9	fe	28.18	42.71	19.91	35.90	27.09

Table C-12. SHR-D individual time-frequency domain feature performance. Red shading highlights the top five performing features within a given classifier (column).

Time-Frequency Domain		Classifier Accuracy				
Feature		LDA	KNN	RFN	SVM	DT
1	tfstd	41.64	40.87	22.72	40.78	37.32
2	tfvar	37.81	40.42	21.02	37.49	37.30
3	tfwl	41.28	41.65	22.52	38.88	38.81
4	tfe	37.33	40.19	20.97	37.25	36.93
5	tfxabs1	34.68	37.33	19.82	36.75	32.37
6	tfxabs2	37.41	38.29	27.02	39.32	31.20
7	tfzc	26.19	18.83	18.44	26.71	19.52
8	tfmn	11.62	17.44	10.35	18.80	17.15
9	tfmabs	43.70	40.83	23.92	42.00	37.78

**Participant: SHR-E**

Table C-13. SHR-E individual time domain feature performance. Red shading highlights the top five performing features within a given classifier (column).

Time Domain		Classifier Accuracy				
Feature		LDA	KNN	RFN	SVM	DT
1	tmabs	69.64	77.50	52.21	71.72	70.11
2	tstd	65.86	75.12	50.93	67.99	67.25
3	tvar	46.64	69.97	43.56	59.43	67.13
4	twl	68.18	75.90	49.39	70.69	66.56
5	trms	65.53	75.35	51.16	67.89	67.37
6	tzc	62.10	52.40	41.15	60.67	50.39
7	tpks	49.84	49.67	39.49	51.12	42.58
8	tmpks	59.83	71.26	47.05	64.43	64.26
9	tmvel	59.52	66.44	45.01	61.64	61.36
10	tslpch	66.11	60.72	43.81	65.22	57.26
11	tpwr	46.75	69.70	43.79	59.91	66.91
12	tdam	68.27	75.10	49.83	70.29	66.27
13	tmfl	68.42	75.77	49.74	70.63	66.56
14	tfd	40.17	31.97	27.29	40.96	31.02
15	tfdh	58.56	54.36	41.53	57.82	49.44
16	tren	52.72	49.44	36.28	55.84	46.76
17	tcr	70.41	72.19	54.62	74.30	55.96
18	tcv	52.11	61.88	40.65	58.49	56.82
19	tcard	73.81	75.66	54.43	71.47	66.78
20	tHmob	61.80	65.40	44.70	63.75	57.44
21	tHcom	59.06	62.01	42.78	59.42	51.87
22	tskw	36.71	58.49	29.36	41.61	54.15
23	tdasdv	64.91	72.62	48.52	67.22	65.26
24	tkurt	23.23	34.14	23.19	27.97	27.45
25	twam	40.39	46.08	30.32	40.37	48.11
26	tmcer	45.35	67.04	39.98	59.48	60.76
27	tperc75	65.58	70.17	49.07	69.54	67.56
28	tiabs	69.51	80.28	51.72	71.53	69.71
29	thist	44.93	44.54	43.56	49.81	34.11
30	tssi	46.55	73.36	43.89	59.89	67.11
31	tlogd	78.09	79.24	53.47	75.69	72.16

Table C-14. SHR-E individual frequency domain feature performance. Red shading highlights the top five performing features within a given classifier (column).

Frequency Domain		Classifier Accuracy				
Feature		LDA	KNN	RFN	SVM	DT
1	fwl	69.48	72.13	49.16	71.76	67.34
2	fmn	57.29	56.68	41.51	58.01	50.86
3	fmd	49.25	39.07	34.65	49.50	39.22
4	fpmn	64.71	73.40	50.17	67.60	66.48
5	fpmd	64.56	72.06	48.74	66.67	65.42
6	fpstd	62.44	70.74	50.34	68.60	67.35
7	fmxp	31.03	28.12	23.38	33.08	26.81
8	fr	54.50	57.33	39.32	57.46	50.30
9	fe	36.02	50.37	25.81	45.56	38.46

Table C-15. SHR-E individual time-frequency domain feature performance. Red shading highlights the top five performing features within a given classifier (column).

Time-Frequency Domain		Classifier Accuracy				
Feature		LDA	KNN	RFN	SVM	DT
1	tfstd	63.09	71.05	49.63	67.55	65.59
2	tfvar	44.22	64.56	42.79	57.71	65.47
3	tfwl	70.39	76.57	51.53	71.71	69.09
4	tfe	43.88	67.91	42.37	57.43	65.04
5	tfxabs1	53.33	60.24	44.21	57.83	55.37
6	tfxabs2	56.06	59.46	49.73	60.52	54.40
7	tfzc	36.18	25.97	25.49	35.36	26.07
8	tfmn	15.48	25.23	10.88	19.57	23.46
9	tfmabs	65.46	71.70	50.34	69.77	67.98

**Participant: SHR-F**

Table C-16. SHR-F individual time domain feature performance. Red shading highlights the top five performing features within a given classifier (column).

Time Domain		Classifier Accuracy				
Feature		LDA	KNN	RFN	SVM	DT
1	tmabs	70.60	88.41	57.95	79.70	79.05
2	tstd	70.43	87.24	61.50	79.41	78.67
3	tvar	56.72	82.91	56.65	71.50	79.19
4	twl	69.64	88.24	55.95	77.74	77.87
5	trms	70.49	87.62	61.36	79.44	78.47
6	tzc	60.06	52.02	45.29	61.52	47.49
7	tpks	65.75	69.75	44.02	68.19	59.96
8	tmpks	64.86	84.90	54.96	77.92	77.56
9	tmvel	65.08	80.61	55.15	70.94	71.24
10	tslpch	75.81	70.56	50.63	74.43	61.39
11	tpwr	56.94	83.08	56.38	71.50	78.16
12	tdam	69.69	86.26	55.98	78.04	77.97
13	tmfl	69.89	88.34	55.71	78.01	78.04
14	tfd	45.26	35.95	29.25	44.47	32.84
15	tfdh	72.58	66.15	52.33	71.62	58.54
16	tren	46.87	46.78	36.84	52.63	43.43
17	tcr	82.70	85.74	61.12	85.51	74.02
18	tcv	64.33	82.98	48.79	72.43	74.70
19	tcard	78.33	87.94	58.08	80.91	76.49
20	tHmob	71.03	72.53	53.41	71.11	59.23
21	tHcom	70.78	76.84	52.71	72.13	66.96
22	tskw	47.59	65.50	20.59	53.04	66.28
23	tdasdv	69.21	84.91	54.10	77.80	77.99
24	tkurt	38.30	55.90	26.56	44.18	47.61
25	twam	42.07	48.62	23.62	40.45	49.15
26	tmcer	66.71	85.19	58.03	77.88	79.50
27	tperc75	67.48	80.17	54.43	74.90	75.40
28	tiabs	70.58	90.55	58.03	79.29	79.55
29	thist	52.46	53.27	50.05	57.12	43.18
30	tssi	56.68	85.17	56.40	71.46	78.40
31	tlogd	79.29	87.86	56.82	82.42	77.33



Table C-17. SHR-F individual frequency domain feature performance. Red shading highlights the top five performing features within a given classifier (column).

Frequency Domain		Classifier Accuracy				
Feature		LDA	KNN	RFN	SVM	DT
1	fwl	70.22	84.34	57.04	78.62	76.21
2	fmn	65.44	61.18	51.58	66.74	53.96
3	fmd	55.08	42.70	40.80	55.00	39.97
4	fpmn	70.18	86.37	60.71	78.96	77.69
5	fpmd	68.88	84.84	59.97	78.82	76.84
6	fpstd	69.07	80.18	57.35	76.52	72.46
7	fmxp	41.03	37.55	33.04	43.01	37.46
8	fr	63.30	65.57	54.68	65.77	55.25
9	fe	41.94	61.06	26.06	57.54	46.53

Table C-18. SHR-F individual time-frequency domain feature performance. Red shading highlights the top five performing features within a given classifier (column).

Time-Frequency Domain		Classifier Accuracy				
Feature		LDA	KNN	RFN	SVM	DT
1	tfstd	68.14	83.26	59.53	77.67	74.21
2	tfvar	53.92	78.46	53.91	67.20	74.24
3	tfwl	69.98	88.12	59.58	79.56	77.31
4	tfe	53.72	80.38	53.41	67.39	73.51
5	tfxabs1	61.84	74.23	51.44	71.50	66.04
6	tfxabs2	64.69	72.40	55.01	72.44	65.14
7	tfzc	37.48	27.59	26.88	37.66	28.30
8	tfmn	13.75	25.55	9.79	22.56	23.30
9	tfmabs	68.84	82.27	57.89	77.61	73.27

**Participant: SHR-G**

Table C-19. SHR-G individual time domain feature performance. Red shading highlights the top five performing features within a given classifier (column).

Time Domain		Classifier Accuracy				
Feature		LDA	KNN	RFN	SVM	DT
1	tmabs	69.47	76.52	44.35	74.01	72.72
2	tstd	66.70	75.50	41.49	73.08	71.29
3	tvar	49.88	71.55	35.28	57.64	71.32
4	twl	63.72	76.38	38.38	66.25	68.75
5	trms	66.73	75.20	41.67	73.19	71.42
6	tzc	60.62	57.00	44.10	61.23	53.36
7	tpks	52.73	51.16	38.82	54.98	47.64
8	tmpks	60.47	73.33	37.41	66.12	70.56
9	tmvel	59.05	69.07	37.63	63.24	64.79
10	tslpch	62.76	61.27	36.58	65.63	58.28
11	tpwr	49.90	71.53	35.74	57.72	71.56
12	tdam	63.45	73.21	38.17	66.27	68.72
13	tmfl	64.02	76.33	38.14	66.43	68.50
14	tfd	43.19	38.94	32.95	44.26	34.86
15	tfdh	57.10	57.74	43.32	58.69	52.62
16	tren	63.90	63.23	42.50	66.23	60.05
17	tcr	71.44	72.14	55.00	72.69	64.10
18	tcv	55.18	71.76	39.24	67.53	68.83
19	tcard	75.15	78.51	39.34	77.09	72.11
20	tHmob	58.20	64.25	43.98	62.19	55.59
21	tHcom	57.05	63.67	40.84	60.77	56.36
22	tskw	40.48	56.59	30.37	43.50	57.64
23	tdasdv	60.91	72.97	35.56	65.47	67.23
24	tkurt	25.99	41.57	16.61	31.89	35.56
25	twam	57.90	59.05	23.69	60.21	62.61
26	tmcer	55.44	69.84	50.49	66.67	67.34
27	tperc75	65.93	71.21	46.01	70.61	69.54
28	tiabs	69.55	79.07	44.58	74.02	72.56
29	thist	46.67	47.59	43.08	50.65	36.95
30	tssi	49.64	76.25	35.00	57.78	71.17
31	tlogd	75.93	77.07	42.92	76.00	72.58

Table C-20. SHR-G individual frequency domain feature performance. Red shading highlights the top five performing features within a given classifier (column).

Frequency Domain		Classifier Accuracy				
Feature		LDA	KNN	RFN	SVM	DT
1	fwl	66.91	72.55	39.76	72.56	70.07
2	fmn	53.20	55.46	41.93	56.96	51.13
3	fmd	50.04	45.12	39.36	51.77	42.68
4	fpmn	66.41	74.75	41.44	73.34	71.34
5	fpmd	64.85	72.40	38.51	71.49	69.39
6	fpstd	67.66	72.13	46.08	73.70	70.90
7	fmxp	32.50	29.32	24.95	34.15	30.74
8	fr	58.66	61.29	43.87	61.12	51.89
9	fe	35.43	61.47	28.35	57.30	52.82

Table C-21. SHR-G individual time-frequency domain feature performance. Red shading highlights the top five performing features within a given classifier (column).

Time-Frequency Domain		Classifier Accuracy				
Feature		LDA	KNN	RFN	SVM	DT
1	tfstd	65.91	72.90	42.17	71.60	69.83
2	tfvar	49.11	68.45	38.44	57.60	69.83
3	tfwl	69.06	76.60	44.24	73.56	71.92
4	tfe	48.97	72.96	37.83	57.32	69.77
5	tfxabs1	55.31	67.67	36.58	62.10	64.58
6	tfxabs2	57.65	64.76	41.66	65.80	63.21
7	tfzc	37.64	29.43	28.67	37.86	29.97
8	tfmn	22.76	35.17	12.67	26.35	35.06
9	tfmabs	67.89	73.08	44.07	72.77	70.91

**Participant: SHR-H**

Table C-22. SHR-H individual time domain feature performance. Red shading highlights the top five performing features within a given classifier (column).

Time Domain		Classifier Accuracy				
Feature		LDA	KNN	RFN	SVM	DT
1	tmabs	66.12	80.02	48.77	67.88	66.46
2	tstd	63.29	78.32	46.71	63.62	63.07
3	tvar	56.80	75.81	46.18	61.63	62.65
4	twl	57.07	66.35	36.50	53.55	52.85
5	trms	63.05	77.98	46.44	63.46	62.76
6	tzc	47.68	44.54	36.39	50.36	39.38
7	tpks	39.23	35.93	28.85	39.32	32.15
8	tmpks	57.64	70.77	42.41	58.32	58.19
9	tmvel	52.93	55.03	31.83	48.10	45.77
10	tslpch	47.04	45.04	32.65	49.45	40.91
11	tpwr	56.85	75.75	46.03	61.47	62.97
12	tdam	56.87	65.72	36.32	53.33	52.63
13	tmfl	56.87	66.52	36.20	53.35	52.52
14	tfd	32.99	26.67	23.16	33.73	25.12
15	tfdh	46.30	40.41	34.83	45.66	36.22
16	tren	32.78	29.88	22.72	37.07	30.32
17	tcr	74.45	75.99	48.88	74.99	59.66
18	tcv	72.07	74.61	42.02	66.95	61.04
19	tcard	61.48	70.57	42.84	59.70	56.95
20	tHmob	53.28	59.05	35.53	54.82	45.23
21	tHcom	51.71	58.96	36.16	51.47	47.83
22	tskw	33.60	39.44	24.24	34.43	33.77
23	tdasdv	54.34	63.86	36.62	53.24	52.41
24	tkurt	32.53	39.88	29.28	36.06	32.89
25	twam	23.51	21.05	18.50	23.76	27.15
26	tmcer	54.72	64.82	42.13	61.44	56.93
27	tperc75	63.01	74.22	44.67	68.03	66.16
28	tiabs	66.24	81.02	48.32	67.60	66.08
29	thist	36.40	38.19	34.65	42.52	28.70
30	tssi	56.68	76.24	46.05	61.51	62.43
31	tlogd	69.70	79.47	46.62	70.69	67.82

Table C-23. SHR-H individual frequency domain feature performance. Red shading highlights the top five performing features within a given classifier (column).

Frequency Domain						
Feature		Classifier Accuracy				
		LDA	KNN	RFN	SVM	DT
1	fwl	55.54	59.21	38.26	56.04	50.78
2	fmn	43.38	40.98	27.74	45.64	36.21
3	fmd	37.12	29.31	27.41	38.17	29.97
4	fpmn	54.40	72.51	41.55	62.40	59.95
5	fpmd	53.22	63.96	40.82	56.99	53.75
6	fpstd	56.08	72.78	41.49	64.96	65.14
7	fmxp	31.31	29.17	22.85	32.39	31.89
8	fr	41.12	40.30	33.90	41.52	34.08
9	fe	44.20	59.53	30.33	51.32	40.03

Table C-24. SHR-H individual time-frequency domain feature performance. Red shading highlights the top five performing features within a given classifier (column).

Time-Frequency Domain						
Feature		Classifier Accuracy				
		LDA	KNN	RFN	SVM	DT
1	tfstd	59.95	69.26	45.44	63.09	59.65
2	tfvar	52.96	66.92	43.06	59.53	59.33
3	tfwl	62.84	71.30	46.23	63.51	60.32
4	tfe	52.36	66.48	43.02	59.01	58.72
5	tfxabs1	46.29	47.08	32.97	48.58	41.52
6	tfxabs2	51.52	51.33	41.60	54.83	43.94
7	tfzc	37.03	29.97	26.81	37.67	29.76
8	tfmn	16.81	19.88	13.72	19.64	19.04
9	tfmabs	60.11	68.59	46.92	64.10	59.83

**Participant: SHR-I**

Table C-25. SHR-I individual time domain feature performance. Red shading highlights the top five performing features within a given classifier (column).

Time Domain		Classifier Accuracy				
Feature		LDA	KNN	RFN	SVM	DT
1	tmabs	52.58	66.09	35.72	52.10	54.90
2	tstd	52.75	65.38	35.77	51.76	54.60
3	tvar	37.60	62.79	36.81	44.82	55.04
4	twl	49.38	60.89	38.10	48.37	53.35
5	trms	52.96	65.67	35.76	51.36	54.99
6	tzc	40.54	35.22	31.27	42.11	32.31
7	tpks	37.12	38.04	29.70	37.42	34.01
8	tmpks	50.81	61.71	35.15	50.74	52.55
9	tmvel	45.77	55.66	35.19	44.07	49.90
10	tslpch	40.13	41.85	33.47	38.66	37.91
11	tpwr	37.04	62.16	36.66	45.22	54.93
12	tdam	49.17	62.09	38.15	48.28	52.82
13	tmfl	49.23	60.48	38.34	48.10	53.03
14	tfd	28.47	24.29	20.49	29.41	22.95
15	tfdh	39.19	36.96	31.61	41.36	34.18
16	tren	33.80	32.42	29.01	35.88	35.19
17	tcr	56.96	61.88	40.03	60.69	47.61
18	tcv	45.73	60.97	26.48	49.61	50.18
19	tcard	56.96	58.13	33.60	51.43	53.12
20	tHmob	42.41	47.22	31.19	45.95	37.79
21	tHcom	35.71	48.56	33.13	39.18	38.54
22	tskw	33.26	46.31	25.32	38.29	41.46
23	tdasdv	48.66	62.32	37.48	46.96	53.12
24	tkurt	23.16	31.63	16.80	26.88	24.92
25	twam	36.20	30.33	25.66	35.40	39.31
26	tmcer	44.22	59.65	41.27	59.25	56.14
27	tperc75	46.42	52.05	35.06	49.04	50.83
28	tiabs	52.03	64.81	36.01	52.11	55.33
29	thist	31.40	34.13	28.93	35.51	24.54
30	tssi	37.04	64.21	36.65	45.52	54.59
31	tlogd	57.94	63.43	34.76	54.41	53.40

Table C-26. SHR-I individual frequency domain feature performance. Red shading highlights the top five performing features within a given classifier (column).

Frequency Domain		Classifier Accuracy				
Feature		LDA	KNN	RFN	SVM	DT
1	fwl	50.15	56.14	37.41	49.83	50.33
2	fmn	38.69	37.99	29.25	40.43	33.04
3	fmd	29.09	21.19	23.58	29.00	21.61
4	fpmn	52.61	63.26	35.24	52.23	53.18
5	fpmd	50.43	58.27	34.38	50.50	50.24
6	fpstd	52.56	60.70	36.90	53.80	51.22
7	fmxp	22.60	24.56	19.48	25.02	24.63
8	fr	37.80	38.06	30.83	39.09	31.33
9	fe	25.13	45.05	20.15	29.32	28.22

Table C-27. SHR-I individual time-frequency domain feature performance. Red shading highlights the top five performing features within a given classifier (column).

Time-Frequency Domain		Classifier Accuracy				
Feature		LDA	KNN	RFN	SVM	DT
1	tfstd	51.82	58.24	34.69	51.00	50.33
2	tfvar	35.74	55.48	34.89	43.80	51.33
3	tfwl	52.32	59.28	38.25	52.20	53.02
4	tfe	35.23	56.72	34.58	43.56	50.20
5	tfxabs1	44.96	48.06	31.82	45.47	42.78
6	tfxabs2	42.65	45.78	32.91	46.03	40.75
7	tfzc	23.41	19.42	17.65	23.42	19.33
8	tfmn	11.46	17.39	9.44	16.58	19.02
9	tfmabs	49.38	55.74	35.39	50.63	49.84

# Feature set comparisons and performance accuracies

Participant: SHR-A

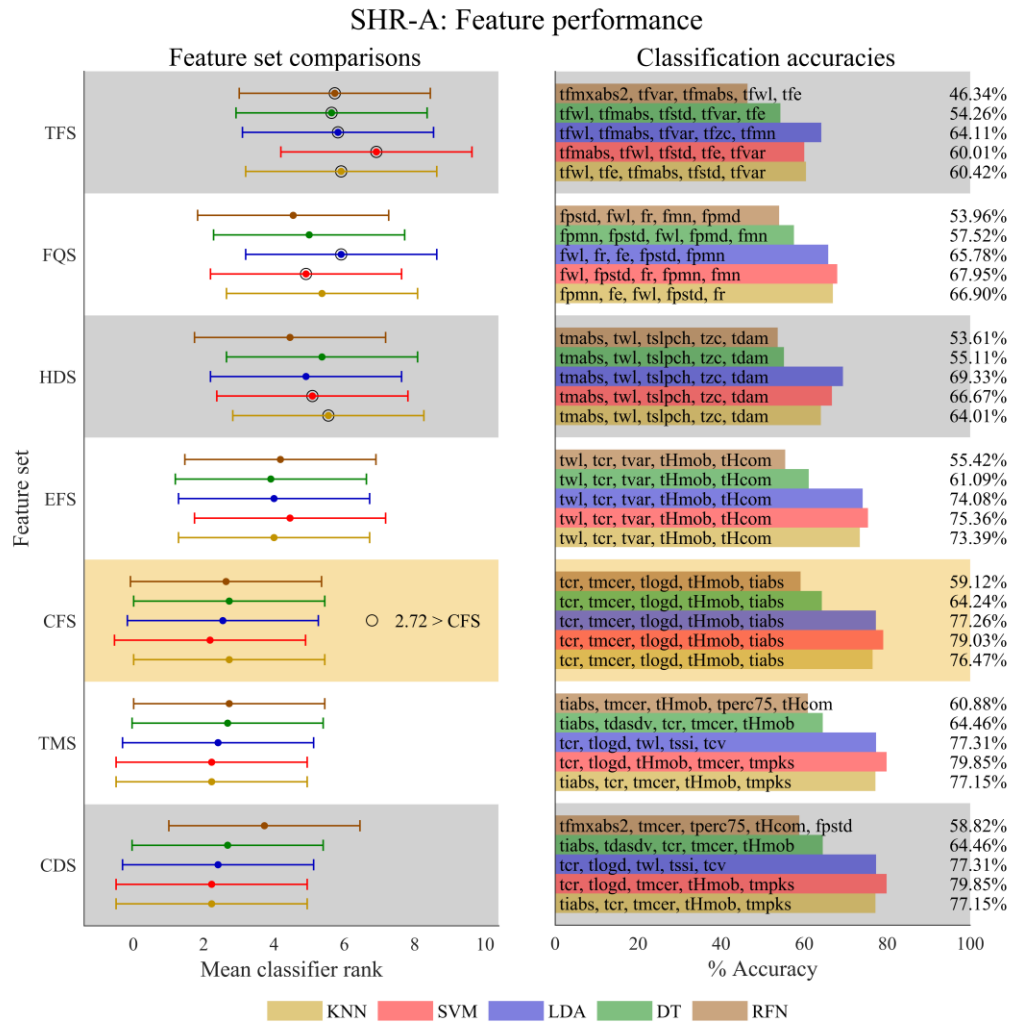


Figure C-1. Investigation of feature set performance for participant SHR-A. The left panel shows the pairwise comparisons for the feature sets on an individual classifier basis. The Friedman test, with a critical value of  $F(6,60) = 2.25$  at  $\alpha = 0.05$ , was used to determine if average accuracy ranks significantly differed from the mean rank. Classifier F Statistics (KNN:  $F_F = 12.95$ , SVM:  $F_F = 26.25$ , LDA:  $F_F = 11.46$ , DT:  $F_F = 6.13$ , RFN:  $F_F = 3.40$ ) confirmed significant differences within each classifier's feature sets. A post-hoc Nemenyi test with a critical distance of 2.72 at  $\alpha = 0.05$  identified superior feature sets as indicated by pairs outside the critical distance marked by the interval bars. Each classifier is color-coded for easy comparison, with lower average ranks indicating better classification accuracy. Feature sets significantly different from the highlighted congenital feature set (CFS) were marked with an outer black ring. The right panel displays classification accuracies, which range from approximately 46% to 80%, alongside the corresponding feature sets, aligning them with the ranked performance shown in the left panel.



**Participant: SHR-B**

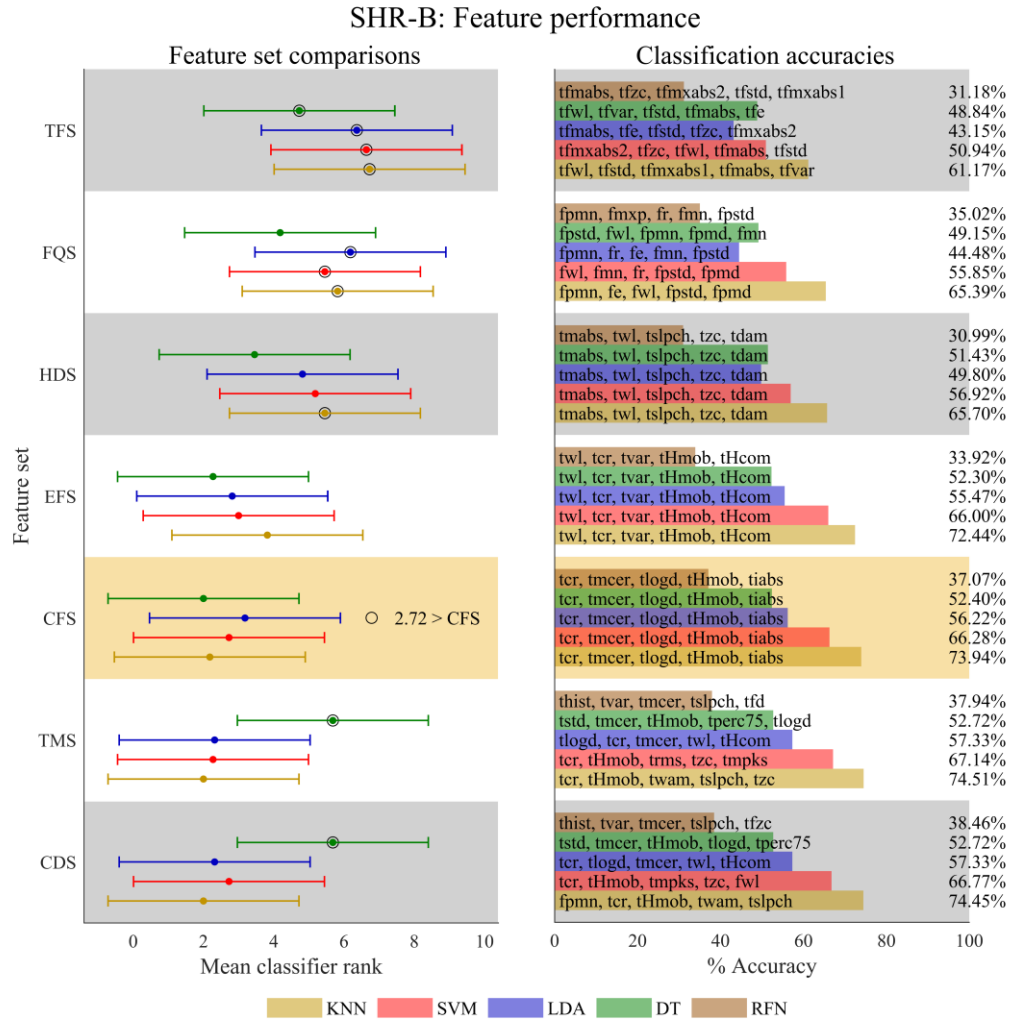


Figure C-2. Investigation of feature set performance for participant SHR-B. The left panel shows the pairwise comparisons for the feature sets on an individual classifier basis. The Friedman test, with a critical value of  $F(6,60) = 2.25$  at  $\alpha = 0.05$ , was used to determine if average accuracy ranks significantly differed from the mean rank. Classifier F Statistics (KNN:  $F_F = 63.65$ , SVM:  $F_F = 17.15$ , LDA:  $F_F = 20.24$ , DT:  $F_F = 9.31$ , RFN:  $F_F = 0.65$ ) confirmed significant differences within each classifier’s feature sets, with the exception of RFN. A post-hoc Nemenyi test with a critical distance of 2.72 at  $\alpha = 0.05$  identified superior feature sets as indicated by pairs outside the critical distance marked by the interval bars. Each classifier is color-coded for easy comparison, with lower average ranks indicating better classification accuracy. Feature sets significantly different from the highlighted congenital feature set (CFS) were marked with an outer black ring. The right panel displays classification accuracies, which range from approximately 31% to 75%, alongside the corresponding feature sets, aligning them with the ranked performance shown in the left panel.

Participant: SHR-C

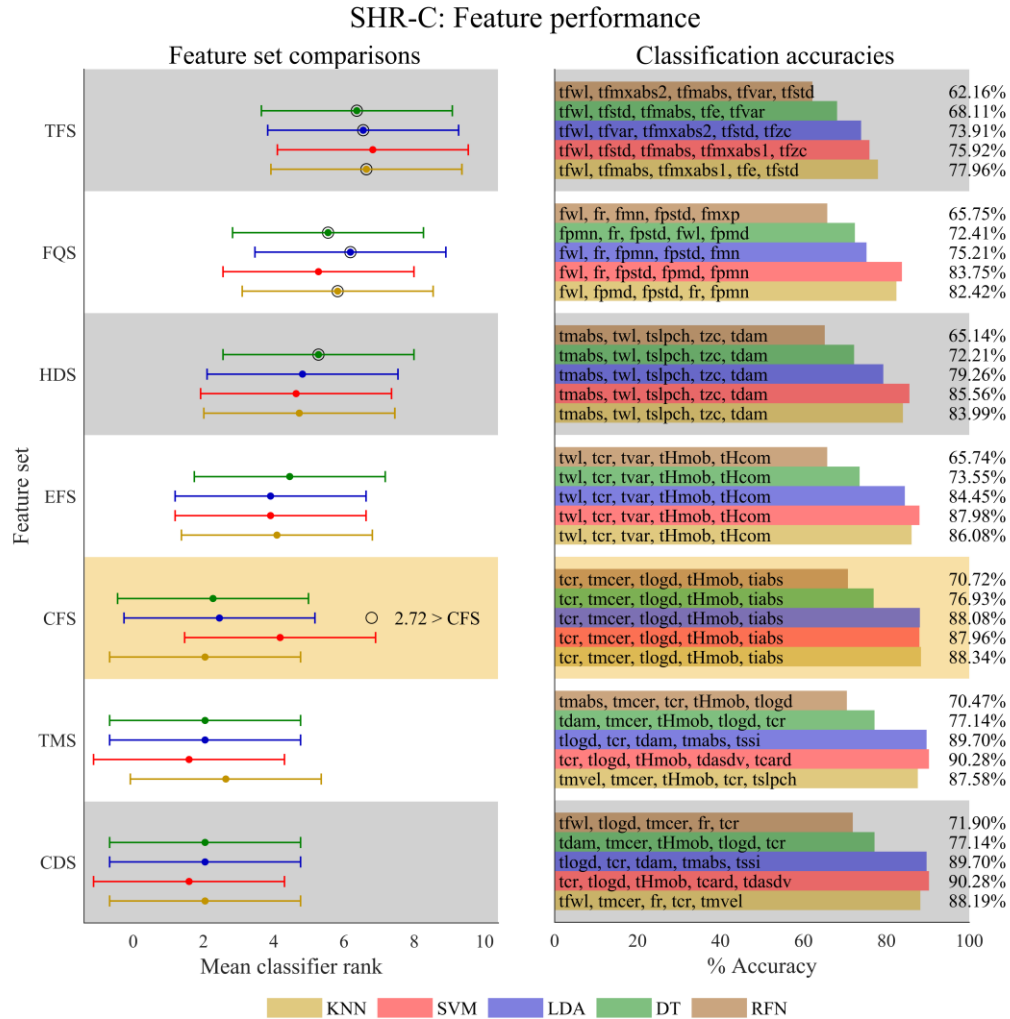


Figure C-3. Investigation of feature set performance for participant SHR-C. The left panel shows the pairwise comparisons for the feature sets on an individual classifier basis. The Friedman test, with a critical value of  $F(6,60) = 2.25$  at  $\alpha = 0.05$ , was used to determine if average accuracy ranks significantly differed from the mean rank. Classifier F Statistics (KNN:  $F_F = 26.33$ , SVM:  $F_F = 33.86$ , LDA:  $F_F = 36.25$ , DT:  $F_F = 26.97$ , RFN:  $F_F = 1.90$ ) confirmed significant differences within each classifier's feature sets, with the exception of RFN. A post-hoc Nemenyi test with a critical distance of 2.72 at  $\alpha = 0.05$  identified superior feature sets as indicated by pairs outside the critical distance marked by the interval bars. Each classifier is color-coded for easy comparison, with lower average ranks indicating better classification accuracy. Feature sets significantly different from the highlighted congenital feature set (CFS) were marked with an outer black ring. The right panel displays classification accuracies, which range from approximately 62% to 90%, alongside the corresponding feature sets, aligning them with the ranked performance shown in the left panel.

**Participant: SHR-D**

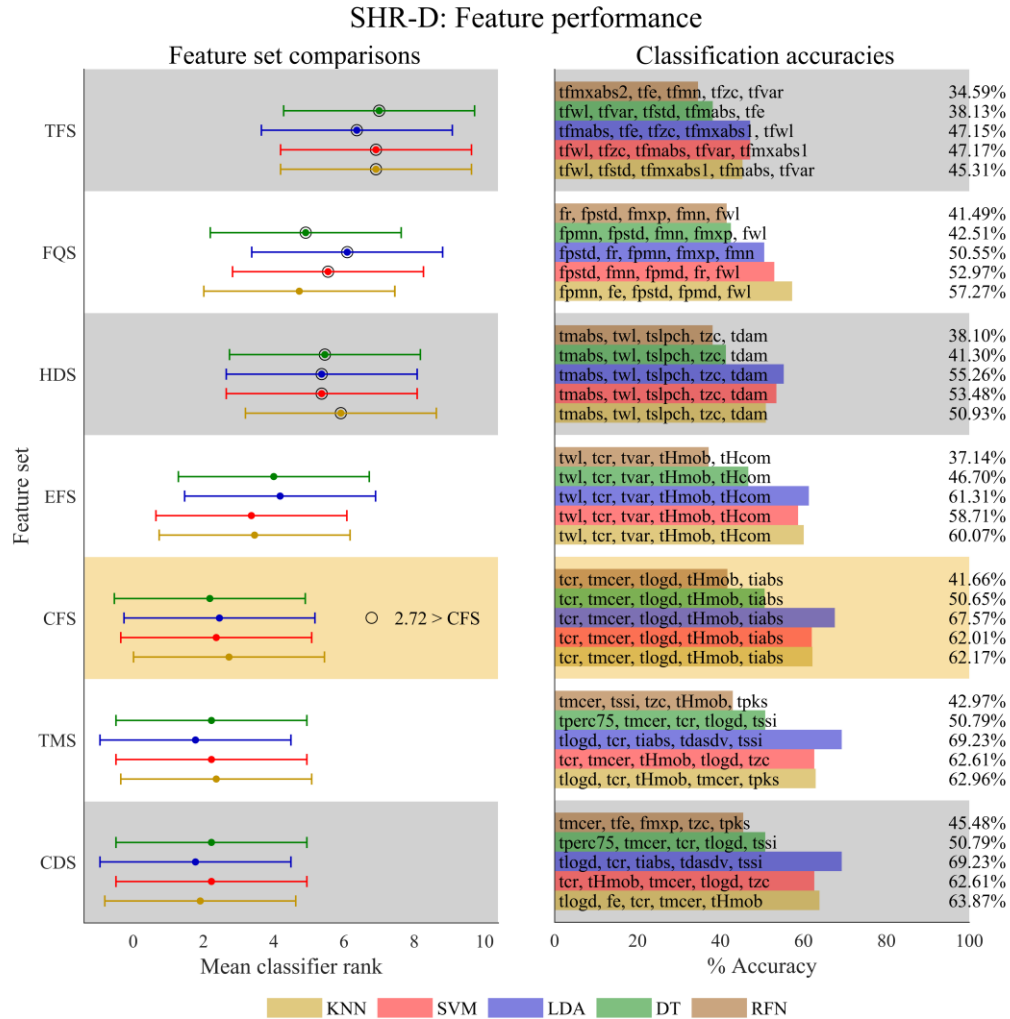


Figure C-4. Investigation of feature set performance for participant SHR-D. The left panel shows the pairwise comparisons for the feature sets on an individual classifier basis. The Friedman test, with a critical value of  $F(6,60) = 2.25$  at  $\alpha = 0.05$ , was used to determine if average accuracy ranks significantly differed from the mean rank. Classifier F Statistics (KNN:  $F_F = 33.77$ , SVM:  $F_F = 37.29$ , LDA:  $F_F = 62.94$ , DT:  $F_F = 33.30$ , RFN:  $F_F = 1.20$ ) confirmed significant differences within each classifier's feature sets, with the exception of RFN. A post-hoc Nemenyi test with a critical distance of 2.72 at  $\alpha = 0.05$  identified superior feature sets as indicated by pairs outside the critical distance marked by the interval bars. Each classifier is color-coded for easy comparison, with lower average ranks indicating better classification accuracy. Feature sets significantly different from the highlighted congenital feature set (CFS) were marked with an outer black ring. The right panel displays classification accuracies, which range from approximately 35% to 69%, alongside the corresponding feature sets, aligning them with the ranked performance shown in the left panel.

Participant: SHR-E

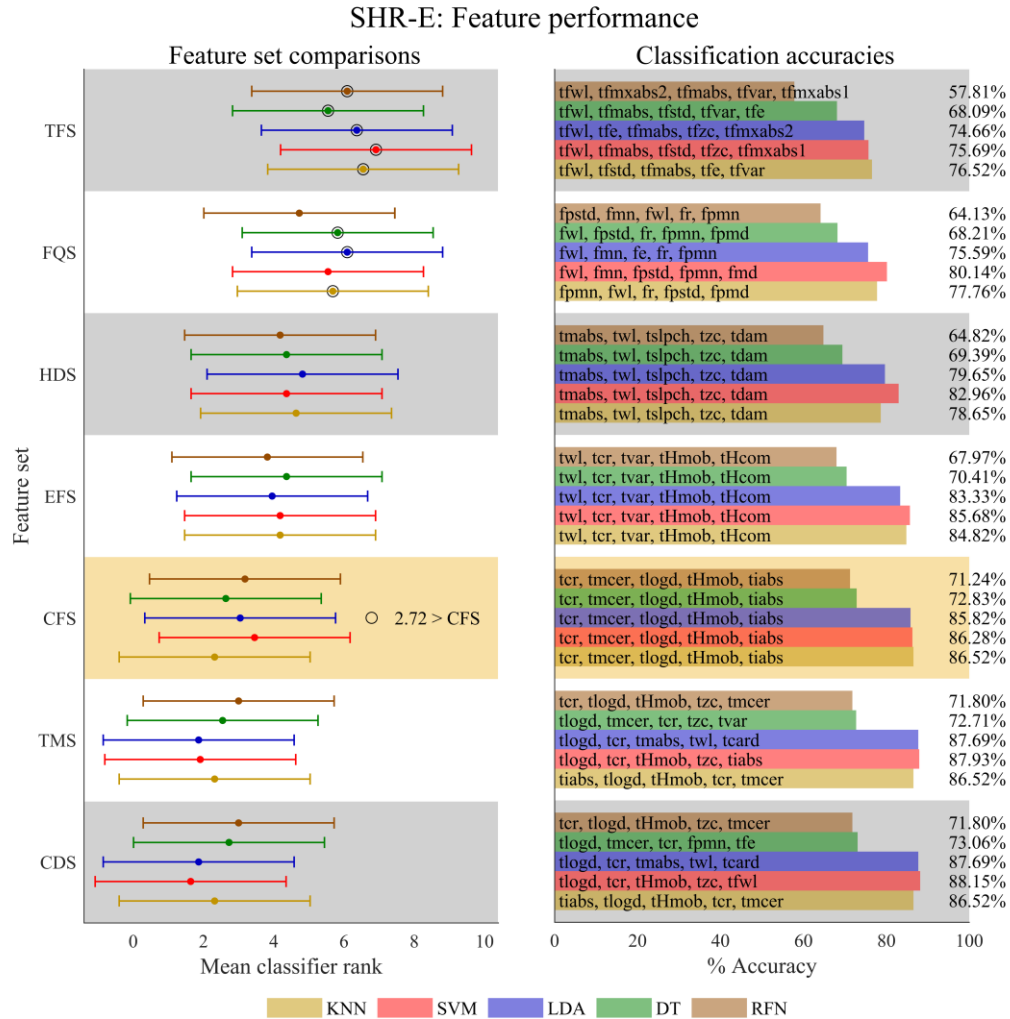


Figure C-5. Investigation of feature set performance for participant SHR-E. The left panel shows the pairwise comparisons for the feature sets on an individual classifier basis. The Friedman test, with a critical value of  $F(6,60) = 2.25$  at  $\alpha = 0.05$ , was used to determine if average accuracy ranks significantly differed from the mean rank. Classifier F Statistics (KNN:  $F_F = 18.66$ , SVM:  $F_F = 31.62$ , LDA:  $F_F = 28.20$ , DT:  $F_F = 7.03$ , RFN:  $F_F = 3.70$ ) confirmed significant differences within each classifier's feature sets. A post-hoc Nemenyi test with a critical distance of 2.72 at  $\alpha = 0.05$  identified superior feature sets as indicated by pairs outside the critical distance marked by the interval bars. Each classifier is color-coded for easy comparison, with lower average ranks indicating better classification accuracy. Feature sets significantly different from the highlighted congenital feature set (CFS) were marked with an outer black ring. The right panel displays classification accuracies, which range from approximately 58% to 88%, alongside the corresponding feature sets, aligning them with the ranked performance shown in the left panel.

Participant: SHR-F

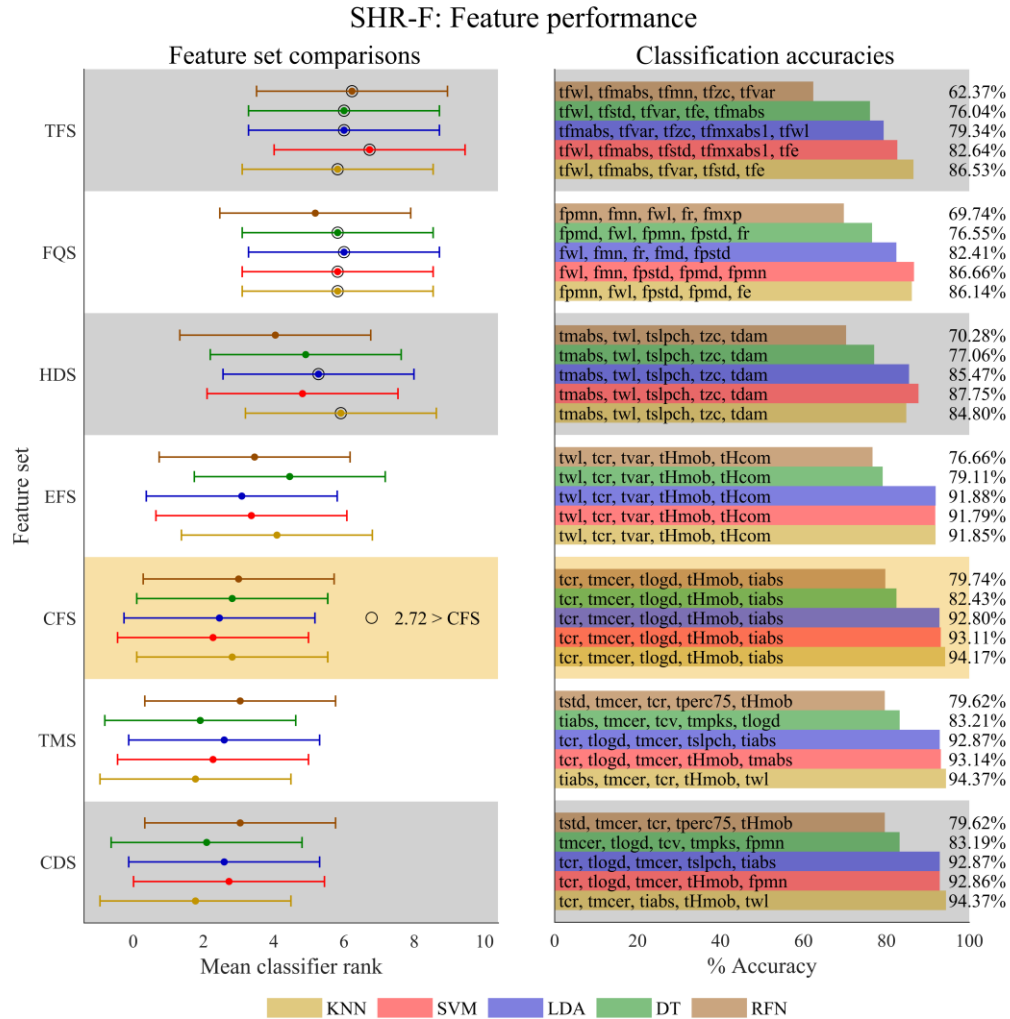


Figure C-6. Investigation of feature set performance for participant SHR-F. The left panel shows the pairwise comparisons for the feature sets on an individual classifier basis. The Friedman test, with a critical value of  $F(6,60) = 2.25$  at  $\alpha = 0.05$ , was used to determine if average accuracy ranks significantly differed from the mean rank. Classifier F Statistics (KNN:  $F_F = 33.63$ , SVM:  $F_F = 22.58$ , LDA:  $F_F = 15.01$ , DT:  $F_F = 17.32$ , RFN:  $F_F = 5.10$ ) confirmed significant differences within each classifier's feature sets. A post-hoc Nemenyi test with a critical distance of 2.72 at  $\alpha = 0.05$  identified superior feature sets as indicated by pairs outside the critical distance marked by the interval bars. Each classifier is color-coded for easy comparison, with lower average ranks indicating better classification accuracy. Feature sets significantly different from the highlighted congenital feature set (CFS) were marked with an outer black ring. The right panel displays classification accuracies, which range from approximately 62% to 94%, alongside the corresponding feature sets, aligning them with the ranked performance shown in the left panel.

Participant: SHR-G

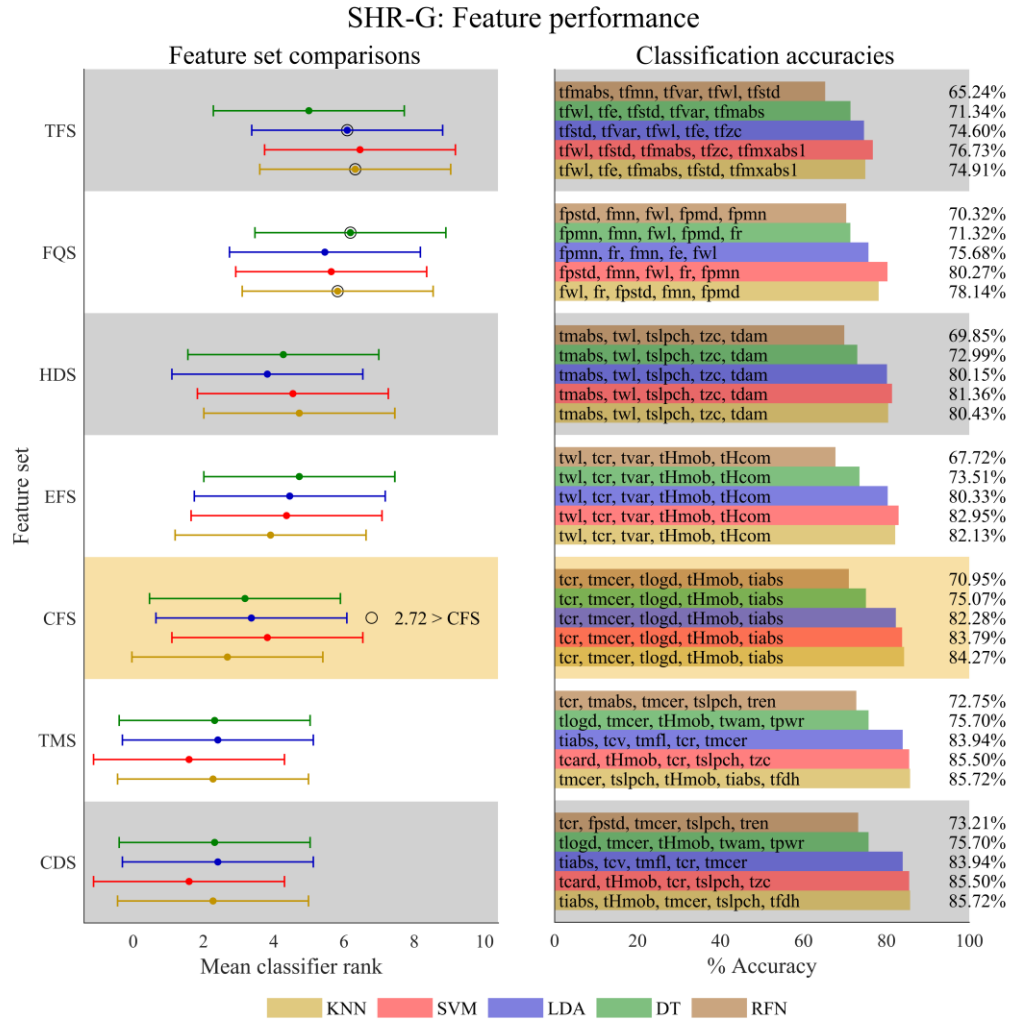


Figure C-7. Investigation of feature set performance for participant SHR-G. The left panel shows the pairwise comparisons for the feature sets on an individual classifier basis. The Friedman test, with a critical value of  $F(6,60) = 2.25$  at  $\alpha = 0.05$ , was used to determine if average accuracy ranks significantly differed from the mean rank. Classifier F Statistics (KNN:  $F_F = 15.27$ , SVM:  $F_F = 28.74$ , LDA:  $F_F = 7.72$ , DT:  $F_F = 8.29$ , RFN:  $F_F = 1.30$ ) confirmed significant differences within each classifier's feature sets, with the exception of RFN. A post-hoc Nemenyi test with a critical distance of 2.72 at  $\alpha = 0.05$  identified superior feature sets as indicated by pairs outside the critical distance marked by the interval bars. Each classifier is color-coded for easy comparison, with lower average ranks indicating better classification accuracy. Feature sets significantly different from the highlighted congenital feature set (CFS) were marked with an outer black ring. The right panel displays classification accuracies, which range from approximately 65% to 86%, alongside the corresponding feature sets, aligning them with the ranked performance shown in the left panel.

**Participant: SHR-H**

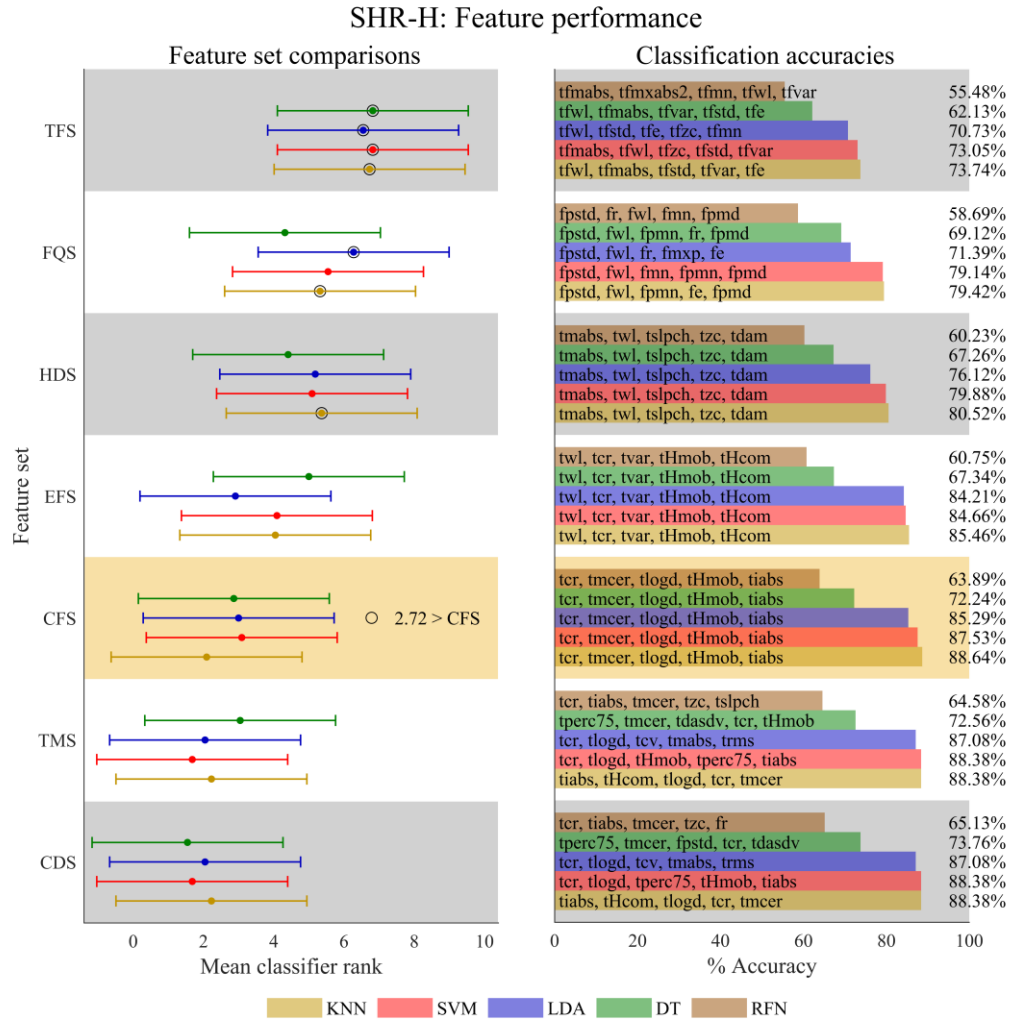


Figure C-8. Investigation of feature set performance for participant SHR-H. The left panel shows the pairwise comparisons for the feature sets on an individual classifier basis. The Friedman test, with a critical value of  $F(6,60) = 2.25$  at  $\alpha = 0.05$ , was used to determine if average accuracy ranks significantly differed from the mean rank. Classifier F Statistics (KNN:  $F_F = 29.81$ , SVM:  $F_F = 47.18$ , LDA:  $F_F = 44.60$ , DT:  $F_F = 16.51$ , RFN:  $F_F = 2.20$ ) confirmed significant differences within each classifier's feature sets, with the exception of RFN. A post-hoc Nemenyi test with a critical distance of 2.72 at  $\alpha = 0.05$  identified superior feature sets as indicated by pairs outside the critical distance marked by the interval bars. Each classifier is color-coded for easy comparison, with lower average ranks indicating better classification accuracy. Feature sets significantly different from the highlighted congenital feature set (CFS) were marked with an outer black ring. The right panel displays classification accuracies, which range from approximately 55% to 89%, alongside the corresponding feature sets, aligning them with the ranked performance shown in the left panel.

**Participant: SHR-I**

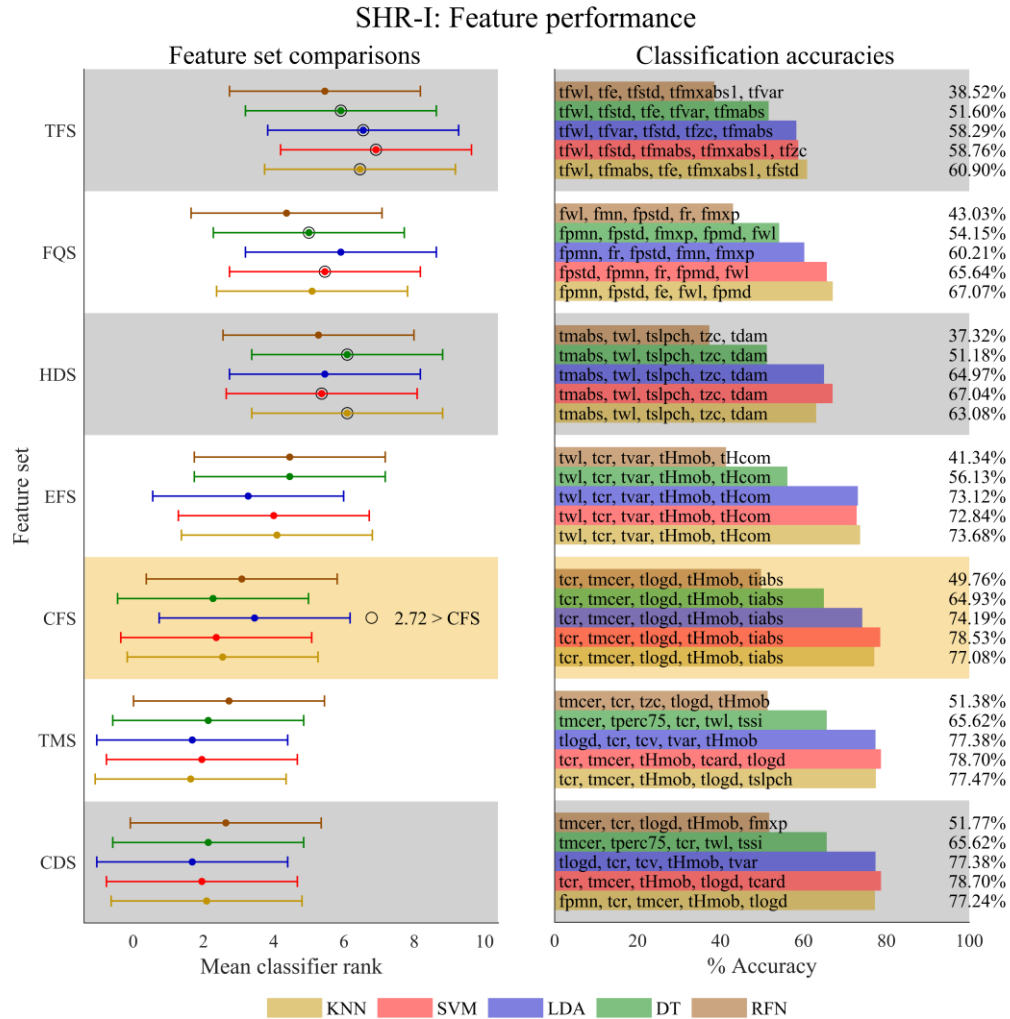


Figure C-9. Investigation of feature set performance for participant SHR-I. The left panel shows the pairwise comparisons for the feature sets on an individual classifier basis. The Friedman test, with a critical value of  $F(6,60) = 2.25$  at  $\alpha = 0.05$ , was used to determine if average accuracy ranks significantly differed from the mean rank. Classifier F Statistics (KNN:  $F_F = 45.36$ , SVM:  $F_F = 51.99$ , LDA:  $F_F = 56.89$ , DT:  $F_F = 21.63$ , RFN:  $F_F = 4.3$ ) confirmed significant differences within each classifier's feature sets. A post-hoc Nemenyi test with a critical distance of 2.72 at  $\alpha = 0.05$  identified superior feature sets as indicated by pairs outside the critical distance marked by the interval bars. Each classifier is color-coded for easy comparison, with lower average ranks indicating better classification accuracy. Feature sets significantly different from the highlighted congenital feature set (CFS) were marked with an outer black ring. The right panel displays classification accuracies, which range from approximately 39% to 79%, alongside the corresponding feature sets, aligning them with the ranked performance shown in the left panel.



## Appendix D: Real-time feature space trial differences

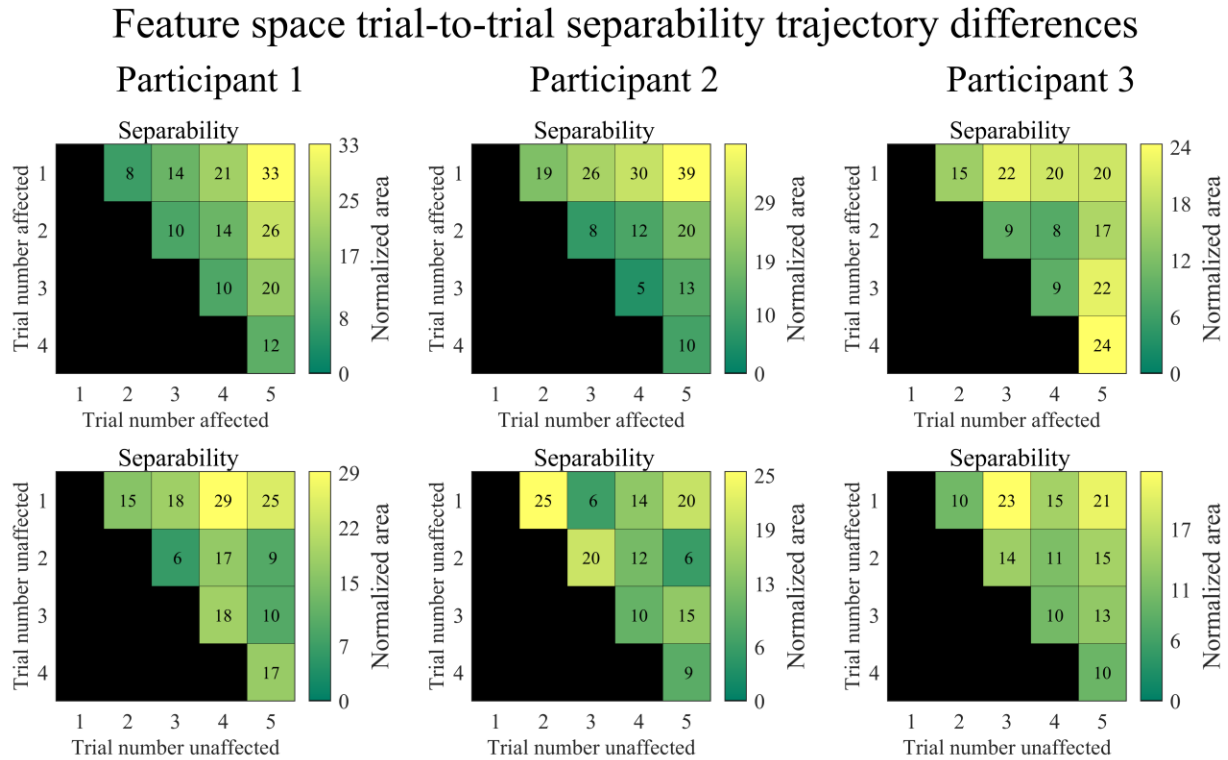


Figure D-1. Feature space trial-to-trial separability trajectory differences. Each column represents the trial-to-trial area of the normalized separability trajectory for the affected limb (top) and unaffected limb (bottom). Lighter yellow coloring indicates a larger area between two normalized trajectories. The affected limb consistently exhibits an increase in area from trial 1 to trial 5 across all participants, whereas the unaffected limb shows indiscernible behavior. Note that the area is rounded to the nearest whole number.

## Feature space trial-to-trial consistency trajectory differences

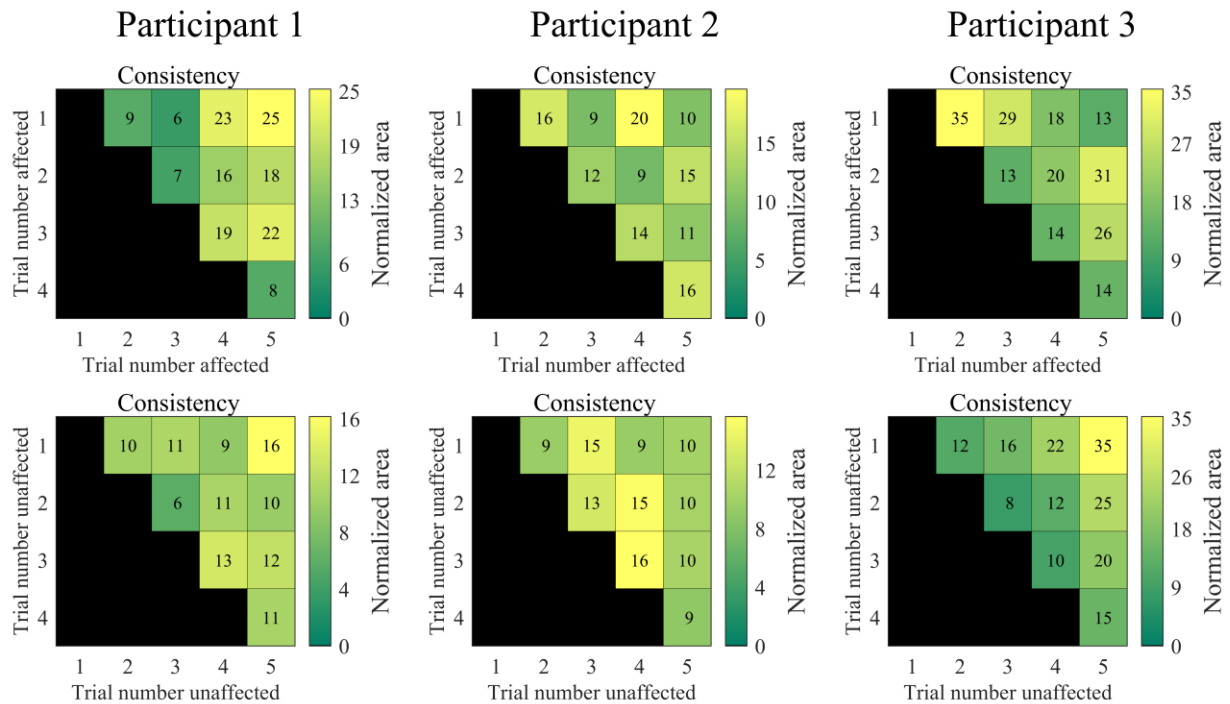


Figure D-2. Feature space trial-to-trial consistency trajectory differences. Each column represents the trial-to-trial area of the normalized consistency trajectory for the affected limb (top) and unaffected limb (bottom). Lighter yellow coloring indicates a larger area between two normalized trajectories. The affected and unaffected limbs show no trends in behavior. This comes with the exception of participant 3's unaffected limb where an increase in area from trial 1 to trial 5 is observed. Note that the area is rounded to the nearest whole number.

## Feature space trial-to-trial variability trajectory differences

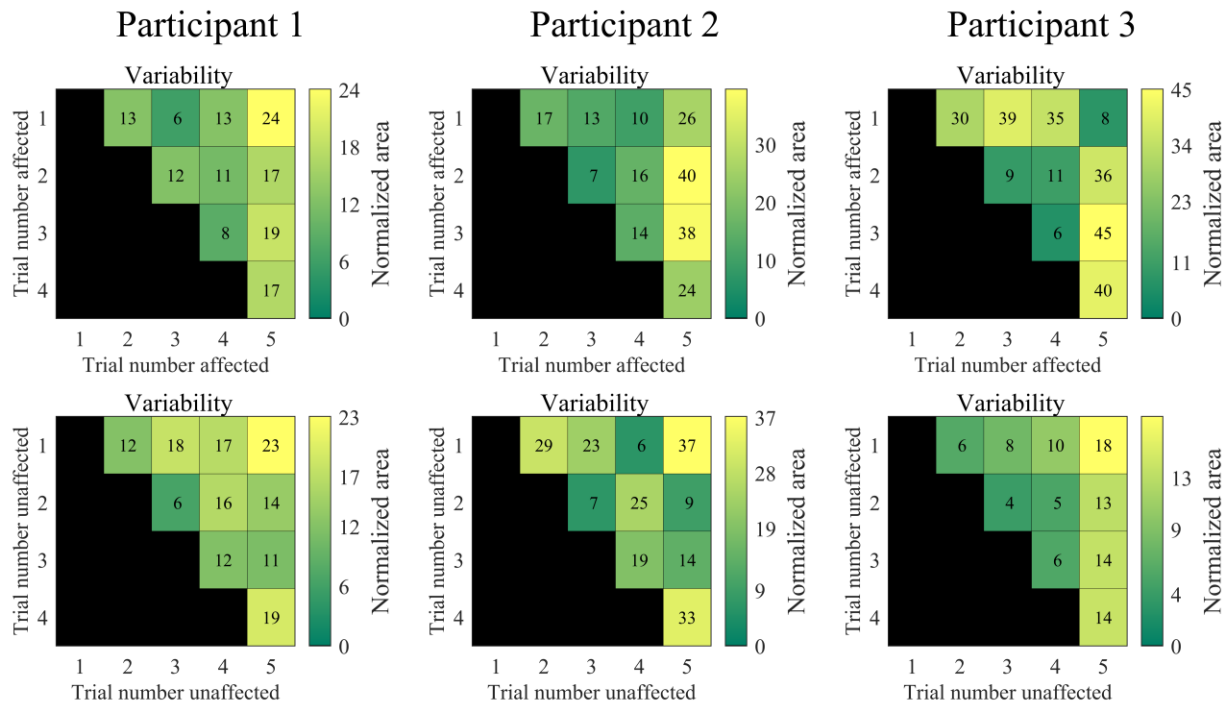


Figure D-3. Feature space trial-to-trial variability trajectory differences. Each column represents the trial-to-trial area of the normalized variability trajectory for the affected limb (top) and unaffected limb (bottom). Lighter yellow coloring indicates a larger area between two normalized trajectories. The affected and unaffected limbs show no trends in behavior. This comes with the exception of participant 3's unaffected limb where an increase in area from trial 1 to trial 5 is observed. Note that the area is rounded to the nearest whole number.